
Effects of Gradation and Cohesion on Bridge Scour, Vol. 1. Effect of Sediment Gradation and Coarse Material Fraction on Clear Water Scour Around Bridge Piers

PUBLICATION NO. FHWA-RD-99-183

DECEMBER 1999

PB2000-103270



U.S. Department of Transportation

Federal Highway Administration

Research, Development, and Technology
Turner-Fairbank Highway Research Center
6300 Georgetown Pike
McLean, VA 22101-2296

REPRODUCED BY:
U.S. Department of Commerce
National Technical Information Service
Springfield, Virginia 22161

NTIS



FOREWORD

This report is volume 1 of a six volume series describing detailed laboratory experiments conducted at Colorado State University for the Federal Highway Administration as part of a study entitled "Effects of Sediment Gradation and Cohesion on Bridge Scour". Volume 1 describes the effects of sediment gradation and coarse material fraction on local clear water pier scour. This six volume series will be distributed to NTIS only and will not be printed by FHWA. A separate summary report which describes the key results from the six volume series will be published by FHWA and distributed to the FHWA Division Offices.



T. Paul Teng, P.E.
Director, Office of Infrastructure
Research and Development

NOTICE

This document is disseminated under the sponsorship of the Department of Transportation in the interest of information exchange. The United States Government assumes no liability for the contents or use thereof. This report does not constitute a standard, specification, or regulation.

The United States Government does not endorse products or manufacturers. Trade and manufacturers names appear in this report only because they are considered essential to the object of the document.

PROTECTED UNDER INTERNATIONAL COPYRIGHT
ALL RIGHTS RESERVED
NATIONAL TECHNICAL INFORMATION SERVICE
U.S. DEPARTMENT OF COMMERCE

Reproduced from
best available copy.



1. Report No. FHWA-RD-99-183	2. PB2000-103270 	3. Recipient's Catalog No.	
4. Title and Subtitle EFFECTS OF GRADATION AND COHESION ON BRIDGE SCOUR Vol. 1. Effect of Sediment Gradation and Coarse Material Fraction on Clear Water Scour Around Bridge Piers		5. Report Date December 1999	6. Performing Organization Code
7. Author(s) Albert Molinas and Mohamad I. Abdou		8. Performing Organization Report No.	
9. Performance Organization Name and Address Colorado State University Engineering Research Center Fort Collins, Colorado		10. Work Unit No. (TRAIS) NCP# 3D3C1-582	11. Contract or Grant No. DTFH61-91-C-00004
12. Sponsoring Agency and Address Office of Engineering Research and Development Federal Highway Administration 6300 Georgetown Pike McLean, Va 22101		13. Type of Report and Period Covered Laboratory Final Report Jan 1991 - Jan 1996	
14. Sponsoring Agency Code			
15. Supplementary Notes Contracting Officer's Technical Representative: J. Sterling Jones HNR-10			
16. Abstract <p>The effects of gradation and coarse bed material fraction on pier scour were investigated experimentally in the eight-foot-wide by two-hundred-foot-long tilting flume at the Engineering Research Center, Colorado State University. Six different sand mixtures with the same median diameter, D_{50}, of 0.75 mm, but with gradation coefficients ranging from 1.38 to 3.4 were used in the experiments. To study the coarse material fraction effects, mixtures with same median diameter, D_{50}, and gradation coefficient, σ_g, but with varying D_{90} and D_{95} sizes were subjected to same scour conditions. The experiments were limited to clear water scour around a circular pier with a diameter of 7.0 inches (178 mm). Flow intensities starting with incipient conditions were increased in the experiments until live-bed conditions were encountered. Extensive bed material samples from the scour hole and the approach were obtained and analyzed. A regression equation was derived to fit the experimental data specific to the particular pier and flow conditions that were used in the experiments and is not intended for general application. Experiments reveal that the coarse material fraction, rather than the gradation coefficient, is the controlling sediment property factor in pier scour.</p> <p>This publication is the first volume of a six volume series. The other volumes are as follows:</p> <ul style="list-style-type: none"> Vol. 2. Experimental Study of Sediment Gradation and Flow Hydrograph Effects on Clear Water Scour Around Circular Piers Vol. 3. Abutment Scour for Nonuniform Mixtures Vol. 4. Experimental Study of Scour Around Circular Piers in Cohesive Soils Vol. 5. Effect of Cohesion on Bridge Abutment Scour Vol. 6. Abutment Scour in Uniform and Stratified Sand Mixtures 			
17. Key Words Bridge Scour, Pier Scour, Abutment Scour, Gradation, Coarse Sediment, Cohesion, Clay Scour		18. Distribution Statement No restrictions. This document is available to the public through the National Technical Information Service, Springfield, Va. 22161	
19. Security Classif. (of this report) Unclassified	20. Security Classif. (of this page) Unclassified	21. No. of Pages 199	22. Price

SI* (MODERN METRIC) CONVERSION FACTORS

APPROXIMATE CONVERSIONS TO SI UNITS

APPROXIMATE CONVERSIONS FROM SI UNITS

Symbol	When You Know	Multiply By	To Find	Symbol	When You Know	Multiply By	To Find	Symbol
LENGTH								
in	inches	25.4	millimeters	mm	millimeters	0.039	inches	in
ft	feet	0.305	meters	m	meters	3.28	feet	ft
yd	yards	0.914	meters	m	kilometers	1.09	yards	yd
mi	miles	1.61	kilometers	km		0.621	miles	mi
AREA								
in ²	square inches	645.2	square millimeters	mm ²	square millimeters	0.0016	square inches	in ²
ft ²	square feet	0.093	square meters	m ²	square meters	10.764	square feet	ft ²
yd ²	square yards	0.836	square meters	m ²	hectares	1.195	square yards	yd ²
ac	acres	0.405	hectares	ha	square kilometers	2.47	acres	ac
mi ²	square miles	2.59	square kilometers	km ²		0.386	square miles	mi ²
VOLUME								
fl oz	fluid ounces	29.57	milliliters	mL	milliliters	0.034	fluid ounces	fl oz
gal	gallons	3.785	liters	L	liters	0.264	gallons	gal
ft ³	cubic feet	0.028	cubic meters	m ³	cubic meters	35.71	cubic feet	ft ³
yd ³	cubic yards	0.765	cubic meters	m ³		1.307	cubic yards	yd ³
NOTE: Volumes greater than 1000 l shall be shown in m ³ .								
MASS								
oz	ounces	28.35	grams	g	grams	0.035	ounces	oz
lb	pounds	0.454	kilograms	kg	kilograms	2.202	pounds	lb
T	short tons (2000 lb)	0.907	megagrams (or "metric ton")	Mg (or "t")	megagrams (or "metric ton")	1.103	short tons (2000 lb)	T
TEMPERATURE (exact)								
°F	Fahrenheit temperature	5(F-32)/9 or (F-32)/1.8	Celcius temperature	°C	Celcius temperature	1.8C + 32	Fahrenheit temperature	°F
ILLUMINATION								
fc	foot-candles	10.76	lux	lx	lux	0.0929	foot-candles	fc
fl	foot-Lamberts	3.426	candela/m ²	cd/m ²	candela/m ²	0.2919	foot-Lamberts	fl
FORCE and PRESSURE or STRESS								
lbf	poundforce	4.45	newtons	N	newtons	0.225	poundforce	lbf
lbf/in ²	poundforce per square inch	6.89	kilopascals	kPa	kilopascals	0.145	poundforce per square inch	lbf/in ²

(Revised September 1993)

* SI is the symbol for the International System of Units. Appropriate rounding should be made to comply with Section 4 of ASTM E380.

EFFECTS OF GRADATION AND COHESION ON BRIDGE SCOUR

VOLUME I

TABLE OF CONTENTS

CHAPTER 1 INTRODUCTION	1
1.1 General	1
1.2 Objectives	3
1.3 Scope of Study	4
CHAPTER 2 EXPERIMENTAL EQUIPMENT AND PROCEDURE	7
2.1 Introduction	7
2.2 Equipment	8
2.2.1 Flume	8
2.2.2 Piers	10
2.2.3 Bed Materials Used in Experiments	11
2.3 Experimental Procedure	17
2.4 Individual Measurements	19
2.4.1 Flow Discharge	19
2.4.2 Flow Depth	20
2.4.3 Slope	21
2.4.4 Flow Temperature	21
2.4.5 Scour Hole Measurements	21
2.4.6 Scour versus Time Measurements	22

2.4.7	Velocity Measurements	23
2.4.8	Sampling of the Armor Layer	24
2.4.9	Grain Size Analysis	28
2.4.9.1	Required Apparatus	29
2.4.9.2	Procedure	29
CHAPTER 3 ARMORING PATTERNS AROUND CIRCULAR BRIDGE PIERS		31
3.1	Introduction	31
3.2	Flow Conditions	32
3.3	Critical Shear Stress for Sediment Mixtures	35
3.4	Ratio of Average Bed Shear Stress to Critical Shear	37
3.5	Armoring Process	47
3.5.1	Armoring Patterns around Bridge Piers for Set 1	49
3.5.2	Armoring Patterns around Bridge Piers for Sets 2 and 3	53
3.5.3	Gradation Patterns at Different Areas around Bridge Piers	60
CHAPTER 4 ANALYSIS AND DISCUSSION OF RESULTS		71
4.1	Introduction	71
4.2	Geometry of Scour Hole	72
4.3	Influence of Mean Approach Velocity on Local Scour	72
4.4	Repeatability of Results	79
4.5	Scour Depth Comparison in Uniform and Non-Uniform Beds	83
4.5.1	Clear-Water Scour Depth as a Function of Froude Number	83

4.5.2	Scour Profile Along Cross-Sections	86
4.5.3	Time Development of Scour Depth to Account for the Effect of Gradation Coefficient	86
4.5.4	Effect of Gradation Coefficient on Armoring Patterns around Bridge Piers	92
4.6	Effect of Increasing Coarse Material Fraction on Resulting Scour Depths	93
4.6.1	Scour Depth as a Function of Froude Number	97
4.6.2	Scour Profile Along Cross-Sections	100
4.6.3	Time Development of Scour Depth to Account for the Effect of Increasing Coarse Material Fraction	100
4.6.4	Conclusions from the Time Development of Scour Depth	110
4.6.5	Effect of Increasing Coarse Material Fraction on Armoring Patterns	114
4.7	Comparison between Scour Depths for Sediment Mixtures with $\sigma_g = 2.43$ Enriched d_{90} and Mixtures with $\sigma_g = 3.4$	114
4.7.1	Resulting Armor Layers at Bridge Piers	118
4.7.2	Development of Scour Depth with Time.	121
4.8	Comparison of Measured Local Scour Depths with other Prediction Equations	121
4.8.1	Contraction Scour	124

4.8.2	Local Pier Scour	124
4.8.3	Comparison with CSU Equation	124
4.8.4	Comparison with the Froehlich Equation	125
4.8.5	Comparison with New Zealand Equations	127
4.9	Regression Analysis	136
4.9.1	Regression Analysis for Experimental Data	136
4.10	Comparison between Predicted Clear-Water Scour Equations from Present Study and other Equations	141
4.11	Comparison between Newly Developed Equations and other Researcher's Measured Data	149
4.12	General Equation for Local Scour Depth Based on the Present Study	150
CHAPTER 5 SUMMARY, CONCLUSIONS AND RECOMMENDATIONS . .		159
5.1	Summary	159
5.2	Conclusions	161
5.3	Recommendations	167
REFERENCES		169
APPENDIX A -Dimensional Analysis to Determine Parameters		
	Influencing Clear-Water Scour Around Bridge Piers	174

EFFECTS OF GRADATION AND COHESION ON BRIDGE SCOUR

VOLUME I

LIST OF FIGURES

Figure 2.1	View of the 8-ft Flume Used in Experiments	9
Figure 2.2	Gradation Curves for Sediment Mixtures Used in Set 1	14
Figure 2.3	Gradation Curves for Sediment Mixtures for Set 2	15
Figure 2.4	Gradation Curves for Sediment Mixtures for Set 3	16
Figure 2.5	Measured and Calculated Velocities From Orifice Equation	26
Figure 3.1	Initial and Final Bed Elevations in the Approach of Pier 1 for Run 6	38
Figure 3.2	Initial and Final Bed Elevations in the Approach of Pier 1 for Run 13	39
Figure 3.3	Initial and Final Bed Elevations in the Approach of Pier 3 for Run 21	40
Figure 3.4	Initial and Final Bed Elevations In the Approach of Pier 3 for Run 22	41
Figure 3.5	Scour Hole and Approach Bed Profiles of Pier 3 for Run 22	42
Figure 3.6	Scour Hole and Approach Bed Profiles of Pier 3 for Run 23	42
Figure 3.7	Scour Hole and Approach Bed Profiles of Pier 3 for Run 24	43
Figure 3.8	Scour Hole and Approach Bed Profiles of Pier 3 for Run 25	43
Figure 3.9	Sediment Size Distribution Curves Around Scour Holes Formed	

	at Piers 2 and 3 During Run 2	50
Figure 3.10	Sediment Size Distribution Curves Around Scour Holes Formed at Piers 1, 2 and 3 During Run 4	51
Figure 3.11	Sediment Size Distribution Curves Around Scour Holes Formed at Piers 1 and 2 During Run 5	52
Figure 3.12	Sediment Size Distribution Curves Around Scour Holes for Runs 2 through 6	54
Figure 3.13	Effect of Coarse Material Fraction at Piers 1, 2 and 3 for Run 14	56
Figure 3.14	Effect of Coarse Material Fraction at Piers 1,2 and 3 for Run 16	57
Figure 3.15	Effect of Coarse Material Fraction at Piers 1 and 2 for Run 23	58
Figure 3.16	Effect of Coarse Material Fraction at Piers 1 and 2 for Run 24	59
Figure 3.17	Sediment Size Distribution Curves Around Pier 2 for Run 7 . . .	61
Figure 3.18	Sediment Size Distribution Curves Around Pier 1 for Run 10 . .	62
Figure 3.19	Sediment Size Distribution Curves Around Pier 2 for Run 18 . .	63
Figure 3.20	Sediment Size Distribution Curves Around Pier 2 for Run 17 . .	64
Figure 3.21	Sediment Size Distribution Curves Around Pier 1 for Run 22 . .	65
Figure 3.22	Sediment Size Distribution Curves Around Pier 1 for Run 23 . .	66
Figure 3.23	Sediment Size Distribution Curves Around Pier 1 for Run 24 . .	67

Figure 3.24	Sediment Size Distribution Curves Around Pier 1 for Run 25	.. 68
Figure 3.25	Sediment Size Distribution Curves Around Pier 2 for Run 27	.. 69
Figure 4.1	View of the Scour Hole Geometry for Pier 1 at the end of Run 7 (Q = 11.41 cfs)	.. 73
Figure 4.2	View of the Scour Hole Geometry for Pier 2 at the end of Run 7 (Q = 11.41 cfs)	.. 73
Figure 4.3	View of the Scour Hole Geometry for Pier 3 at the end of Run 7 (Q = 11.41 cfs)	.. 74
Figure 4.4	View of the Scour Hole Geometry for Pier 1 at the end of Run 10 (Q = 13.79 cfs)	.. 74
Figure 4.5	View of the Scour Hole Geometry for Pier 2 at the end of Run 10 (Q = 13.79 cfs)	.. 75
Figure 4.6	View of the Scour Hole Geometry for Pier 3 at the end of Run 10 (Q = 13.79 cfs)	.. 75
Figure 4.7	Dimensionless Scour Depth as a Function of the Approach Velocity for Various Gradation Coefficients	.. 77
Figure 4.8	Sediment Size Distribution Curves Around Scour Holes Formed at Piers 1 and 3 during Run 6	.. 80
Figure 4.9	Sediment Size Distribution Curves Around Scour Holes Formed at Piers 2 and 3 during Run 7	.. 81
Figure 4.10	Sediment Size Distribution Curves Around Scour Holes Formed at Piers 1, 2, and 3 during Run 10	.. 82

Figure 4.11	Effect of the Non-Uniformity of Sediments on Pier Scour Depth	85
Figure 4.12	Cross Sections Passing through Center Lines of Piers 1 and 2 for Runs 17 and 23 ($Q = 9.16$ cfs)	87
Figure 4.13	Cross Sections Passing through Center Lines of Piers 1, 2 and 3 for Runs 13 and 24 ($Q = 11.10$ cfs)	88
Figure 4.14	Cross Sections Passing through Center Lines of Piers 1, 2 and 3 for Runs 18 and 25 ($Q = 13.43$ cfs)	89
Figure 4.15	Effect of Sediment Gradation on Scour versus Time for $Q = 9.16$ cfs	90
Figure 4.16	Effect of Sediment Gradation on Scour versus Time for $Q = 11.10$ cfs	91
Figure 4.17	Surface Sediment Size Distribution Curves at the Upstream of Piers 1 and 2 for Runs 14 and 22	94
Figure 4.18	Surface Sediment Size Distribution Curves at the Upstream of Piers 1 and 2 for Runs 17 and 23	95
Figure 4.19	Surface Sediment Size Distribution Curves at the Upstream of Piers 1 and 2 for Runs 18 and 25	96
Figure 4.20	Effect of Increasing d_{90} and d_{95} on Scour Depth ($\sigma_g = 2.43$)	98
Figure 4.21	Effect of Increasing d_{90} on Scour Depth ($\sigma_g = 3.40$)	99
Figure 4.22	Cross Sections Passing through Center Lines of Piers 1 and 2 for Run 17 ($Q = 9.16$ cfs)	101
Figure 4.23	Cross Sections Passing through Center Lines of Piers 1 and 2 for	

	Run 13 (Q = 11.10 cfs)	102
Figure 4.24	Cross Sections Passing through Center Lines of Piers 1 and 2 for Run 18 (Q = 13.43 cfs)	103
Figure 4.25	Cross Sections Passing through Center Lines of Piers 1 and 2 for Run 23 (Q = 9.16 cfs)	104
Figure 4.26	Cross Sections Passing through Center Lines of Piers 1 and 2 for Run 24 (Q = 11.10 cfs)	105
Figure 4.27	Cross Sections Passing through Center Lines of Piers 1 and 2 for Run 25 (Q = 13.40 cfs)	106
Figure 4.28	Effect of Coarse Material Fraction on Scour versus Time (Q = 9.19 cfs)	107
Figure 4.29	Effect of Coarse Material Fraction on Scour versus Time (Q = 11.10 cfs)	108
Figure 4.30	Effect of Coarse Material Fraction on Scour versus Time (Q = 13.43 cfs)	109
Figure 4.31	Effect of Coarse Material Fraction on Scour versus Time (Q = 9.16 cfs)	111
Figure 4.32	Effect of Coarse Material Fraction on Scour versus Time (Q = 11.10 cfs)	112
Figure 4.33	Effect of Coarse Material Fraction on Scour versus Time (Q = 13.40 cfs)	113
Figure 4.34	Surface Sediment Size Distribution Curves at the Upstream of	

	Piers 1, 2 and 3 for Run 18	115
Figure 4.35	Effect of Increasing d_{90} Size for Mixtures with $\sigma_g = 2.43$ and $\sigma_g = 3.4$	117
Figure 4.36	Surface Sediment Size Distribution Curves at the Upstream of Pier 2 for Runs 14 and 22	119
Figure 4.37	Surface Sediment Size Distribution Curves at the Upstream of Pier 2 for Runs 18 and 25	120
Figure 4.38	Time Development of Scour for Sediment Mixtures with Increased d_{90} size for $\sigma_g = 2.43$ and $\sigma_g = 3.40$ ($Q = 9.16$ cfs)	122
Figure 4.39	Time Development of Scour for Sediment Mixtures with Increased d_{90} size for $\sigma_g = 2.43$ and $\sigma_g = 3.40$ ($Q = 11.40$ cfs)	123
Figure 4.40	Comparison between Measured Data and CSU Equation	126
Figure 4.41	Comparison between Measured Data and Froehlich Equation	128
Figure 4.42	Function of K_σ versus σ_g by Ettema (1976)	130
Figure 4.43	Comparison Between Measured Data and New Zealand Equations for $\sigma_g = 1.38$	133
Figure 4.44	Comparison between Measured Data and New Zealand Equations for $\sigma_g = 2.43$	134
Figure 4.45	Comparison between Measured Data and New Zealand Equations for $\sigma_g = 3.40$	135
Figure 4.46	Comparison between Newly Developed Prediction Equation and other Equations for $\sigma_g = 1.38$	142

Figure 4.47	Comparison between Newly Developed Prediction Equation and other Equations for $\sigma_g = 1.38$	143
Figure 4.48	Comparison between Newly Developed Prediction Equation and other Equations for $\sigma_g = 2.43$	144
Figure 4.49	Comparison between Newly Developed Prediction Equation and other Equations for $\sigma_g = 2.43$	145
Figure 4.50	Comparison between Newly Developed Prediction Equation and other Equations for $\sigma_g = 3.40$	146
Figure 4.51	Comparison between Newly Developed Prediction Equation and other Equations for $\sigma_g = 3.40$	147
Figure 4.52	Comparison between Newly Developed Prediction Equation and Chiew's Data	151
Figure 4.53	Comparison between Newly Developed Prediction Equation and Chiew's Data	152
Figure 4.54	Comparison between Newly Developed Prediction Equation and Chee's Data	153
Figure 4.55	Comparison between Newly Developed Prediction Equation and Chee's Data	154
Figure 4.56	Comparison between Newly Developed Prediction Equation and Baker's Data	155
Figure 4.57	Comparison between Newly Developed Prediction Equation and Baker's Data	156

Figure 5.1	Variation of Dimensionless Scour Depth with Approach Velocity for Experimental Tests Conducted During this Study	162
Figure 5.2	Variation of Dimensionless Scour Depth with Approach Velocity for Various D_{90} Sizes Used in Experiments ($D_{50} = 0.75$ mm) . . .	163
Figure 5.3	Variation of Dimensionless Scour Depth with Approach Froude Number for Various D_{90} Sizes Used in Experiments ($D_{50} = 0.75$ mm) .	164

EFFECTS OF GRADATION AND COHESION ON BRIDGE SCOUR

VOLUME I

LIST OF TABLES

Table 2.1. Sediment Mixture Properties for Set No. 1	13
Table 2.2. Sediment Mixture Properties for Set No. 2	13
Table 2.3. Sediment Mixture Properties for Set No. 3	13
Table 2.4. Cross-Section Integrated Velocities	25
Table 3.1. Summary of Experimental Data (T = 60 - 65 °F)	33
Table 3.2. Critical Shear Stress for Sediment Mixtures	37
Table 3.3. Calculations of Average Bed Shear Stress	44
Table 4.1. Effect of Sediment Gradation on Clear-Water Scour Depth	84
Table 4.2. Comparison between Scour Depths for d_{90} enriched $\sigma_g = 2.43$ and $\sigma_g = 3.40$	118

LIST OF SYMBOLS

<u>Symbol</u>	<u>Definition</u>
A	Cross-sectional area
B	Flume (channel) width
b	Pier width or diameter
b'	Pier width projected normal to the approach flow
d_{avg}	Mean diameter of the initial mixture
d_{avga}	Mean diameter of the armor coat
d_g	Geometric mean diameter of the sediment mixture
d_{16}	Sediment size (diameter) for which 16% of the sediment material by weight is finer
d_{50}	Median sediment size or, sediment size (diameter) for which 50% of the sediment material by weight is finer
d_{84}	Sediment size (diameter) for which 84% of the sediment material by weight is finer
d_{90}	Sediment size (diameter) for which 90% of the sediment material by weight is finer
F_r, Fr	Froude number
g	Acceleration due to gravity

k	Proportionality constant
K	Coefficient for pier type in Froehlich equation (Equation 4.2)
K_1	Correction factor for pier shape
K_2	Correction factor for pier alignment
K_d	Sediment size factor
K_I	Flow intensity factor
K_s	Pier shape factor
K_y	Flow depth factor
K_a	Pier alignment factor
K_σ	Sediment gradation factor
K_o	A coefficient which is less than or equal to 1.0 in Ettema equation (Equation 4.6). This coefficient is the ratio of the scour depth in graded material to that in uniform material
L	Pier length
P	Wetted perimeter of the total cross section
Q	Water discharge
R	Hydraulic radius of the cross section, $R = A/P$
S_e	Slope of the energy grade line
S_w	Water surface slope
S_0	Bed surface slope
S_s	Specific gravity of the sediment grains
T	Average water temperature ($^{\circ}$ F)

t	Time
U	Mean flow velocity, $U = Q/A$
U_c	Critical velocity
U_*	Shear velocity
U_{*c}	Critical shear velocity
V_1	Approach velocity to each pier
Y_1	Average approach flow depth in front of each pier
Y_s	Local scour depth
Y_s/b	Relative scour depth with respect to pier diameter
Y_s/Y_1	Relative scour depth with respect to flow depth
α	Angle of attack = angle between flow direction and pier axis
σ_g	Geometric standard deviation of sediment mixtures, $\sigma_g = (d_{84}/d_{16})^{0.5}$
γ_w	Specific weight of water
γ_s	Specific weight of sediment
ρ	Density of water
ρ_s	Density of sediment
ν	Kinematic viscosity of water
τ_0, τ_b	Mean bed shear stress
τ_{cm}	Critical shear stress for sediment mixtures

CHAPTER 1

INTRODUCTION

1.1 General

Bridge failures during floods cause great damage and loss of life throughout the world. One of the main reasons for bridge failures is the scouring or undermining of bridge foundations by the action of the flow. The damage can be attributed to the presence of obstructions to the flow such as piers or abutments which cause disturbances in the flow creating vortices that cause local scour. The interaction between the bridge structure and the river flows through bridge piers and abutments causes local scour in the area around piers and abutments.

During the past 50 years, many problems associated with local scour have been recognized and much effort has been devoted to studies of local scour. In this field, good progress has been made. Equations have been derived or developed for predicting local scour depths around bridge piers taking into consideration the major parameters that affect scour phenomenon, including flow, fluid properties, sediment, pier geometry and time.

Most pier scour equations are based on physical models (laboratory tests) using dimensional analysis to identify the major parameters that affect local scour. Physical models still remain the principal tool for estimating expected depths of scour because theoretical solutions of the equations that describe the complex interaction between the

flow around a bridge pier and the erodible sediment bed surrounding it are not available. Also, accurate field measurements have been difficult to obtain because of the severe three-dimensional flow patterns that occur at bridges during high flows, and the problems and costs associated with collecting data during peak flow periods.

The general nature and principles of scour and the different variables that affect scour are well-known from the studies of Laursen and Toch (1956) and Melville (1975). These authors formulated a wide variety of empirical equations based upon a limited range of data to predict the scour depth. These equations apply to different modes of transport, clear water or live bed scour, and they treat bed sediments as uniform in terms of some median or mean particle size only. However, natural fluvial sediments seldom have a uniform particle size composition and most natural sediment deposits have a non-uniform grain size distribution.

The laboratory experiments on local scour conducted during the last two decades by Nicollet (1971), Hancu (1971), Ettema (1976), and Baker (1986) indicate that the maximum clear water scour depends upon both the sediment size and sediment gradation. Ettema (1976) and Baker (1986) show that the local scour in graded bed material is much less than uniform bed material scour. This result is a consequence of an armor layer which forms within the scour hole as the sediment mixture non-uniformity increases. Due to the importance of gradation of bed materials on the resulting scour depth, and because most design practices do not account for this effect, it was decided to study the effect of non-uniformity of bed sediments on the resulting local scour depth around bridge piers in clear water conditions.

1.2 Objectives

The primary goal of this study is to investigate the effects of sediment gradation and coarse material fraction of sediment mixtures on clear-water scour depth and to develop a new bridge pier scour predictor accounting for non-uniformity of bed material. The study also includes an extensive investigation of the final bed material gradation in the area around each pier after having been subjected to certain flow conditions. These objectives were achieved through:

1. a survey of previous experimental, theoretical and field studies, and the evaluation of the available scour depth predictors through an extensive literature review;
2. collection and compilation of data and results obtained from previous experimental laboratory work and field data collected by previous investigators for local scour depth around bridge piers.
3. Performing bridge pier scour experiments using Six different bed materials with gradation coefficients ranging between 1.0 and 4.0. One of the sediment mixtures was chosen to be almost ($\sigma_g = 1.38$) a uniform sand to compare armored scour hole depths with those which do not exhibit armoring effect (i.e. uniform material) under the same flow conditions;
4. analyzing the results to produce new scour predictors which account for armoring (gradation) effects as well as the flow effects;

This study was limited to clear-water scour adjacent to circular cylindrical piers.

1.3 Scope of Study

In order to fulfill the objectives listed in Section 1.2, a physical model study was conducted in the Hydraulics Laboratory at the Engineering Research Center, Colorado State University using a tilting 8-ft wide, 200-ft long flume. Six different sand mixtures having the same median diameter of d_{50} of 0.75 mm and having gradation coefficients (σ_g) of 3.4, 2.43, and 1.38 were used in the experiments. The gradation coefficient σ_g is defined as $(d_{84}/d_{16})^{1/2}$. In the bridge pier scour experiments the sediment mixture with a gradation coefficient of 1.38 was considered to be uniform sand bed material.

Three sets of runs were performed using three identical plexiglass circular piers having an outside diameter of 7.0 inches (0.583 feet). The three piers were spaced along the length of the flume along the center line. The leading upstream pier was 45.0 ft from the head box of the flume, the second pier was 80.0 ft from the head, and the third pier was 120.0 ft from the head. The approach flow depth for each pier was almost constant in the range of $1.0 \text{ ft} \pm 0.1 \text{ ft}$ except in two of the runs where the flow depth was increased to 1.2-1.3 ft to study the change in the resulting scour depth keeping all other conditions the same except flow depth. The main variables varied in the experiments were the flow discharge, (and therefore the velocity and Froude number), size of the coarse material, and the coefficient of gradation for bed material around each pier. During two sets of the runs, d_{90} was increased and during one set of runs d_{95} was increased while keeping the gradation coefficient constant. In the series of experiments the discharge was gradually increased until the bed began to move at the end of each set of runs, and a complete range of data for clear-water scour conditions

for each gradation was obtained. In the first set of runs the bed material properties were kept the same with σ_g of 2.43 and d_{50} of 0.75 mm, around each of the three piers to check the repeatability of results. During the second set of runs, the bed material around pier 1 was kept the same as the first set of runs with σ_g of 2.43 and d_{50} of 0.75 mm. Around pier 2, σ_g was 2.43 but d_{90} size was increased, and around pier 3, σ_g was 2.43 but d_{95} size was increased. Lastly, during the third set of runs, a sediment mixture with a coefficient of gradation σ_g of 3.4 and d_{50} of 0.75 mm was used around pier 2. Around pier 1, σ_g and d_{50} were the same but d_{90} size was increased. Around pier 3 an almost uniform mixture with σ_g of 1.38 and d_{50} of 0.75 mm was used.

In this study, new local scour depth prediction equations have been developed that account for the effect of bed material gradation. Also, new scour predictors were developed taking into account the effect of increasing d_{90} in the original sediment mixture. The work was performed in three phases: 1) Literature review; 2) Experimentation; and 3) Data Reduction and Analysis.

Due to its volume, the literature review and compilation of existing bridge pier scour data are presented and are being published separately through CSU as a Civil Engineering Report. Chapter 2 briefly describes the flume used in experiments, sediment mixtures used in this study, the methods employed in the measurement of different hydraulic variables, and the procedures used to collect the data. Chapter 3 details the armoring patterns encountered around circular bridge piers during the experiments. Chapter 4 is on the data reduction and analysis and discussion of the results. In the analysis, new equations for bridge pier scour accounting for gradation

effects were developed. Chapter 5 includes a summary, conclusions, and recommendations for future studies. Appendix A presents the dimensional analysis for the involved and influencing parameters on bridge pier scour.

This research aims at estimating the local scour depth for bridge piers in non-uniform bed material, a problem which is of fundamental importance in the design of safe bridge pier foundations under clear-water scour conditions. It is hoped that the data from this study will be a valuable contribution to researchers who are working in the field of bridge scour, since it will expand the data base against which to compare their future research results.

CHAPTER 2

EXPERIMENTAL EQUIPMENT & PROCEDURE

2.1 Introduction

This chapter describes the sediment mixtures used in the experimental program as bed materials, and the piers, the flume, the experimental procedure, as well as the individual measurements employed in this study.

The experimental program consisted of three main series: the first series was conducted by subjecting three identical piers to specified flow conditions. The purpose of this set of runs was to check the repeatability of results for scour depth at the three piers subjected to the same flow conditions. This first set (Runs 1 through 12) was performed using a graded sand mixture with a geometric standard deviation, σ_g of 2.43 and d_{50} of 0.75 mm. The second set (Runs 13 through 19) was performed using the same sand with σ_g of 2.43 and d_{50} of 0.75 mm as the bed material around pier 1. Around piers 2 and 3 the size of coarse material fraction in the original sediment mixture corresponding to 10% (around pier 2) and to 5% (around pier 3) was increased. The gradation coefficient, σ_g and d_{50} were kept constant at 2.43 and 0.75 mm respectively. The purpose of this second set of runs was to examine the behavior of the scour depth with increasing the sizes of sediments for the fraction above d_{90} and d_{95} in the original sediment mixture without changing the gradation coefficient. The third set (Runs 20 through 27), was conducted using a sediment mixture with σ_g of 3.4 and d_{50}

of 0.75 mm as the bed material around pier 2 and increasing the coarse fraction above d_{90} in the same sediment mixture as the bed material around pier 1. For pier 3, a uniform sand with σ_g of 1.38 and d_{50} of 0.75 mm was used. The purpose of sets No. 2 and 3 was to investigate the effect of increasing coarse material fraction and gradation of bed materials on local pier scour depth.

2.2 Equipment

This section briefly describes the flume, the bed materials and other instruments used in carrying out the experiments.

2.2.1 Flume

Experimental work for this study was conducted using the 8-ft flume shown in Figure 2.1 which is housed in the Hydraulics Laboratory at the Engineering Research Center at Colorado State University. The flume tilts and recirculates water and sediment, is 200 ft long, 8 ft wide, and 4 ft deep. The flume can be adjusted to any desired slope up to 3% . The flume is supported by a steel structure that holds it about six feet from the floor of the laboratory.

Water is pumped into the flume from a sump tank by using a system of three pumps through the main pipelines to the head box which contains vertical and horizontal flow straighteners and a mesh box of gravel followed by a concrete ramp to reduce the

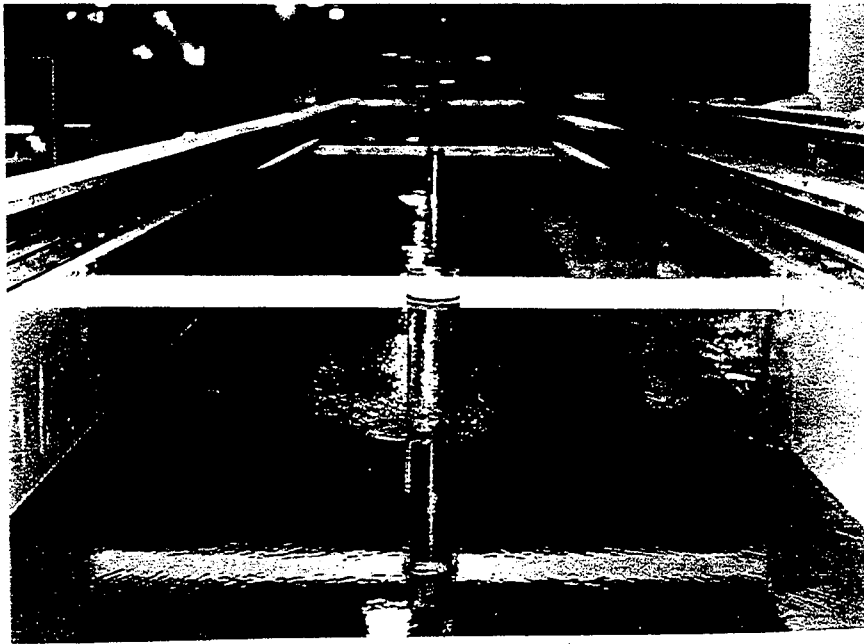


Figure 2.1 View of the 8-ft Flume Used in Experiments

turbulent eddies induced at the flume entrance. A wooden floating frame is placed at the upstream end of the flume to absorb the surface waves induced by the water entering the flume. Water leaving the flume falls into a sump connected to the pumps. The flow in all runs was subcritical and therefore was subjected to downstream control. A vertical, adjustable tail gate at the downstream end of the flume was used to maintain desired flow conditions and to control the water depth. The test reach was 130.0 ft long beginning from the zero (head) of the flume, and extending up to station 160.0 ft where a 20 ft long sediment trap consisting of two vertical wooden walls rising from the bottom to the bed was placed. The function of the first wooden wall is to retain the bed material and the second wall function is to trap the sediment coming from the flume for

the movable bed conditions. Flume discharge is measured by a calibrated orifice meter installed on each of the three main pipelines of the pumps. The combined maximum discharge is approximately 100 cfs.

A motorized instrument carriage runs longitudinally on the flume rails mounted on the walls of the flume. A point gage of accuracy 0.01 ft is mounted on the carriage. It supports a depth measuring device for the bed and water surface elevations and the current meter used to take all velocity measurements.

2.2.2 Piers

Three identical cylindrical piers of clear plexiglass 4-ft high with an outside diameter of 7 inches were utilized in the pier scour experiments. Circular piers were used because of their symmetry and the abundance of data available for comparative purposes. All three piers were placed at the center line of the flume for each run. In the longitudinal direction, the leading pier was 45 feet from the head box of the flume, the second one was 80 feet from the head of the flume, and the third one was 120 feet from the head of the flume.

In order to keep side-wall effects insignificant, the maximum pier size (for use in the 8-ft wide flume) was kept at 7 inches, i.e. a flume width to pier width ratio, B/b of 13.7. This value is higher than the B/b value of 8 suggested by Shen et al. (1966) since it was found by Chiew (1984) during some trials that a blockage ratio of 8 or smaller could produce significant wall effect.

The depth measurements for pier scour with time were achieved utilizing visual techniques. For this purpose, the piers were constructed of transparent plexiglass material and three measuring scales were glued to the front, side and back of each pier, in addition to a mirror with handle angled at 45° placed at the base of the pier. The base of the scour hole and the deepest point of the scour hole at any time could be easily identified and recorded by sliding the mirror within the plexiglass and reading the corresponding measurement on the scale. In this way, scour depth with elapsed time could be obtained up to an accuracy of ± 0.005 ft (1.5 mm). A bright light located above the water surface was used to improve the visibility of the scour region under clear water scour conditions.

2.2.3 Bed Materials Used in Experiments

It has been indicated by many researchers such as Blench (1952), Fleming (1970), and Vanoni et al.(1961) that there is a very strong tendency for alluvial sediments to follow the log normal size distributions. Such size distribution can be represented by a straight line on logarithmic-normal probability paper and in this case d_{50} becomes the geometric mean diameter d_g of the sediment mixture where d_{50} is the sediment diameter for which 50% of the sediment material by weight is finer. Also, the geometric standard deviation σ_g is given by:

$$\sigma_g = \frac{d_{84}}{d_{50}} = \frac{d_{50}}{d_{16}} \quad (2.1)$$

or

$$\sigma_g = \frac{1}{2} \left[\frac{d_{84}}{d_{50}} + \frac{d_{50}}{d_{16}} \right] \quad (2.2)$$

or

$$\sigma_g = \sqrt{\frac{d_{84}}{d_{16}}} \quad (2.3)$$

where: d_{16} , d_{50} , and d_{84} are the sediment diameters for which 16%, 50%, and 84% of the sediment material is finer by weight respectively. The log-normal distribution function is a 2-parameter distribution and is completely defined by d_{50} and σ_g . However, most natural sediments show an approximate log-normal distribution only through the mid part of the distribution, say $d_{50} \pm \sigma$, but they usually have long tails in both the coarse and fine fractions. Thus, Equations 2.1 through 2.3 are for gradation coefficients that measure the spread of the distribution only between d_{84} and d_{16} in most natural sediments. The presence of coarse material in sediment mixtures are better defined by sizes of different quantities, such as d_{98} , d_{95} , d_{90} , etc. For the work here, d_{50} and σ_g were held constant and sizes of d_{90} , d_{95} , d_{98} , etc. were changed since armoring in the scour hole involves mostly the coarser fractions of the mixture.

Proposed Sediment Mixtures. There is a specific requirement that needs to be met in determining the gradation of the initial grain size distribution for the sediment mixtures. This requirement is to keep the median size diameter constant throughout the study. The median diameter was chosen to be 0.75 mm, then gradation coefficients were chosen to be between 1.0 and 4.0. The properties of the sediment mixtures used throughout the present series of tests are indicated in Tables 2.1 through 2.3.

Table 2.1. Sediment Mixture Properties for Set No. 1

Pier No.	D ₁₆ (mm)	D ₅₀ (mm)	D ₈₄ (mm)	D ₉₀ (mm)	D ₉₅ (mm)	σ_g
1	0.31	0.75	1.83	2.10	2.36	2.43
2	0.31	0.75	1.83	2.10	2.36	2.43
3	0.31	0.75	1.83	2.10	2.36	2.43

Table 2.2. Sediment Mixture Properties for Set No. 2

Pier No.	D ₁₆ (mm)	D ₅₀ (mm)	D ₈₄ (mm)	D ₉₀ (mm)	D ₉₅ (mm)	σ_g
1	0.31	0.75	1.83	2.10	2.36	2.43
2	0.31	0.75	1.83	2.80	5.00	2.43
3	0.31	0.75	1.83	2.10	2.36	2.43

Table 2.3. Sediment Mixture Properties for Set No. 3

Pier No.	D ₁₆ (mm)	D ₅₀ (mm)	D ₈₄ (mm)	D ₉₀ (mm)	D ₉₅ (mm)	σ_g
1	0.23	0.75	2.65	4.76	6.40	3.40
2	0.23	0.75	2.65	3.20	4.20	3.40
3	0.55	0.75	1.05	1.18	1.22	1.38

Figures 2.2, 2.3, and 2.4 show the sediment size gradation curves of bed sediments used around the three piers during sets of runs No. 1, 2, and 3.

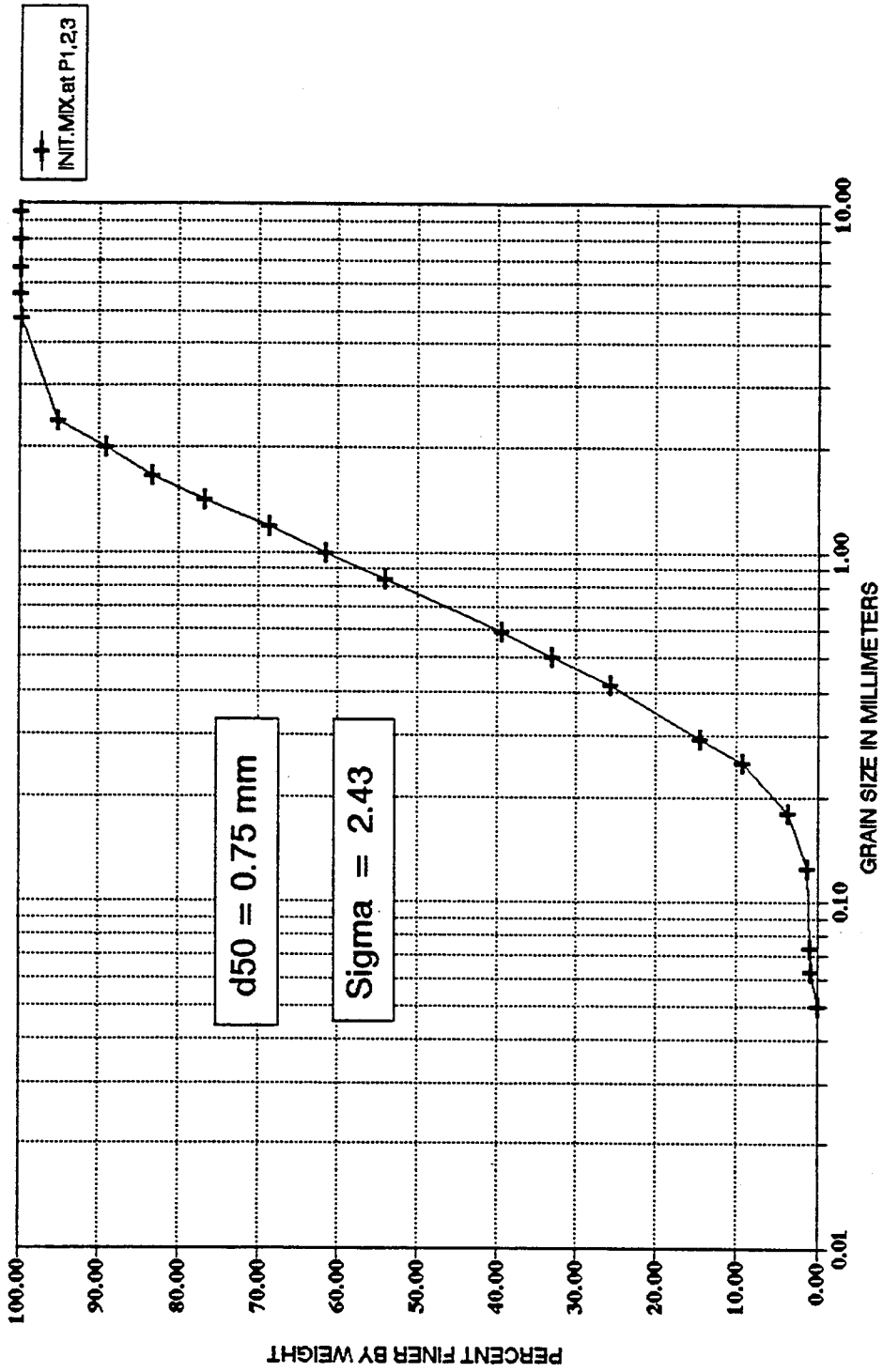


Figure 2.2 Gradation Curves for Sediment Mixtures Used in Set 1

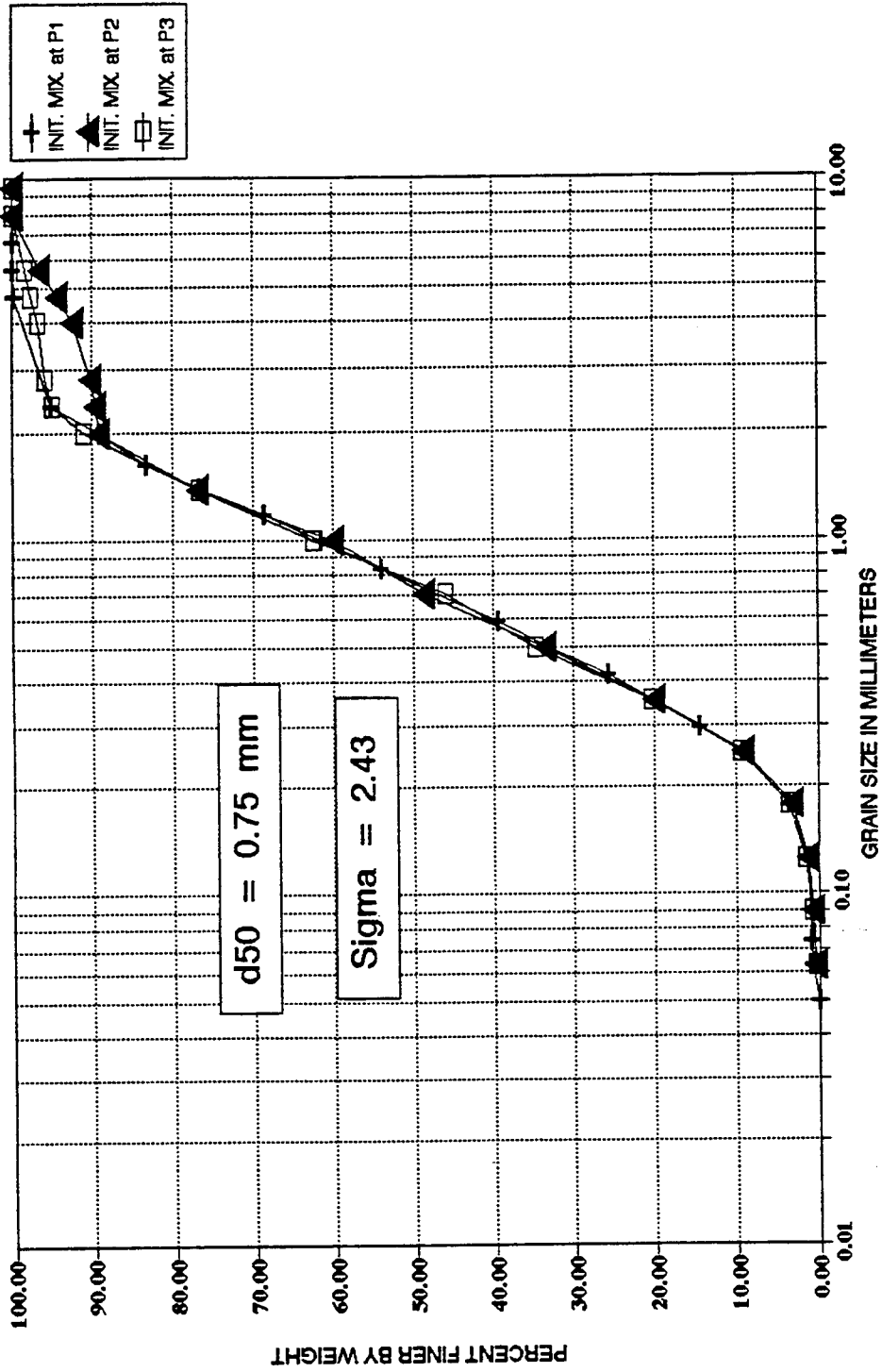


Figure 2.3 Gradation Curves for Sediment Mixtures for Set 2

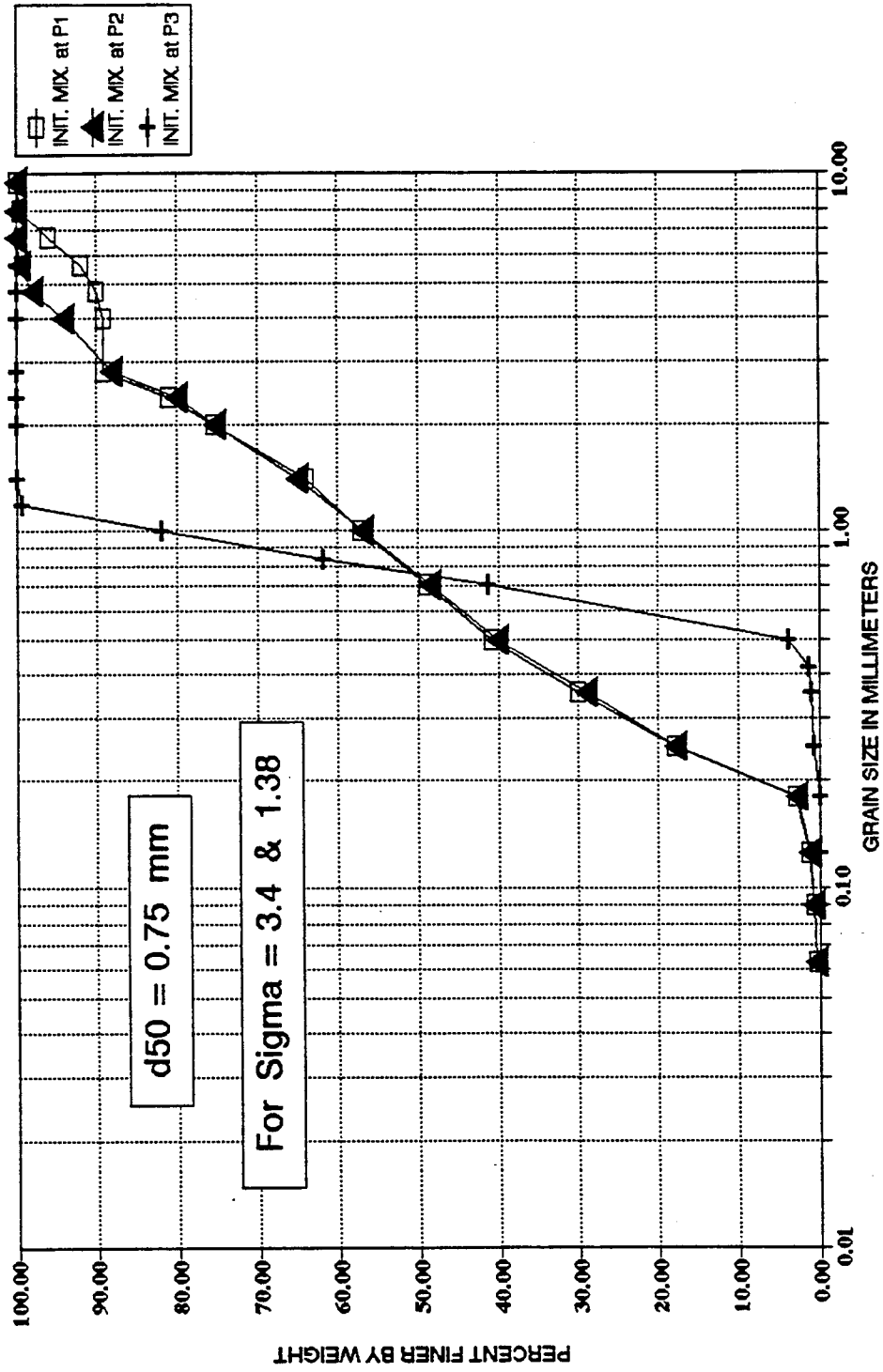


Figure 2.4 Gradation Curves for Sediment Mixtures for Set 3

2.3 Experimental Procedure

Preparation for the scour test was initiated by leveling the bed. Prior to each run, the sediment bed was levelled with the aid of a flat wood plate that has the same width as the flume and was connected vertically to the instrument carriage by clamps. By employing the point gage mounted on the carriage, initial bed elevations were taken to check the levelling of the flume and calculate the average initial bed elevation around each pier.

The gate was kept closed until the flume was filled with water. Then the gate was adjusted to get the desired depth, and the valves of the pump were adjusted to get the desired discharge which was determined with an orifice inserted in the recirculating pipeline. Flow depth for all runs was maintained at $1.0 \text{ ft} \pm 0.1 \text{ ft}$ and water surface and bed slopes were almost parallel.

Once the requested flow conditions were verified, the carriage and the point gage were moved along the flume in such a way that any point in the study area could be reached with the measuring devices. It was possible to obtain good measurements of the velocity in the approach of each pier. Water surface profile was measured along the length of the flume to calculate the water surface slope. Following scour with time along the period of each run was also done. Every test ran for 16 hours to allow maximum scour to be reached and the final scour hole geometry to be established. This period was enough to maintain the maximum scour depth constant for at least 3 to 4 hours.

At the end of each run, to drain the flume without any disturbance, the tail gate was slowly closed and the pump stopped. Then the flume was slowly drained with the aid of an efficient drainage system on the floor of the flume with its end open towards the tail gate.

The bed was then allowed to dry over a 24-hr period, photos of scour holes around each pier were taken, and measurements of the final bed elevations were recorded to determine the maximum scour depth around each pier and the final bed slope. The bed was allowed to dry another 24 hours and then the armor layers around each pier and different areas in the approach and downstream of the piers were sampled using the flour paste technique described by Ahmed (1989). Sieve analysis was then performed on the samples using U.S. standard sieves (the sieving of the sediment samples was completed by using a series of sieves at intervals of $\sqrt{2}$ x sieve diameter).

This procedure was repeated for each run. The area around each pier within 20 feet had to be refilled with the proper mixtures and remixed, then the bed was leveled and saturated with water. Flow conditions were verified, and velocity was measured at the approach of each pier in addition to the water surface profile measurements and scour depth with time. After the scour depth became constant with time for at least 3.0 to 4.0 hours, the flow was stopped to let the bed dry, then the final bed elevations were taken. Finally, the surface layer around each pier as well as the approach and downstream of each pier was sampled to determine the size distribution of the armored layers.

2.4 Individual Measurements

In order to obtain a satisfactory correlation between the variation of scour depth, flow parameters, and the change in bed material gradation, it was necessary during each experimental run to take measurements of the following variables, noting in order to maintain the clear water scour process, no sediment inflow was allowed throughout the duration of the experimental investigation:

- Flow discharge
- Flow depth
- Water surface slope
- Mean bed slope
- Mean bed elevations
- Water temperature
- Scour hole measurements
- Scour versus time measurements
- Velocity measurements
- Armoring measurements (bed sediment samples)

2.4.1 Flow Discharge

The flow discharge was measured by an orifice meter mounted on the main discharge pipeline. The differential head on the meter was measured by a mercury manometer and by reading the difference in pressure head upstream and downstream of the calibrated orifice meter. The discharge was regulated by means of a valve in the

main pipeline. Knowing the differential head ΔH in inches, discharge was determined in cfs using the following calibrated orifice meter relationship:

$$Q = 5.29 * (\Delta H)^{0.5} \quad (2.4)$$

The flow discharge was also estimated by integrating the velocity profile over the entire cross-section of the flume at several locations. Good agreement between the two methods was obtained.

2.4.2 Flow Depth

In the case of non-uniform material, bed irregularities affect the accuracy of measurements because the theoretical bed surface is not known and the bed elevation reading at any section actually depends on the position of the needle tip of the point gage relative to the larger grains on the bed. To reduce such error, three different point gage readings were taken at each of the test sections and the actual bed reading was then considered to be the average of the three readings.

The corresponding water surface readings were determined and the depth of flow was calculated as the average difference between the water surface and the bed surface elevations at the specified test sections. For all experimental runs a uniform flow depth over the entire flume length was maintained at $1.0 \text{ ft} \pm 0.1 \text{ ft}$ by regulating the tail gate at the flume exit. The local flow depth varied along the flume length during runs No. 12, 19, and 27, in response to the presence of bed features.

2.4.3 Slope

Slope in laboratory flumes is one of the most difficult quantities to measure. Special attention was devoted to reduce the error in slope measurements as much as possible. For this reason bed levels were measured using the point gage, then corrected through conversion factors obtained from a careful leveling of the carriage along the entire flume using a surveyor's level and rod. The bed slope was then computed as the slope of the line of best fit based on a least square-criteria. The water surface slope was calculated in a similar manner.

2.4.4 Flow Temperature

Measurements of water temperatures during each run are obtained by using a mercury thermometer. Temperature was measured by inserting the thermometer into the flume at about the middle of the flume length. The temperature was observed at regular intervals of time and averaged to obtain the mean temperature of each individual experimental run. Temperatures ranged from 61°F to 65°F and averaged 63°F.

2.4.5 Scour Hole Measurements

At the completion of each experiment the scour hole profiles around each pier were recorded with the point gage supported by the mobile carriage. After using the conventional method (stopping the flow and then measure the bed using a point gage), it became apparent that the method would not yield the correct scour depths around each pier because the scoured holes were partially filled in as the flow stopped. Thus, it was

necessary to let the bed dry for at least 24 hours to drain the flume completely in order to get accurate measurements of scour.

Very intensive grids were applied when measuring the scour around each pier, also contouring the region around each pier was done very carefully by employing as many points as possible because the maximum scour depth was the main concern of this study. The maximum scour depth value for each run was calculated as the difference between the mean initial bed elevation and the lowest measured point of scour around each pier.

2.4.6 Scour versus Time Measurements

The depth measurement for pier scour utilized visual techniques. The piers were constructed out of transparent plexiglass material. A series of lights was used to facilitate the observation of the scour hole and to help in photographing the bed after each run, especially for the armored layer around each pier.

As mentioned before, the piers were made out of plexiglass and measuring grid tapes were pasted on the interior wall at the front, side, and back of each pier. Using a mirror with a handle, it was easy to follow (trace) the development of scour with time without interference with the flow. The depth of scour was recorded at regular intervals as the scour hole formed. The frequency of scour depth measurements decreased as the rate of scouring decreased. The experiments were stopped when no change occurred to the maximum depth of the scour hole over a minimum period of four hours.

2.4.7 Velocity Measurements

The measurements of flow velocities during the experiments were carried out utilizing a one-dimensional Marsh-McBirney magnetic probe, Model 2000 portable water flowmeter. This type of current meter was designed for use in both the field and the laboratory. The unit measures velocity in one direction from an electromagnetic sensor placed in a conductive liquid such as water. The velocity measurement is displayed on a digital display as feet per second (ft/sec) or meters per second (m/s). Marsh Mc-Birney rates the accuracy of these flow meters at $\pm 2\%$ of the reading, and their range from -0.5 ft/s to 19.99 ft/s (-0.15 m/s to 6.0 m/s). From an environmental point of view, the sensor is accurate in the range of 32°F to 160°F (0°C to 65°C).

The velocity was measured in the approach of each pier at three specified sections: 7 ft, 5 ft, and 2 ft upstream of each pier (about 12, 6, and 3 pier diameters). The velocity was measured at 10, 20, 30...90% of the flow depth measured from the bed of the flume. The velocity profiles were then averaged at each section to calculate the overall mean flow velocity in the approach of each pier. The discharge was calculated by the integration method using the continuity equation:

$$Q = U * A \quad (2.5)$$

where

Q = flow discharge in (ft³/sec);

U = mean approach flow velocity in (ft/sec); and

A = cross-sectional area in (ft²).

The flume discharge determined by integrating the velocity distribution across the entire section was compared to discharge from the calibrated orifice meter. Good agreement was obtained between the two values. As shown in Table 2.4, the percentage error in the discharge determined from the integration of the velocity distribution and computed from the orifice equation is on the order of -1.35% to -7.97%. This percentage of error was found to be within the acceptable limits of laboratory measurements for such measurements. Figure 2.5 shows the values of the measured velocities and velocities calculated from the orifice discharge measurements of the flow. The measured velocities average about 5% less than those calculated from the orifice discharge.

2.4.8 Sampling of the Armor Layer

At the end of each experiment, the particle size distribution of the armor layers formed around each pier in the scour hole, approach bed to each pier, and downstream of the pier were measured from samples obtained by the flour paste technique described by Ahmed (1989). Sieve analysis was then performed on the samples using U.S. standard sieves and the available shaker in the Sediment Laboratory of the Engineering Research Center, Colorado State University.

To determine the grain size distribution of the armor layer, it was required to collect all grains in the top layer only. The most common method used by previous researchers for such purpose is the wax method. Gessler (1967) used molten resin at 200°C, Little and Mayer (1972) used purified bee's wax at 65°C to 68°C, Davis (1974)

Table 2.4 Cross-Section Integrated Velocities

Run No.	Discharge (cfs) from the orifice	Discharge (cfs) calculated from integration	Error%
1	7.29	7.056	-3.21
2	8.69	8.573	-1.35
3	10.58	10.377	-1.91
4	10.58	9.900	-6.42
5	9.31	8.846	-4.98
6	9.90	9.592	-3.11
7	11.41	10.957	-3.97
8	12.74	11.787	-6.40
9	9.43	9.058	-3.95
10	13.79	13.011	-5.65
11	15.15	14.160	-6.53
12	16.73	16.000	-4.35
13	11.10	10.515	-5.27
14	7.29	6.757	-7.31
15	5.16	4.880	-5.43
16	8.36	7.744	-7.37
17	9.16	8.429	-7.97
18	13.43	12.670	-5.64
19	16.85	16.407	-2.63
20	5.20	5.010	-3.66
21	6.50	6.127	-5.73
22	7.30	6.912	-5.31
23	9.16	8.702	-4.99
24	11.10	10.773	-2.95
25	13.40	12.557	-6.29
26	16.90	15.974	-4.65
27	18.30	16.738	-7.90

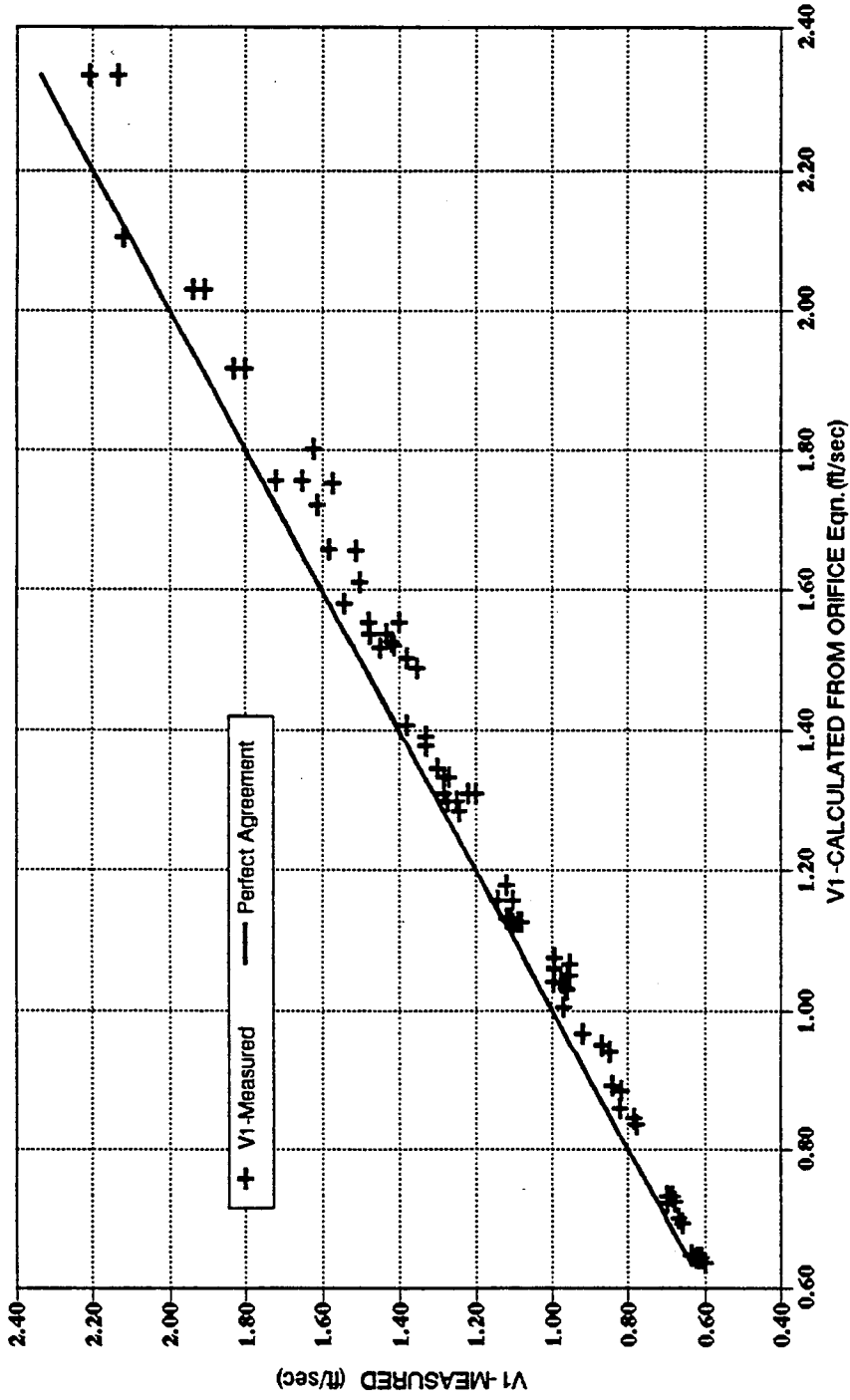


Figure 2.5 Measured and Calculated Velocities from Orifice Equation

used molten petroleum wax at 76°C to 78°C and Proffitt (1980) used paraffin wax at 55°C to 57°C. In previous work, the measured grain size distribution of the armor layers was found to be highly affected by the temperature at which the wax was poured onto the bed. If the temperature is outside the narrow ranges specified above, the wax either permeates down before solidifying or solidifies before all grains in the top layer adhere to it.

Day (1976) used the paint method to identify grains in the top layer but still used the wax method to lift it up. This method predicted a coarser grain size distribution of the armor layer than the wax method. Day explained this to be caused by the penetration of the wax below the armor layer.

In the present study, the flour paste technique, developed by Ahmed (1989) was used. The procedure proved to be much easier than the wax method in terms of preparation, use, time elapsed, and separation of the grains adhering to the paste. The paste is sticky enough for all grain sizes to adhere easily and thick enough so that it did not penetrate further than the surface layer.

After the bed was allowed to dry, the paste was placed on the surface of the bed. A gentle uniform pressure was applied downward on the paste to pick up all the grain sizes on the surface layer. The paste was then lifted up bringing with it the grains that had been the surface layer. The separation process of the grains adhering to the paste was achieved simply by washing the surface of the paste with warm water and gently brushing by hand. A visual observation of the paste surface clearly indicated that all grains, even the finest, were separated from the paste. The material was then dried,

weighed, sieved, and the grain size distribution of the armor layer at a specific area for a given flow condition was obtained. Detailed figures which show the grain size distribution curves of the armored bed and scour holes for certain flow conditions are presented in Chapters 3 and 4.

2.4.9 Grain Size Analysis

Mechanical (or sieve) analysis was used to determine the particle sizes and their relative distribution for particles greater than 0.074 mm (0.0029 in.). The smallest sieve size used in this analyses was the U.S. No. 200. The sieve number corresponds to the number of openings per linear inch; for example, the U.S. Bureau of Standards No. 8 sieve has eight openings per inch.

To accomplish the mechanical analysis, sieves were stacked one on top of the other in the shape of a nest of sieves, in which the largest screen opening (smallest sieve number) was on top, progressing to the sieve with the smallest screen openings (largest sieve number) on the bottom of the nest. A lid was placed on top of the nest and a pan was placed below the bottom sieve to catch any sediment that passes through the smallest opening.

A 10-minute shaking period was used in this procedure. A larger sample required a longer shaking period. Similarly, a sample comprised primarily of fine-grained material requires a longer shaking period than a coarser-grained sample of equal weight.

Particles that appear to be stuck in the sieve screen were never forced through the mesh, because forcing particles through the screen distorts the grain size results and can damage the screen. Particles caught in the screen were removed by brushing with the proper sieve brush (wire-bristled brush for coarse screens and a hair brush for fine screens). Brushing was done from the underside of the screen in order that the particles could be brushed out of the screen in the same direction that they entered the screen opening.

2.4.9.1 Required Apparatus

- a) A set of U.S. Standard sieves, lid and pan.
- b) Set of sieve brushes for cleaning sieves.
- c) Balance, sensitive to 0.1 gram.
- d) Large pans for air drying after cleaning the samples.

2.4.9.2 Procedure

- a) Separate all grains from the paste material and then wash with warm water to remove any paste that adhered to the particles.
- b) Samples were thoroughly air dried.
- c) The pan that was used in weighing the retained weights on each sieve after shaking the sample was cleaned and dried.
- d) If the total sample is sufficiently large, select a representative sample by using the quartering method.

- e) Weigh the sample to the nearest 0.1 gram.
- f) Sieve the sample of soil through a set (or "nest") of sieves by using a mechanical shaker for at least 10 minutes.
- g) Carefully separate the nest of sieves and weigh and record each weight that was retained on each sieve to the nearest 0.1 gram.
- h) The results of the grain size analysis were reported in the form of a grain size distribution curve on semi-log paper.

CHAPTER 3

ARMORING PATTERNS AROUND CIRCULAR BRIDGE PIERS

3.1 Introduction

Armoring measurements were performed after each run at different areas or positions around the piers to show sediment size distributions patterns in response to different flow conditions. This chapter presents the basic data and information about the armoring measurements around circular bridge piers. A brief discussion using the measured sediment size distribution curves for armor layers to satisfy the objectives of the three sets of runs performed during this study is also presented. Three sets of runs were performed to study the effects of bed material gradation, as well as increasing the size of coarse sediment fractions existing in the original sediment mixture, on bridge pier scour.

During the first set of runs the mixture was the same around piers No. 1, 2, and 3, having a mean diameter d_{50} of 0.75 mm and a geometric standard deviation σ_g of 2.43, as shown in Figure 2.2. The purpose of the first set of runs was to check the repeatability of armoring results under almost the same flow conditions.

In the second set of runs, the mixture around the three piers had the same d_{50} of 0.75 mm and σ_g of 2.43. Around pier 1 the mixture was the same as the first set of runs, around pier 2 the coarse material fraction size above d_{90} was increased, and around pier 3 the coarse material fraction size above d_{95} was increased as shown in

Figure 2.3. The purpose of this second set of runs was to study the effect of increasing the coarse material fraction size of the original sediment mixture on the local scour depth keeping d_{50} and σ_g at 0.75 mm and 2.43 respectively.

During the third set of runs, the mixture around pier 2 had the same mean diameter of 0.75 mm and σ_g of 3.4. Around pier 1 the mixture had the same d_{50} and σ_g as pier 2, but the size of fraction above d_{90} was increased, and around pier 3 a uniform sand of d_{50} of 0.75 mm and σ_g of 1.38, Figure 2.4, was used as a bed material. The purpose of this third set of runs was to study the effect of increasing the coarse fraction size above d_{90} in the original sediment mixture on the resulting scour depth. The resulting armoring patterns, and comparisons of scour in non-uniform materials with that resulting in uniform bed material were studied.

3.2 Flow Conditions

The flow conditions which were tested during this study are summarized in Table 3.1. The measured and computed data listed in Table 3.1 are the median sediment size, d_{50} , the geometric standard deviation for each of the six sediment mixtures used in this study, σ_g , the flow discharge, Q , the approach flow depth, Y_1 , the approach velocity to each pier, V_1 , the calculated energy line slope S_e , the calculated Froude Number, F_r , the measured scour depth, Y_s , and duration of each experiment, t (hours).

Table 3.1 Summary of Experimental Measured Data (T = 60 - 65°F)

Set No. 1 (Runs 1 through 12)										
Run No.3	Mixture No.	D ₅₀ mm	σ_g	Q cfs	Y ₁ ft	V ₁ ft/s	S _e	Fr	Y _s ft	t hr
1-1	1	0.75	2.43	7.29	1.26	0.7	0.0002	0.109	0.12	8
1-2	1	0.75	2.43	7.29	1.3	0.67	0.0002	0.104	0.12	8
1-3	1	0.75	2.43	7.29	1.31	0.66	0.0002	0.102	0.11	8
2-1	1	0.75	2.43	8.69	0.94	1.14	0.0004	0.207	0.25	8
2-2	1	0.75	2.43	8.69	0.96	1.12	0.0004	0.201	0.22	8
2-3	1	0.75	2.43	8.69	0.96	1.11	0.0004	0.2	0.22	8
3-1	1	0.75	2.43	10.6	0.94	1.38	0.0006	0.25	0.55	19
3-2	1	0.75	2.43	10.6	0.95	1.33	0.0006	0.24	0.47	19
3-3	1	0.75	2.43	10.6	0.96	1.33	0.0006	0.24	0.47	19
4-1	1	0.75	2.43	10.6	1.25	0.99	0.0004	0.156	0.16	12
4-2	1	0.75	2.43	10.6	1.23	0.99	0.0004	0.157	0.16	12
4-3	1	0.75	2.43	10.6	1.24	0.95	0.0004	0.151	0.15	12
5-1	1	0.75	2.43	9.31	1.16	0.97	0.00042	0.159	0.15	8
5-2	1	0.75	2.43	9.31	1.13	0.96	0.00042	0.158	0.15	8
5-3	1	0.75	2.43	9.31	1.12	0.97	0.00042	0.161	0.13	8
6-1	1	0.75	2.43	9.9	1.1	1.09	0.00045	0.183	0.29	12
6-2	1	0.75	2.43	9.9	1.1	1.09	0.00045	0.183	0.27	12
6-3	1	0.75	2.43	9.9	1.1	1.08	0.00045	0.182	0.26	12
7-1	1	0.75	2.43	11.41	1.06	1.3	0.0006	0.224	0.48	16
7-2	1	0.75	2.43	11.41	1.07	1.28	0.0006	0.218	0.44	16
7-3	1	0.75	2.43	11.41	1.07	1.27	0.0006	0.217	0.44	16
8-1	1	0.75	2.43	12.74	1.05	1.45	0.00065	0.251	0.61	12
8-2	1	0.75	2.43	12.74	1.07	1.35	0.00065	0.23	0.6	12
8-3	1	0.75	2.43	12.74	1.06	1.38	0.00065	0.236	0.6	12
9-1	1	0.75	2.43	9.43	1.05	1.1	0.00043	0.189	0.3	16
9-2	1	0.75	2.43	9.43	1.02	1.1	0.00043	0.192	0.26	16
9-3	1	0.75	2.43	9.43	1	1.12	0.00043	0.197	0.26	16

Table 3.1 Continued

10-1	1	0.75	2.43	13.79	1.09	1.54	0.0007	0.26	0.64	10
10-2	1	0.75	2.43	13.79	1.07	1.5	0.0007	0.255	0.61	10
10-3	1	0.75	2.43	13.79	1.04	1.51	0.0007	0.26	0.6	10
11-1	1	0.75	2.43	15.15	1.1	1.61	0.00073	0.27	0.68	14
11-2	1	0.75	2.43	15.15	1.08	1.57	0.00073	0.266	0.65	14
11-3	1	0.75	2.43	15.15	1.05	1.62	0.00073	0.279	0.68	14
12-1	1	0.75	2.43	16.73	1.19	1.65	0.00085	0.266	0.65	16
12-2	1	0.75	2.43	16.73	1.19	1.72	0.00085	0.277	0.64	16
12-3	1	0.75	2.43	16.73	1.26	1.58	0.00085	0.249	0.66	16

Set No. 2 (Runs 13 through 19)										
Run No.	Mixture No.	D ₅₀ mm	σ_g	Q cfs	Y ₁ ft	V ₁ ft/s	S _e	Fr	Y _s ft	t hr
13-1	1-A	0.75	2.43	11.1	1.06	1.28	0.00055	0.219	0.51	16
13-2	1-B	0.75	2.43	11.1	1.06	1.2	0.00055	0.193	0.16	16
13-3	1-C	0.75	2.43	11.1	1.06	1.22	0.00055	0.209	0.22	16
14-1	1-A	0.75	2.43	7.29	1.02	0.84	0.00029	0.146	0.16	16
14-2	1-B	0.75	2.43	7.29	1.03	0.82	0.00029	0.142	0.04	16
14-3	1-C	0.75	2.43	7.29	1.03	0.82	0.00029	0.142	0.09	16
15-1	1-A	0.75	2.43	5.16	1	0.62	0.00022	0.108	0.03	16
15-2	1-B	0.75	2.43	5.16	1.01	0.6	0.00022	0.105	0.01	16
15-3	1-C	0.75	2.43	5.16	1	0.61	0.00022	0.107	0.02	16
16-1	1-A	0.75	2.43	8.36	1.08	0.92	0.00045	0.156	0.27	16
16-2	1-B	0.75	2.43	8.36	1.1	0.87	0.00045	0.145	0.09	16
16-3	1-C	0.75	2.43	8.36	1.11	0.85	0.00045	0.141	0.15	16
17-1	1-A	0.75	2.43	9.16	1.08	0.99	0.0005	0.168	0.3	16
17-2	1-B	0.75	2.43	9.16	1.09	0.96	0.0005	0.161	0.1	16
17-3	1-C	0.75	2.43	9.16	1.09	0.95	0.0005	0.16	0.16	16
18-1	1-A	0.75	2.43	13.43	1.08	1.48	0.00062	0.25	0.7	16
18-2	1-B	0.75	2.43	13.43	1.08	1.4	0.00062	0.238	0.28	16
18-3	1-C	0.75	2.43	13.43	1.1	1.42	0.00062	0.238	0.42	16
19-1	1-A	0.75	2.43	16.85	1.1	1.8	0.00098	0.302	0.74	16
19-2	1-B	0.75	2.43	16.85	1.1	1.83	0.00098	0.307	0.59	16
19-3	1-C	0.75	2.43	16.85	1	2.12	0.00098	0.374	0.66	16

Table 3.1 Continued

Set No. 3 (Runs 20 through 27)										
Run No.	Mixture No.	D ₅₀ mm	σ_g	Q cfs	Y ₁ ft	V ₁ ft/s	S _e	Fr	Y _s ft	t hr
20-1	2-E	0.75	3.4	5.2	1	0.64	0.00047	0.112	0.01	16
20-2	2-D	0.75	3.4	5.2	1.01	0.62	0.00047	0.108	0.01	16
20-3	3	0.75	1.38	5.2	1.01	0.61	0.00047	0.107	0.03	16
21-1	2-E	0.75	3.4	6.5	1.12	0.68	0.0005	0.113	0.03	16
21-2	2-D	0.75	3.4	6.5	1.11	0.69	0.0005	0.115	0.04	16
21-3	3	0.75	1.38	6.5	1.11	0.7	0.0005	0.117	0.13	16
22-1	2-E	0.75	3.4	7.3	1.06	0.82	0.00054	0.141	0.04	16
22-2	2-D	0.75	3.4	7.3	1.08	0.79	0.00054	0.133	0.05	16
22-3	3	0.75	1.38	7.3	1.09	0.78	0.00054	0.131	0.21	16
23-1	2-E	0.75	3.4	9.16	1.1	1.00	0.00062	0.167	0.06	16
23-2	2-D	0.75	3.4	9.16	1.1	0.98	0.00062	0.164	0.07	16
23-3	3	0.75	1.38	9.16	1.11	0.96	0.00062	0.161	0.42	16
24-1	2-E	0.75	3.4	11.1	1.07	1.27	0.0007	0.216	0.1	16
24-2	2-D	0.75	3.4	11.1	1.08	1.24	0.0007	0.21	0.17	16
24-3	3	0.75	1.38	11.1	1.07	1.25	0.0007	0.213	0.7	16
25-1	2-E	0.75	3.4	13.4	1.09	1.48	0.0009	0.25	0.23	16
25-2	2-D	0.75	3.4	13.4	1.09	1.43	0.0009	0.241	0.28	16
25-3	3	0.75	1.38	13.4	1.1	1.41	0.0009	0.237	0.82	16
26-1	2-E	0.75	3.4	16.9	1.04	1.94	0.0015	0.335	0.62	16
26-2	2-D	0.75	3.4	16.9	1.04	1.91	0.0015	0.33	0.62	16
27-1	2-E	0.75	3.4	18.3	0.98	2.21	0.002	0.393	0.72	16
27-2	2-D	0.75	3.4	18.3	0.98	2.14	0.002	0.38	0.66	16

3.3 Critical Shear Stress for Sediment Mixtures

To investigate the effect of sediment gradation and increasing size of coarse material fraction on local scour depth in the clear-water scour, the bed in the approach of each pier should not be in motion. However, for each run, some finer particles were moved from the approach channel, so the bed upstream of the piers degraded slightly

(in the order of 0.01 ft) and gradually armored. After that, there was no further bed motion and clear-water scour took place around the piers. Generally, clear-water scour at bridge piers will occur so long as the approach shear stress does not exceed the critical shear stress for the sediment mixture composing the bed.

The criteria for calculating critical shear stress for the sediment mixture forming the approach bed of each pier was achieved using Gessler's method. Gessler (1971) defined the critical shear stress of a sediment mixture as the bed shear stress which will develop the coarsest armor coat, and can be calculated using the formula:

$$\tau_{c_m} = 0.047 (\gamma_s - \gamma_w) D_{avg_{a_{max}}} \quad (3.1)$$

where τ_{c_m} is the critical shear stress for sediment mixtures, and $D_{avg_{a_{max}}}$ is the maximum mean diameter of the armor layers for that mixture.

In the present study, the surface armor layer in the approach of each pier was sampled and the grain size distribution curves for different sediment mixtures were developed. From these curves the mean diameter of each of the armor layers were determined. For each of the sediment mixtures the mean diameter of the coarsest armor layer in the approach of each pier resulting from experiments was used in calculating the critical shear stress for that sediment mixture. Table 3.2 shows the values of the corresponding critical shear stresses for the bed materials used in this study.

Table 3.2 Critical Shear Stress for Sediment Mixtures

Mixture No.	d_{50}	σ_g	$D_{avg \text{ } amax}$		τ_{cm} (lb/ft ²)
			(mm)	(ft)	
1	0.75	2.43	2.50	0.0082	0.0397
2	0.75	3.40	5.60	0.0184	0.0890
3	0.75	1.38	---	---	0.0120

3.4 Ratio of Average Bed Shear Stress to Critical Shear

Observations and photographs of the bed confirmed, without any need for further calculations that no bed material motion upstream of each pier occurred.

Figures 3.1 through 3.4 are some examples for the initial bed and final bed elevations in the approach of the piers, clearly indicating that no bed movement occurred in front of the piers. The photographs presented in Figures 3.5 through 3.8 confirm these observations.

Values of the average bed shear stress in the approach of the three piers are presented in Table 3.3. The average bed shear stress can be calculated as:

$$\tau_b = \gamma_w R S_e \quad (3.2)$$

where τ_b = bed shear stress;

γ_w = the specific weight of water;

R = the hydraulic radius, ($R=A/P$);

A = cross sectional area;

P = wetted perimeter; and

S_e = slope of the energy gradient.

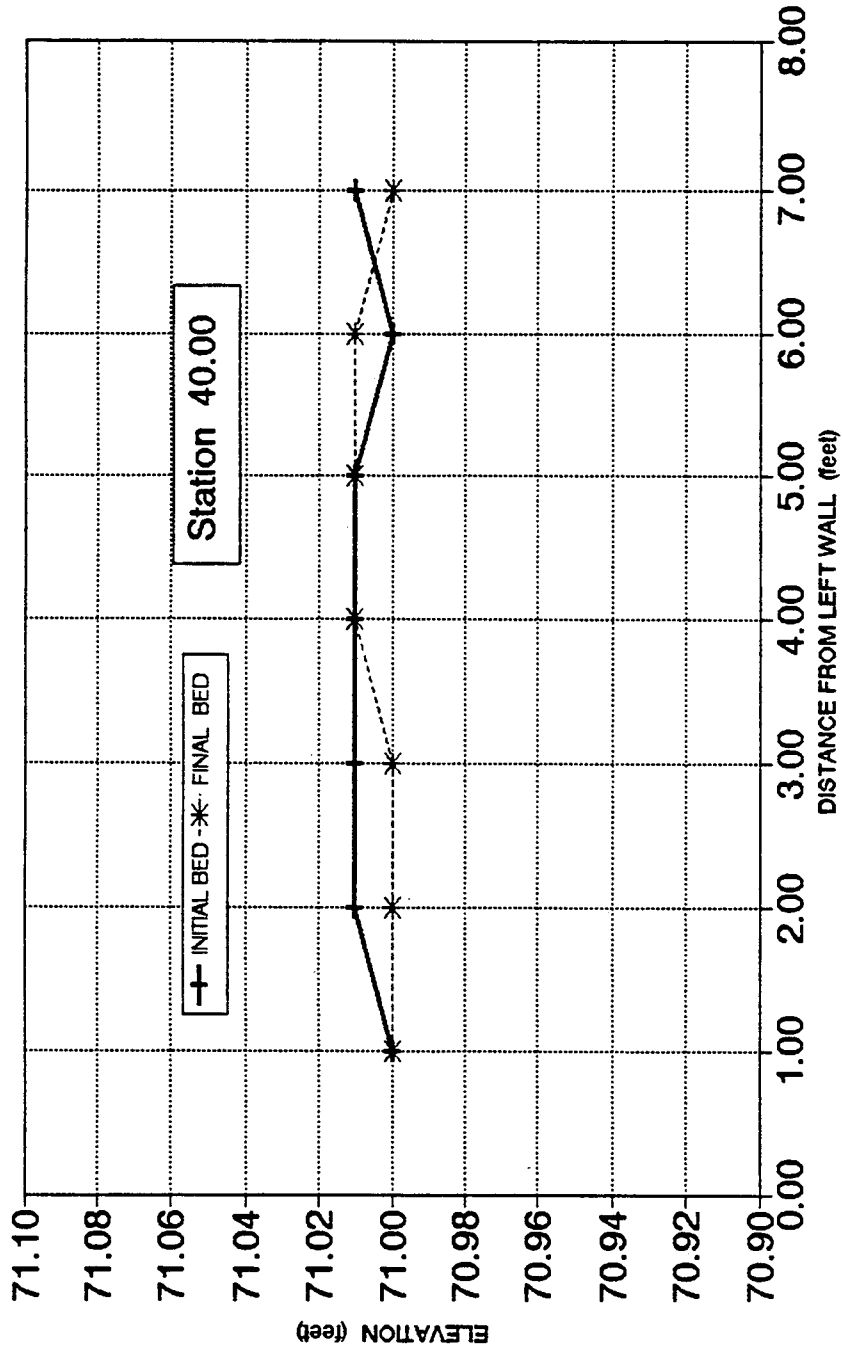


Figure 3.1 Initial and Final Bed Elevations in the Approach of Pier 1 for Run 6

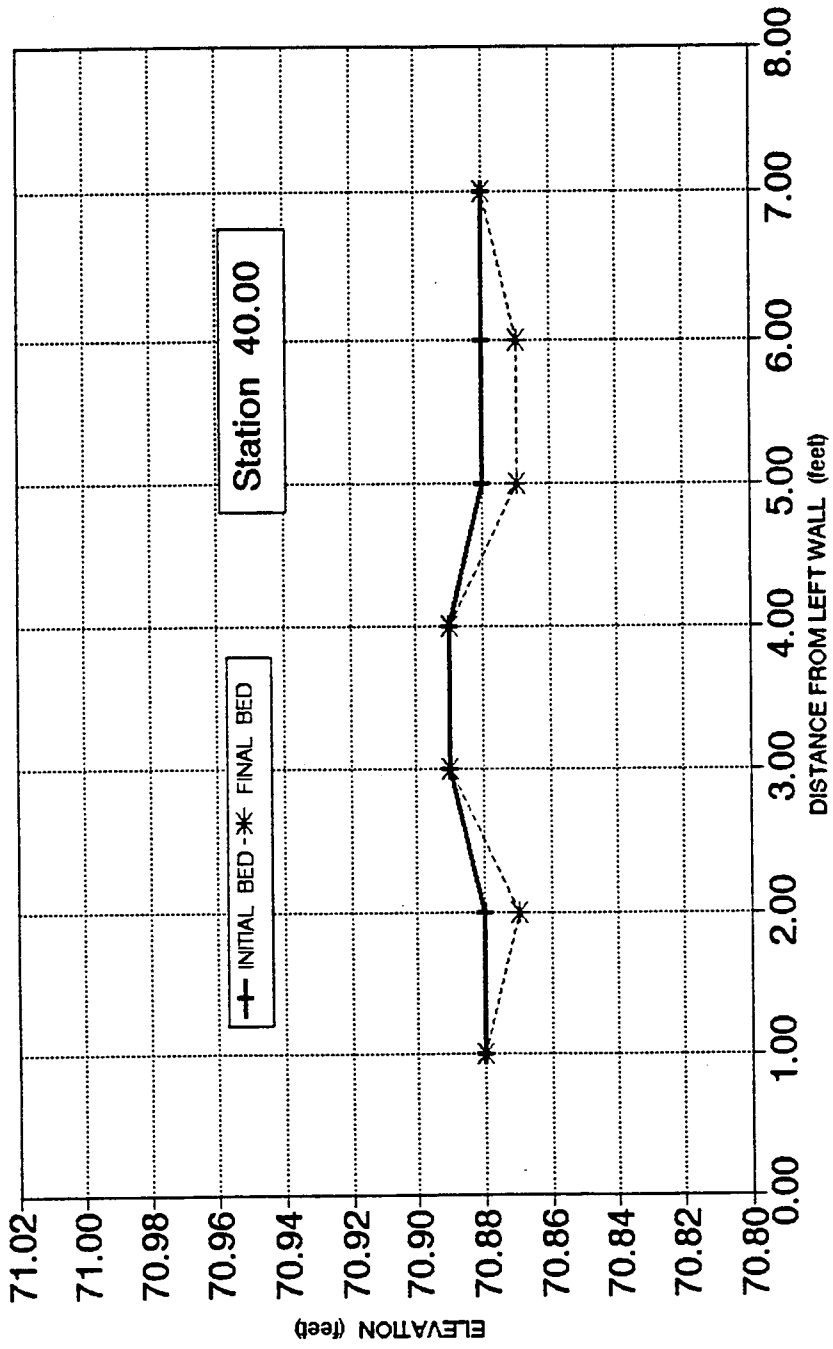


Figure 3.2 Initial and Final Bed Elevations in the Approach of Pier 1 for Run 13

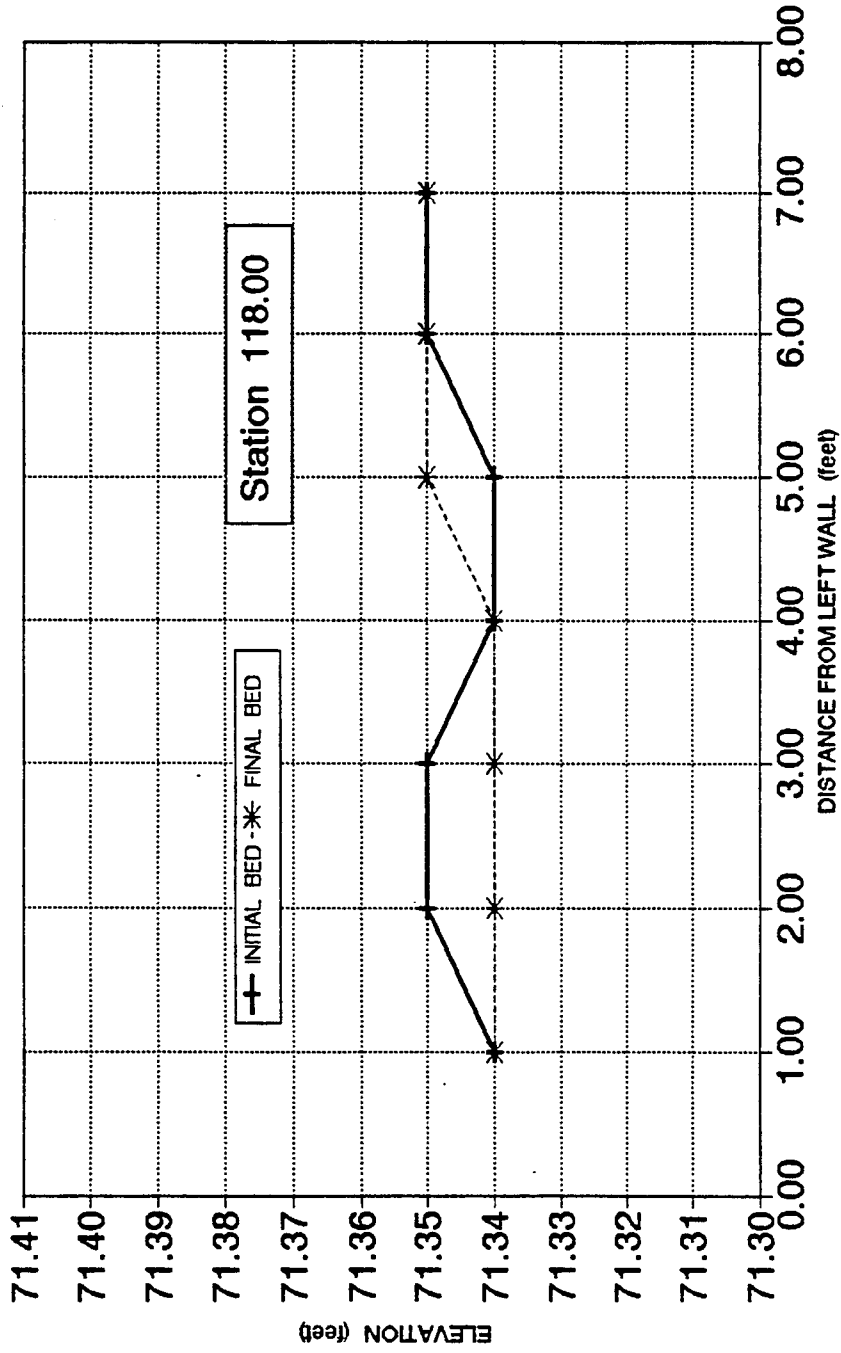


Figure 3.3 Initial and Final Bed Elevations in the Approach of Pier 3 for Run 21

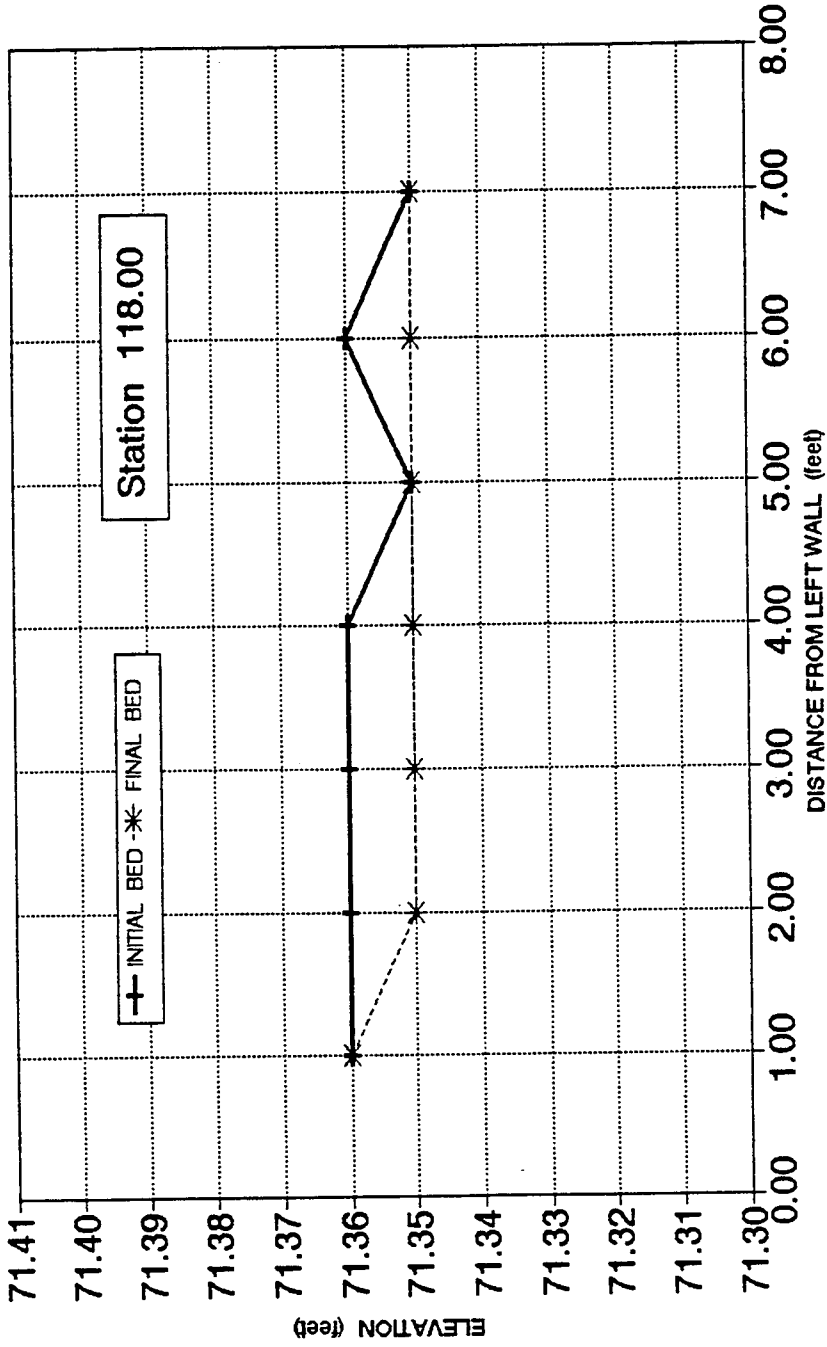


Figure 3.4 Initial and Final Bed Elevations In the Approach of Pier 3 for Run 22

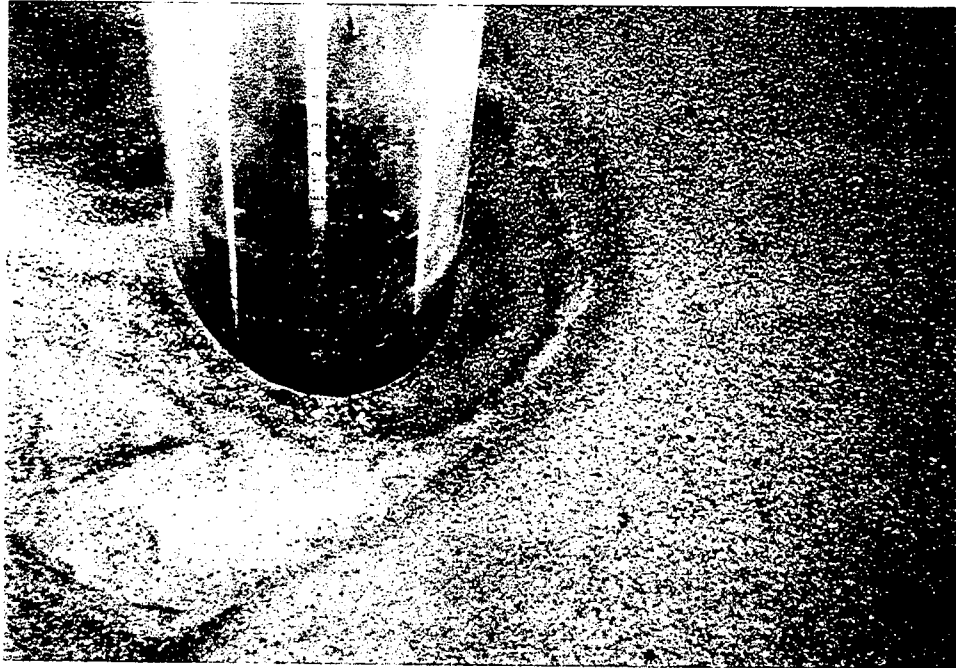


Figure 3.5 Scour Hole and Approach Bed Profiles of Pier 3 Run 22

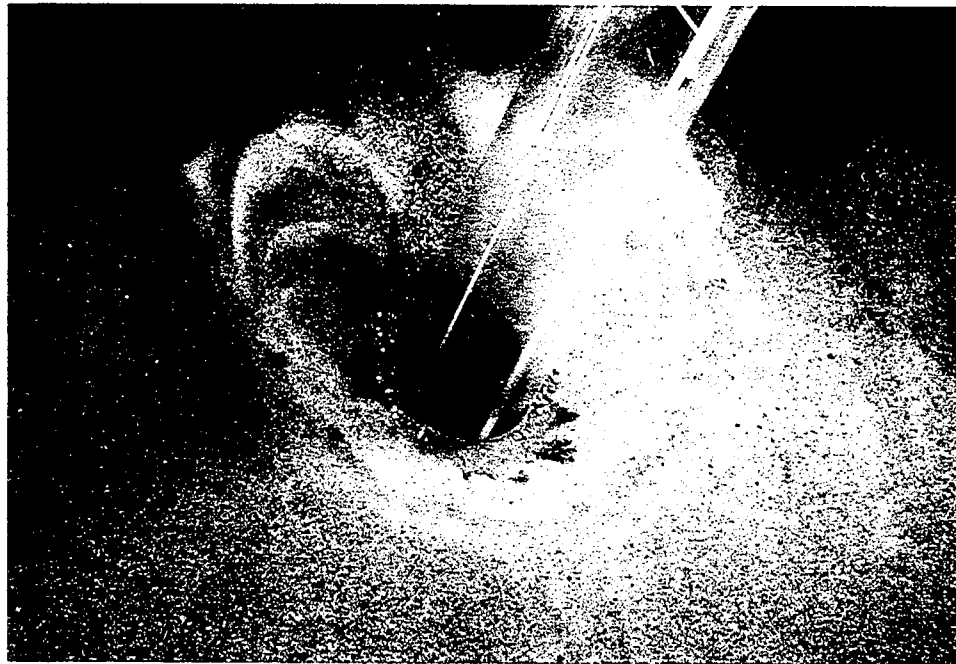


Figure 3.6 Scour Hole and Approach Bed Profiles of Pier 3 Run 23



Figure 3.7 Scour Hole and Approach Bed Profiles of Pier 3 Run 24



Figure 3.8 Scour Hole and Approach Bed Profiles of Pier 3 Run 25

Table 3.3 Calculations of Average Bed Shear Stress

Set No. 1 (Runs 1 through 12)										
Run #	Q ft ³ /s	Y ft	A ft ²	P ft	R ft	Slope	τ_o lb/ft ²	U* ft/sec	U*c ft/sec	U*/U*c
1-1	7.29	1.26	10.08	10.52	0.958	0.0002	0.011958	0.078553	0.143052	0.549
1-2	7.29	1.3	10.4	10.6	0.981	0.0002	0.012245	0.079489	0.143052	0.556
1-3	7.29	1.31	10.48	10.62	0.987	0.0002	0.012315	0.079719	0.143052	0.557
2-1	8.69	0.94	7.52	9.88	0.761	0.0004	0.018998	0.099012	0.143052	0.694
2-2	8.69	0.96	7.68	9.92	0.774	0.0004	0.019324	0.099858	0.143052	0.698
2-3	8.69	0.96	7.68	9.92	0.774	0.0004	0.019324	0.099858	0.143052	0.698
3-1	10.58	0.94	7.52	9.88	0.761	0.0006	0.028497	0.121265	0.143052	0.848
3-2	10.58	0.95	7.6	9.9	0.768	0.0006	0.028742	0.121785	0.143052	0.851
3-3	10.58	0.96	7.68	9.92	0.774	0.0006	0.028986	0.122301	0.143052	0.855
4-1	10.58	1.25	10	10.5	0.952	0.0004	0.023771	0.110755	0.143052	0.774
4-2	10.58	1.23	9.84	10.46	0.941	0.0004	0.023481	0.110075	0.143052	0.769
4-3	10.58	1.24	9.92	10.48	0.947	0.0004	0.023626	0.110416	0.143052	0.772
5-1	9.31	1.16	9.28	10.32	0.899	0.00042	0.023567	0.110277	0.143052	0.771
5-2	9.31	1.13	9.04	10.26	0.881	0.00042	0.023092	0.10916	0.143052	0.764
5-3	9.31	1.12	8.96	10.24	0.875	0.00042	0.022932	0.108782	0.143052	0.760
6-1	9.9	1.1	8.8	10.2	0.863	0.00045	0.024226	0.111809	0.143052	0.782
6-2	9.9	1.1	8.8	10.2	0.863	0.00045	0.024226	0.111809	0.143052	0.782
6-3	9.9	1.1	8.8	10.2	0.863	0.00045	0.024226	0.111809	0.143052	0.782
7-1	11.41	1.06	8.48	10.12	0.838	0.0006	0.031373	0.127236	0.143052	0.889
7-2	11.41	1.07	8.56	10.14	0.844	0.0006	0.031606	0.127709	0.143052	0.893
7-3	11.41	1.07	8.56	10.14	0.844	0.0006	0.031606	0.127709	0.143052	0.893
8-1	12.74	1.05	8.4	10.1	0.832	0.00065	0.033733	0.131936	0.143052	0.922
8-2	12.74	1.07	8.56	10.14	0.844	0.00065	0.03424	0.132924	0.143052	0.929
8-3	12.74	1.06	8.48	10.12	0.838	0.00065	0.033987	0.132432	0.143052	0.926
9-1	9.43	1.05	8.4	10.1	0.832	0.00043	0.022316	0.10731	0.143052	0.750
9-2	9.43	1.02	8.16	10.04	0.813	0.00043	0.021808	0.106082	0.143052	0.742
9-3	9.43	1	8	10	0.800	0.00043	0.021466	0.105246	0.143052	0.736
10-1	13.79	1.09	8.72	10.18	0.857	0.0007	0.037415	0.138951	0.143052	0.971
10-2	13.79	1.07	8.56	10.14	0.844	0.0007	0.036874	0.137941	0.143052	0.964
10-3	13.79	1.04	8.32	10.08	0.825	0.0007	0.036053	0.136398	0.143052	0.953
11-1	15.15	1.1	8.8	10.2	0.863	0.00073	0.0393	0.142407	0.143052	0.995
11-2	15.15	1.08	8.64	10.16	0.850	0.00073	0.038737	0.141384	0.143052	0.988
11-3	15.15	1.05	8.4	10.1	0.832	0.00073	0.037885	0.13982	0.143052	0.977
12-1	16.73	1.19	9.52	10.38	0.917	0.00085	0.048646	0.158437	0.143052	1.107
12-2	16.73	1.19	9.52	10.38	0.917	0.00085	0.048646	0.158437	0.143052	1.107
12-3	16.73	1.26	10.08	10.52	0.958	0.00085	0.050822	0.161942	0.143052	1.132

Table 3.3 Continued

Set No. 2 (Runs 13 through 19)										
Run #	Q ft ³ /s	Y ft	A ft ²	P ft	R ft	Slope	τ_0 lb/ft ²	U* ft/sec	U*c ft/sec	U*/U*c
13-1	11.1	1.06	8.48	10.12	0.838	0.00055	0.028758	0.12182	0.143052	0.852
13-2	11.1	1.06	8.48	10.12	0.838	0.00055	0.028758	0.12182	0.143052	0.852
13-3	11.1	1.06	8.48	10.12	0.838	0.00055	0.028758	0.12182	0.143052	0.852
14-1	7.29	1.02	8.16	10.04	0.813	0.00029	0.014708	0.087117	0.143052	0.609
14-2	7.29	1.03	8.24	10.06	0.819	0.00029	0.014822	0.087456	0.143052	0.611
14-3	7.29	1.03	8.24	10.06	0.819	0.00029	0.014822	0.087456	0.143052	0.611
15-1	5.16	1	8	10	0.800	0.00022	0.010982	0.075281	0.143052	0.526
15-2	5.16	1.01	8.08	10.02	0.806	0.00022	0.01107	0.075581	0.143052	0.528
15-3	5.16	1	8	10	0.800	0.00022	0.010982	0.075281	0.143052	0.526
16-1	8.36	1.08	8.64	10.16	0.850	0.00045	0.023879	0.111005	0.143052	0.776
16-2	8.36	1.1	8.8	10.2	0.863	0.00045	0.024226	0.111809	0.143052	0.782
16-3	8.36	1.11	8.88	10.22	0.869	0.00045	0.024398	0.112206	0.143052	0.784
17-1	9.16	1.08	8.64	10.16	0.850	0.0005	0.026532	0.11701	0.143052	0.818
17-2	9.16	1.09	8.72	10.18	0.857	0.0005	0.026725	0.117435	0.143052	0.821
17-3	9.16	1.09	8.72	10.18	0.857	0.0005	0.026725	0.117435	0.143052	0.821
18-1	13.43	1.08	8.64	10.16	0.850	0.00062	0.0329	0.130297	0.143052	0.912
18-2	13.43	1.08	8.64	10.16	0.850	0.00062	0.0329	0.130297	0.143052	0.911
18-3	13.43	1.1	8.8	10.2	0.863	0.00062	0.033378	0.13124	0.143052	0.917
19-1	16.85	1.1	8.8	10.2	0.863	0.00098	0.052759	0.164999	0.143052	1.153
19-2	16.85	1.1	8.8	10.2	0.863	0.00098	0.052759	0.164999	0.143052	1.153
19-3	16.85	1	8	10	0.800	0.00098	0.048922	0.158886	0.143052	1.111
Set No. 3 (Runs 20 through 27)										
Run #	Q ft ³ /s	Y ft	A ft ²	P ft	R ft	Slope	τ_0 lb/ft ²	U* ft/sec	U*c ft/sec	U*/U*c
20-1	5.2	1	8	10	0.800	0.00047	0.023462	0.110033	0.214188	0.514
20-2	5.2	1.01	8.08	10.02	0.806	0.00047	0.02365	0.110471	0.214188	0.516
20-3	5.2	1.01	8.08	10.02	0.806	0.00047	0.02365	0.110471	0.078648	1.416
21-1	6.5	1.12	8.96	10.24	0.875	0.0005	0.0273	0.118691	0.214188	0.554
21-2	6.5	1.11	8.88	10.22	0.869	0.0005	0.027109	0.118275	0.214188	0.552
21-3	6.5	1.11	8.88	10.22	0.869	0.0005	0.027109	0.118275	0.078648	1.516
22-1	7.3	1.06	8.48	10.12	0.838	0.00054	0.028235	0.120707	0.214188	0.564
22-2	7.3	1.08	8.64	10.16	0.850	0.00054	0.028655	0.1216	0.214188	0.568
22-3	7.3	1.09	8.72	10.18	0.857	0.00054	0.028863	0.122042	0.078648	1.565
23-1	9.16	1.1	8.8	10.2	0.863	0.00062	0.033378	0.13124	0.214188	0.613
23-2	9.16	1.1	8.8	10.2	0.863	0.00062	0.033378	0.13124	0.214188	0.613
23-3	9.16	1.11	8.88	10.22	0.869	0.00062	0.033615	0.131706	0.078648	1.688
24-1	11.1	1.07	8.56	10.14	0.844	0.0007	0.036874	0.137941	0.214188	0.644
24-2	11.1	1.08	8.64	10.16	0.850	0.0007	0.037145	0.138448	0.214188	0.646
24-3	11.1	1.07	8.56	10.14	0.844	0.0007	0.036874	0.137941	0.078648	1.768
25-1	13.4	1.09	8.72	10.18	0.857	0.0009	0.048106	0.157555	0.214188	0.736

Table 3.3 Continued

25-2	13.4	1.09	8.72	10.18	0.857	0.0009	0.048106	0.157555	0.214188	0.736
25-3	13.4	1.1	8.8	10.2	0.863	0.0009	0.048452	0.158121	0.078648	2.027
26-1	16.9	1.04	8.32	10.08	0.825	0.0015	0.077257	0.199666	0.214188	0.932
26-2	16.9	1.04	8.32	10.08	0.825	0.0015	0.077257	0.199666	0.214188	0.932
27-1	18.3	0.98	7.84	9.96	0.787	0.002	0.098236	0.22515	0.214188	1.051
27-2	18.3	0.98	7.84	9.96	0.787	0.002	0.098236	0.22515	0.214188	1.051

For the present study, the width/depth aspect ratio utilized during this study was on the order of 7 to 8 in almost all the experiments. For this ratio, calculations to correct the shear stresses to include the side wall effects did not give or result in any significant correction for the wall effect. During this study subcritical flow conditions prevailed, so the flow was subjected to downstream control. By adjusting the downstream tail gate during each experiment, it was possible to obtain almost uniform flow conditions within the study reach. In spite of this fact, the measured bed slope values were slightly different from those of measured water surface slopes. For this reason, the slope of the energy line was used for the calculations of the average bed shear stress.

In the calculations of the bed shear stress, U_* / U_{*c} was used as a criteria for controlling the movement of the approach bed to each pier, where U_* is the shear velocity and is equal to $(\tau_o / \rho)^{0.5}$. In the experiments, the value of the parameter U_* / U_{*c} exceeded the critical value of 1.0 only during runs No. 12, 19, and 27. However, according to Table 3.3 for runs 20-3, 21-3, 22-3, 23-4, 24-3, and 25-3 the U_* / U_{*c} values exceed the value of 1.0 which falsely gives the impression that the approach bed has been moving during these runs. However, both the observations and measurements of the bed proved that clear-water scour occurred along these runs. It has been found

for this reason that the calculation of shear stresses for graded bed materials is compatible with the energy slope measurements and therefore shear velocity values were compatible with the data and observations. Measured shear velocities were not compatible with observations and measured data for the uniform material used during the third set of runs. This is probably due to the fact that the Shields diagram, which is used for the calculation of critical shear stress and the critical shear velocity, U_{*c} by using d_{50} for representing the bed material for the initiation of the motion may not be applicable to the tested material conditions.

3.5 Armoring Process

Armoring is a phenomena that happens in graded bed materials. During the armoring process, the fine materials of the mixture are washed out, the rate of sediment transport is decreased because less and less movable material is available for transport, and the top-most layer of bed material becomes coarser. When the flow conditions remain constant for enough time, the sediment transport rate approaches zero and an armor coat forms which protects material below from erosion or scour.

During the first set of runs (run 1 through 12), the armor layer samples around the perimeter of the bridge piers were taken as single sample. Other samples in the approach and ridge of each pier were also taken in addition to samples from the deposition region directly behind the pier to show the variation of the material sizes of the surface layers around bridge piers. For Sets No. 2 (runs 13 through 19) and No. 3 (runs 20 through 27), the armor layer around the perimeter of the pier was divided

further into 3 subsections: in front of the pier (nose), at the side of the pier, and in the downstream area directly behind the pier. Other sediment sample sites were the same as in first set of runs: the approach, ridge, and the tail of depositional area downstream from the piers. In summary, the only difference in sampling the armor layer around the perimeter of the piers was during the first set of runs where the region next to the pier was sampled as a single unit while during Sets No. 2 and 3, it was taken as 3 separate units (front, side and downstream area).

In order to clarify the definition of legends used in various sediment size distribution curves in chapters 3 and 4, an explanation of the short-hand definitions of legends is included next.

Orig. Mix. (or Init. Mix.): the original (initial) mixture corresponding to the set of runs in which the specific experiment was performed.

Arm. Lay.: the (surface) armor layer from around the perimeter of the pier for the Set No. 1 runs which were taken as a single sample.

Scour Hole: a single sample taken from the surface layer around the perimeter of pier.

Upper Slope: surface sample taken from the upper part of the front slope of the scour hole.

Lower Slope: surface sample taken from the lower part of the front slope of the scour hole.

Ridge: surface sample taken from the downstream area of the pier where the flow lines converge again. Usually, this area is where the coarse particles behind each pier are encountered.

P1,P2,P3: Pier No. 1 placed at 45 ft from the head of the flume, Pier No. 2 placed at 80 ft from the head, and Pier No. 3 at 120 ft from the head of the flume, respectively.

R3-P1: Run No. 3 for pier 1;

R2-P2: Run No. 2 for pier 2;

U/S. SURF.: Surface sample from the front part of armor layer.

SIDE SURF.: Surface sample from the side part of the armor layer.

D/S. SURF.: Surface sample from the downstream part of the armor layer just behind the pier.

APPROACH: Surface sample from the armor layer formed at the approach of each pier.

Q : the specified discharge for certain run in cubic feet per second.

Fr: Froude Number for certain specified run.

3.5.1 Armoring Patterns around Bridge Piers for Set No.1

Presented here are some examples of the armor layer gradation patterns around bridge piers during Set No. 1. Figures 3.9 through 3.11 represent three different discharges of 8.69, 10.58, and 9.31 cfs and show the repeatability of the armor layer measurements around piers 1, 2, and 3. In these figures, piers subjected to identical flow conditions develop nearly identical sediment size gradation curves.

Other armoring examples are also presented in Chapter 4. The main factor in the present experiments controlling the scour and the armoring pattern is the shear stress

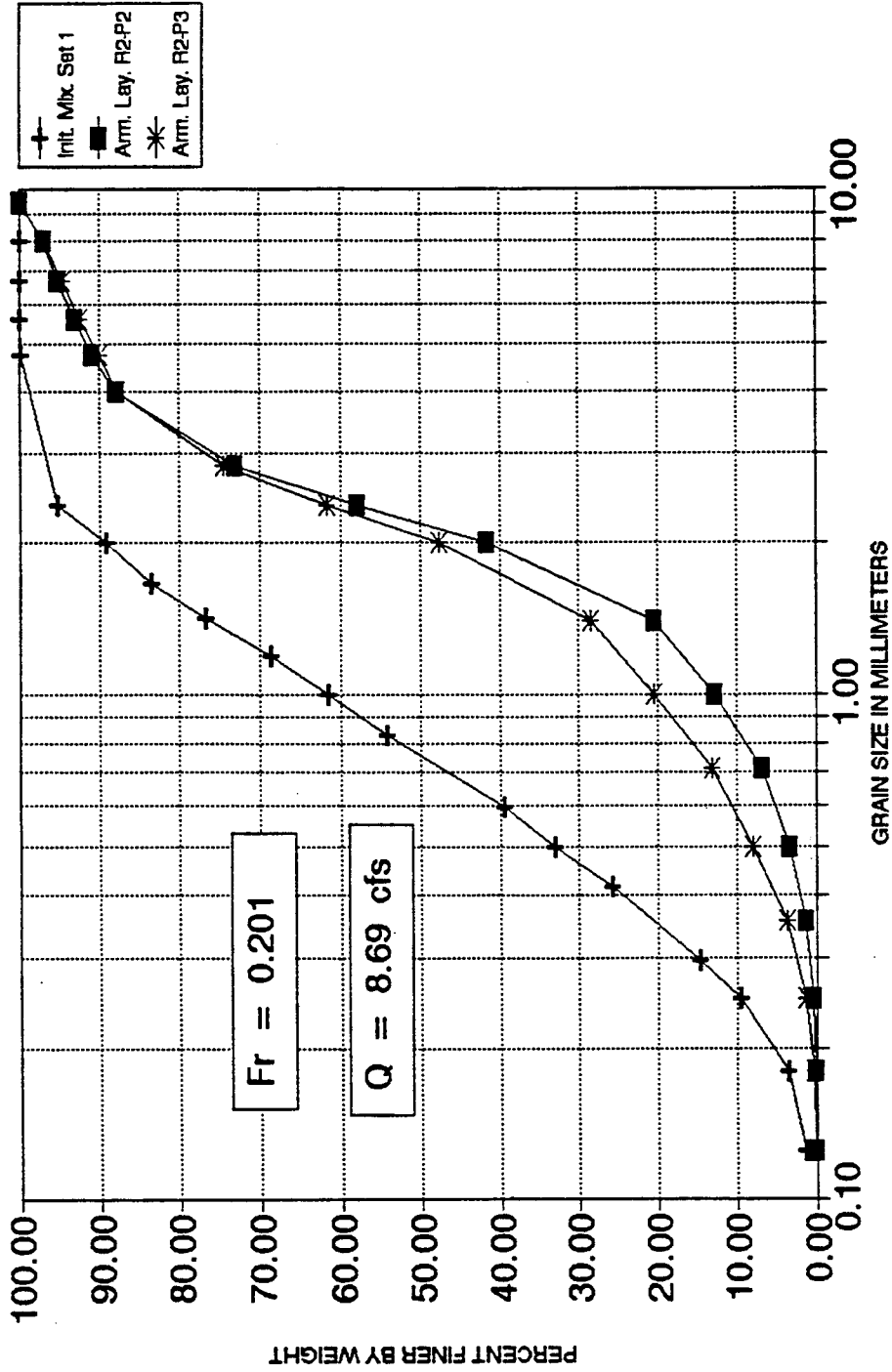


Figure 3.9 Sediment Size Distribution Curves Around Scour Holes Formed at Piers 2 and 3 During Run 2

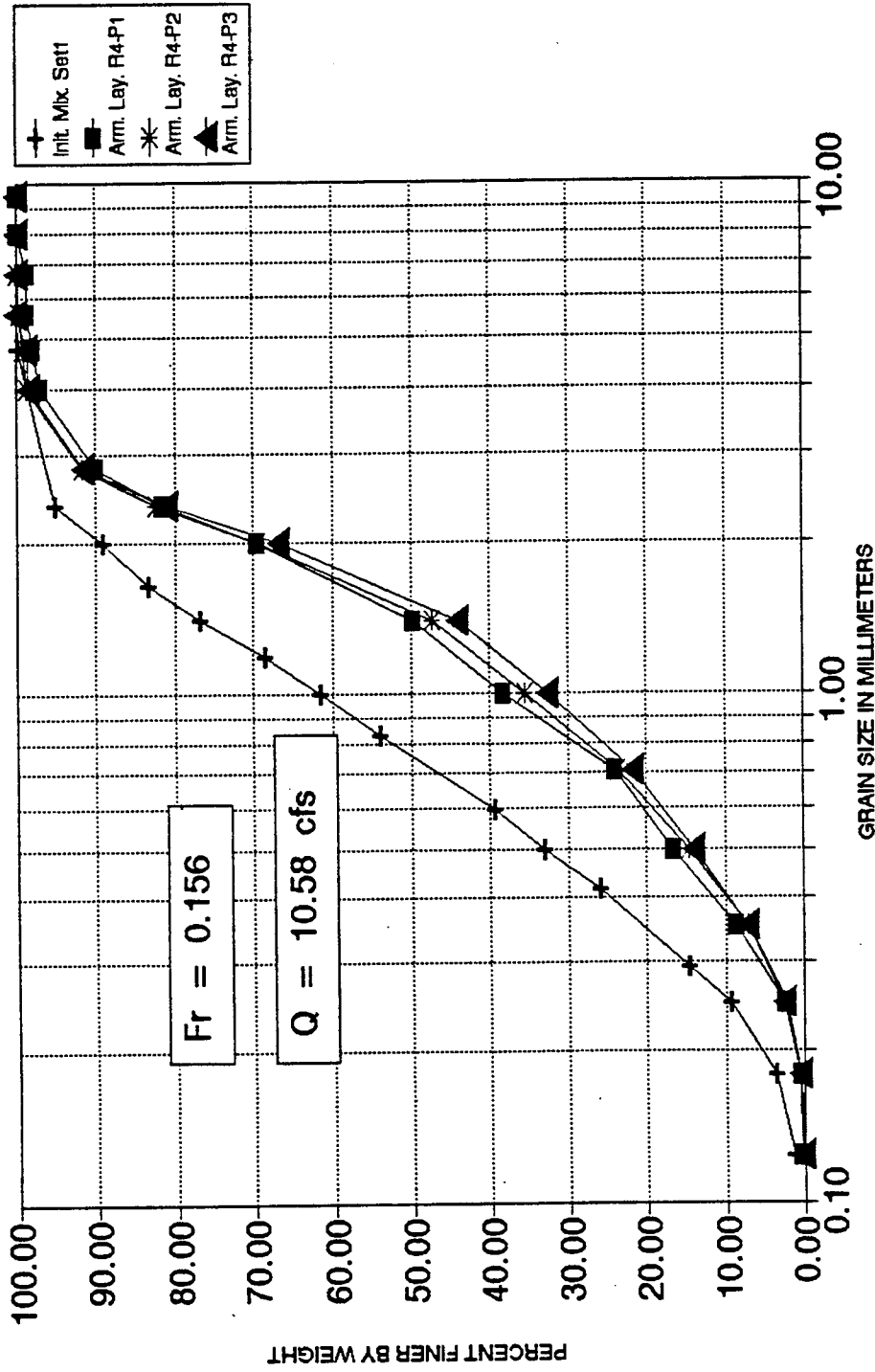


Figure 3.10 Sediment Size Distribution Curves Around Scour Holes Formed at Piers 1, 2 and 3 During Run 4

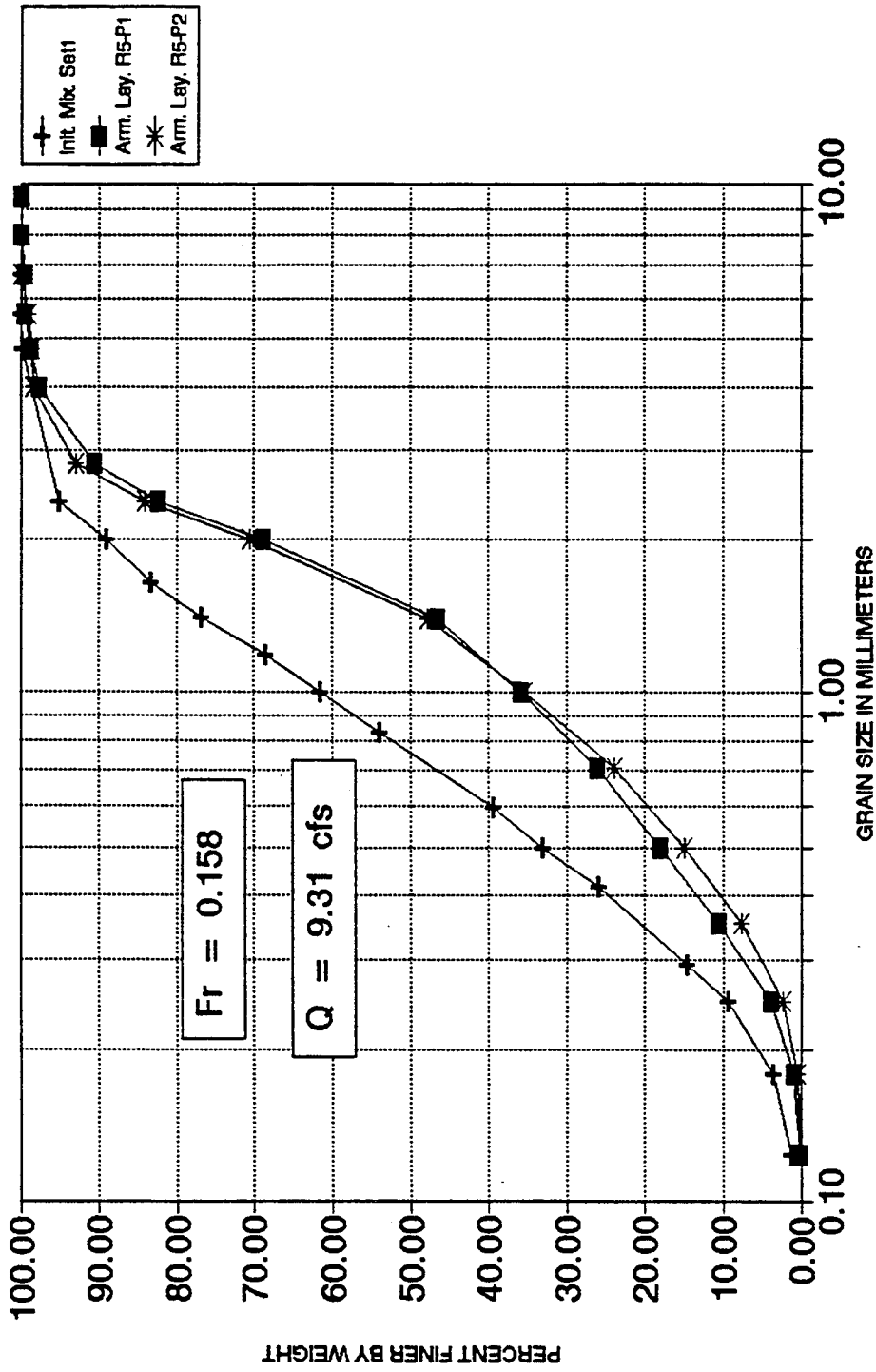


Figure 3.11 Sediment Size Distribution Curves Around Scour Holes Formed at Piers 1 and 2 During Run 5

which is a function of the stream velocity. The higher the flow velocity, the coarser the armor layer at the pier site. The Froude number, which is a function of the stream velocity, plays an important role in controlling the scour process.

Figure 3.12 shows armoring patterns for the discharges of 8.69, 10.58, 10.58, 9.31, and 9.90 cfs. These patterns show that the coarseness of the armor layers is proportional to the Froude Number of the flow which is a good indicator that the flow velocity is an important parameter in the scour process. In this figure, during runs 3 and 4 the flow discharge was the same at 10.58 cfs, but the velocity during run 3 was higher than that for run 4 due to lower flow depth. As a consequence, larger scour depths resulted for runs 4 and 5. The flow discharge during run 5 was 9.31 cfs which was less than that for run 4 (10.58 cfs), but the velocities and the corresponding Froude Numbers were almost the same resulting in the same armoring patterns.

The armoring pattern examples for set No. 1 proved the repeatability of armoring patterns and scour depths for almost the same flow conditions. Based on the observations and measurements, it can be concluded that the flow velocity and Froude Number are more important than the flow discharge itself in controlling the scour process and the resulting scour depth value.

3.5.2 Armoring Patterns Around Bridge Piers for Sets No. 2 and 3

The goal of experiments conducted for set No. 2 (runs 13 through 19) and set No.3 (runs 20 through 27) was to check the effect of increasing the size of coarse material fraction above the d_{90} and d_{95} size. For the experiments for set No. 2 the d_{90}

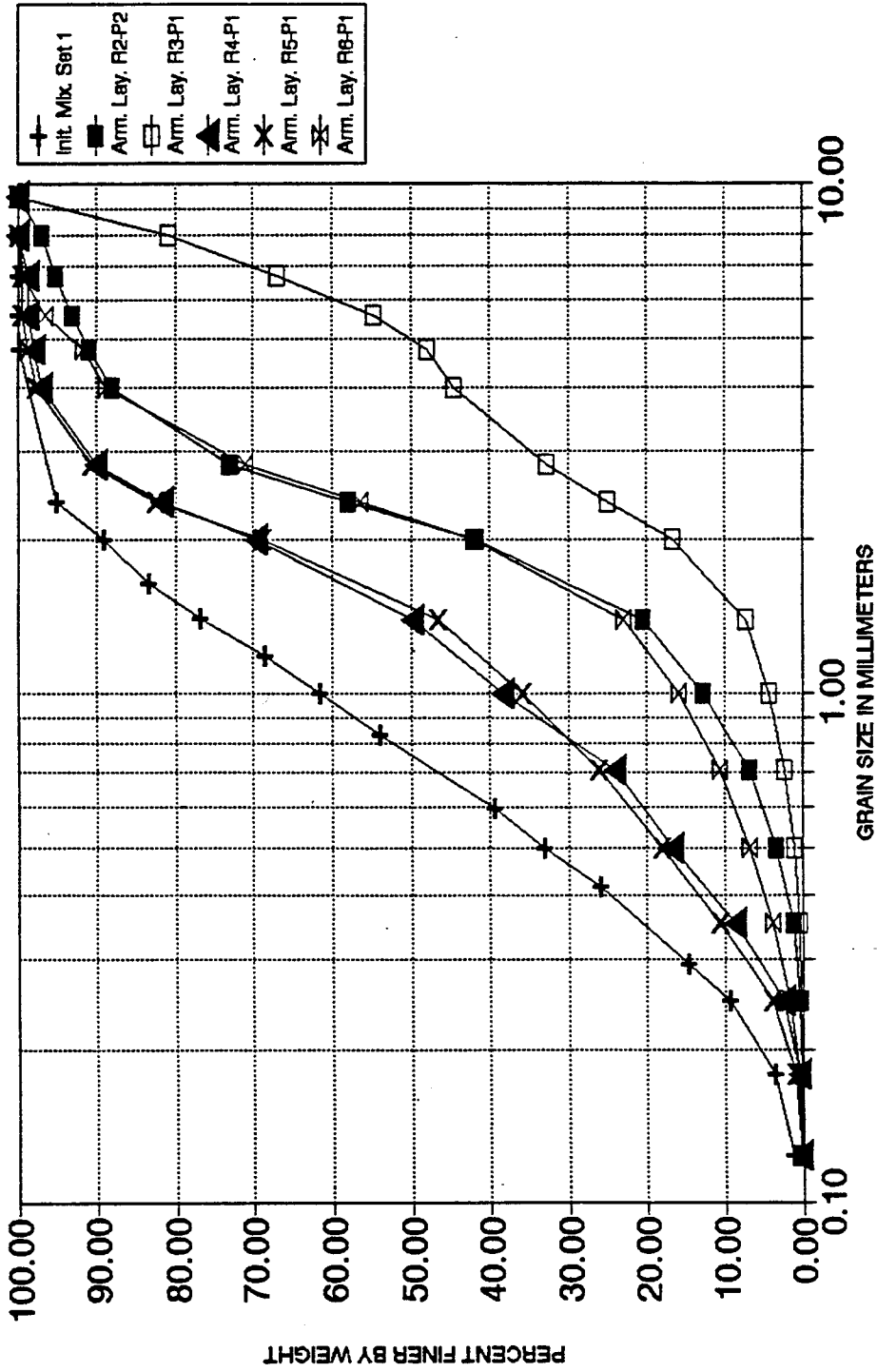


Figure 3.12 Sediment Size Distribution Curves Around Scour Holes for Runs 2 through 6

and d_{95} sizes were increased; for set No. 3 only d_{90} size was increased. The resulting scour depth and hence the armor pattern when keeping σ_g at the same value of 2.43 for set No. 2 and 3.4 for set No. 3 were significantly lower than uniform material.

Figures 3.13 and 3.14 present some of the resulting size distribution curves for set No. 2 and Figures 3.15 and 3.16 present the same information for set No. 3. Other examples are presented in Chapter 4 for further discussions of the effect of increasing the coarse material fraction on the scour process. The outcome of increasing the size of coarse material fraction above the limit that defines σ_g is to increase the strength of the bed material to resist higher shear stresses and to withstand the higher erosive forces around the piers and hence to reduce the scour depth. For discharges of 7.29 cfs and 8.36 cfs during set No. 2, Figures 3.13 and 3.14 present the variation of armor patterns for the same σ_g but with increased d_{90} and d_{95} sizes around piers 2 and 3, respectively. Around the pier 1 there was no significant change in bed material composition. It is clear that the coarseness of the armor layer results in a dramatic reduction in scour depths. Also, during the third set of runs shown in Figures 3.15 and 3.16 for Q of 9.16 and 11.1 cfs the behavior of the armor pattern, when increasing the size of the fraction above d_{90} while keeping σ_g of 3.4, is the same as the second set of runs. However, in this case the variation in armor patterns is not as large as the case of σ_g of 2.43 since the mixture with a σ_g value of 3.4 is originally much coarser. The percentage reduction in scour depths for this case is therefore smaller than the previous case.

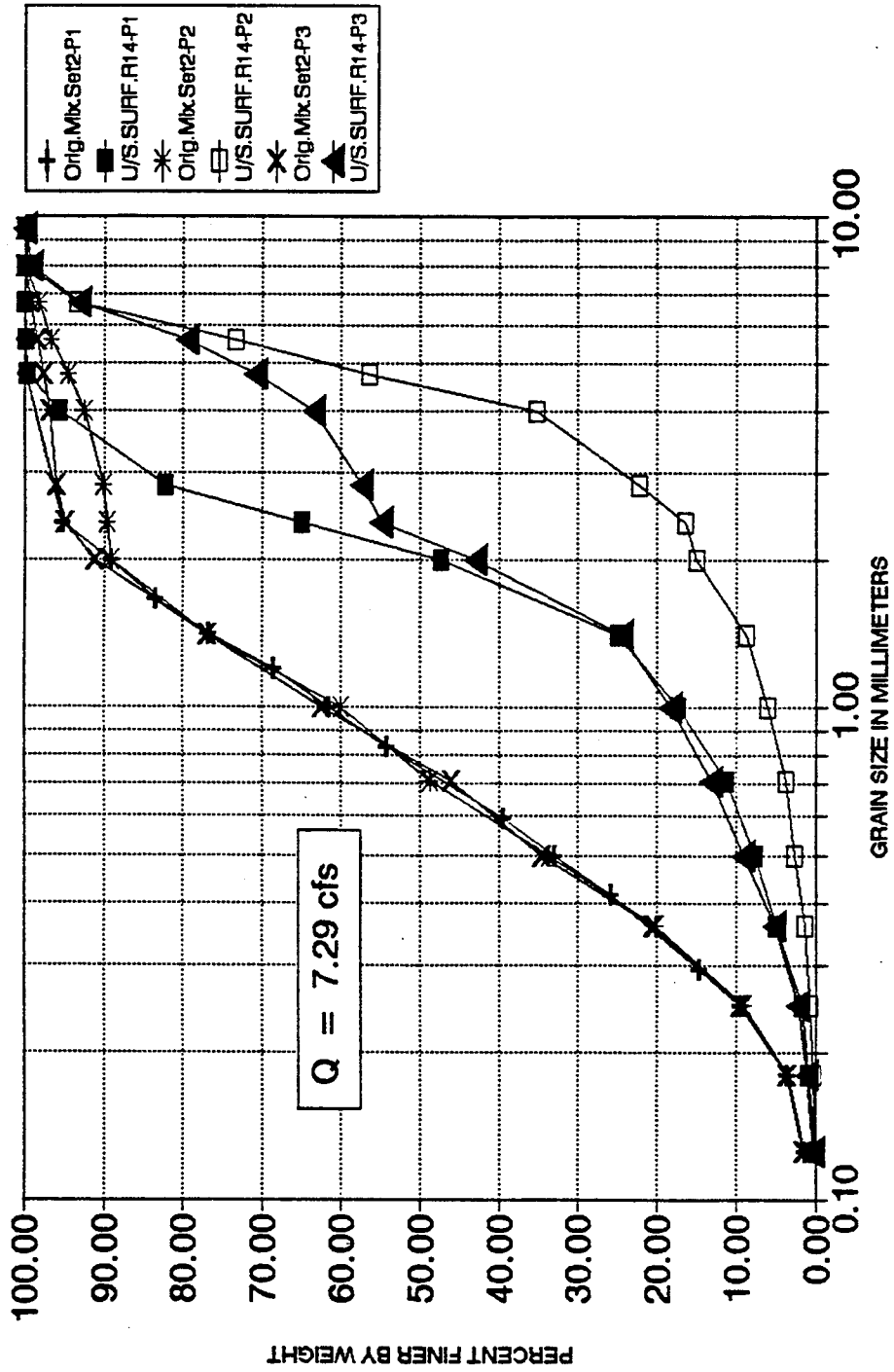


Figure 3.13 Effect of Coarse Material Fraction at Piers 1, 2 and 3 for Run 14

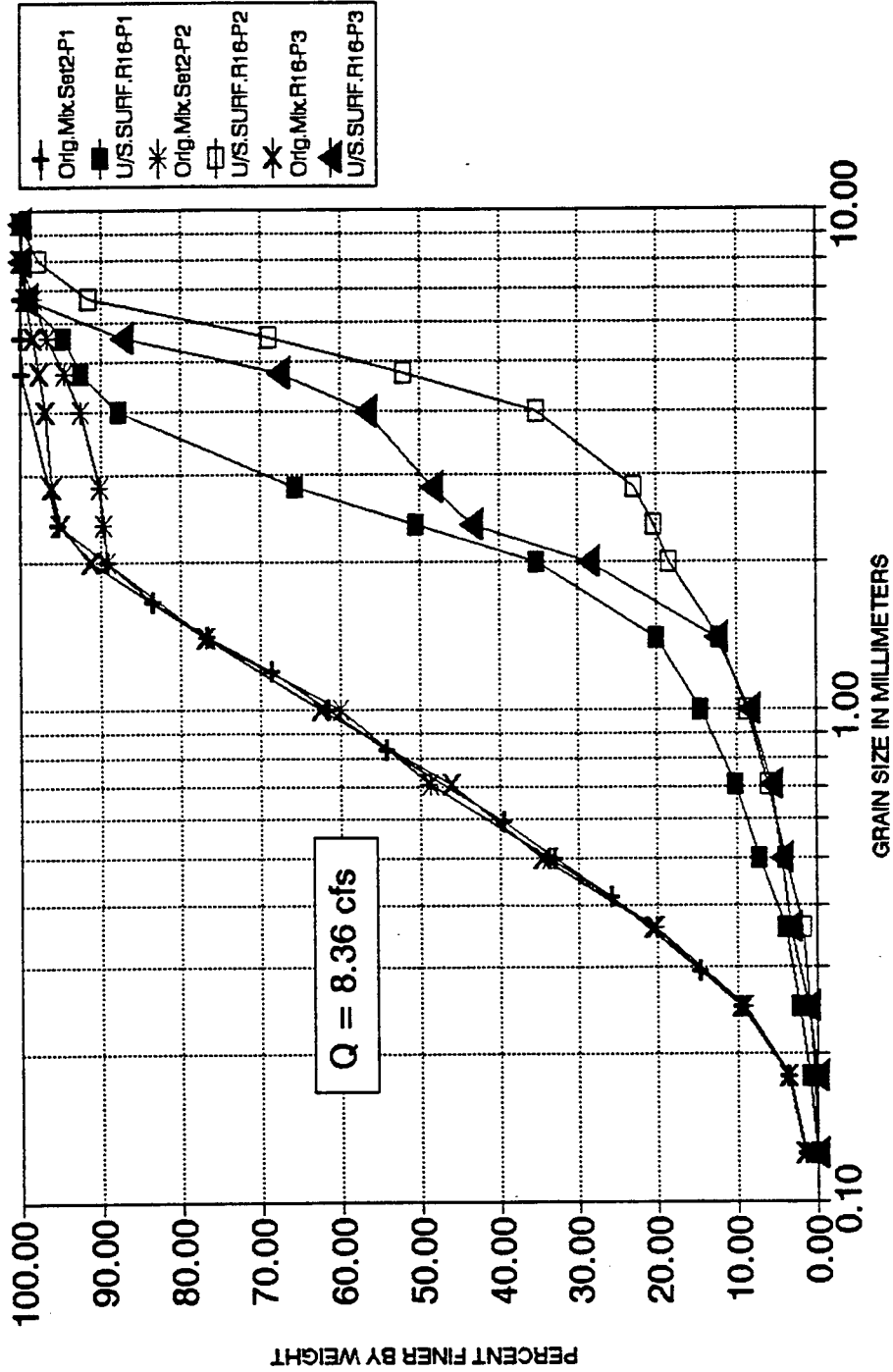


Figure 3.14 Effect of Coarse Material Fraction at Piers 1, 2 and 3 for Run 16

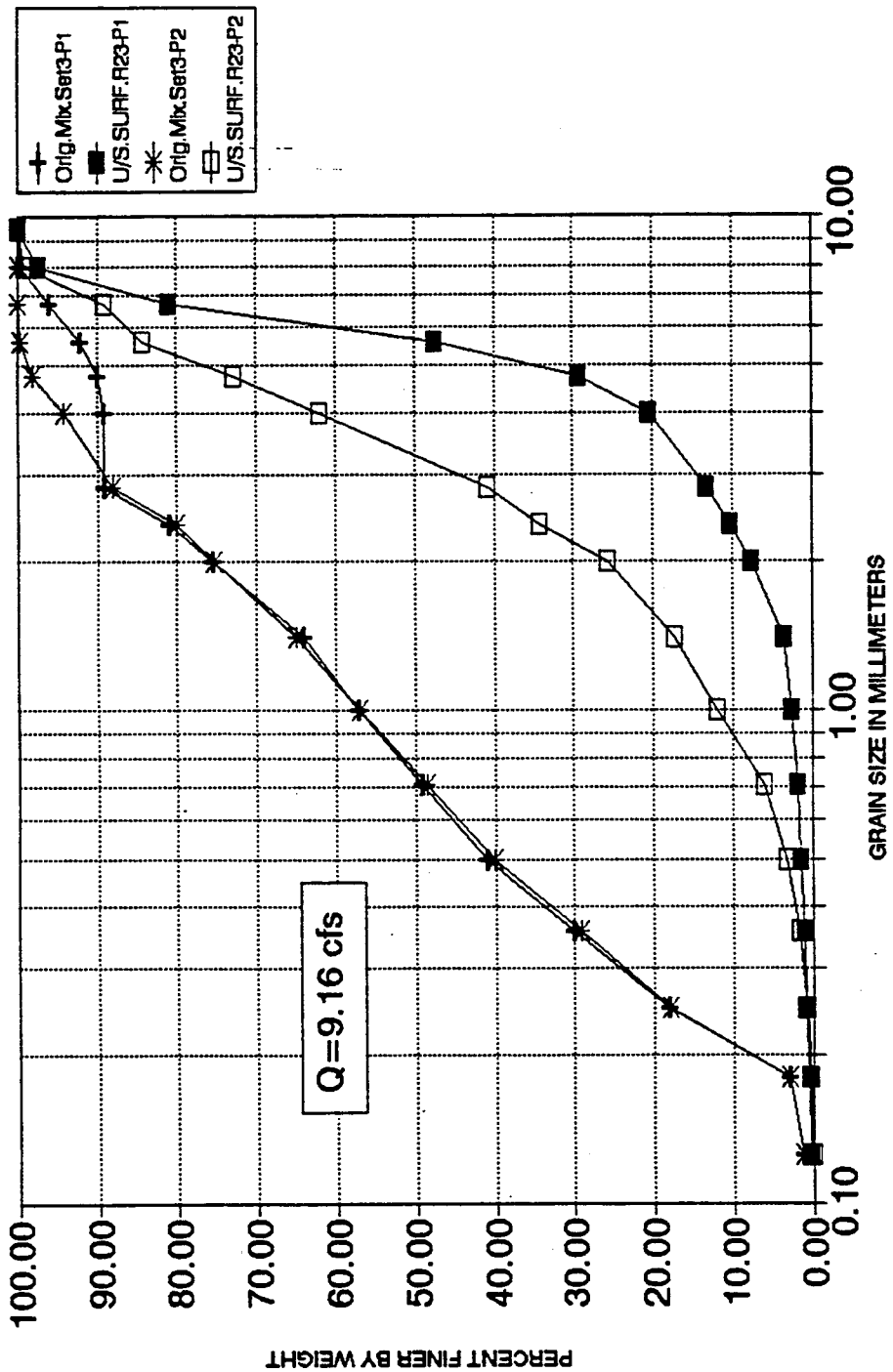


Figure 3.15 Effect of Coarse Material Fraction at Piers 1 and 2 for Run 23

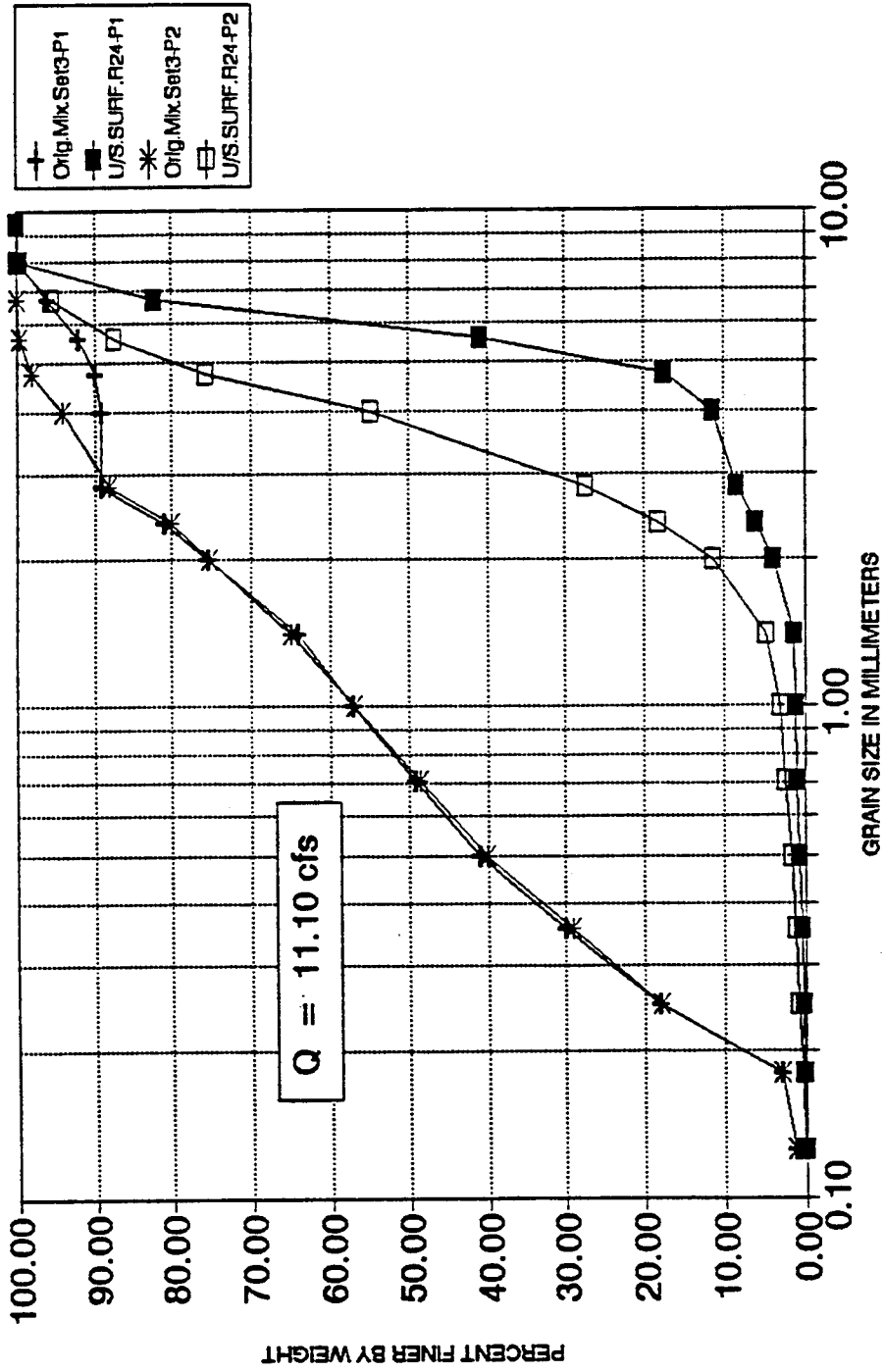


Figure 3.16 Effect of Coarse Material Fraction at Piers 1 and 2 for Run 24

3.5.3 Gradation Patterns at Different Areas around Bridge Piers

In this section, the sediment size distribution patterns for the Set No. 3 runs are presented. Additionally, some sediment size patterns from Sets No. 1 and 2 are presented at the approach of each pier, the upstream (nose) of piers, sides, downstream, and the ridge to show the variation of armoring patterns around the same pier with the same original bed material.

In the approach area of each pier the applied shear stress compared to that at the pier is relatively small. This is because the velocity in the approach of the piers compared to the velocities required to initiate the scour around the piers is in the order of $(1/2)$ to $(1/\sqrt{8})$ of the velocity required to initiate the scour. Since the shear stress is proportional to the square of the velocity, shear stresses at the approach regions are in the order of $1/4$ to $1/8$ to those experienced around the piers. These conclusions are supported by the formation of the coarsest armor patterns around the piers shown in Figures 3.17 through 3.25.

At the nose and sides of the pier, the applied shear stresses are higher than at any other area around the pier. Scouring process is most severe at these two positions and therefore the scour depths are larger than at any other area. This is reflected on the armoring behavior shown at these locations (coarsest armor). Directly downstream of the pier a wake zone exists. In this zone a finer size armor layer is measured.

From the potential flow theory, it is expected that the stream lines passing around the piers carry or move to some degree the coarse particles and settle them past the pier at the ridge zone. After diverging from upstream edge of the pier to

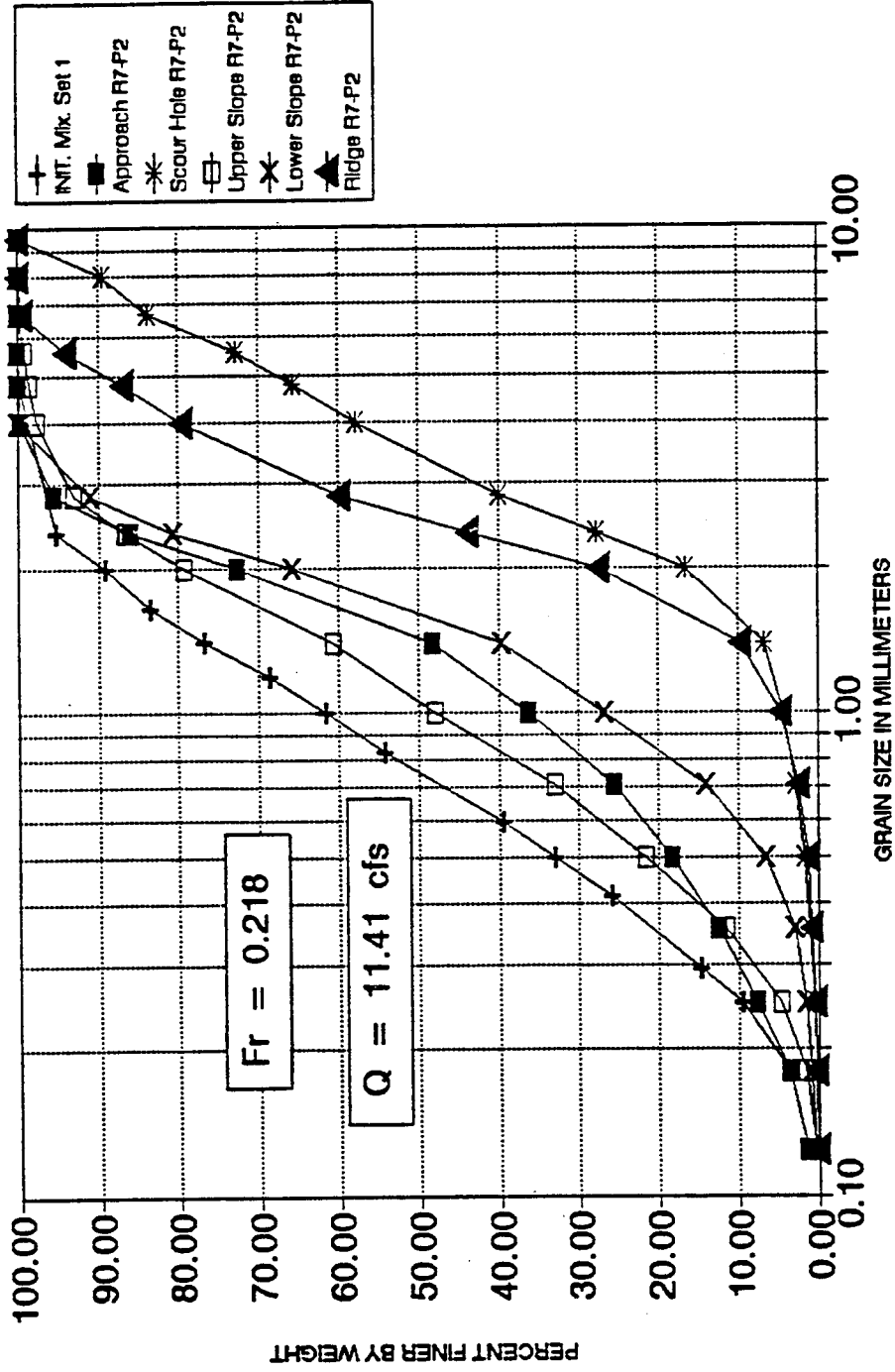


Figure 3.17 Sediment Size Distribution Curves around Pier 2 for Run 7

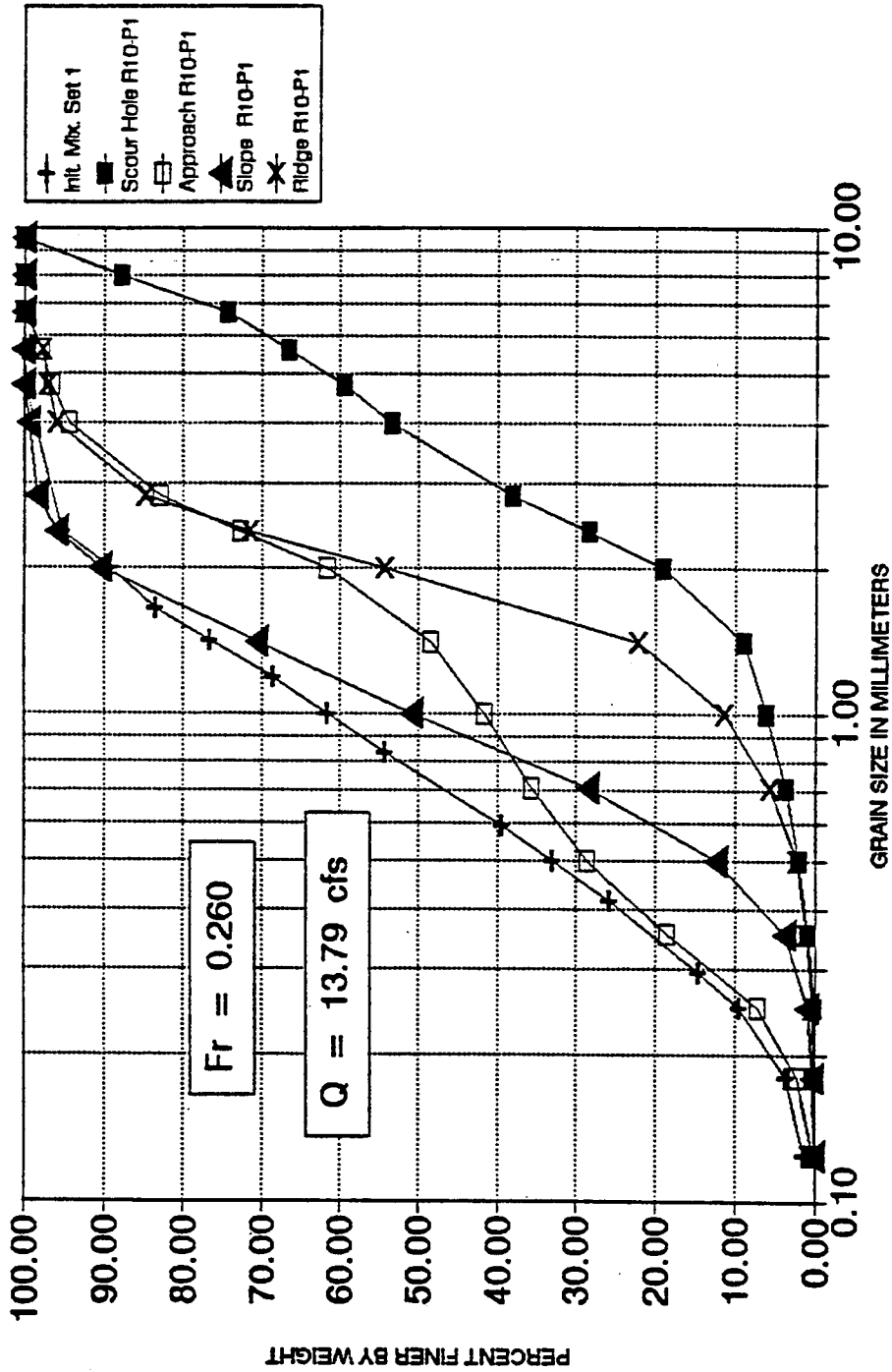


Figure 3.18 Sediment Size Distribution Curves Around Pier 1 for Run 10

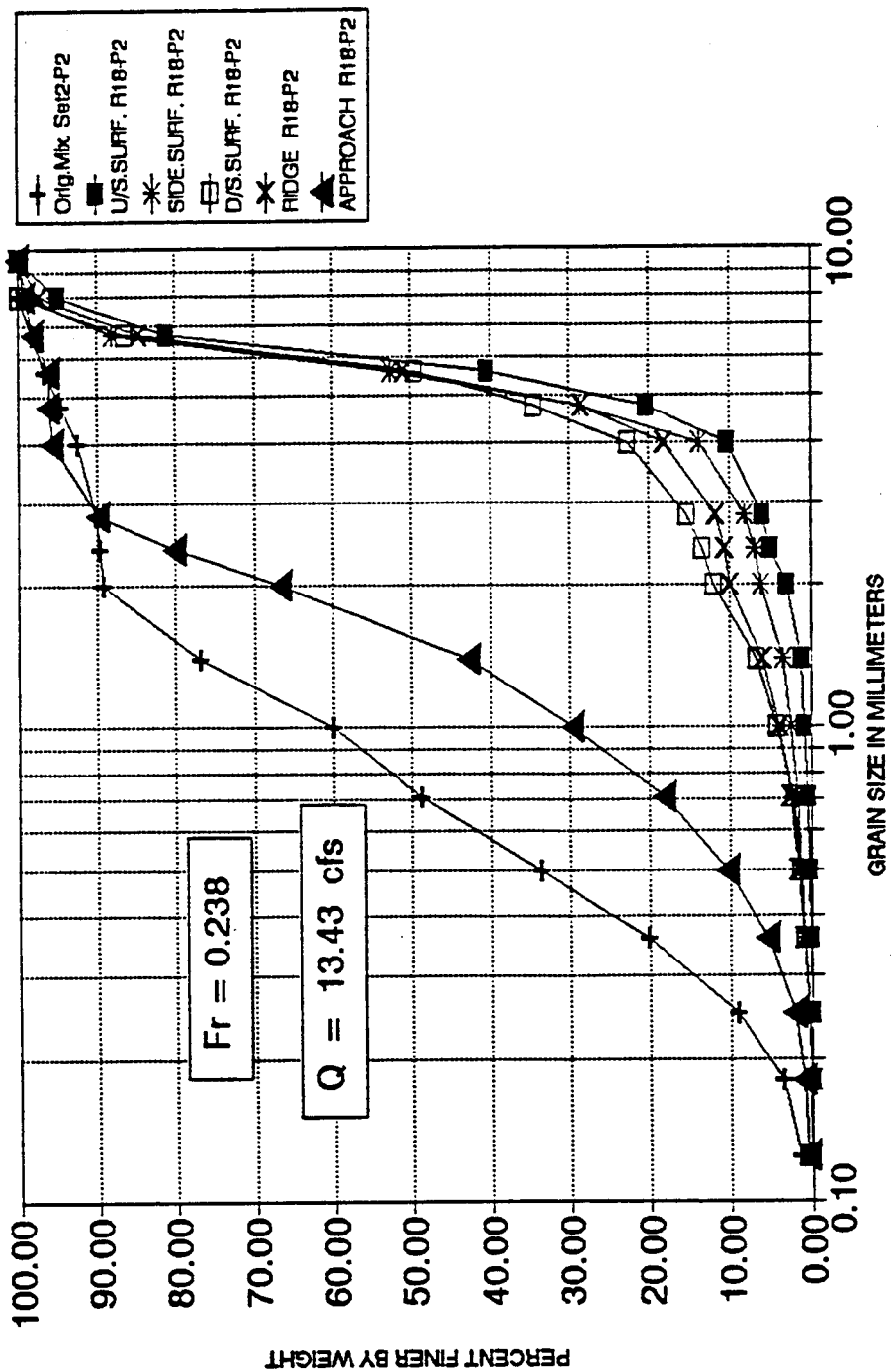


Figure 3.19 Sediment Size Distribution Curves Around Pier 2 for Run 18

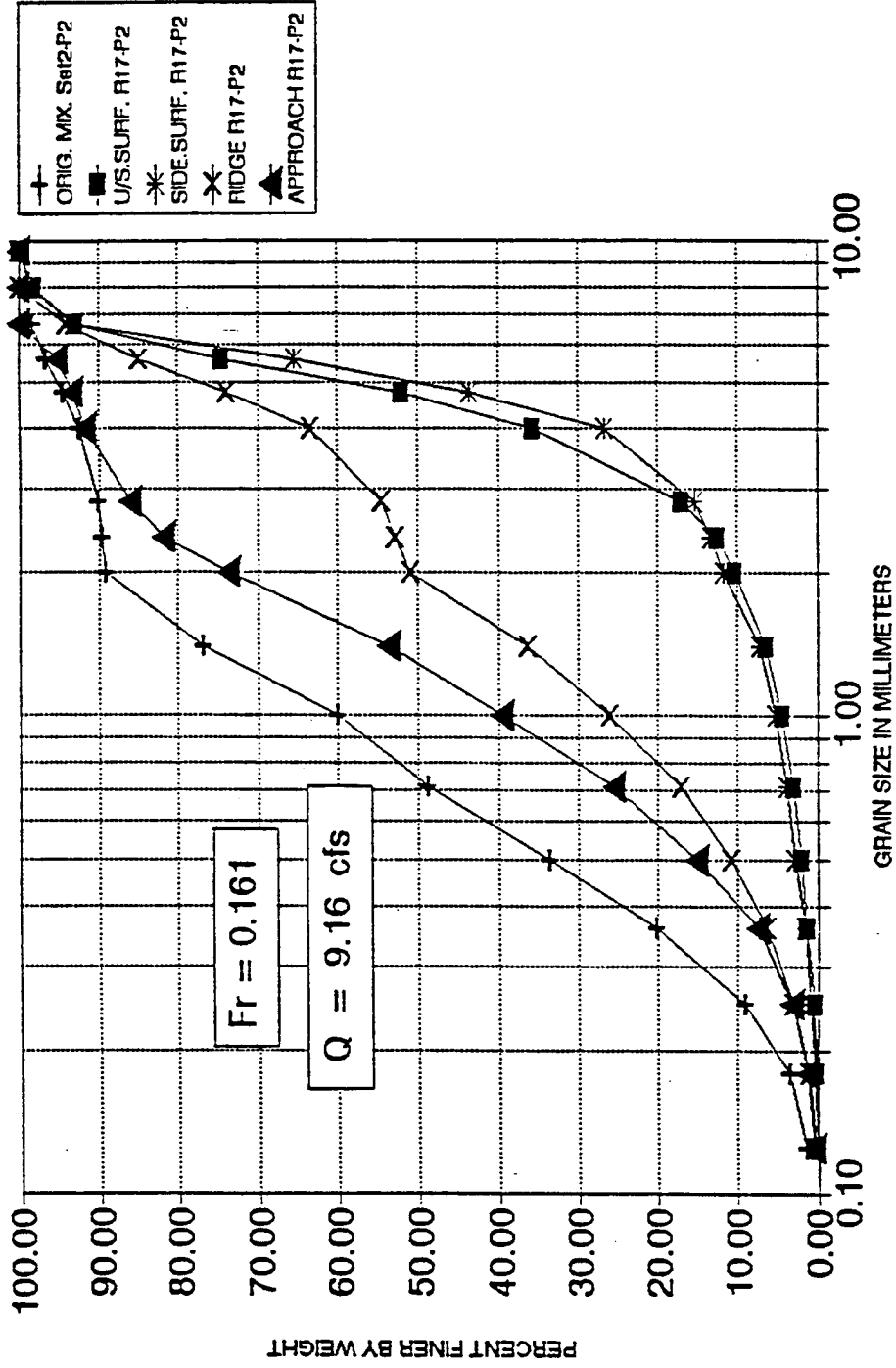


Figure 3.20 Sediment Size Distribution Curves Around Pier 2 for Run 17

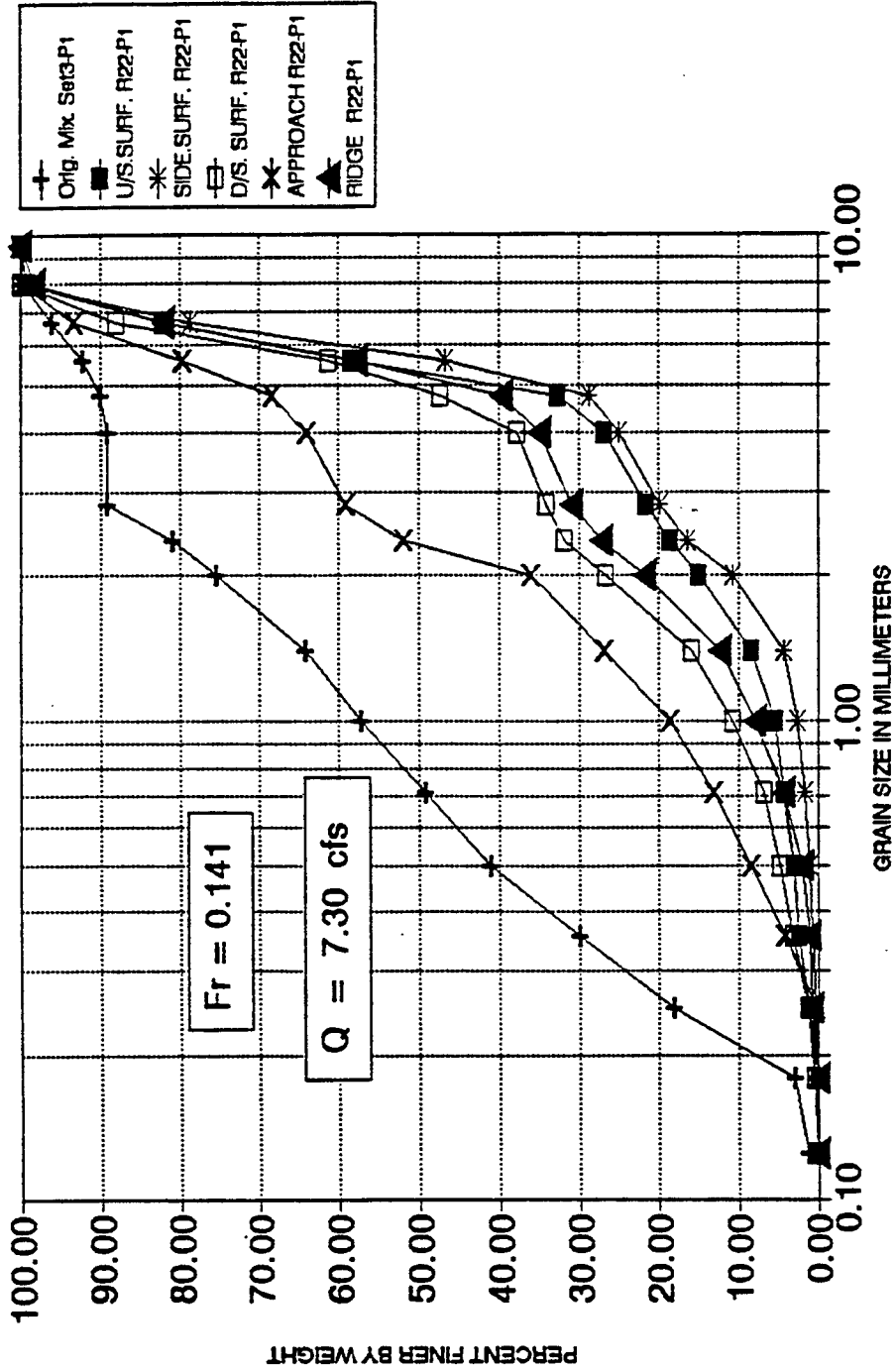


Figure 3.21 Sediment Size Distribution Curves Around Pier 1 for Run 22

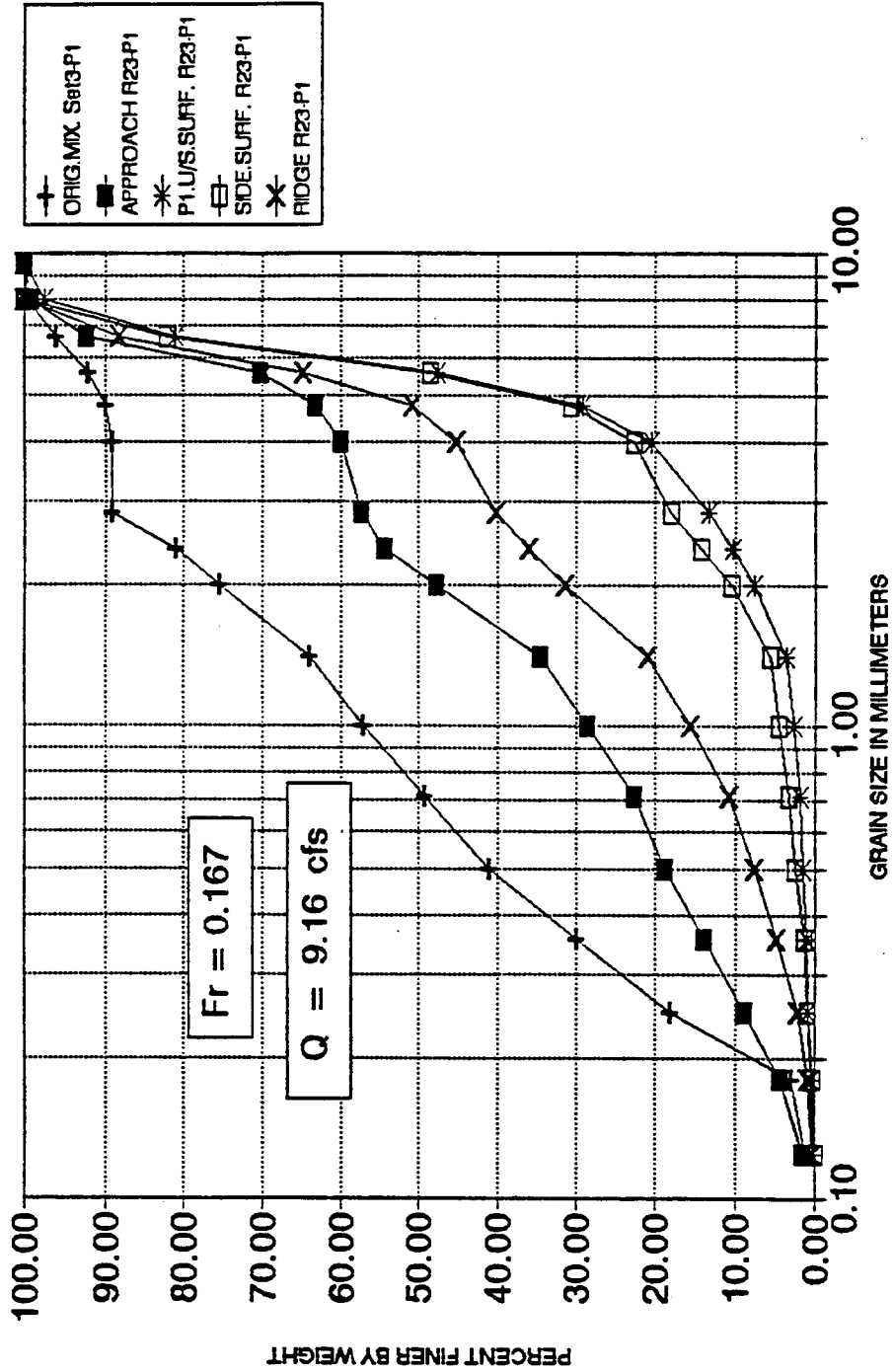


Figure 3.22 Sediment Size Distribution Curves Around Pier 1 for Run 23

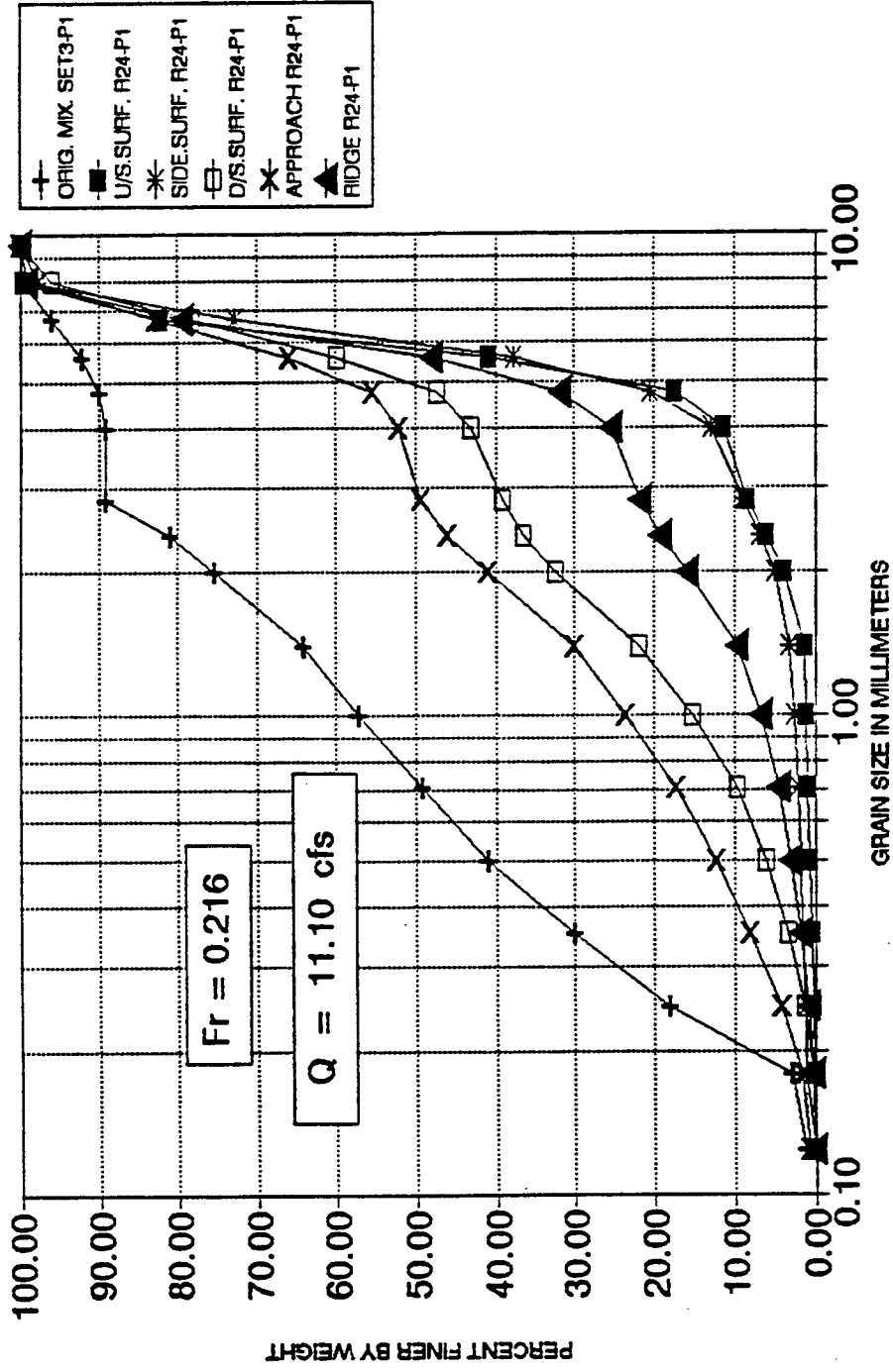


Figure 3.23 Sediment Size Distribution Curves Around Pier 1 for Run 24

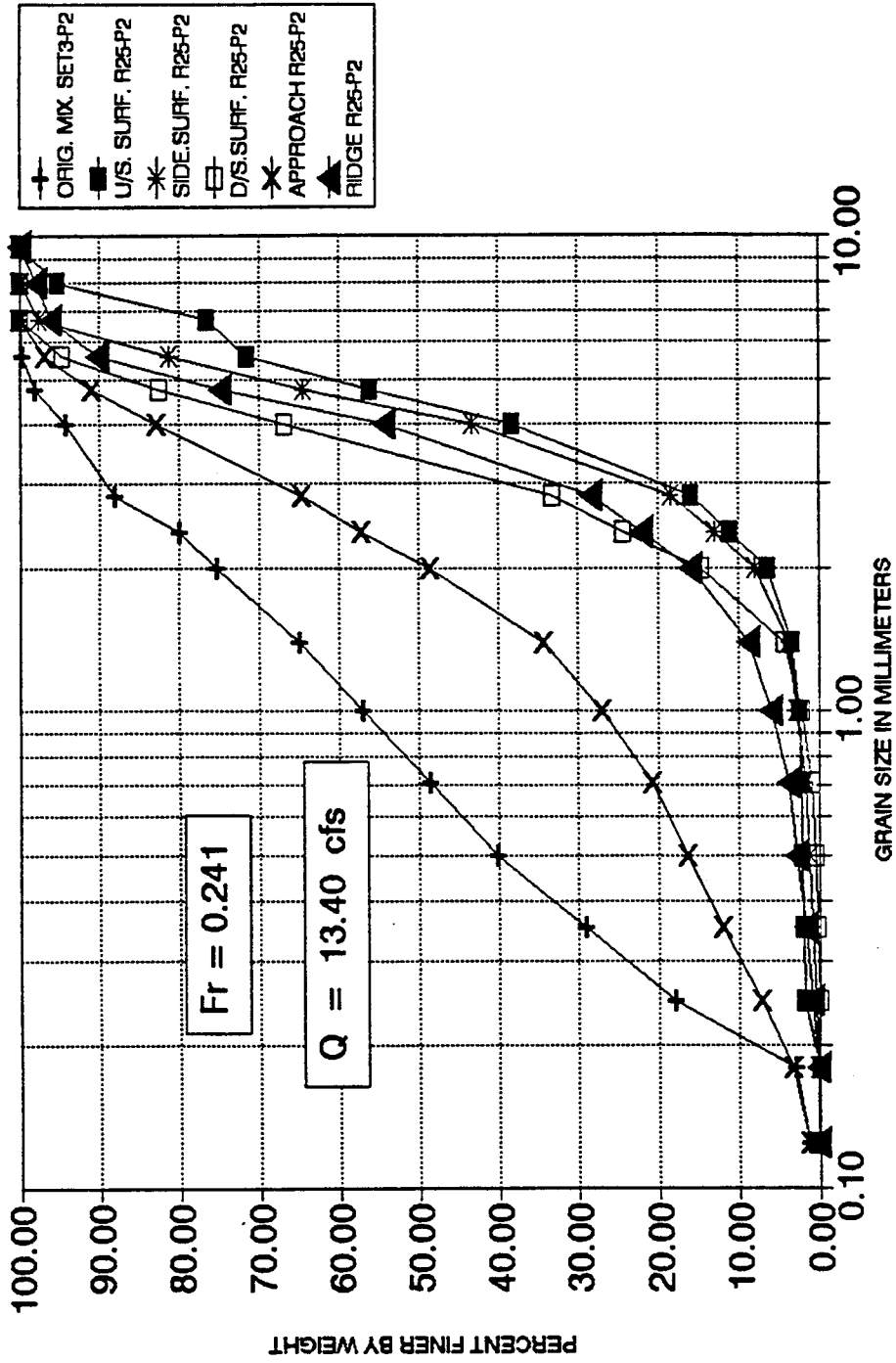


Figure 3.24 Sediment Size Distribution Curves Around Pier 2 for Run 25

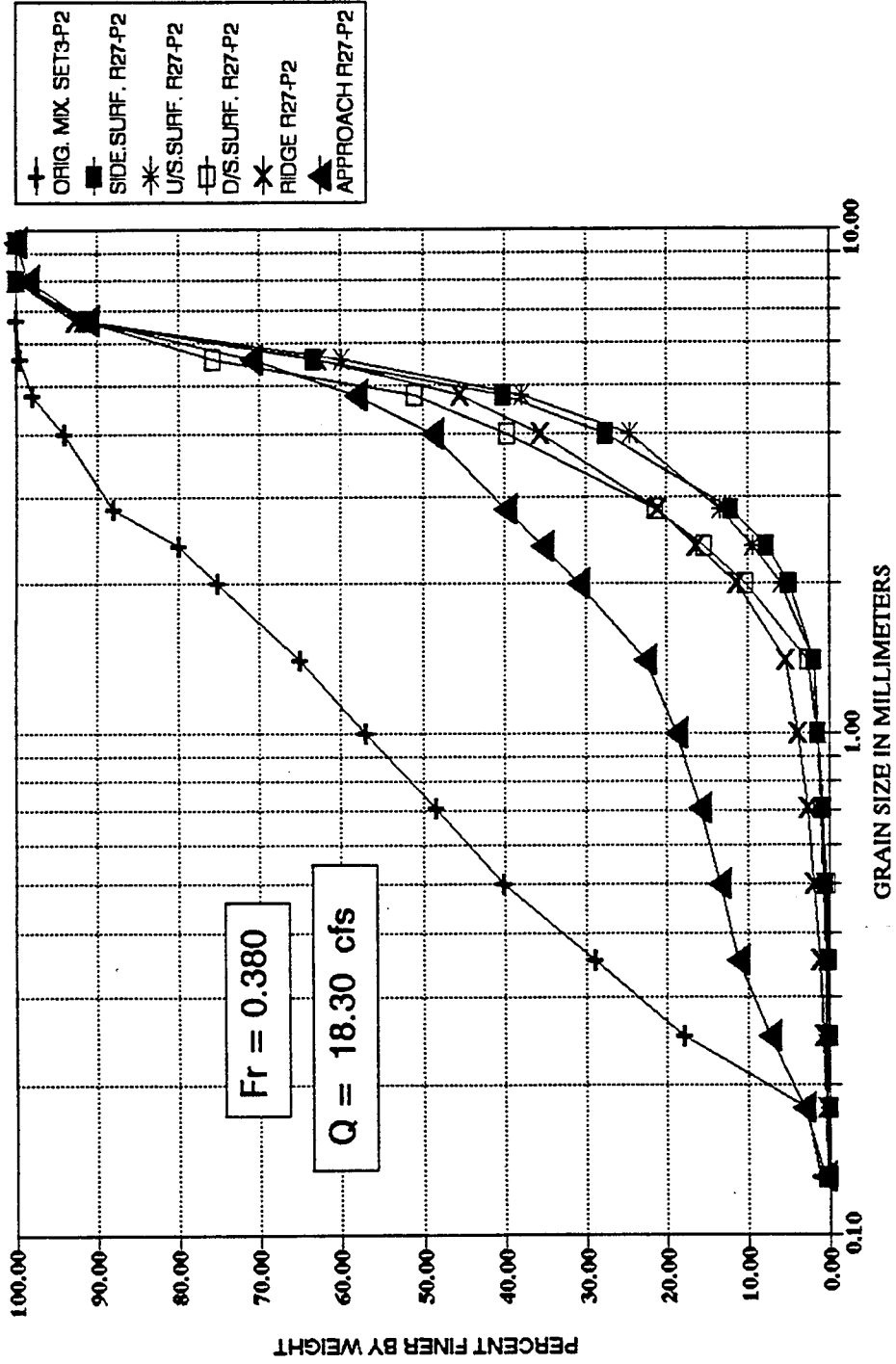


Figure 3.25 Sediment Size Distribution Curves Around Pier 2 for Run 27

the sides, the stream lines tend to converge again downstream of the piers.

At the tail of the horseshoe shape, at the wake zone finer materials is found. This is because the flow in this region is very weak compared to that at the sides of the pier resulting in the deposition of the fine particles eroded from the upstream of scour holes at this area. From the observations and measurements of armoring patterns at the different areas around bridge piers, it can be concluded that the coarsest armor layers exist in front (at the nose) and sides of the piers (with some small differences since the applied shear stress differs slightly at these two areas).

A less coarser armor layer is found at the ridge downstream of the piers. Still, a finer size distribution is observed at the downstream area behind the pier directly at the wake zone. Lastly, the finest layer is measured at the tail end of the depositional zone of the horseshoe vortex, away from the pier site. Further discussions on the armoring patterns will be presented in Chapter 4.

CHAPTER 4

ANALYSIS AND DISCUSSION OF RESULTS

4.1 Introduction

This chapter discusses the effect of sediment gradation and the coarse material fraction on the behavior of the local scour depth around circular cylindrical piers, keeping all other parameters constant except the stream velocity and sediment size properties. The pier shape was circular with a 7 in outside diameter and aligned with the flow direction. The approach flow depth was almost constant in the range of 1.0 ft and the mean sediment size for all the three sediment mixtures used was kept constant at 0.75 mm. The only parameter that varied was the flow velocity against the scour depth for each of the six sediment mixtures. Due to these facts, the stream velocity or Froude number are appropriate measures of the flow strength to analyze the behavior of scour depth corresponding to each sediment mixture under certain flow conditions.

The complete experimental records of this study are presented as a part of the data supplement for the project No. DTHF 61-91-C-00004 entitled "Effect of Sediment Gradation and Cohesion on Scour" for the U.S. Federal Highway Administration. All experiments were carried out under uniform flow conditions. Seventy-nine runs were conducted: 71 of them were classified as clear-water scour and eight of them were live bed scour.

4.2 Geometry of Scour Hole

The deepest scour depths for all experiments were observed to be located at the upstream nose of the piers. This observation agreed with those of previous investigators. Also, all the scour holes which formed around the piers were observed to have roughly the shape of a frustum of an inverted cone, similar to observations reported earlier.

In each of the clear-water runs, the upstream slope of the scour hole was observed to be approximately or near the static angle of repose, α . This is consistent with a scour mechanism in which scouring occurs at a base of the scour hole, with material sliding down the slope from above. From cross-sections for different scour holes for different flow conditions and sediment mixtures, it can be seen that scour holes and volume of scoured materials are larger for uniform materials than for graded mixtures. Figures 4.1 through 4.6 present the geometry of scour holes which are formed under different flow conditions and different bed materials.

4.3 Influence of Mean Approach Velocity on Local Scour

During the present study, all the parameters affecting scour depth were approximately constant except the approach velocity to each pier. As a result, the scour depth was varied only as a function of the approach velocity for each sediment gradation that was used. As mentioned in Chapter 2, the approach velocity for each pier was the average of seven vertical velocity profiles in front of each pier.

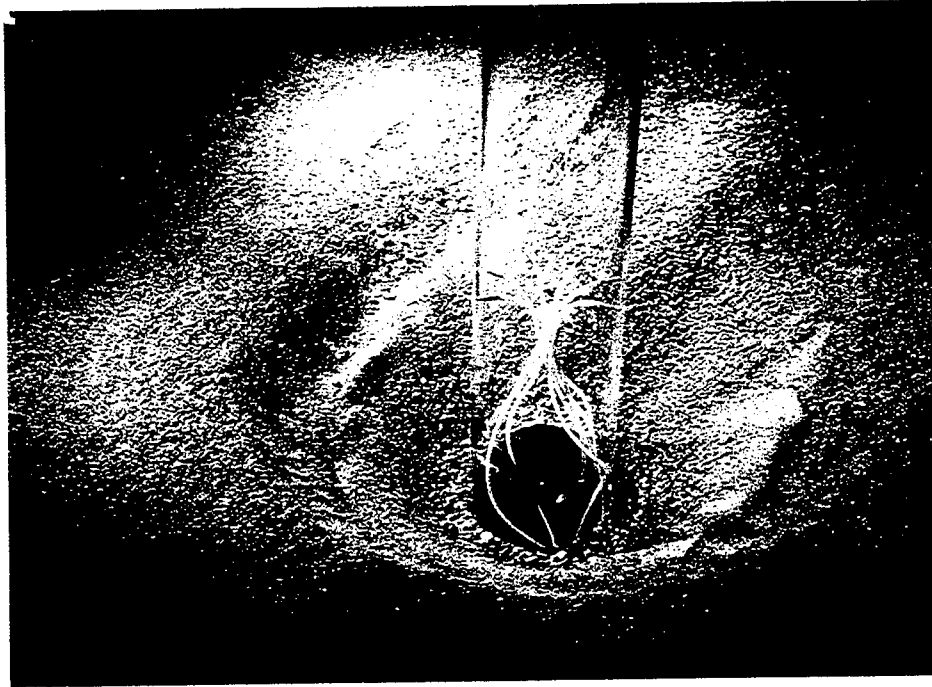


Figure 4.1 View of the Scour Hole Geometry for Pier 1 at the end of Run 7,

$$Q = 11.41 \text{ cfs}$$

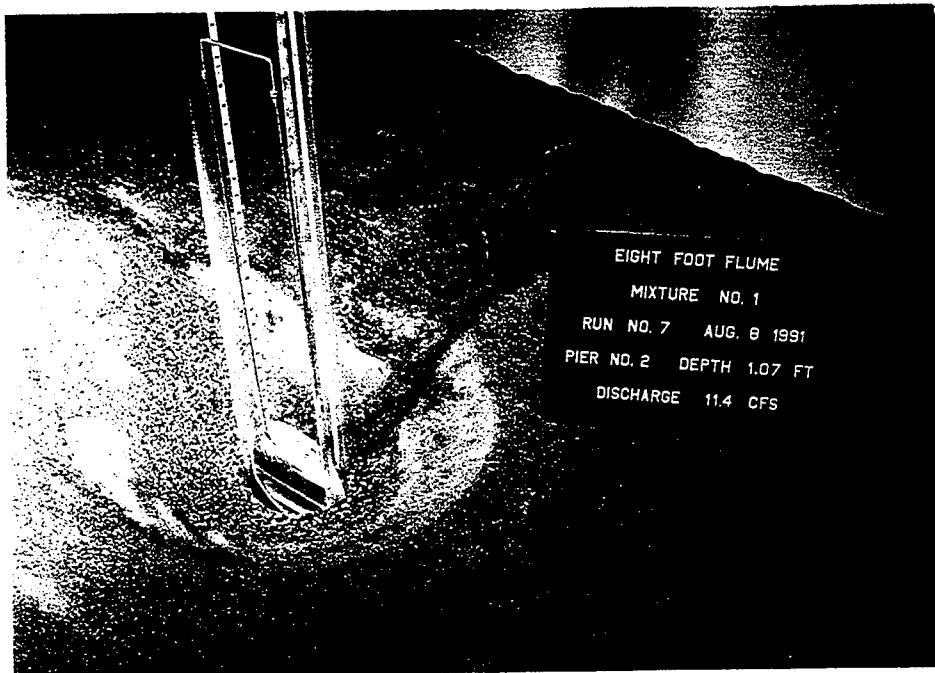


Figure 4.2 View of the Scour Hole Geometry for Pier 2 at the end of Run 7,

$$Q = 11.41 \text{ cfs}$$



Figure 4.3 View of the Scour Hole Geometry for Pier 3 at the end of Run 7,

$Q = 11.41$ cfs



Figure 4.4 View of the Scour Hole Geometry for Pier 1 at the end of Run 10,

$Q = 13.79$ cfs

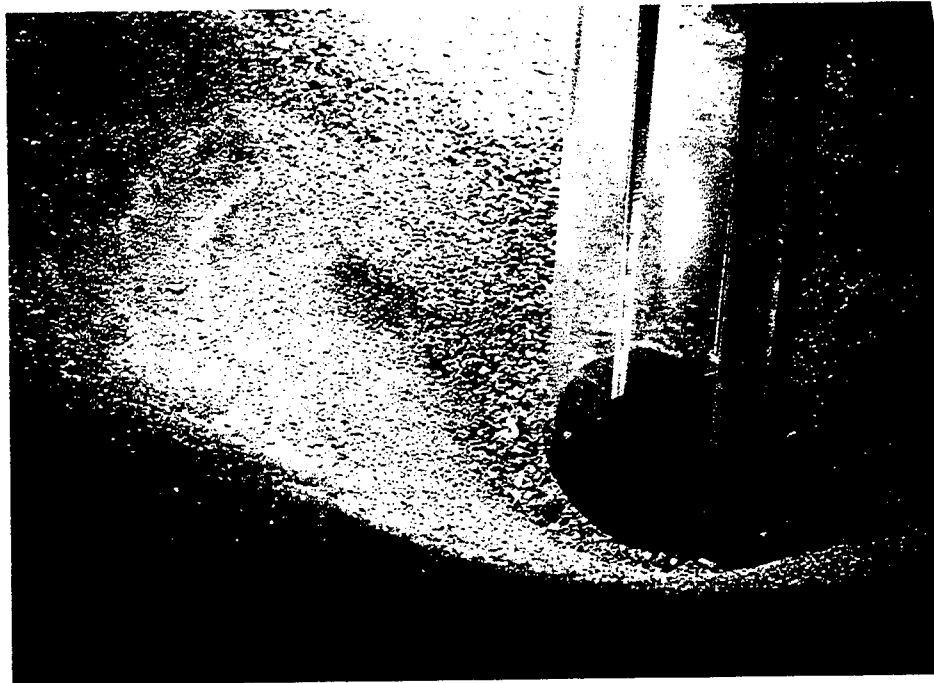


Figure 4.5 View of the Scour Hole Geometry for Pier 2 at the end of Run 10,

$$Q = 13.79 \text{ cfs}$$

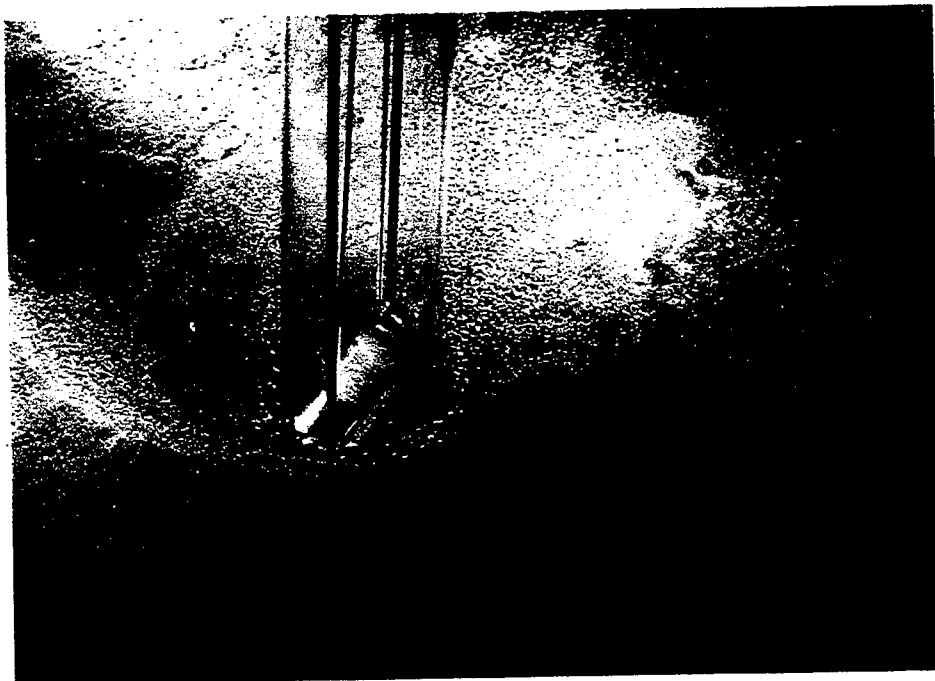


Figure 4.6 View of the Scour Hole Geometry for Pier at the end of 3 Run 10,

$$Q = 13.79 \text{ cfs}$$

The mean velocity of flow for each run was calculated from the water continuity equation as $U = Q/A$ where Q was pump discharge from orifice equation and A was the corresponding flow area measured during experiments. Good agreement between the two velocities indicated uniform approach flow conditions.

The symmetry of velocities around the center line of the piers (flume) were verified from intensive measurements that were performed in the approach of each pier, points at equal distances from the axis of the pier turned out to be satisfactorily close to each other. A complete list of all the measurements is reported in the publication of the measurements concerning all the measurements of the project.

Plots of the relative scour depth Y_s/b , against the mean approach velocity V_1 for different sediment mixtures with a constant mean diameter, d_{50} of 0.75 mm are shown in Figure 4.7. A definite trend in each of the curves is apparent.

The scour depth developed in the clear-water, as shown by previous investigations of Chabert and Engeldinger (1956) and Raudkivi and Sutherland (1981), increases almost linearly with increasing mean velocity to a maximum at about threshold velocity. Note that when the flow velocity is increased gradually, the strength of the scouring mechanism increases correspondingly and the stream power which is a function of the stream velocity, erodes more and more with velocity increases. This trend continues with further flow velocity increases until live bed conditions are reached.

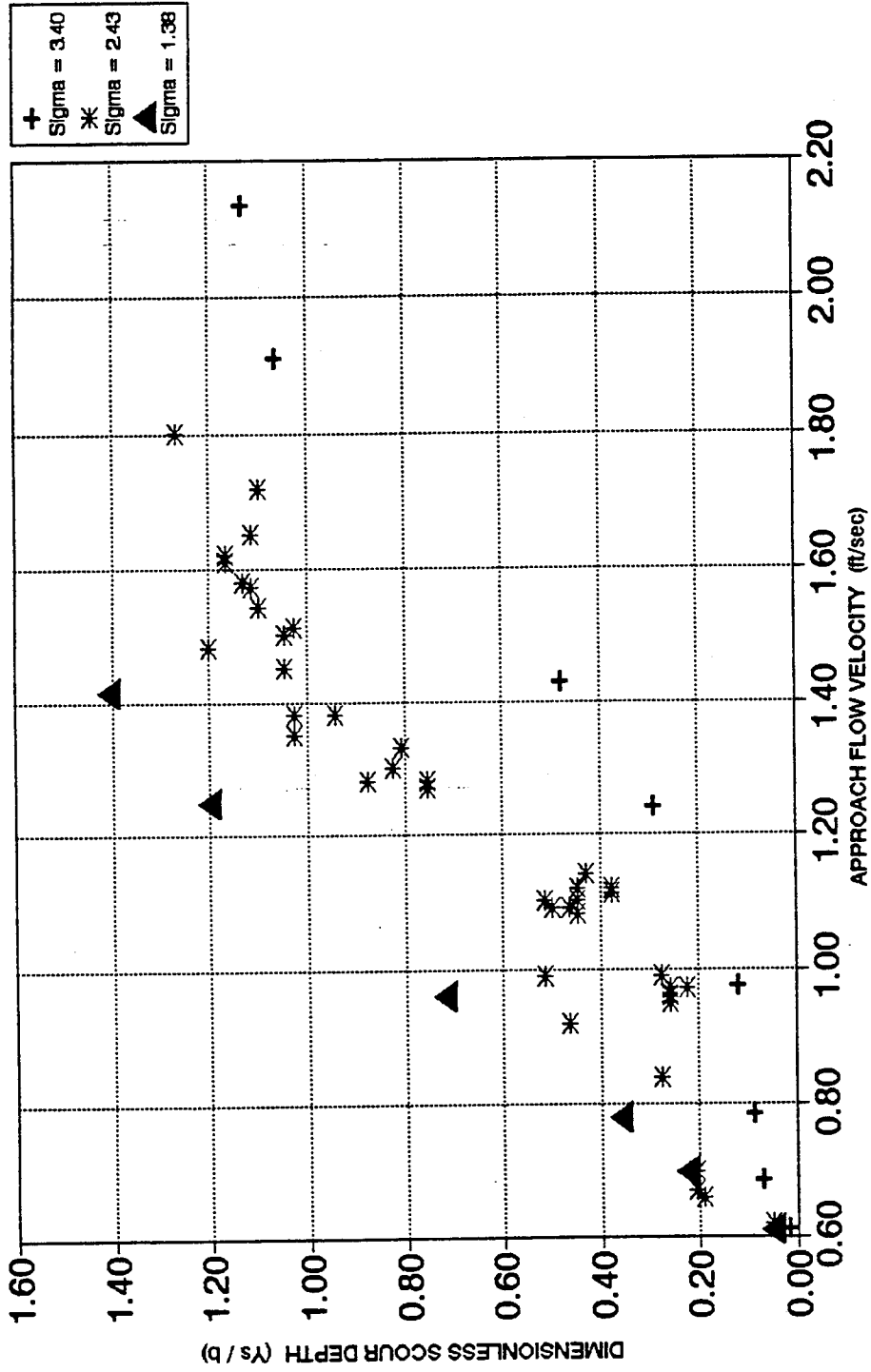


Figure 4.7 Dimensionless Scour Depth as a Function of the Approach Velocity for Various Gradation Coefficients

In this study, the critical velocities for the three sediment mixtures beyond which live-bed conditions are expected are calculated using the Neill (1973) equation:

$$V_c = 12.0 h^{1/6} d^{1/3} \quad (4.1)$$

where:

V_c = the critical velocity in ft/sec,

h = the mean flow depth in ft, and

d = the representative diameter of bed material in ft.

This Equation 4.1 gives a value of 1.60 ft/sec as a critical value for the uniform material used around pier 3 during third set of runs which can be comparable to the measured value which was in the range between 1.50 and 1.90 ft/sec, this range is between velocity value of run 25 and run 26 at which the uniform material moved. Also, Equation 4.1 gives good results for the values of critical velocities for mixtures No. 1 and No. 2 when d_{90} was used as a representative size for the mixtures instead of d_{50} , because as it has been seen from results that d_{50} is no longer valid for representing the sediment mixtures as usual with uniform ones. The critical velocity for sediment mixture No. 1 was calculated to be 2.28 ft/s for d_{90} size of 2.10 mm while the measured critical velocity one was in the range of 1.60 ft/sec to 1.80 ft/sec depending on the flow depth used during runs 12 and 19. The critical velocity for mixture No. 2 was calculated as 2.60 ft/sec for d_{90} size of 3.2 mm while the measured critical velocity was about 2.20 ft/s. The difference between computed and measured critical velocities can be attributed to the circumstances in which Neill equation was developed which were not compatible with the present experimental conditions.

During the second and third set of runs, when d_{90} increased for mixtures 1 and 2, V_c was increased indicating that in order to initiate motion for sediment mixtures one must count for moving its d_{90} size as well.

4.4 Repeatability of Results

Three sets of runs were performed during this investigation. The purpose of the first run set (runs 1 through 12), was to check if it was possible to get the same scour depth for graded sediments when passing the same flow conditions at the site of each pier under investigation. Table 3.1 shows clearly that this function was satisfied since each of the three piers was subjected to almost the same flow conditions and the resulting bed material size distribution was almost the same around each pier. Correspondingly, the measured scour depths were almost the same too. Figures 4.8 through 4.10 show some examples of the sediment size distribution curves for the armor layers around the three piers during runs 6, 7, and 10 for three different discharges of 9.90, 11.41, and 13.79 cfs respectively. From these figures it can be said that repeatability of results to obtain armor layers were satisfied to a large degree taking into account the possibility of acceptable mistakes during the sampling of armor layers, using any technique for removing the surface layer around each pier, and also the sensitivity of analysis while performing the sieving analysis.

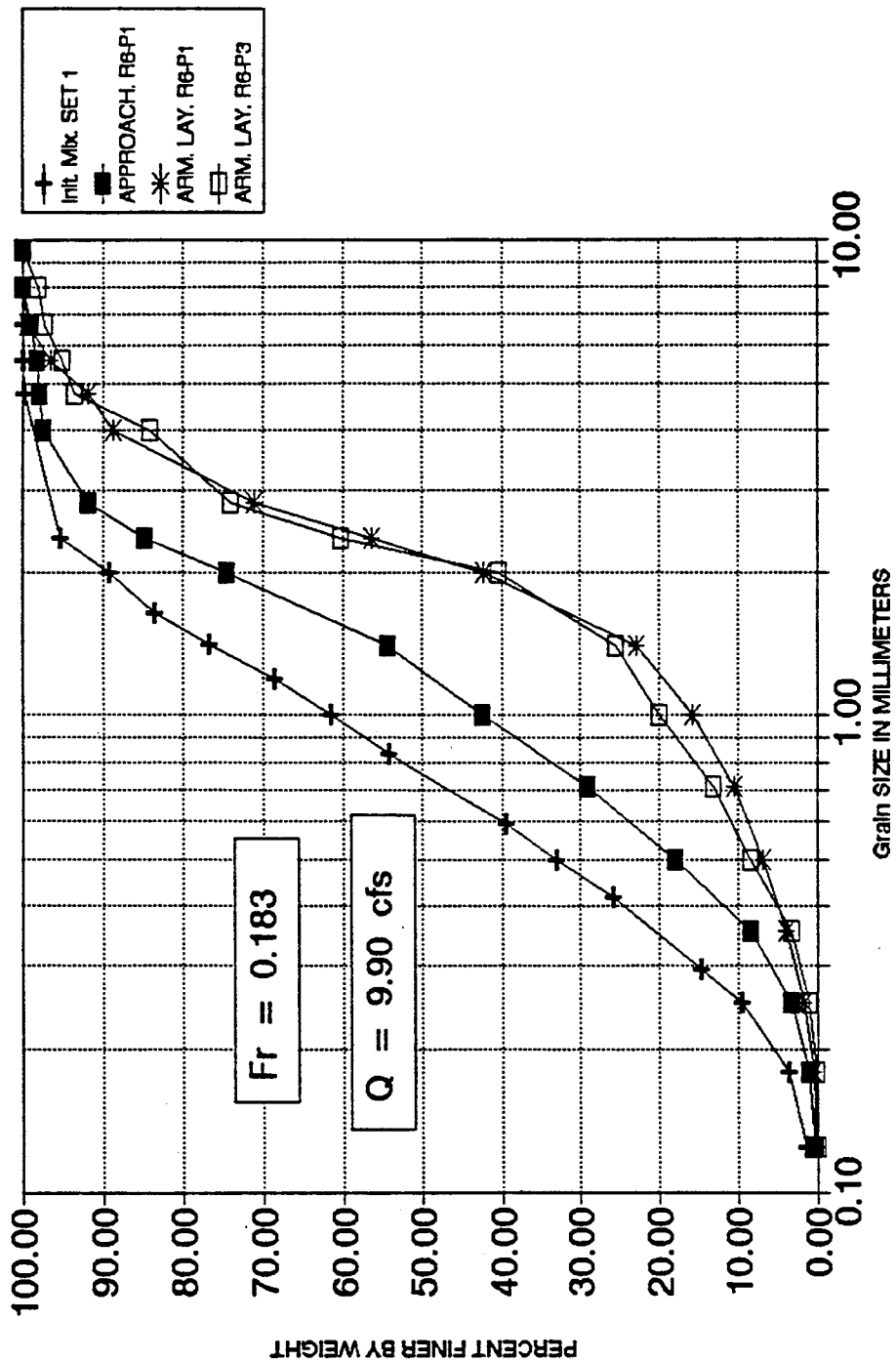


Figure 4.8 Sediment Size Distribution Curves Around Scour Holes Formed at Piers 1 and 3 during Run 6

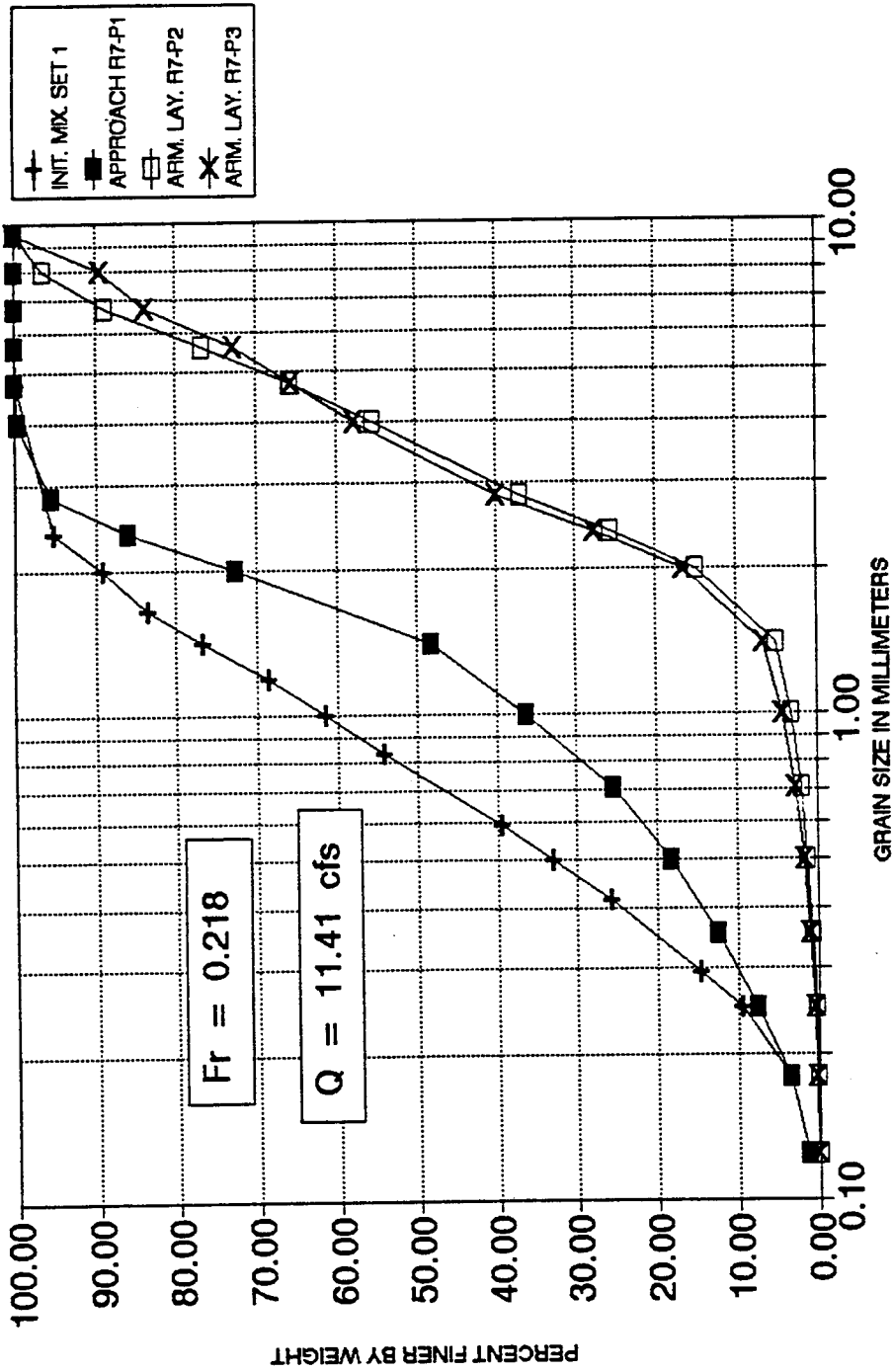


Figure 4.9 Sediment Size Distribution Curves Around Scour Holes Formed at Piers 2 and 3 during Run 7

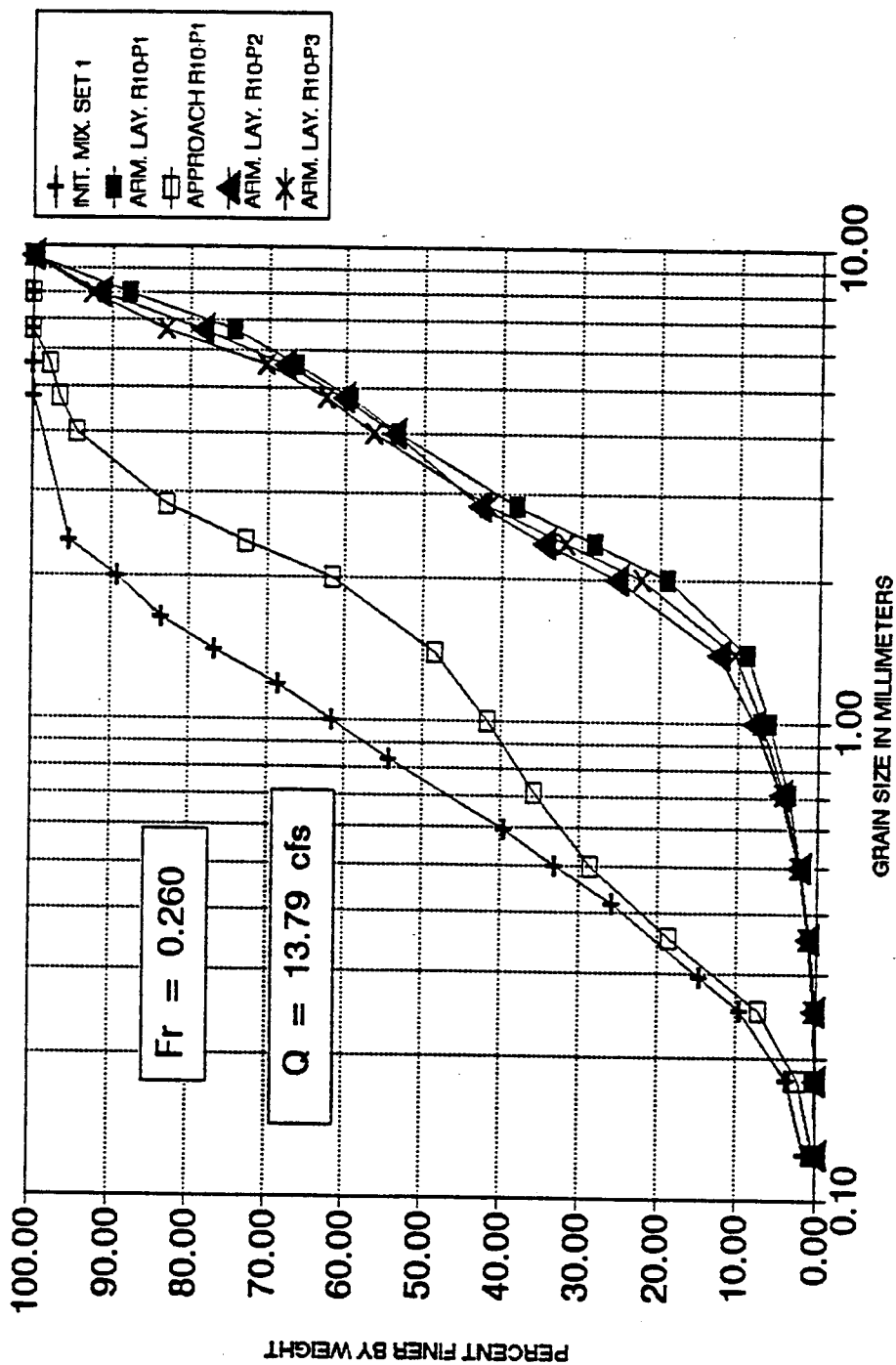


Figure 4.10 Sediment Size Distribution Curves Around Scour Holes Formed at Piers 1, 2, and 3 during Run 10

4.5 Scour Depth Comparison in Uniform and Non-Uniform Beds

Very few investigations in the past have looked at the influence of bed material gradation on the development of scour. Recently, Ettema and Raudkivi (1977) confirmed Nicollet's (1971) experiments and stated that sediment gradation has a stronger influence on the reduction of the equilibrium depth of clear water scour for non-uniform beds than those of uniform ones. As a rule of thumb it can be said that the higher the sediment non-uniformity, the lower the equilibrium scour depth will be.

4.5.1 Clear-Water Scour Depths as a Function of Froude Number

In the present study the effect of sediment gradation on equilibrium scour depth has in principle confirmed the investigations done by Ettema (1976, 1980). During this experimental investigation, for graded materials with a gradation coefficient (σ_g) of 2.43 and 3.4, an armor layer around each pier was observed after passing certain flow conditions. This phenomenon did not exist for the nearly uniform materials with σ_g of 1.38. This armor layer, once formed, acts as a coating or protection for the underlying fine materials and prevents more scour from happening.

The armoring phenomena exists only in graded materials and does not happen in uniform ones. When the flow passes the pier and scouring begins, fine particles are washed away downstream of the pier. Coarser particles which exist in the initial sediment mixture, slide down into the scour hole and form the coating which in return stabilize and prevent more scour from happening. In the case of uniform materials, since almost all particles have the same size and since the material washed from around

the pier is the same size as the material which will stay in the hole after the scouring processes, the scour rate is reduced only after maximum equilibrium scour depth is attained for that flow condition. Referring to Figure 4.11, it is clear that the scour depths around the piers in graded mixtures having σ_g of 2.43 and 3.4 are less than those with σ_g of 1.38 for almost the same flow conditions. Values of scour depths in non-uniform and uniform beds corresponding to the various test conditions are shown in Table 4.1.

Table 4.1. Effect of Sediment Gradation On Clear-Water Scour Depth

Q (cfs)	$\sigma_g = 1.38$		$\sigma_g = 2.43$		$\sigma_g = 3.40$	
	F_r	Y_s (ft)	F_r	Y_s (ft)	F_r	Y_s (ft)
5.20	.107	.030	.108	.030	.108	.010
7.30	.131	.210	.146	.160	.133	.050
9.16	.161	.420	.168	.300	.164	.070
11.10	.213	.700	.219	.510	.210	.170
13.40	.237	.820	.250	.700	.241	.280

In comparing the scour depths in Table 4.1, it can be seen that for a given F_r of the flow the scour depth reduces from σ_g of 1.38 to σ_g of 2.43 to σ_g of 3.4. From Figure 4.11 which relates F_r to scour depth it can be said that the regressed line which represents data of scour depth corresponding to σ_g of 3.4 has the lowest slope compared to the other two lines corresponding to those of σ_g of 2.43 and 1.38, and the lower the slope of the line, the higher the gradation coefficient and consequently the lower the scour depth.

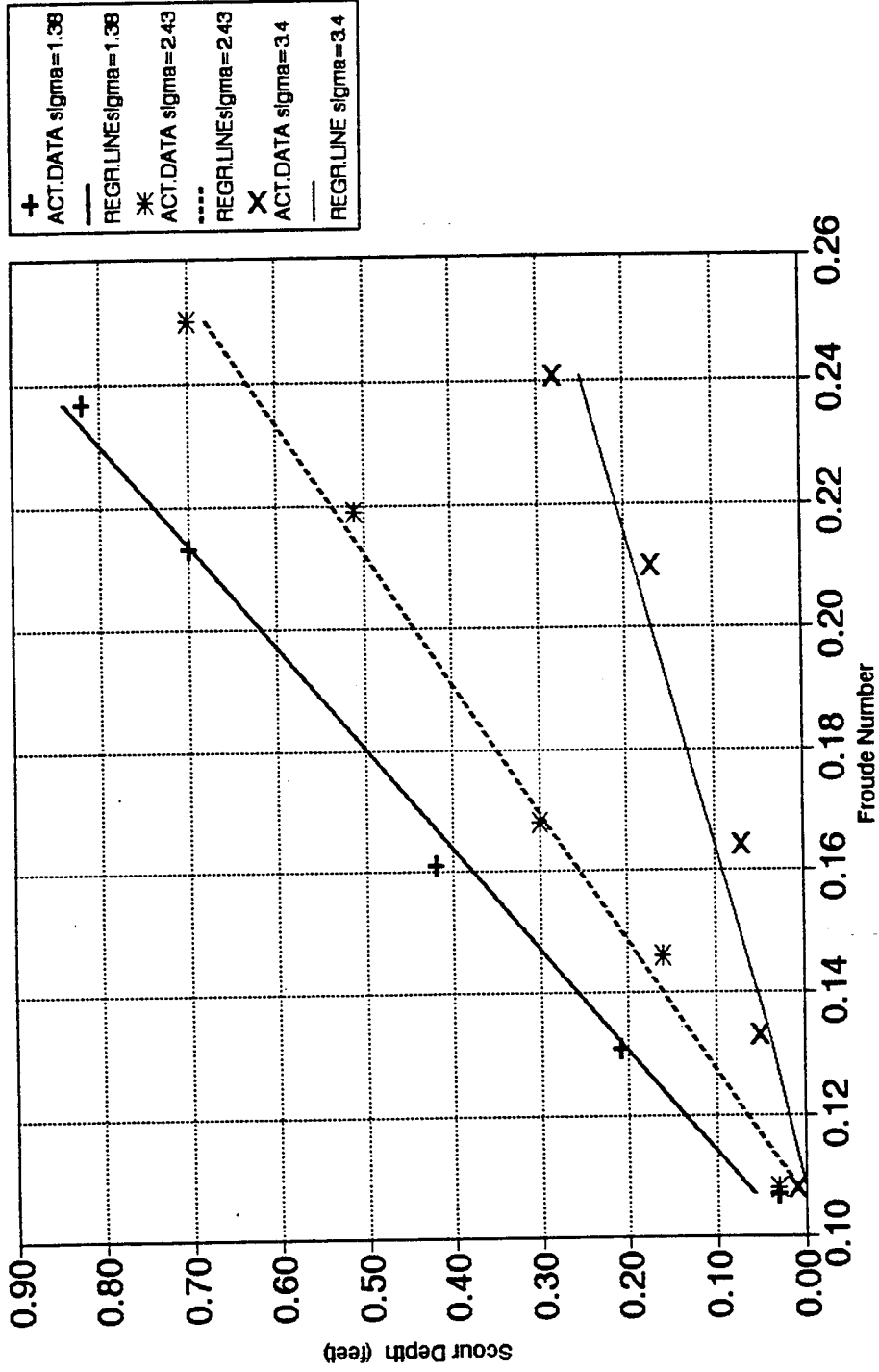


Figure 4.11 Effect of the Non-Uniformity of Sediments on Pier Scour Depth

4.5.2 Scour Profile Along Cross-Sections

To investigate the effect of gradation coefficient on scour hole geometry a comparison between different cross sections passing through the center line of piers were made for various σ_g values. Figures 4.12 through 4.14 can be used to demonstrate and explain how the dimensions of each scour hole vary with flow conditions and also how they vary with changing gradation coefficients. Flow conditions corresponding to Q of 9.16, 11.10, and 13.43 cfs have been chosen to show the change of the cross-sections geometry when σ_g is increased from 1.38 to 2.43 to 3.4. It is clear that the effect of increasing σ_g is to reduce the depth and the width of the scour hole but the geometry of the scour hole is almost constant.

4.5.3 Time Development of Scour Depth to Account for the Effect of Gradation Coefficient

The development of scour hole depth (Y_s) with time (t) does not appear to have been sufficiently investigated (Franzetti et al., 1982). In this investigation, scour depth development with time was monitored using a mirror inside each plexiglass pier and a scale mounted on the inside walls of the piers.

As shown in Figures 4.15 and 4.16 as an example, based on experimental results it can be said that the function $Y_s(t)$ generally increases over time for clear-water conditions in all runs. Except for the first five runs, all experiments were conducted with 16 hours test duration in order to be sure that the equilibrium scour depth was reached and became constant for a sufficient period of time. Longer test runs also was

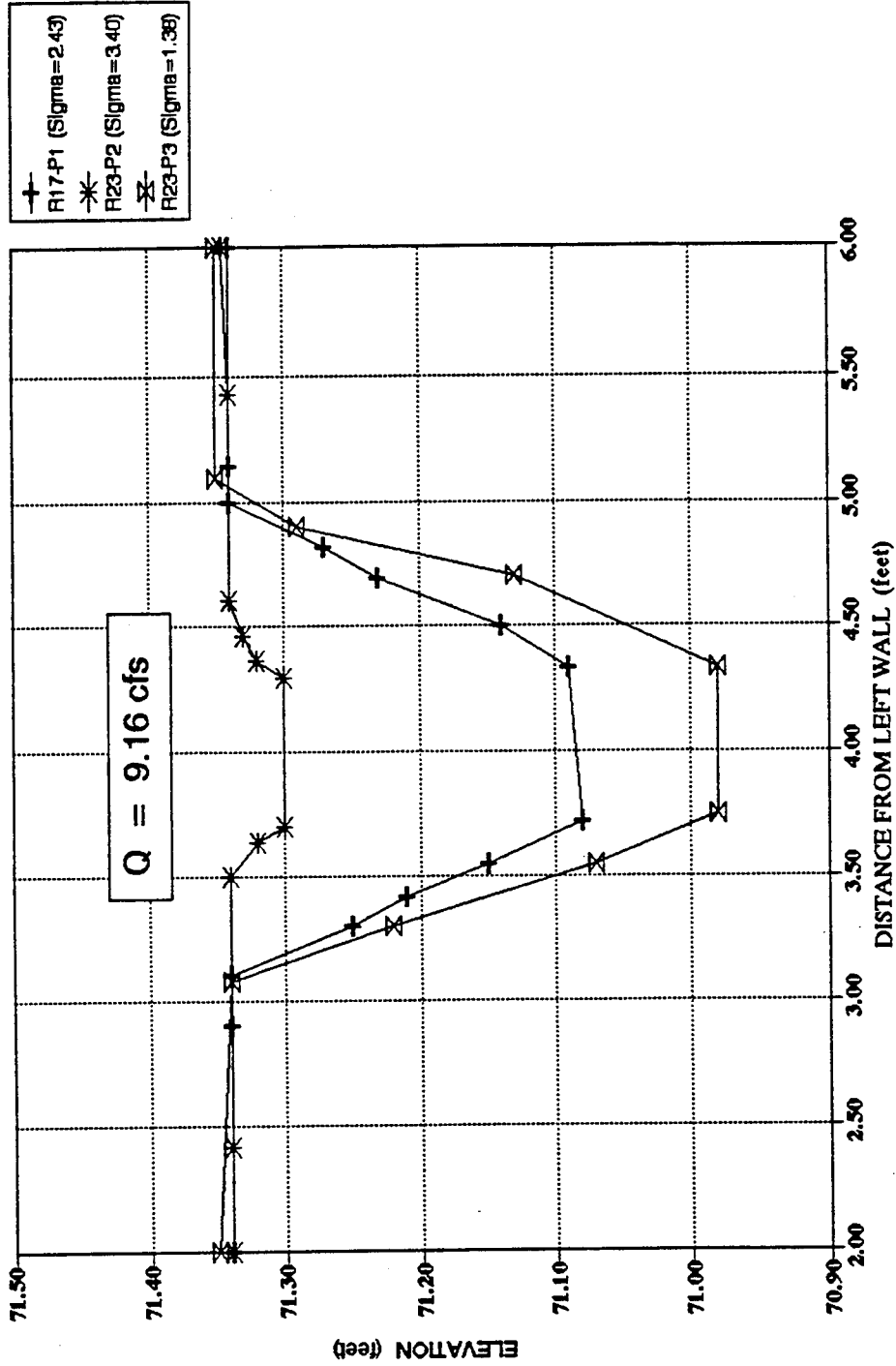


Figure 4.12 Cross Sections Passing through Center Lines of Piers 1 and 2 for Runs 17 and 23 (Q = 9.16 cfs)

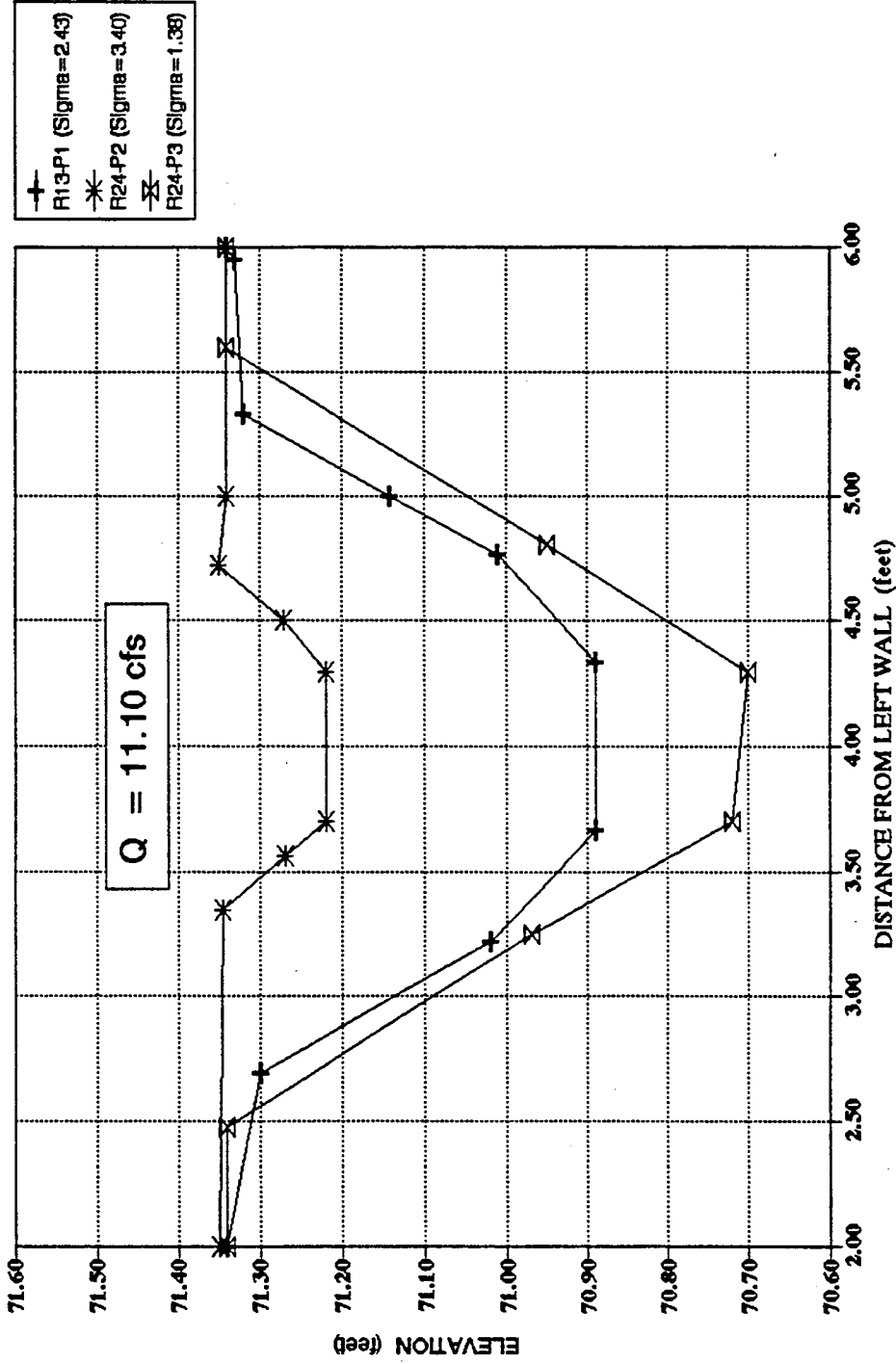


Figure 4.13 Cross Sections Passing through Center Lines of Piers 1, 2 and 3 for Runs 13 and 24 (Q = 11.10 cfs)

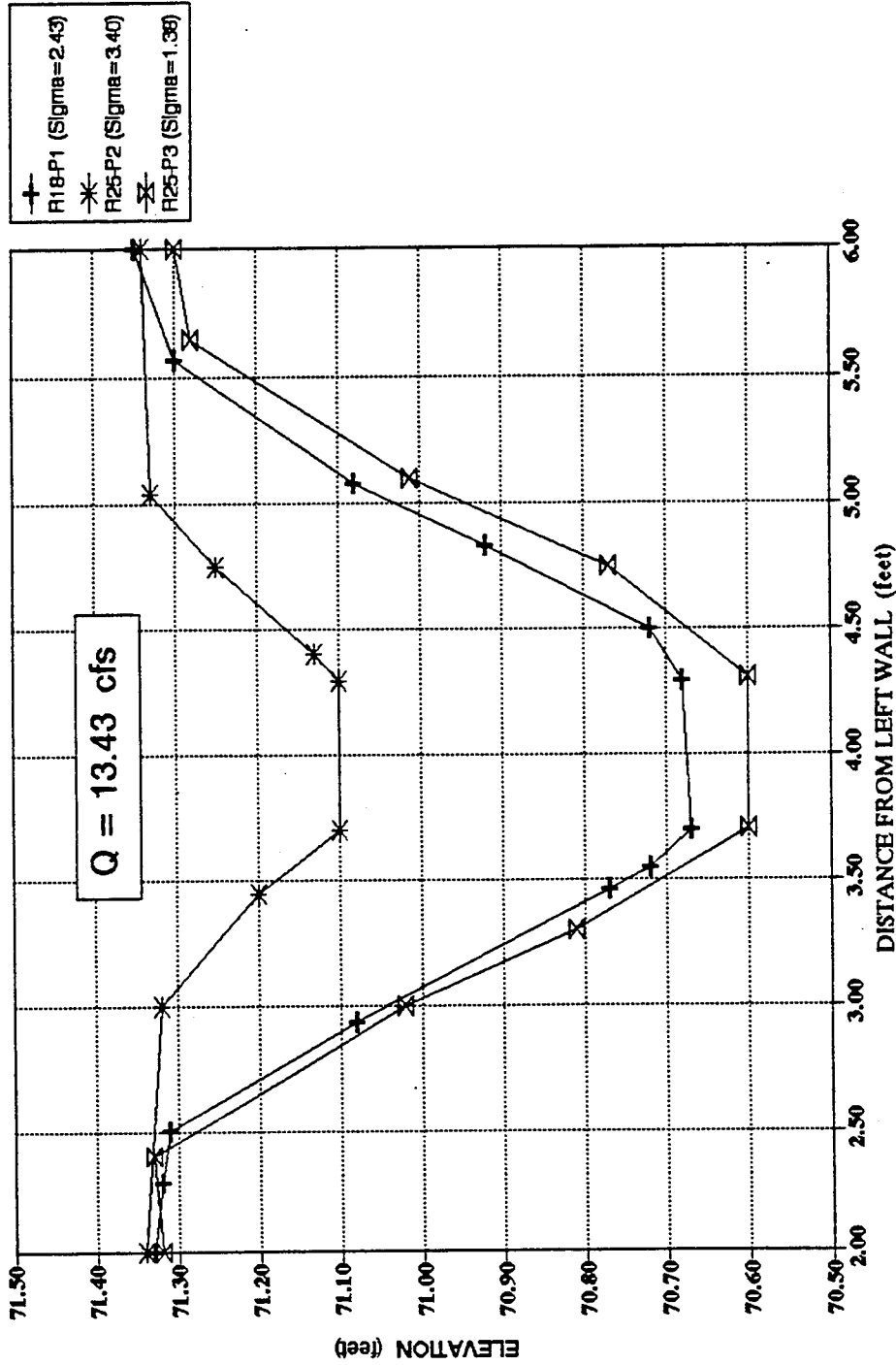


Figure 4.14 Cross Sections Passing through Center Lines of Piers 1, 2 and 3 for Runs 18 and 25 (Q = 13.43 cfs)

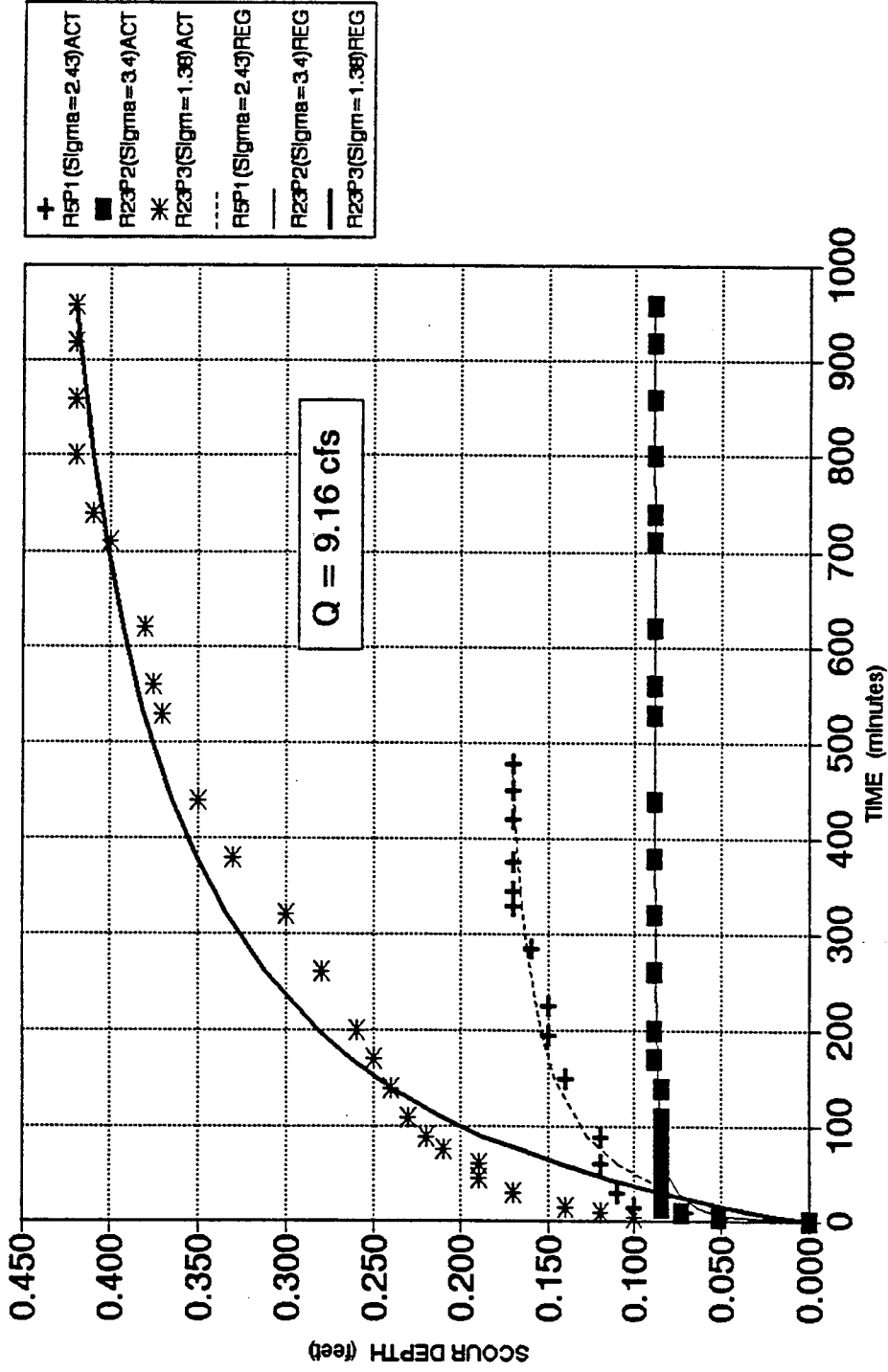


Figure 4.15 Effect of Sediment Gradation on Scour versus Time for $Q = 9.16 \text{ cfs}$

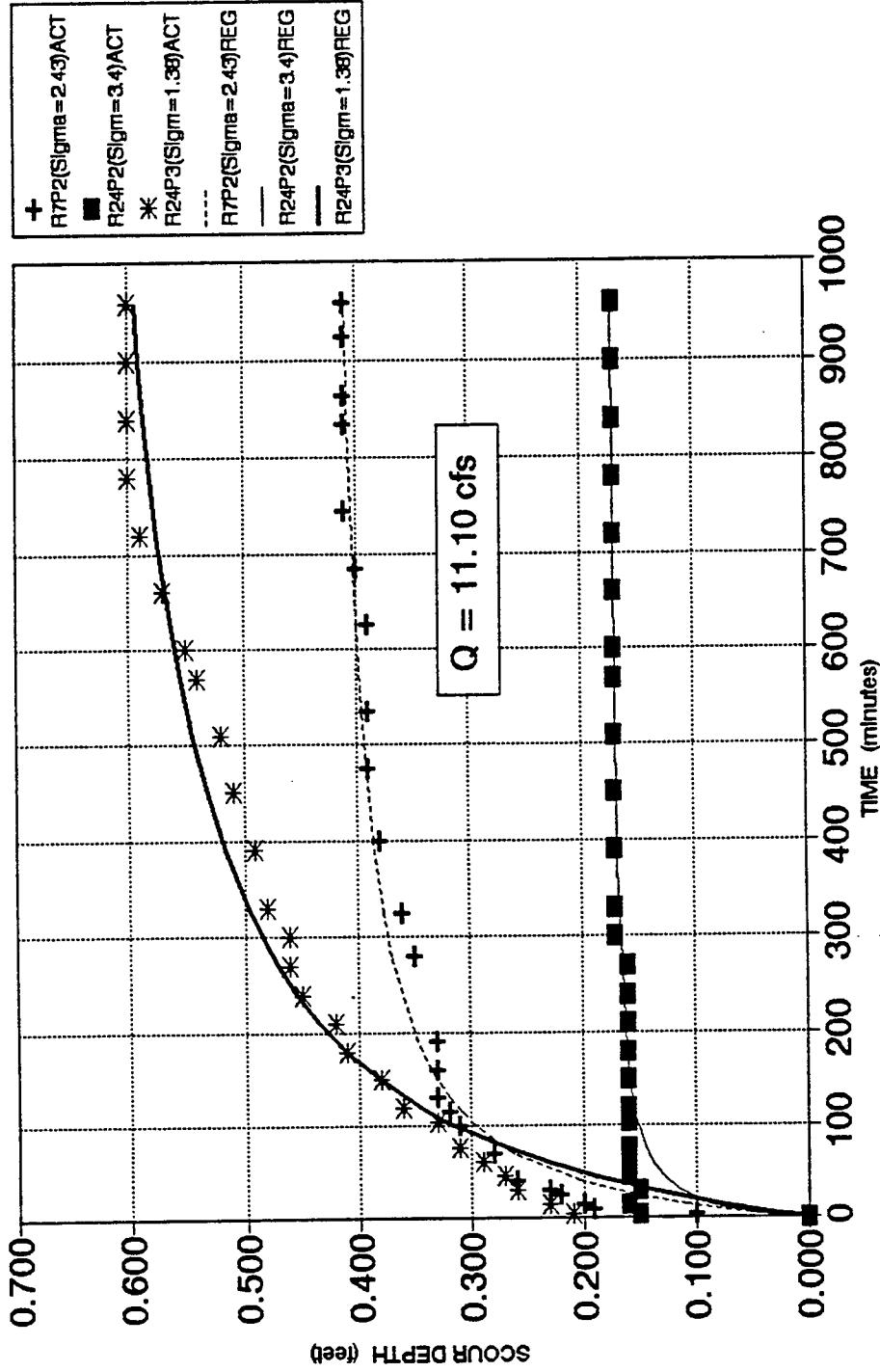


Figure 4.16 Effect of Sediment Gradation on Scour versus Time for Q = 11.10 cfs

to estimate with sufficient reliability the equilibrium scour depth, Y_s . Franzetti et al., (1982) reported that previous experimental test durations ranged from 2 to 8 hours. As shown in Figures 4.15 and 4.16 the equilibrium scour depth was reached in a relatively short time for σ_g of 3.4 and 2.43 compared to that in σ_g of 1.38. This means that the lower the σ_g value, the longer the time it takes to reach equilibrium. The development of scour with time is a process which can be likened to a balancing act between the shear stress applied at the base of the pier and the strength of the bed material represented by its coarse material. At the beginning of scour process, the shear stress is very high and the horseshoe vortex is very strong, so the rate of erosion is greatest. Then the bed begins to armor to protect itself against this eroding action. At this time as the scour hole develops, the horseshoe vortex begins to weaken, the shear stress decreases and equilibrium is reached when the scour depth becomes constant for a sufficient length of time.

4.5.4 Effect of Gradation Coefficient on Armoring Patterns around Bridge Piers

Six sediment mixtures with different gradation coefficients were used as bed materials. One of the mixtures was considered to be uniform ($\sigma_g=1.38$). The other five mixtures were to check the effect of gradation. The mixture with a gradation coefficient of 2.43 was used as bed material around pier 1 during Set No. 2 and around the three piers during Set No. 1. The third mixture with σ_g of 3.4 was used as bed material around pier 2 during Set No. 3 experiments. As shown in Table 3.1 for the

same flow conditions, the scour depth was observed to be lower at higher σ_g values. Figures 4.17 through 4.19 show coarseness of the armor layers resulting from σ_g of 3.4 compared to those resulting from σ_g of 2.43. It is clear that the mean diameter (d_{50}) of the armor layers corresponding to σ_g of 3.4 is larger than that for σ_g of 2.43. This indicates that for larger gradation coefficients reduction in scour depths are expected due to the formation of coarser armor layers.

4.6 Effect of Increasing Coarse Material Fraction on Resulting Scour Depths

Some of the previous studies of local scour during the last two decades studied various aspects of the effect of sediment gradation on the development of local scour, whether in clear-water scour or in live-bed scour regime. But the effect of changing (or increasing) the coarse material fraction above the upper limits that define σ_g (d_{84}) of the sediment mixture on the local scour depth has not been experimentally investigated previously. The concept is to keep the value of σ_g the same by its standard definition while increasing coarser material sizes. Any changes in the scour depth is therefore due to increasing this small fraction above d_{90} , d_{92} , d_{95} or d_{98} size fractions.

In this present study two cases were used to check this effect. During the second set of runs the coarse material fraction above d_{90} and d_{95} for σ_g of 2.43 around piers No.2 and 3 was increased. During third Set of runs around Pier No. 1 the d_{90} size was increased for σ_g of 3.4.

As shown in Table 3.1 scour depth was significantly reduced by increasing the size of a small coarse size fraction while keeping σ_g unchanged. Ettema (1976)

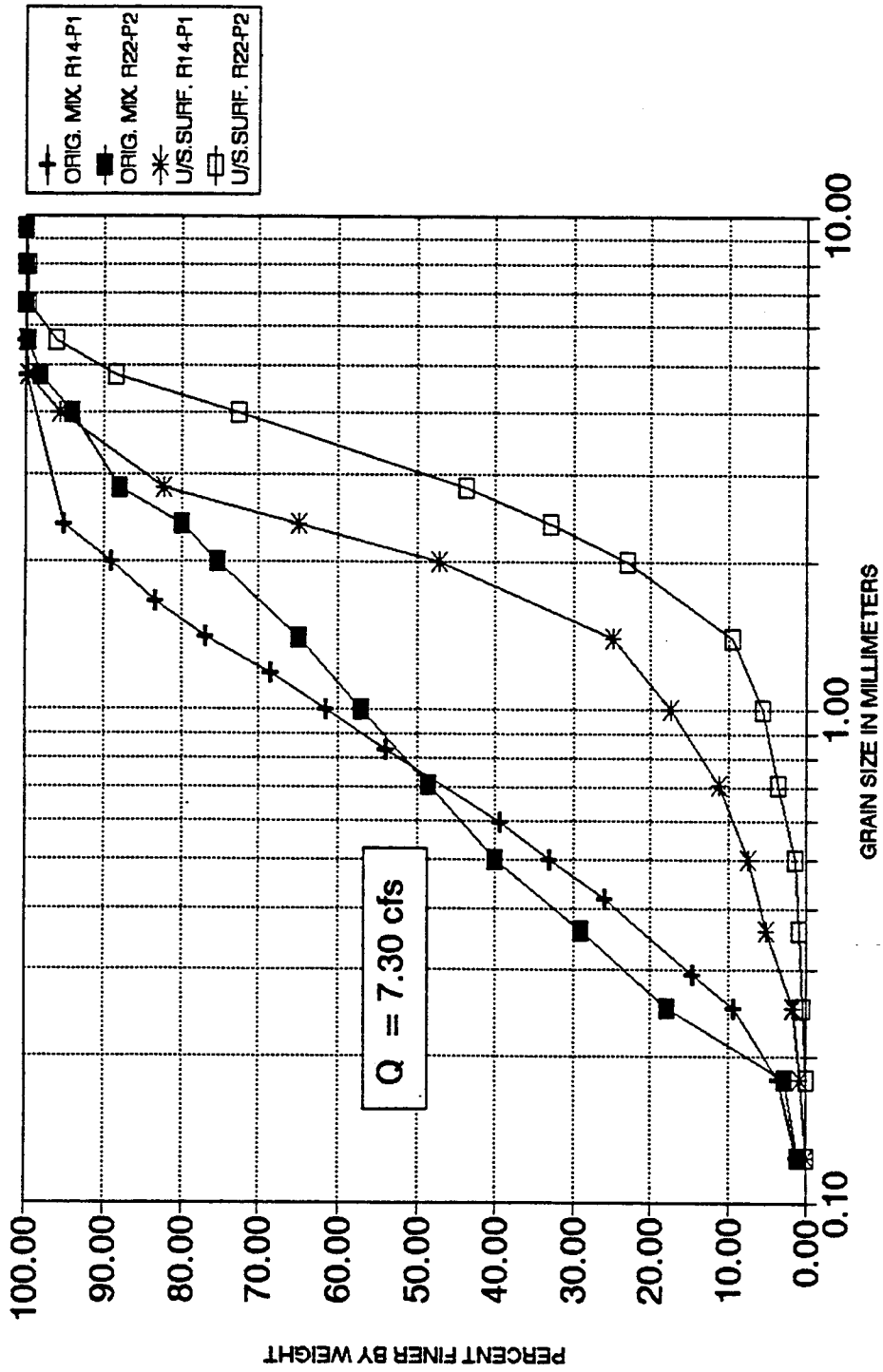


Figure 4.17 Surface Sediment Size Distribution Curves at the Upstream of Piers 1 and 2 for Runs 14 and 22

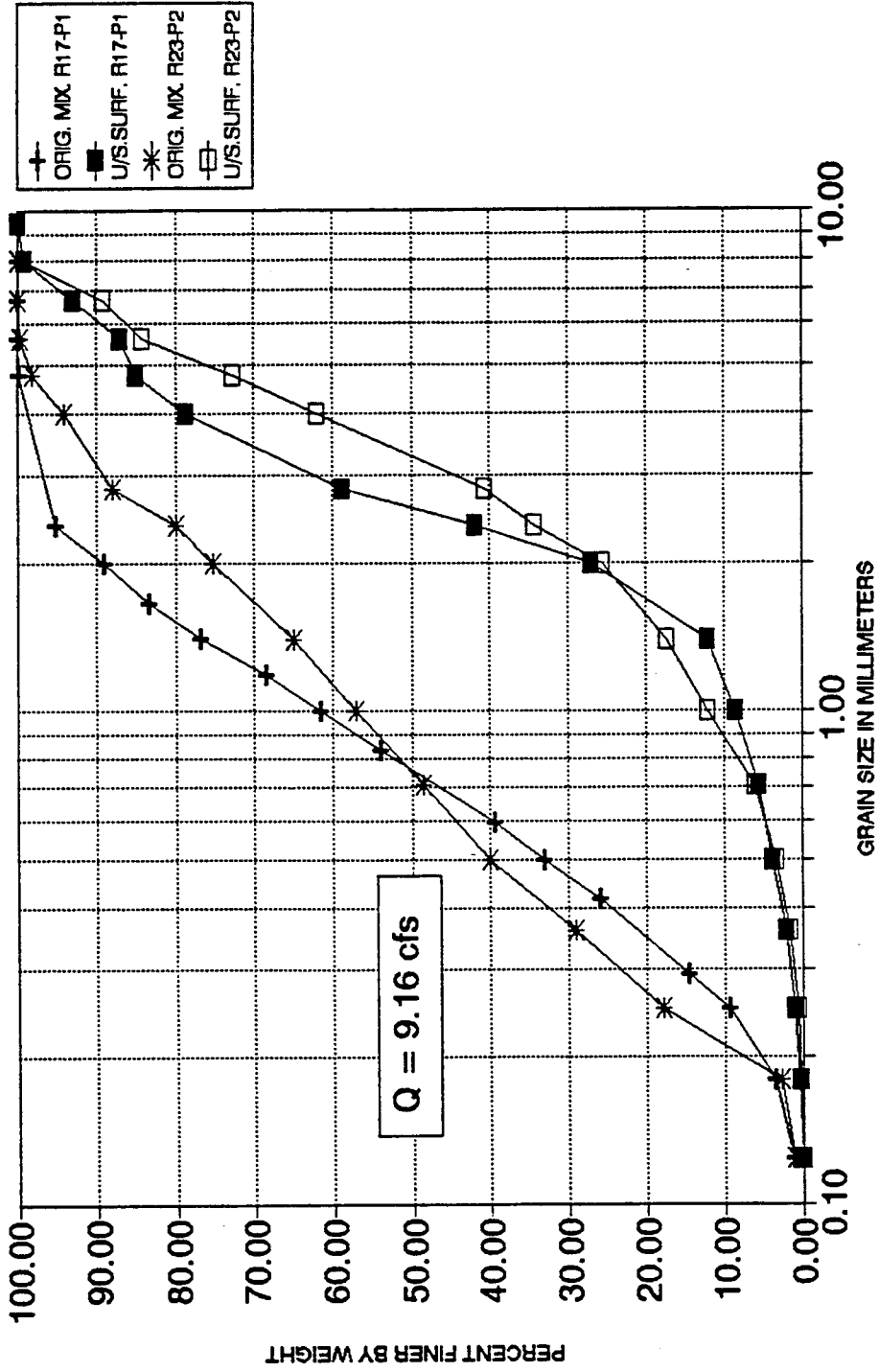


Figure 4.18 Surface Sediment Size Distribution Curves at the Upstream of Piers 1 and 2 for Runs 17 and 23

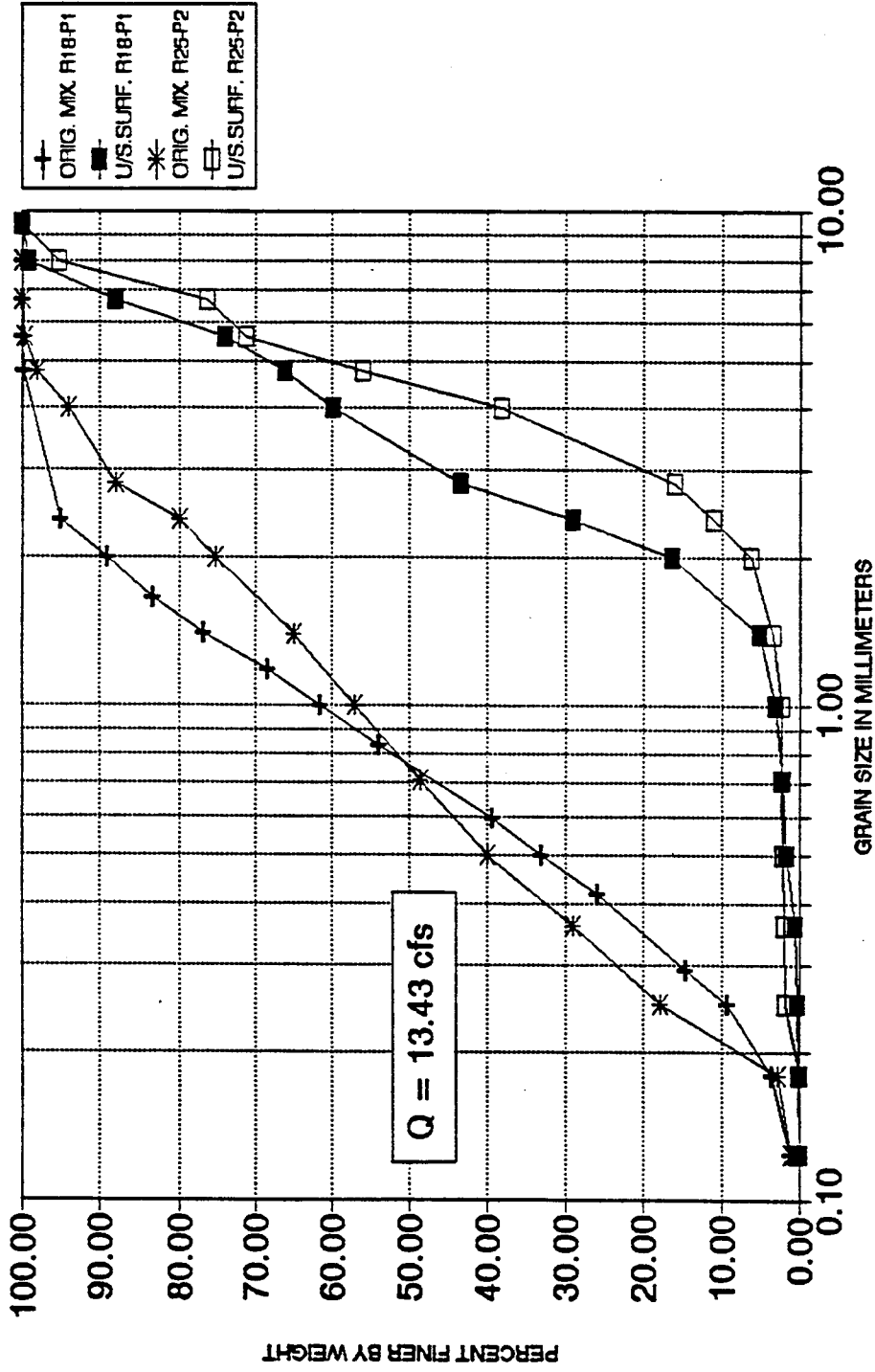


Figure 4.19 Surface Sediment Size Distribution Curves at the Upstream of Piers 1 and 2 for Runs 18 and 25

investigated the effect of sediment gradation on the development of scour depth for clear-water condition and concluded that the scour depths were dramatically reduced due to the effect of sediment gradation. In this work, the dramatic reduction in the scour depth has been observed due to increasing the coarse material fraction above the limits that define σ_g in the sediment mixture while keeping the value of σ_g constant. It has been noted in these experiments that coarse material fraction (the upper 10%) is a more significant parameter than σ_g in describing the reduction of the scour depth around bridge piers.

The volume of a scour hole (the inverted cone) is reduced due to the significant reduction in the depth and width of the scour hole. The time development of scour depth was also reduced significantly. This reflects the strong effect of the coarser armor layer formation in comparison to the armor layer formation due σ_g alone.

4.6.1 Scour Depth as a Function of Froude Number

As pointed out in the previous section, increasing σ_g values reduces the scour depth. Taking into account the effect of increasing the size of a coarser fraction, it can be said that the higher the percent of increasing the coarse material fraction, the greater the reduction in the scour depth. The results are shown in Figures 4.20 and 4.21. Figure 4.20 demonstrated that for σ_g of 2.43 when the sediment size for the upper limits above d_{90} and d_{95} were increased the scour depth is reduced. For σ_g of 3.4 only the effect of increasing the limits above d_{90} was checked. For this case too there was a reduction in the scour depth due to increasing coarser fraction above d_{90} . Figures

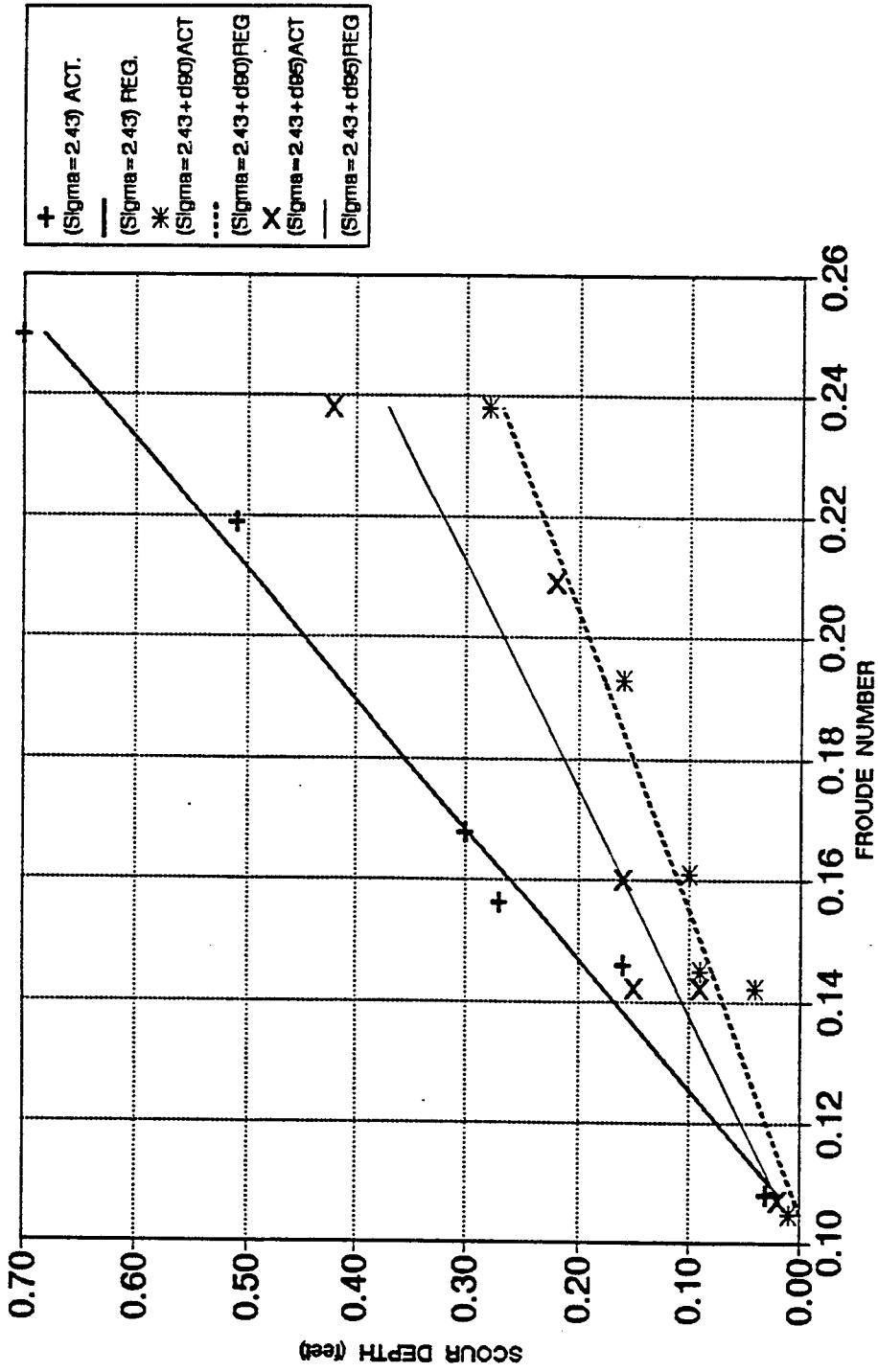


Figure 4.20 Effect of Increasing d_{90} and d_{95} on Scour Depth ($\sigma_g = 2.43$)

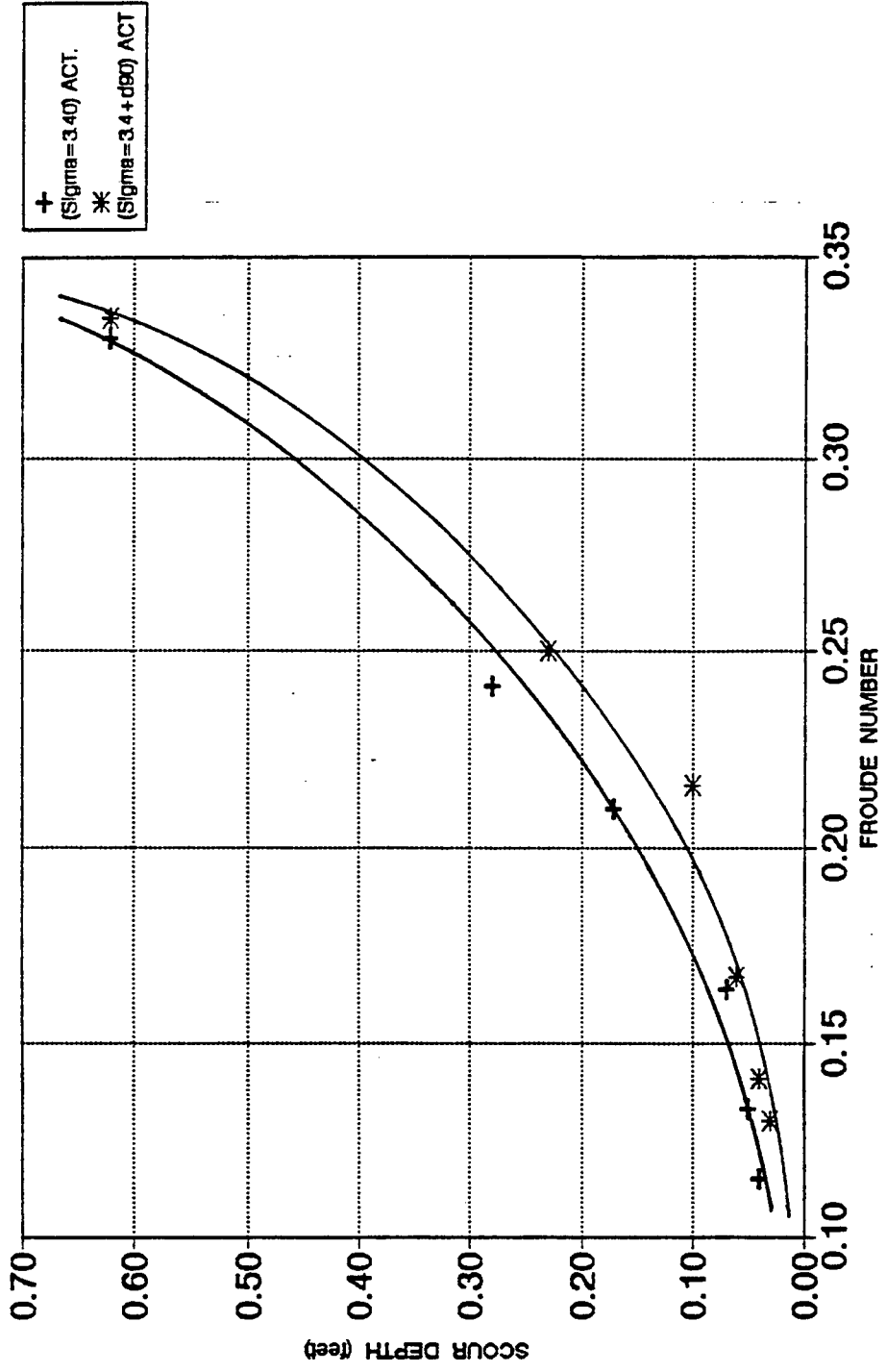


Figure 4.21 Effect of Increasing d_{90} on Scour Depth ($\sigma_g = 3.40$)

4.20 and 4.21 show that the percent of reduction in scour depth taking into account the effect of larger d_{90} is higher for σ_g of 2.43 than that for σ_g of 3.4.

4.6.2 Scour Profile Along Cross-Sections

When the effect of increasing d_{90} size is considered and comparisons with the scour resulting from the original σ_g of 2.43 is made. It is obvious from Figures 4.22 through 4.24 that the scour profile is reduced significantly for the same flow conditions. Conclusions from the case of σ_g of 2.43 are also valid for σ_g of 3.4 as shown in Figures 4.25 through 4.27 for the same flow conditions of $Q=9.16, 11.10$ and 13.40 cfs. A reduction in the scour hole dimensions are also observed. One interpretation is that coarse material fraction in the sediment mixture, when it is increased, can limit the scour depth and consequently the scoured volume.

4.6.3 Time Development of Scour Depth to Account for the Effect of Increasing Coarse Material Fraction

The conclusions for the effect of increasing the gradation coefficient on the development of scour depth are also valid for increasing d_{90} or d_{95} sizes in the two cases studied in this dissertation. For σ_g of 2.43, in Figures 4.28 through 4.30, the scour depth development is affected by the increase of the size of a small percentage of coarse material. A reduction in the scour depth with elapsed time can be observed when increasing the d_{95} and d_{90} sizes from their original sizes corresponding to σ_g of 2.43. The main reason for this reduction is that the coarse particles forming the armor layer

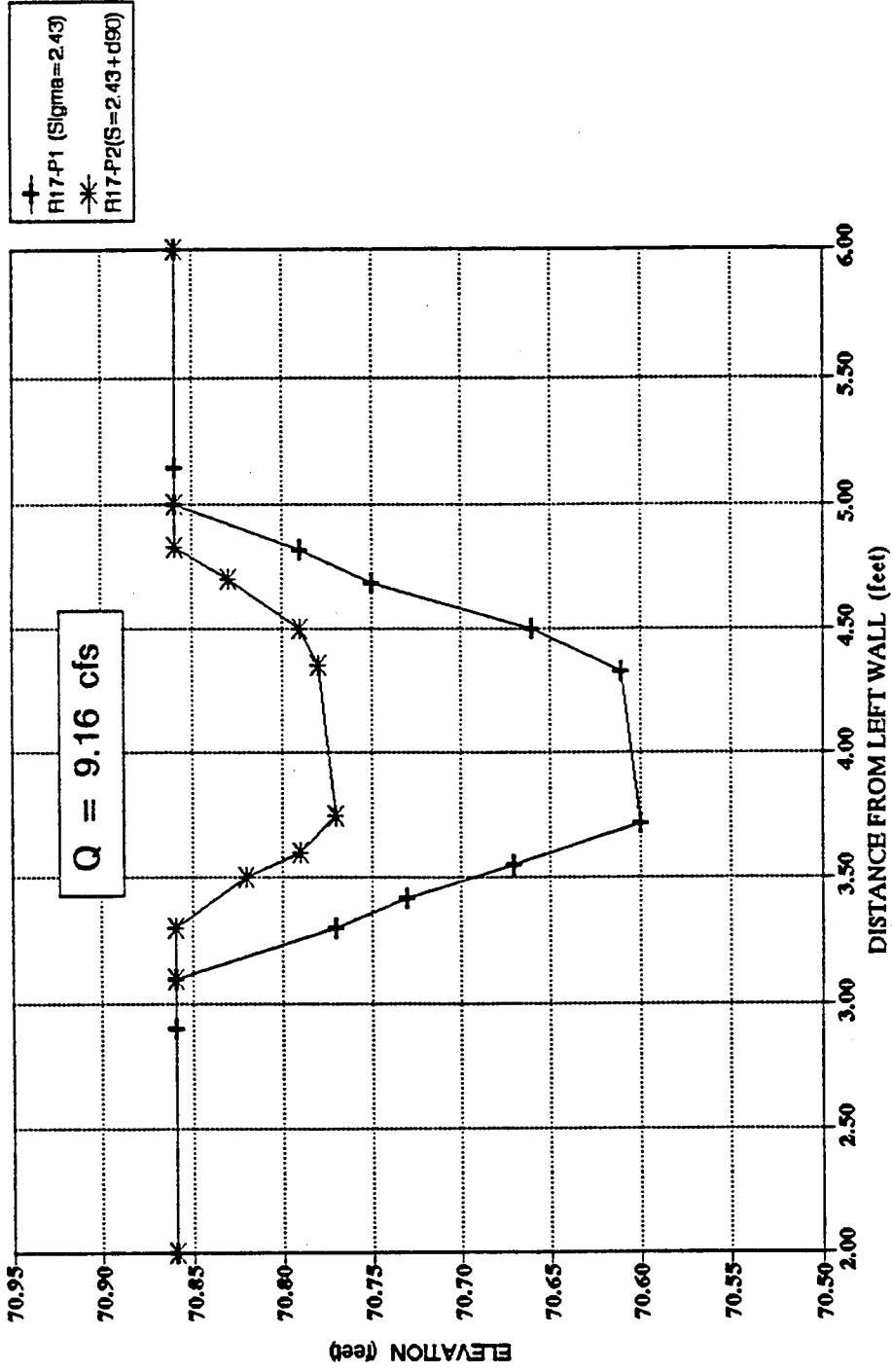


Figure 4.22 Cross Sections Passing through Center Lines of Piers 1 and 2 for Run 17 ($Q = 9.16$ cfs)

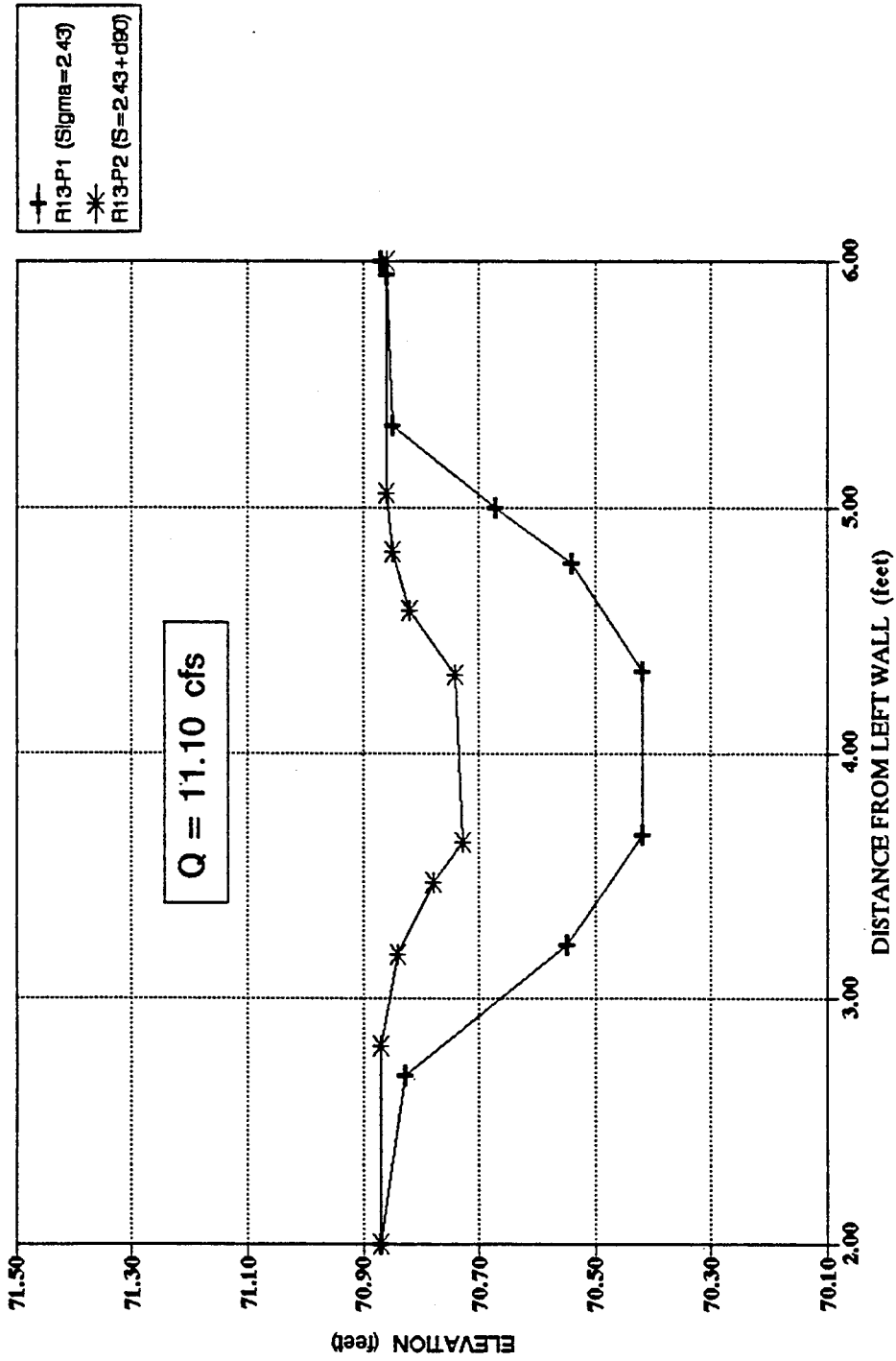


Figure 4.23 Cross Sections Passing through Center Lines of Piers 1 and 2 for Run 13 (Q = 11.10 cfs)

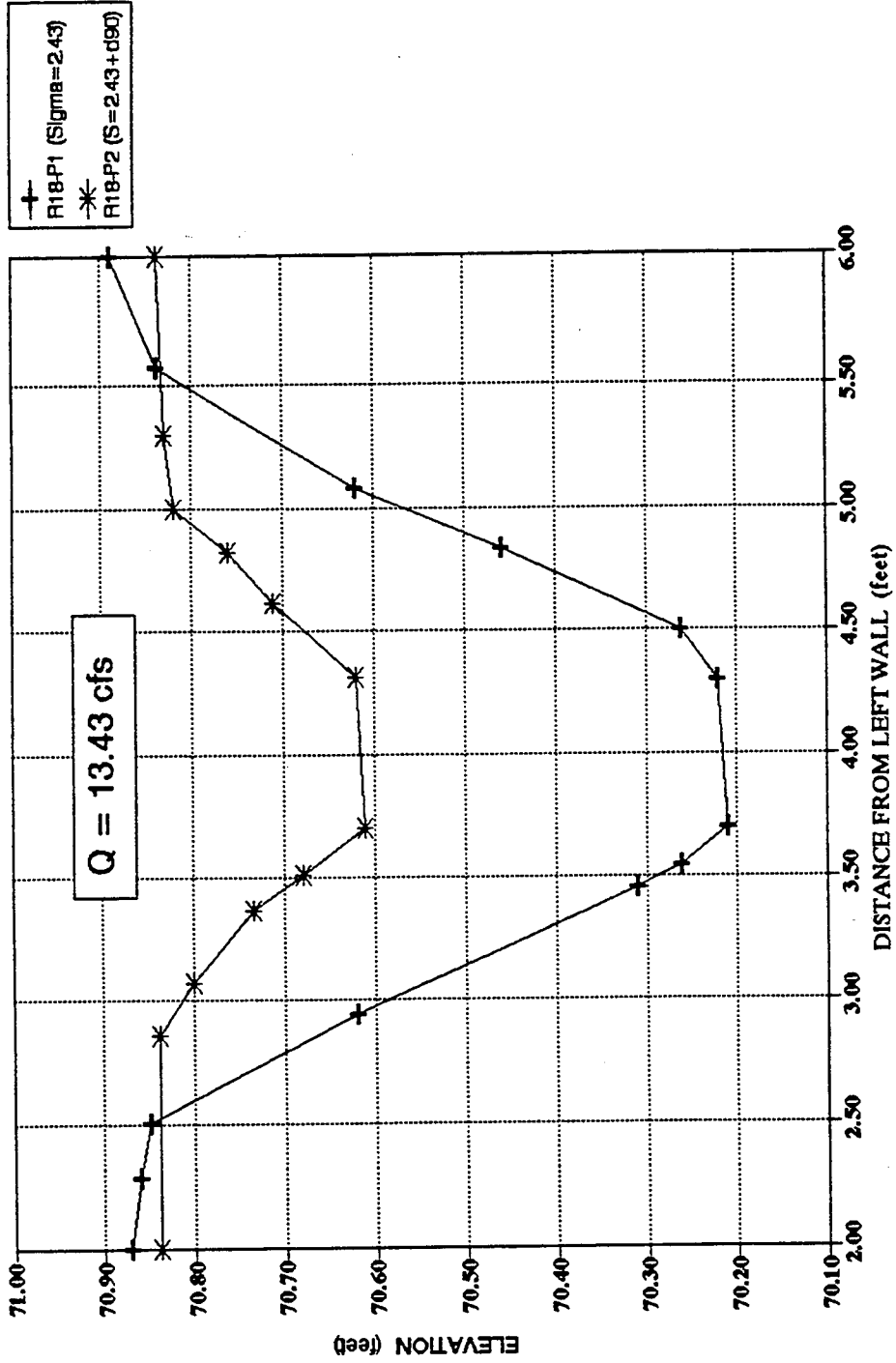


Figure 4.24 Cross Sections Passing through Center Lines of Piers 1 and 2 for Run 18 (Q = 13.43 cfs)

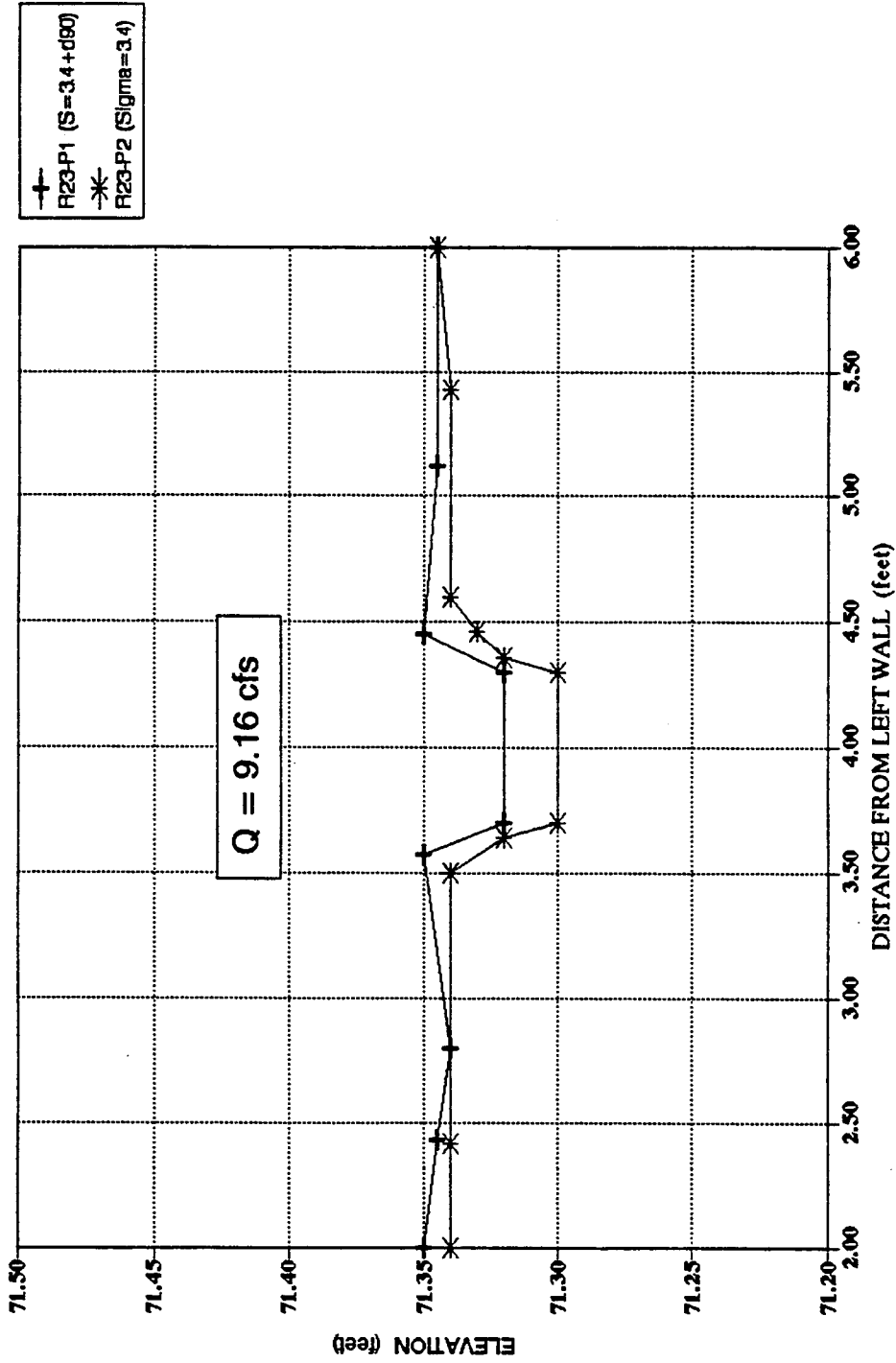


Figure 4.25 Cross Sections Passing through Center Lines of Piers 1 and 2 for Run 23 (Q = 9.16 cfs)

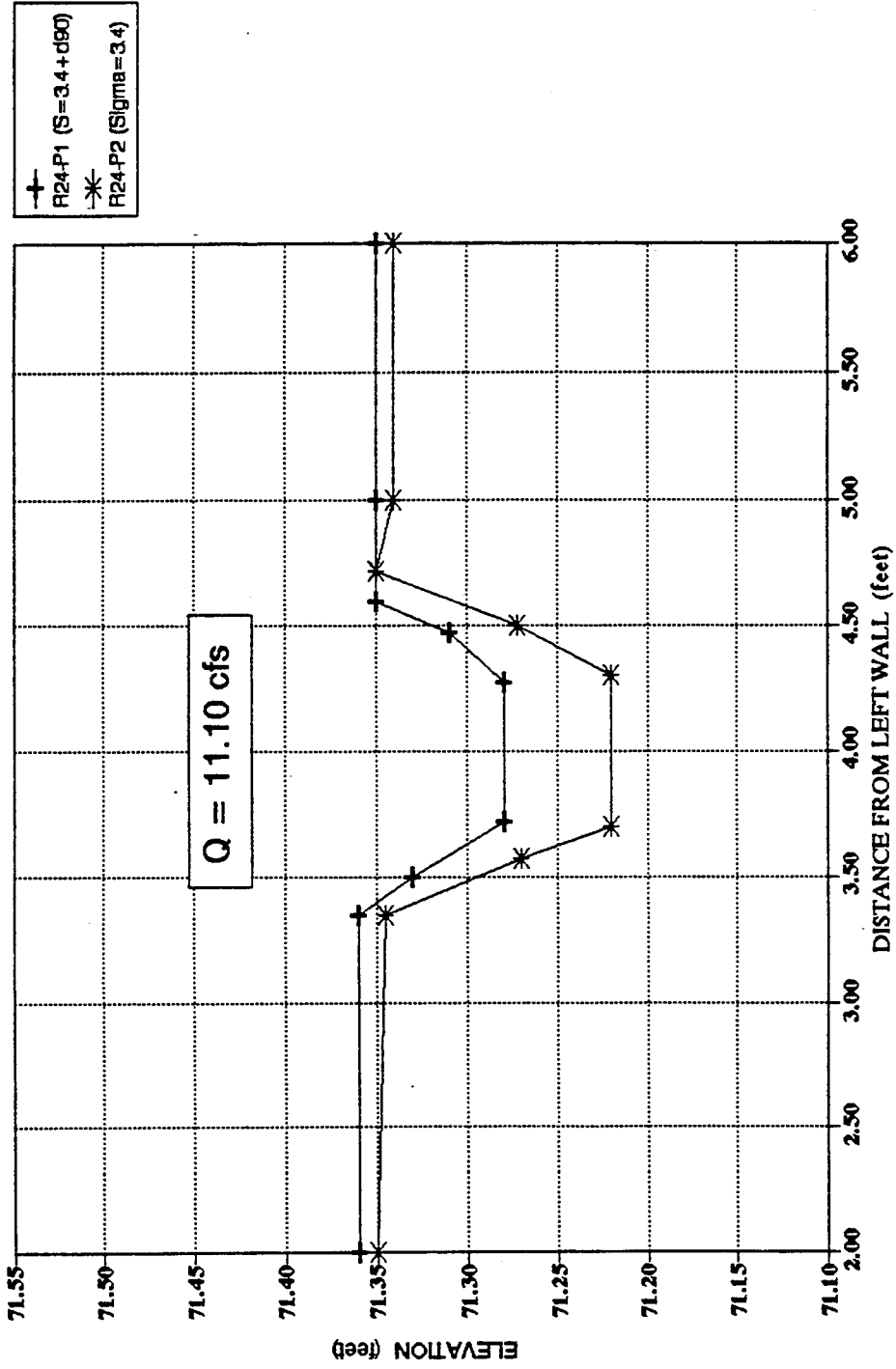


Figure 4.26 Cross Sections Passing through Center Lines of Piers 1 and 2 for Run 24 (Q = 11.10 cfs)

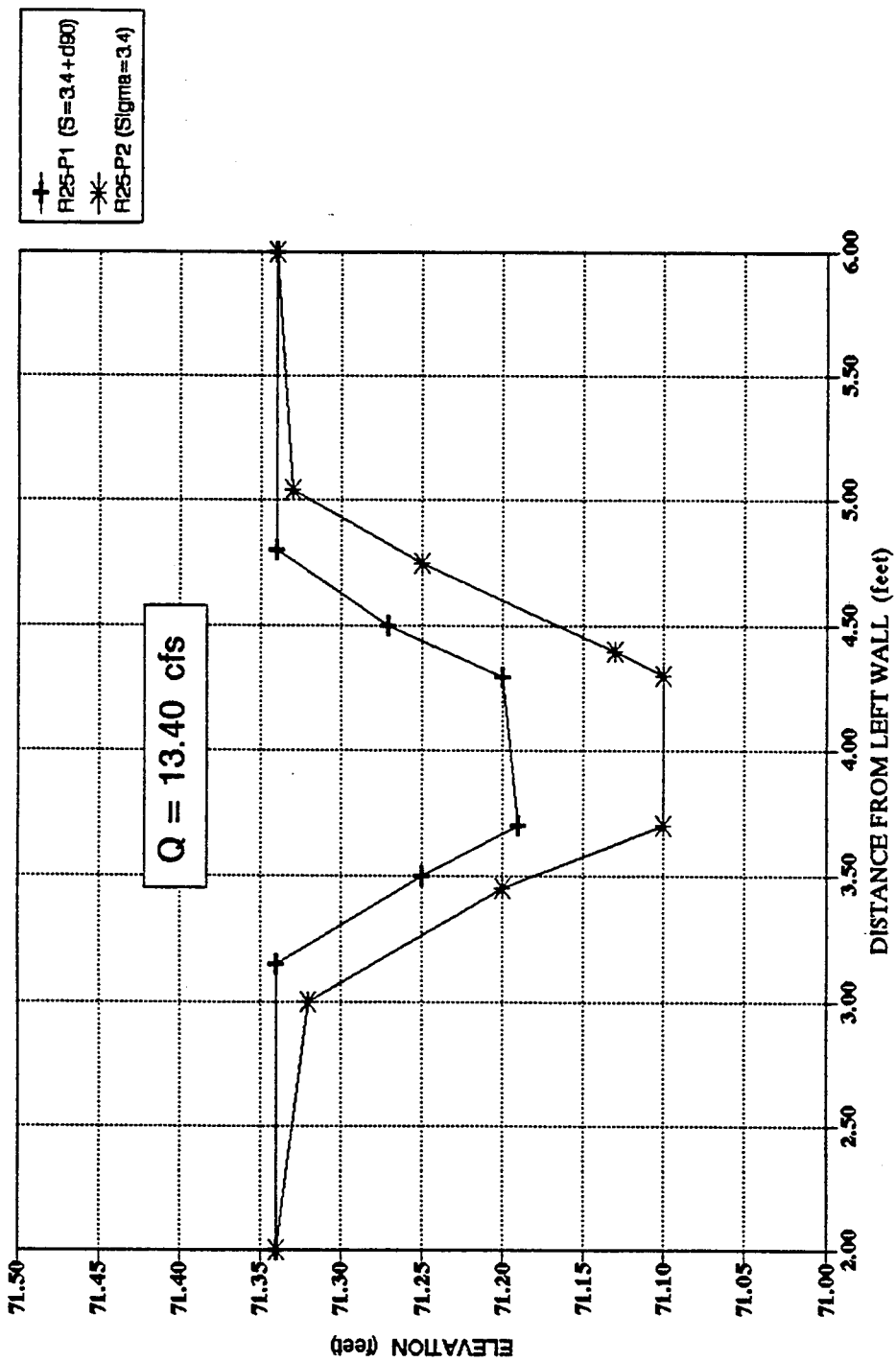


Figure 4.27 Cross Sections Passing through Center Lines of Piers 1 and 2 for Run 25 (Q = 13.40 cfs)

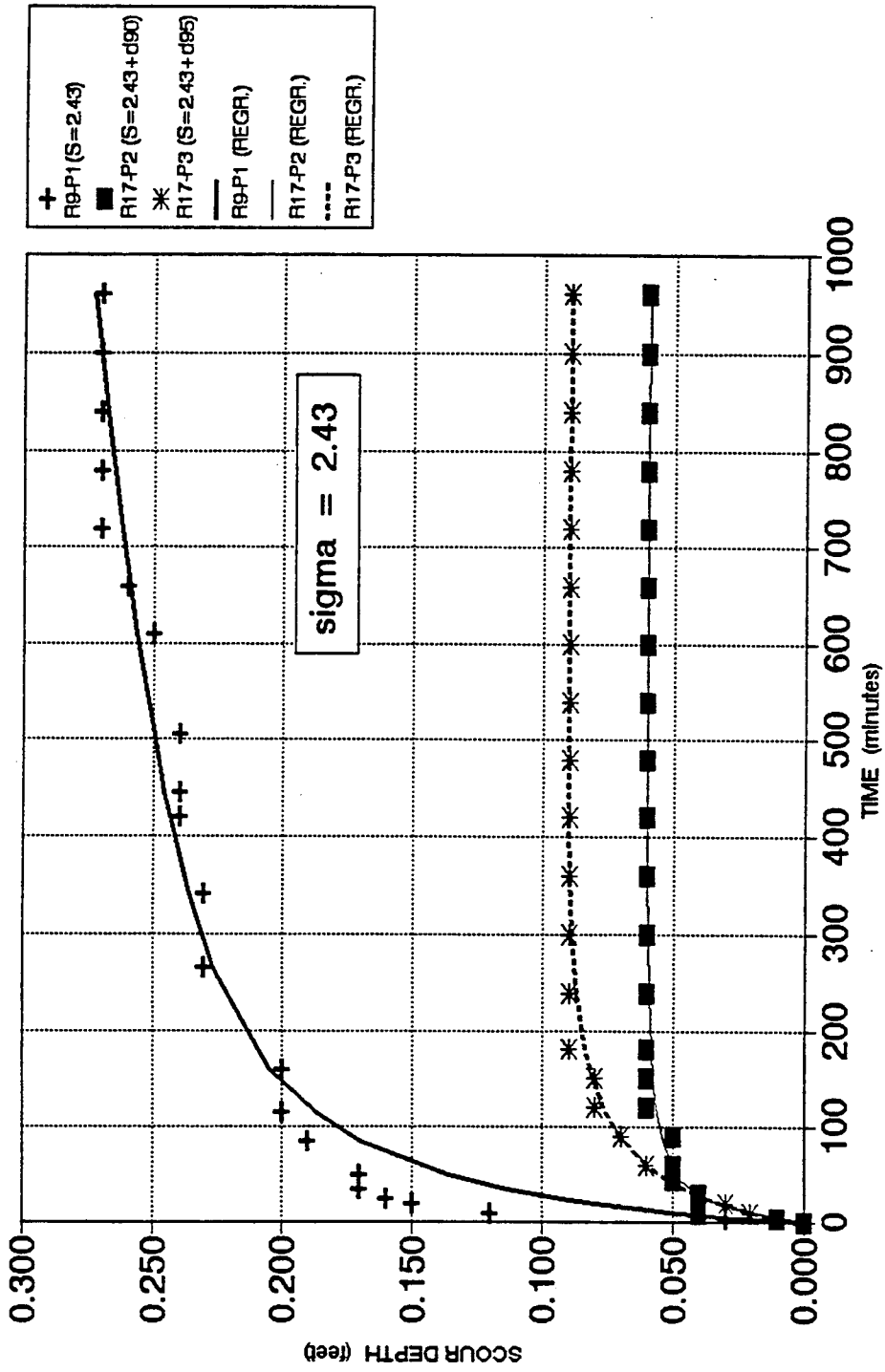


Figure 4.28 Effect of Coarse Material Fraction on Scour versus Time (Q = 9.19 cfs)

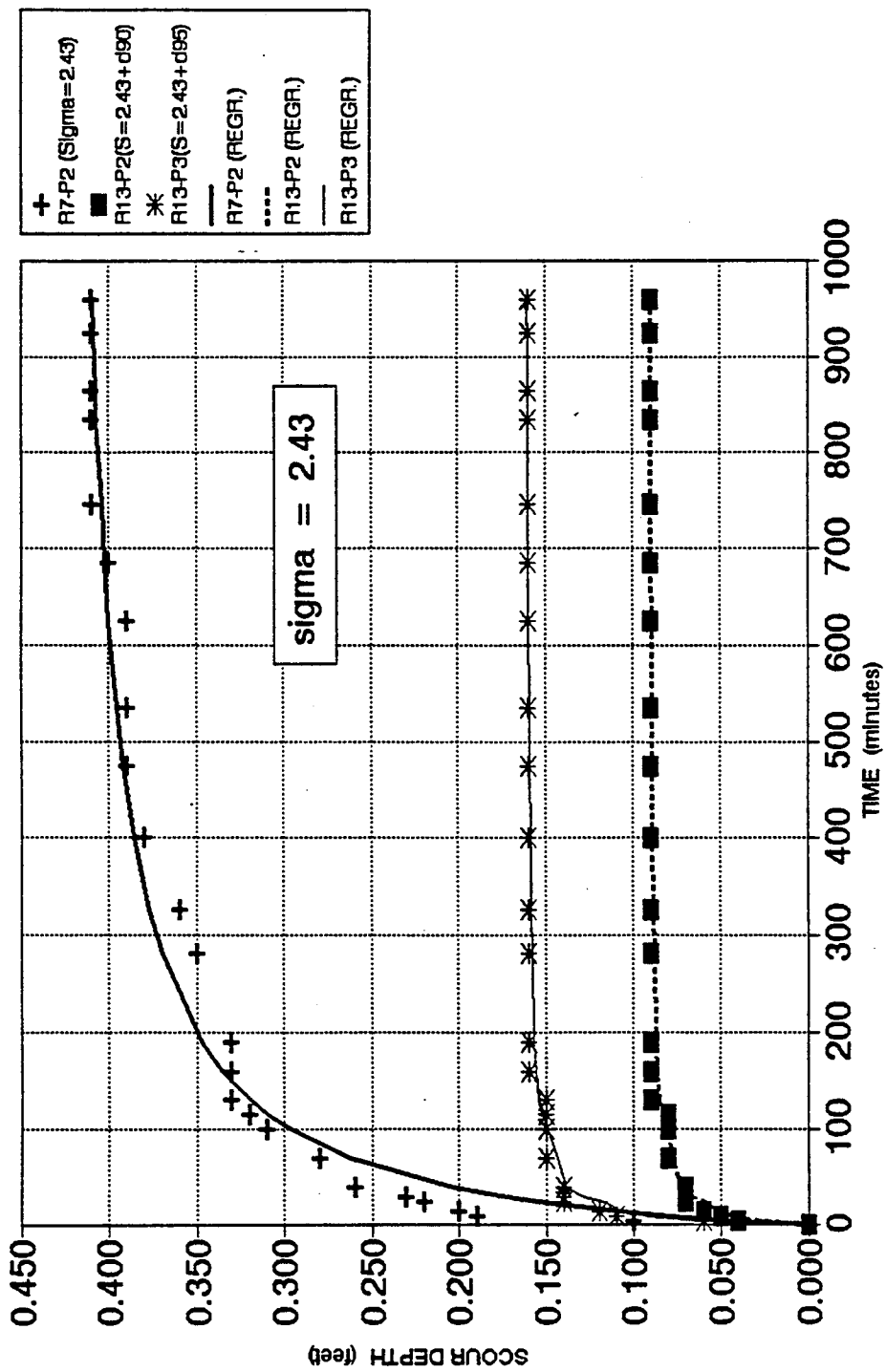


Figure 4.29 Effect of Coarse Material Fraction on Scour versus Time (Q = 11.10 cfs)

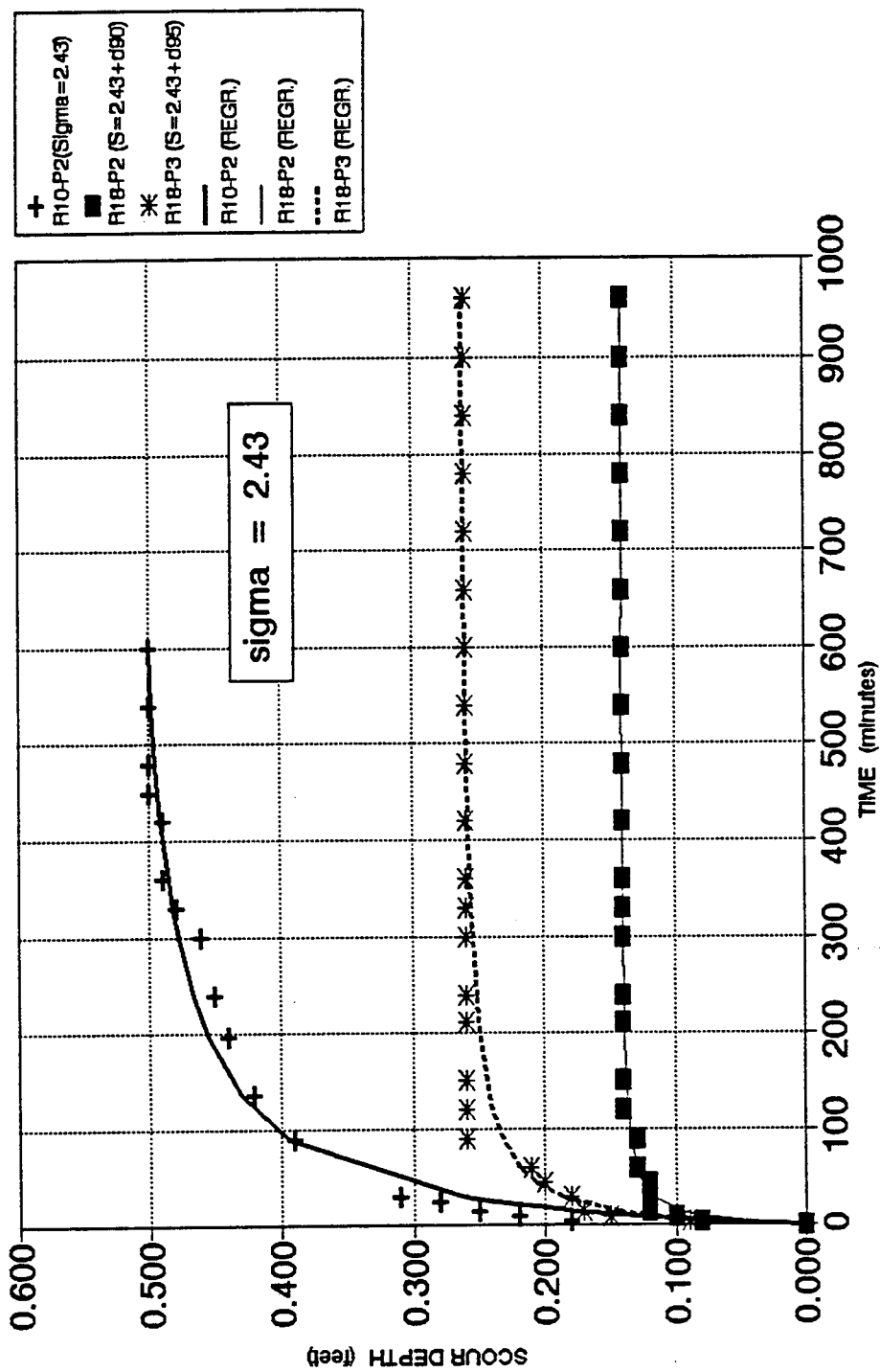


Figure 4.30 Effect of Coarse Material Fraction on Scour versus Time (Q = 13.43 cfs)

around bridge piers resist the scour phenomena and cause the equilibrium scour depth to be reached faster for larger d_{90} than that for larger d_{95} and the latter being faster than the case of the original mixture of σ_g of 2.43.

For the case of σ_g of 3.4, since the original mixture is coarser than in the mixture with σ_g of 2.43, the rate of reduction of scour depth with time is less and the equilibrium is reached very rapidly when size of the fraction of sediment mixture above d_{90} is increased. Figures 4.31 through 4.33 show that the time development of scour depth will be less when d_{90} size is increased and the equilibrium is reached in a shorter time than that for σ_g of 3.4.

4.6.4 Conclusions from the Time Development of Scour Depth

From this study, it was concluded that development of scour depth with time is highly affected by the gradation of bed material at the site of the pier. When σ_g , the non-uniformity coefficient, was equal to 3.4, it was noticed that 80-90% of the equilibrium scour depth is reached in the first 1 to 2 hours, while the same percentage requires the first 4-5 hours when $\sigma_g=2.43$, and from 5 to 10 hours when $\sigma_g=1.38$. Experiments were run for 16 hours to be sure that the final scour depth or the equilibrium depth was reached and also to establish the final bed geometry around each pier.

Depending on the original gradation of the sediment mixture, when increasing the coarse material fraction above d_{90} and d_{95} , it was observed that 80-90% of the equilibrium scour depth was reached in the first 1 to 3 hours. The percentage of

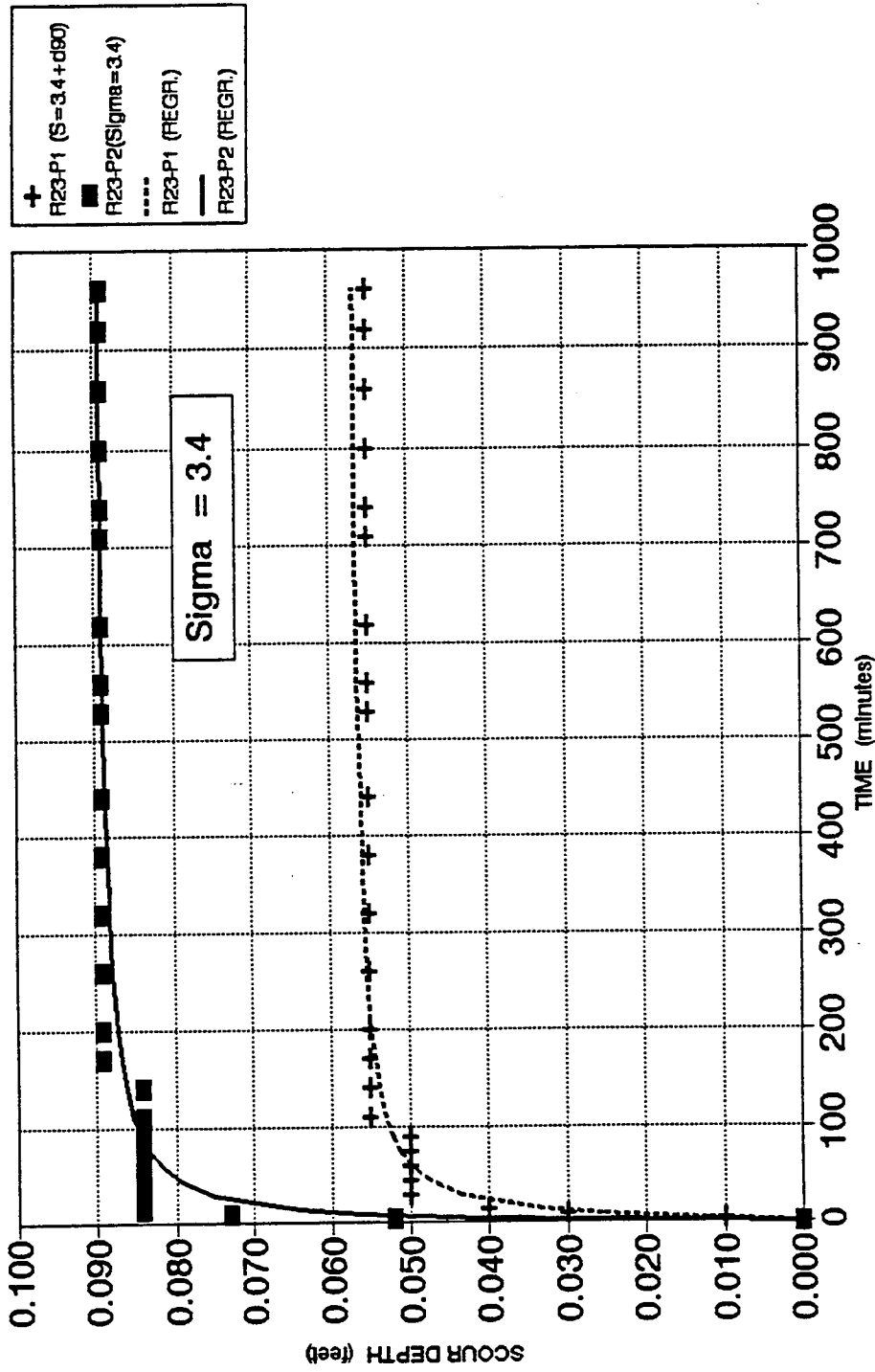


Figure 4.31 Effect of Coarse Material Fraction on Scour versus Time (Q = 9.16 cfs)

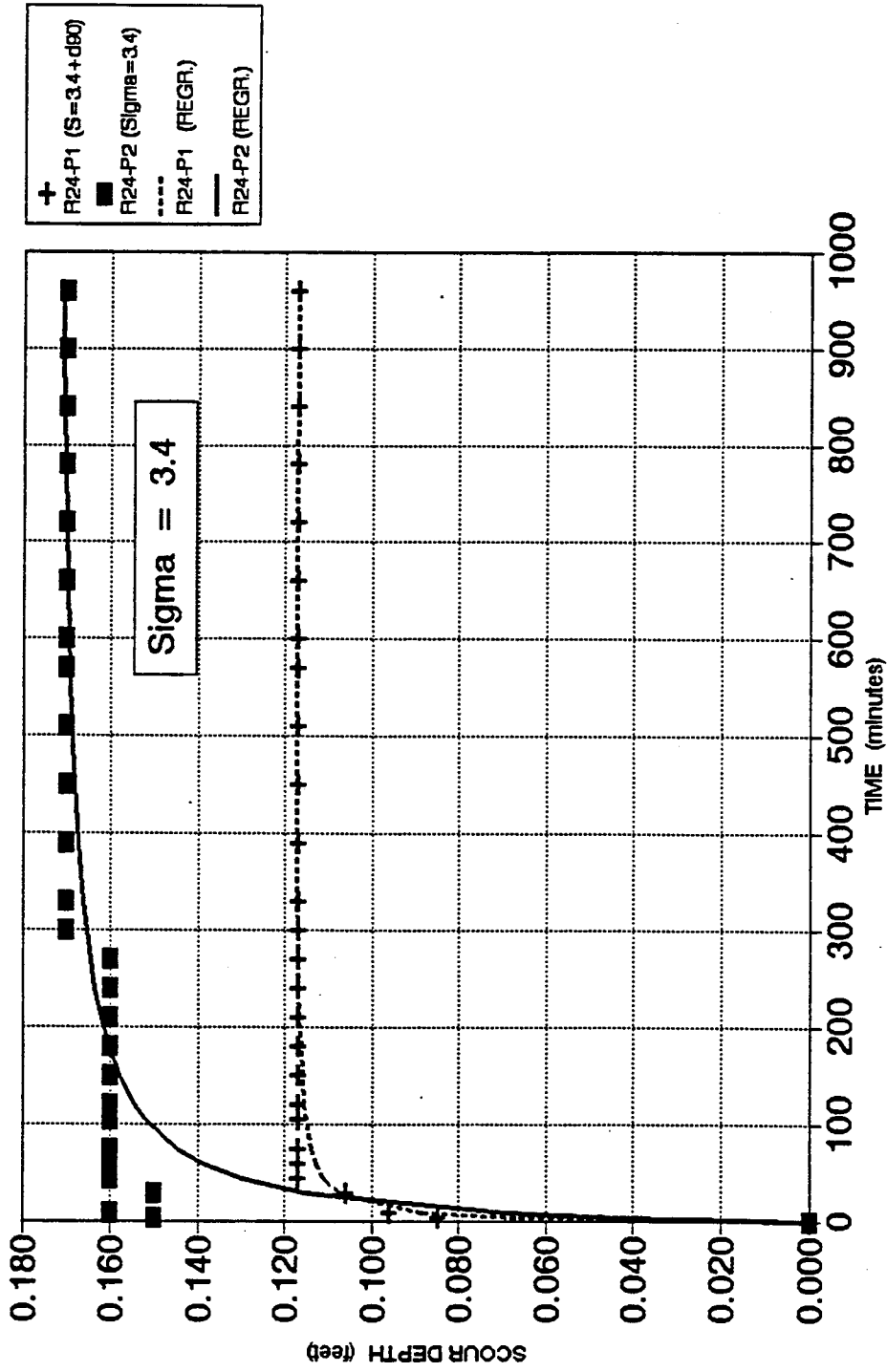


Figure 4.32 Effect of Coarse Material Fraction on Scour versus Time (Q = 11.10 cfs)

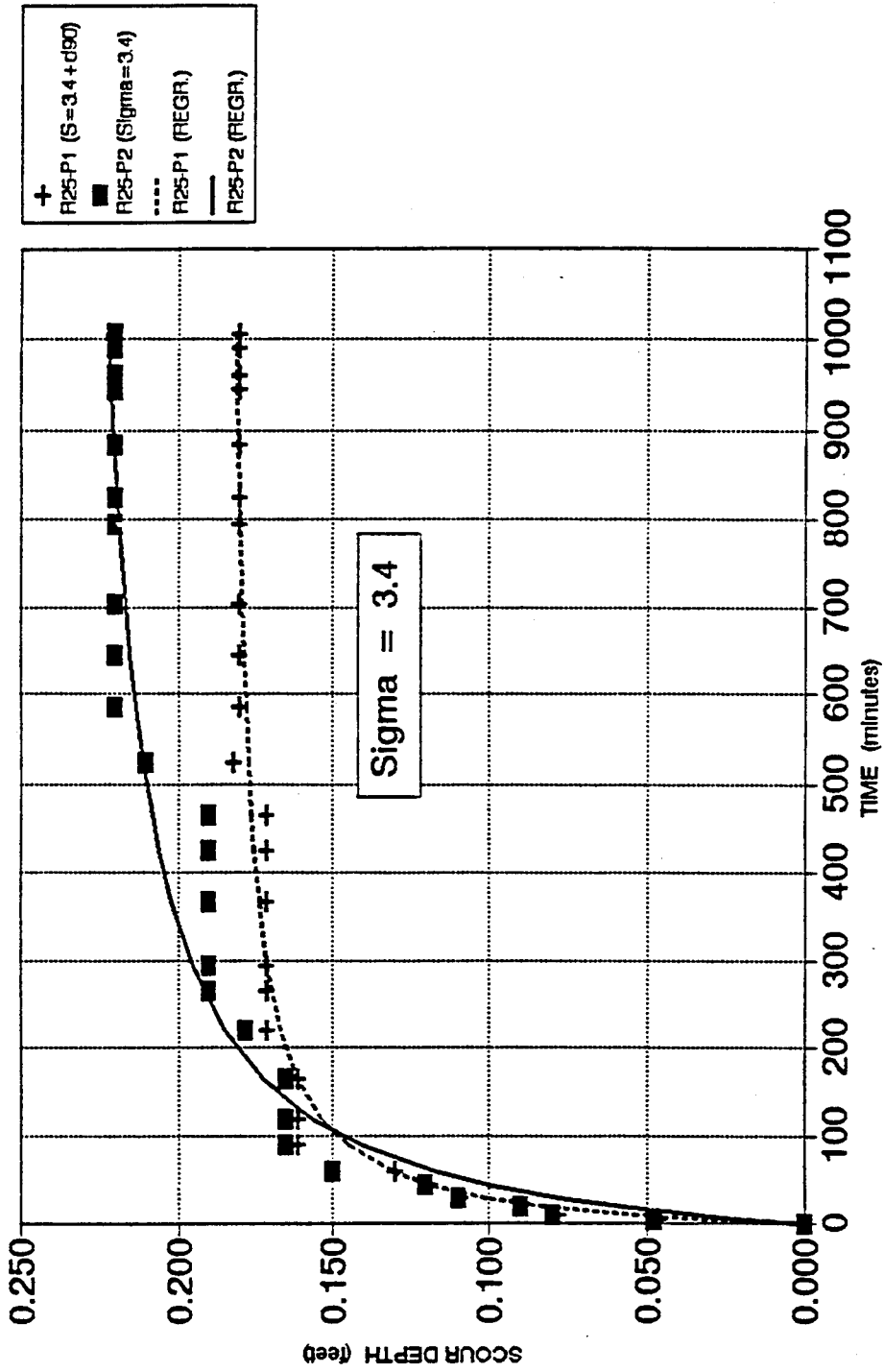


Figure 4.33 Effect of Coarse Material Fraction on Scour versus Time (Q = 13.40 cfs)

increasing the coarse fraction, i.e. the case of σ_g of 2.43 when increasing its d_{90} can be simulated by $\sigma_g=3.4$. The function of the coarser materials in a mixture against the erosion or scouring power of the stream is to resist it and to balance the erosive forces. The large particles in a mixture form a ring around the piers to stop the development of deeper scour holes and stabilize the bed.

4.6.5 Effect of Increasing Coarse Material Fraction on Armoring Patterns

This effect was studied through runs for Sets No. 2 and 3. During Set No. 2 experiments a significant reduction in scour depths at pier 2 as well as at pier 3 was observed due to increasing d_{90} and d_{95} sizes, respectively. Figure 4.34 presents an example to show armoring pattern around the piers during Set 2 for a discharge of 13.43 cfs to show the effects of increasing d_{90} and d_{95} . It is clear that increasing the size of this small sediment fraction reduces the scour depth dramatically due to the formation of the coarse armor layers and this coarseness increases with the increase of the coarse material fraction percentage. Table 3.1 shows the dramatic change in scour depth from Pier 1 to Pier 3 to Pier 2 during Set No. 2 and from Pier 2 to Pier 1 during Set No. 3 to reflect the increase in d_{95} and d_{90} sizes.

4.7 Comparison between Scour Depths for Sediment Mixture with σ_g of 2.43 Enriched d_{90} and Mixtures with σ_g of 3.4

The concept of increasing the coarse material fraction in the sediment mixture provided encouraging results and caused a dramatic reduction in scour depths when

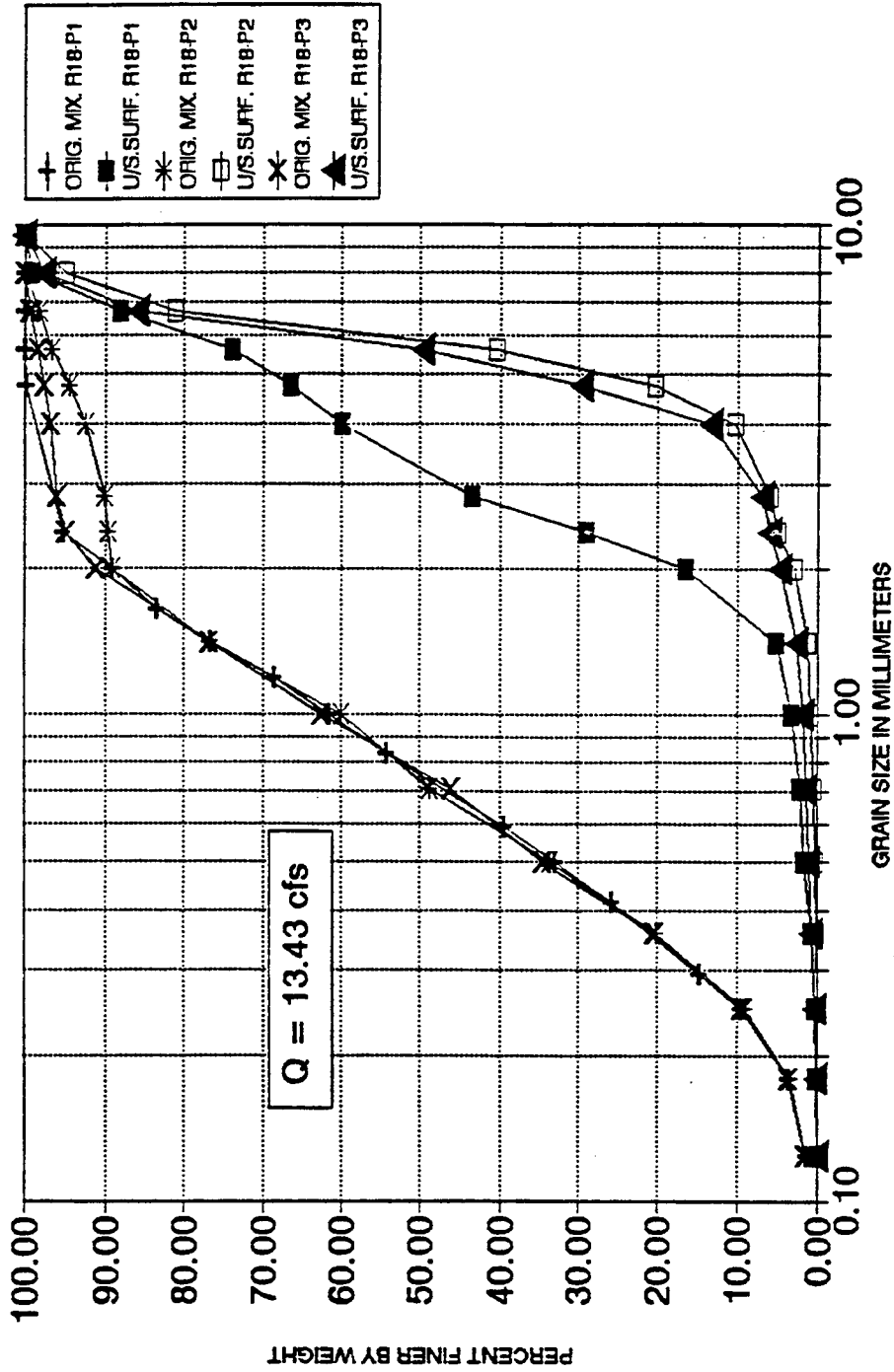


Figure 4.34 Surface Sediment Size Distribution Curves at the Upstream of Piers 1, 2 and 3 for Run 18

compared to the effect with original σ_g of 2.43 and 3.4. Scour depths resulting for bed material with a lower σ_g value of 2.43 were compared with those resulting at bed materials with higher σ_g when the lower σ_g value was strengthened by increasing the fraction above d_{90} .

This comparison was achieved for runs that have almost the same flow conditions, Table 4.2. The scour depths for σ_g of 2.43 when its d_{90} is enriched were almost the same and in some cases less than that for σ_g of 3.4. The coarse material fraction above the upper limits that define σ_g has a stronger effect on reducing scour depths than the effect of σ_g value itself. Figure 4.35 shows this very clearly, for the presented flow conditions that were available from this study, the scour depths were almost the same or sometimes less for σ_g of 2.43 with d_{90} enriched which means that the effect of coarse fraction in resisting scouring action and preventing it to continue for deeper depths is more effective than the effect of σ_g itself. Next, we will consider how the armoring patterns in both cases look like, the development of scour with time and shape of cross section for scour holes in both cases.

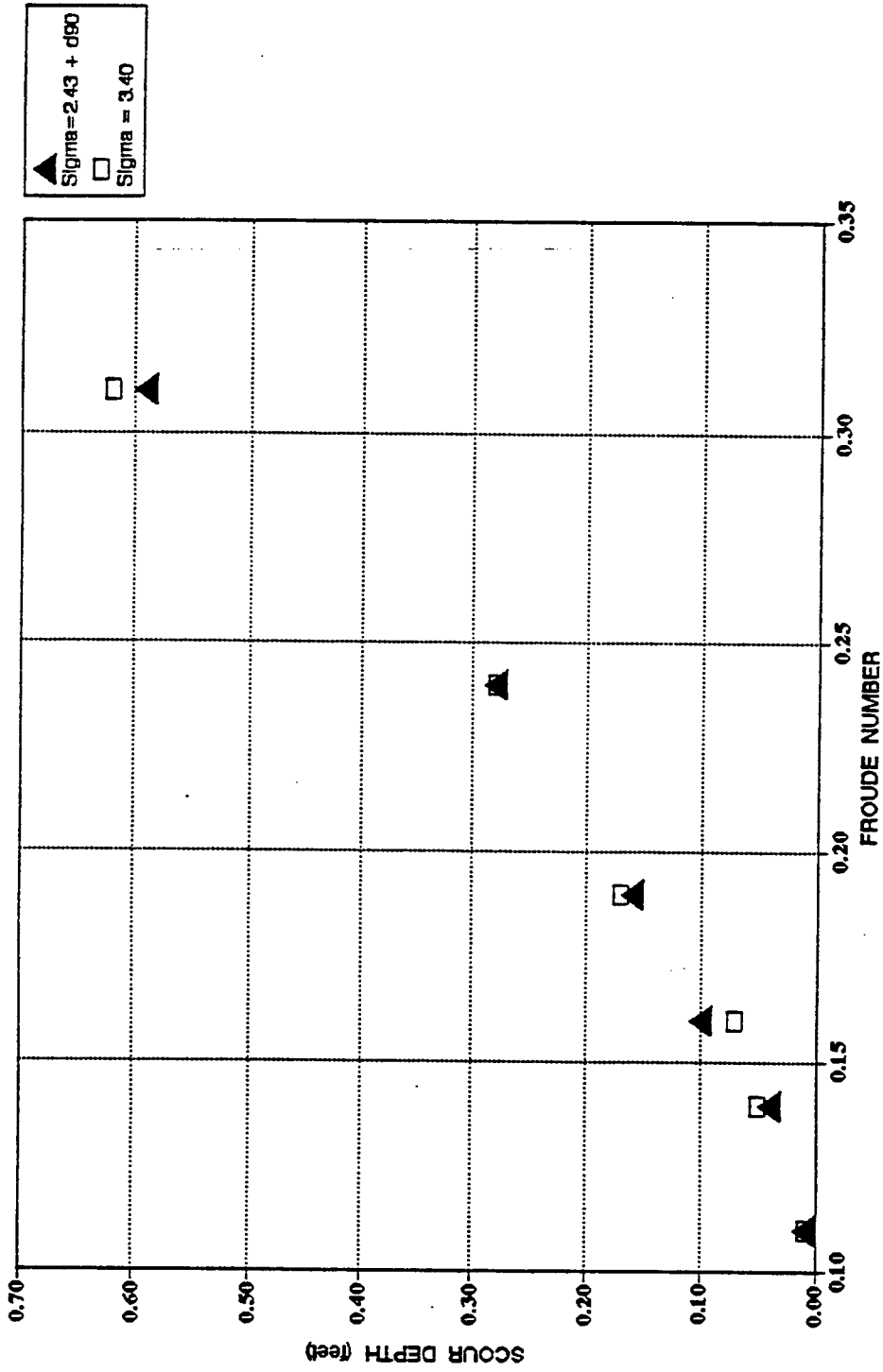


Figure 4.35 Effect of Increasing d_{90} Size for Mixtures with $\sigma_g = 2.43$ and $\sigma_g = 3.4$

Table 4.2. Comparison between Scour depths for d_{90} enriched ($\sigma_g = 2.43$ *) and $\sigma_g = 3.4$

Run No.	Q cfs	V_1 fps	Y_1 ft	F_r	Y_s (ft)	
					$\sigma_g = 2.43^*$	$\sigma_g = 3.4$
15-2	5.16	0.60	1.01	0.105	0.01	0.01
20-2	5.20	0.61	1.01	0.108		
14-2	7.29	0.82	1.03	0.142	0.04	0.05
22-2	7.30	0.78	1.08	0.133		
17-2	9.16	0.96	1.09	0.161	0.10	0.07
23-2	9.16	0.98	1.10	0.164		
13-2	11.10	1.20	1.06	0.193	0.16	0.17
24-2	11.10	1.24	1.08	0.210		
18-2	13.43	1.40	1.08	0.238	0.28	0.28
25-2	13.43	1.43	1.09	0.241		
19-2	16.85	1.83	1.10	0.307	0.59	0.62
26-2	16.90	1.91	1.04	0.33		

4.7.1 Resulting Armor layers at Bridge Piers

Sampling of armor layers in front of Pier 2 during Set No. 2 and Pier 2 during Set No. 3 was performed and sediment size distribution curves for these samples are presented in Figures 4.36 and 4.37. In these figures the original sediment mixtures at Pier 2 during Sets No. 2 and No. 3 were plotted along with the resulting armor layers. The original sediment mixture for σ_g of 3.4 is coarser in the range of d_{50} to almost d_{90} , and finer below d_{50} than the mixture with σ_g of 2.43 to gives a larger value of σ_g . The mixture with a lower σ_g value of 2.43, when strengthened by increasing the size of the fraction above d_{90} resulted in a coarser armor layer than that formed by the mixture with a higher σ_g value of 3.4. This small fraction which represents only 10% of the whole composition of the original gradation caused all the armor layers around the pier

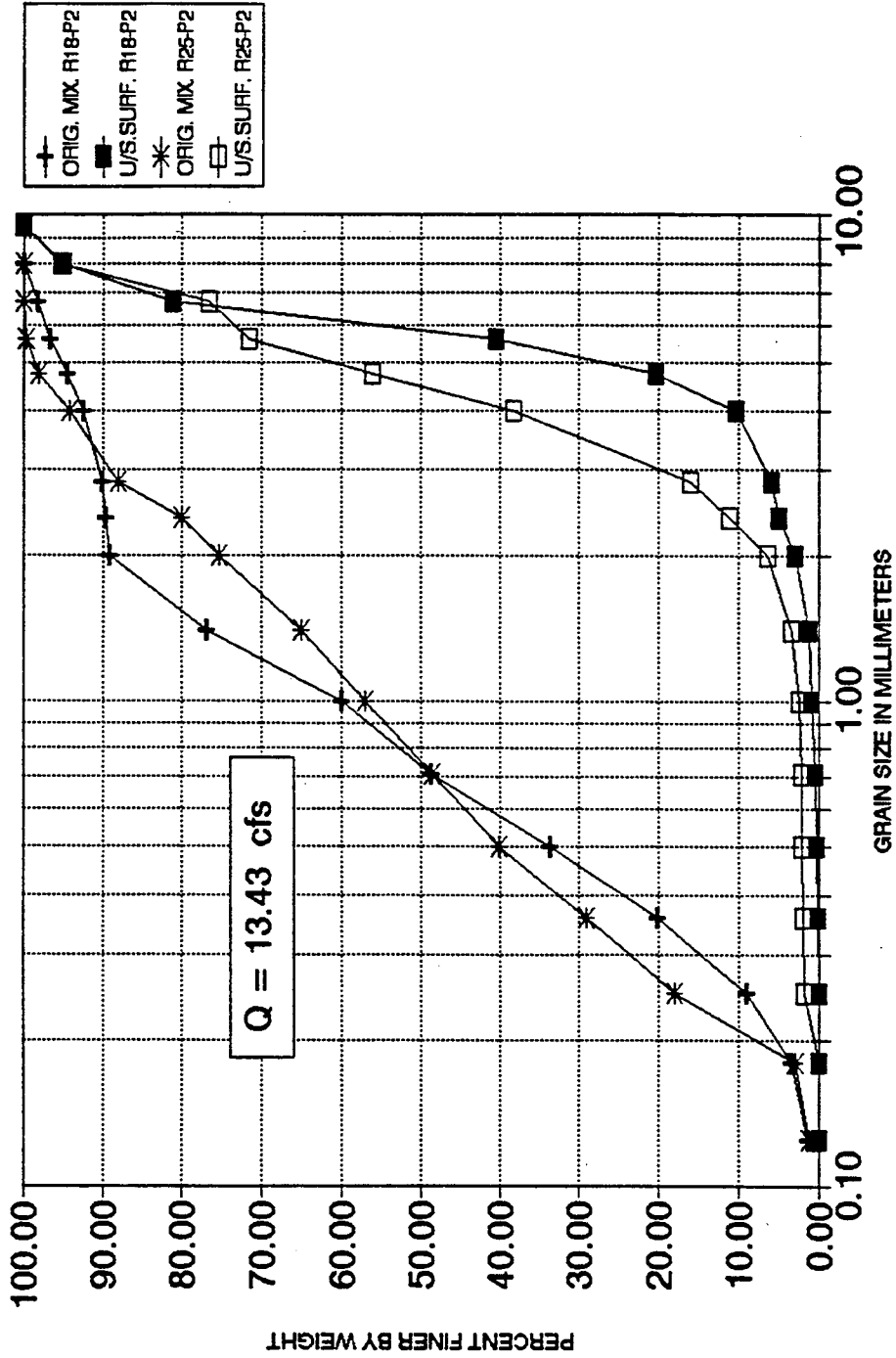


Figure 4.37 Surface Sediment Size Distribution Curves at the Upstream of Pier 2 for Runs 18 and 25

that have lower σ_g value to be coarser than those that occurred at the pier with a higher σ_g value. All grain size distribution curves for armor layers for the presented examples of Q of 7.30 and 13.40 cfs were shifted to the right in the case of increasing d_{90} with the σ_g of 2.43 to be coarser than that of σ_g of 3.4, giving all interpretations for why the scour depth is less and also why the rate of development of scour depth with time is less.

4.7.2 Development of Scour Depth with Time.

Figures 4.38 and 4.39 will be used as examples to explain the development of scour depth with time for the two cases under comparison. From these figures it is clear that the coarse material fraction plays an important role in reducing the rate of scour and the equilibrium scour depth at any σ_g value. This happens mainly due to the formation of coarser armor layers. For these two examples, for $Q=9.16$ and 11.10 cfs, this phenomenon is demonstrated clearly in Figures 4.38 and 4.39.

4.8 Comparison of Measured Local Scour Depths with other Prediction Equations

This section describes the observed and measured experimental results for local scour depths for different bed materials used during this investigation. A comparison between measured scour depths and prediction equations developed by other researchers is made to determine how the results of this study compared to previous work. Details of these experiments for the three sets of run are given in Section 4.1.

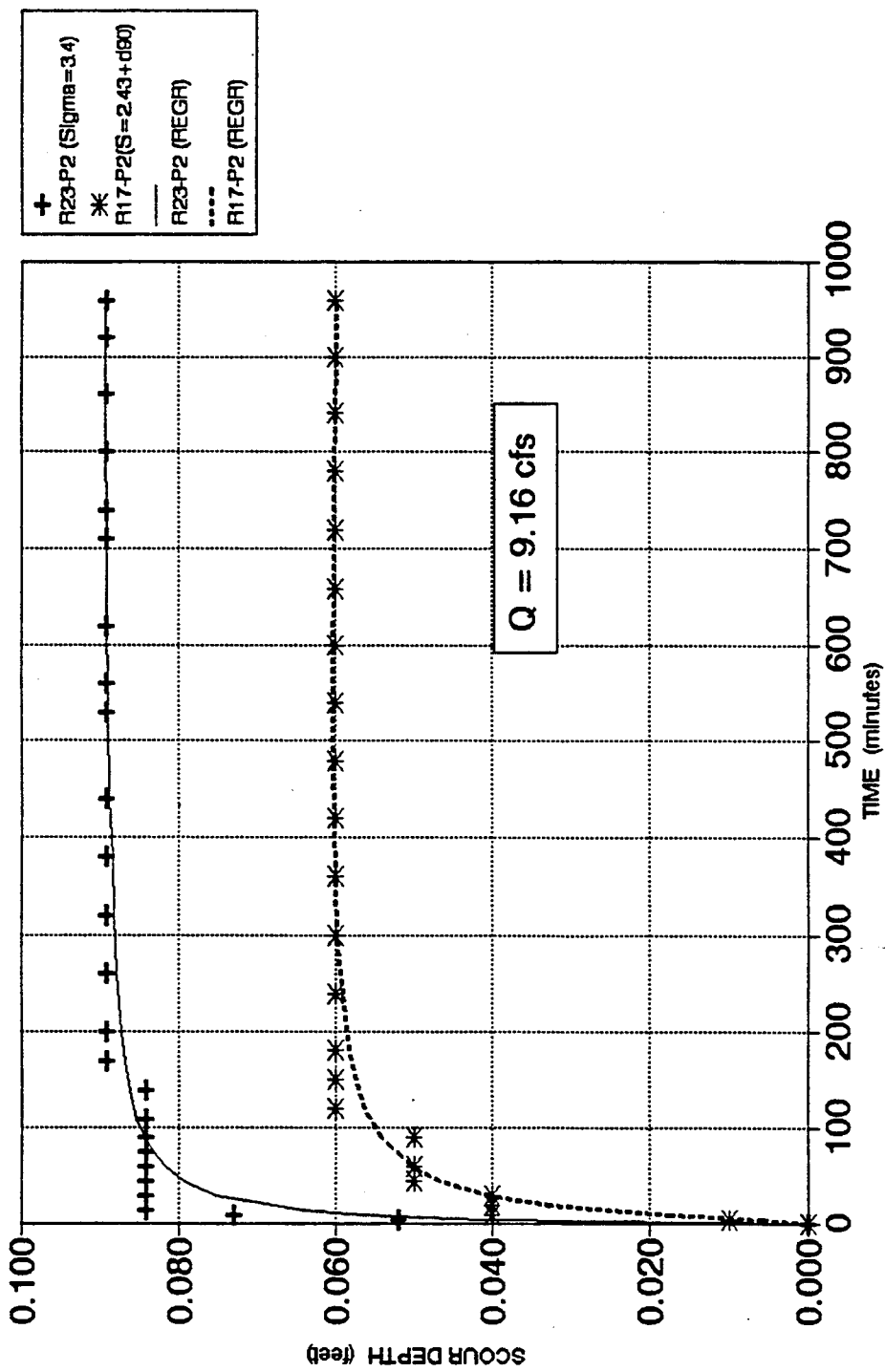


Figure 4.38 Time Development of Scour for Sediment Mixtures with Increased d_{90} size for $\sigma_g = 2.43$ and $\sigma_g = 3.40$ ($Q = 9.16$ cfs)

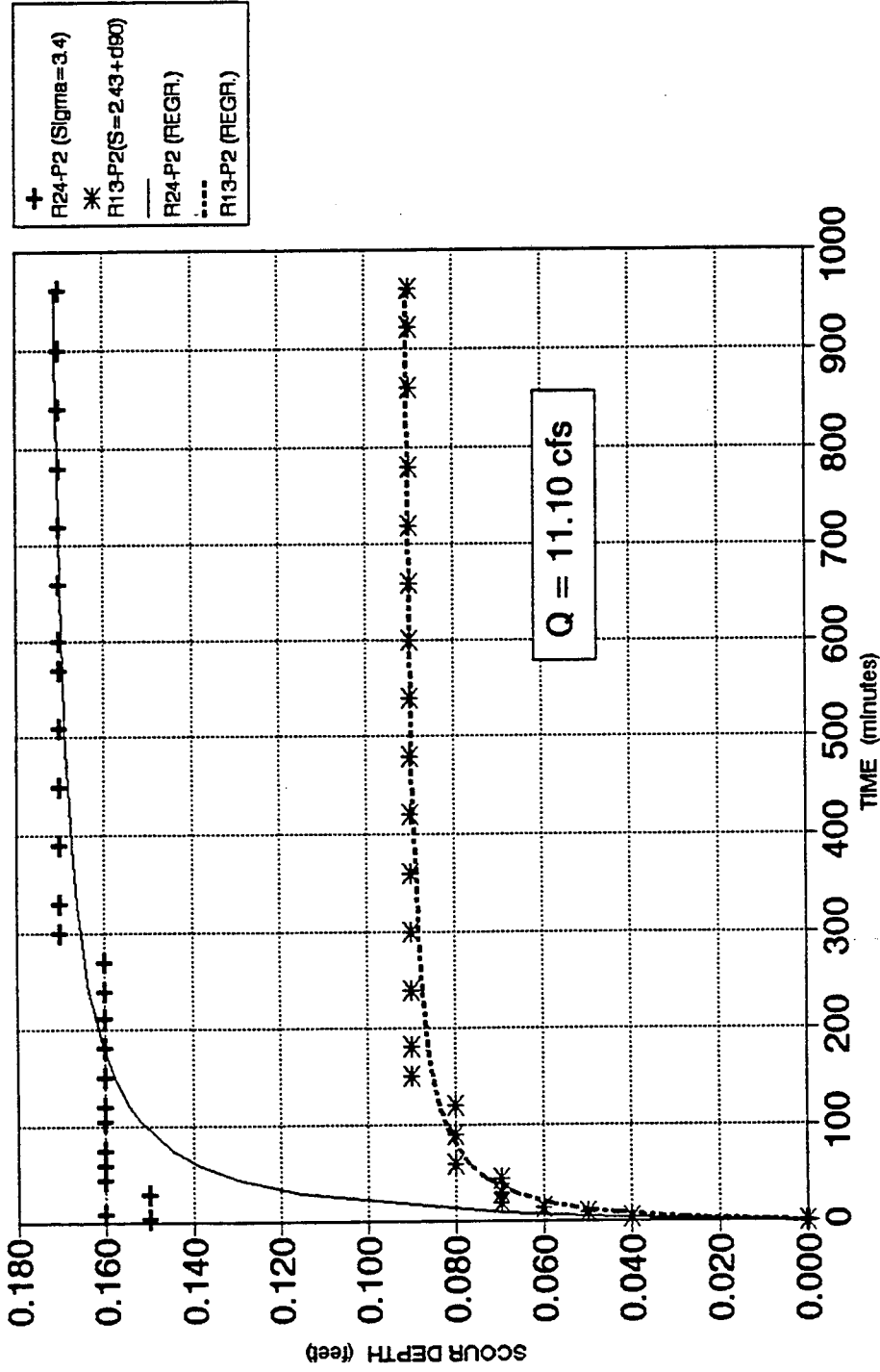


Figure 4.39 Time Development of Scour for Sediment Mixtures with Increased d_{90} size for $\sigma_g = 2.43$ and $\sigma_g = 3.40$ ($Q = 11.40$ cfs)

4.8.1 Contraction Scour

It was observed in all experiment cases that there was no contraction scour. According to Richardson (1989), the contraction scour should be negligible if the contraction of the channel is less than 10 percent. In the present study, the presence of the pier resulted in a contraction of 7.29% only of the channel (flume) width. The observation verified the suggestion provided by Richardson.

4.8.2 Local Pier Scour

The scour hole around the pier had the shape of an inverted cone and the deepest scour always occurred directly in front of the pier, which is in agreement with observations by other investigators. The maximum depth of scour hole increases with an increase in the approach velocity and hence the Froude number.

4.8.3 Comparison with CSU Equation

A comparison was made between the measured data and the CSU equation (Richardson and others, 1975). The CSU equation used in the comparison is:

$$\frac{Y_s}{Y_1} = 2.00 K_1 K_2 \left(\frac{b}{Y_1} \right)^{0.65} (F_r)^{0.43} \quad (4.2)$$

The comparison included the measured value of scour depth corresponding to three values of σ_g of 1.38, 2.43, and 3.4 to cover the range of sediment bed non-uniformity which is frequently used in laboratory tests. The comparison was done for all flow condition ranges that were tested in clear-water scour.

As seen in Figure 4.40, the values of Y_s/Y_1 calculated by the CSU equation were higher than measured values of Y_s/Y_1 for all σ_g values which were tested. The CSU equation over-predicts clear water scour depths and is conservative. It is also clear that the difference between the scour depth calculated by the CSU equation and the measured scour depth is large for small Froude numbers, but the difference tends to decrease with higher Froude numbers. Another fact that should be mentioned here is that this wide range of variation between measured data and the CSU equation values is referred to the fact that the coefficient determined by regression for Equation 4.2 was modified to 2.0 in order to develop a curve that would envelop all the laboratory data available at the time, (Johnson,P. 1992).

4.8.4 Comparison with the Froehlich Equation

A comparison was also made between the measured data and Froehlich's equation (1988). Froehlich's equation used in the comparison is:

$$\frac{Y_s}{Y_1} = 0.32 K \left(\frac{b'}{b}\right)^{0.62} \left(\frac{b}{Y_1}\right)^{0.54} (F_r)^{0.20} \left(\frac{b}{d_{50}}\right)^{0.08} + 1.0 \quad (4.3)$$

in which:

- K = coefficient for pier type
 - = 1.2 for square-nosed pier
 - = 1.0 for round and round-nosed pier
 - = 0.72 for a sharp-nosed pier.
- b' = pier width projected normal to the approach flow.

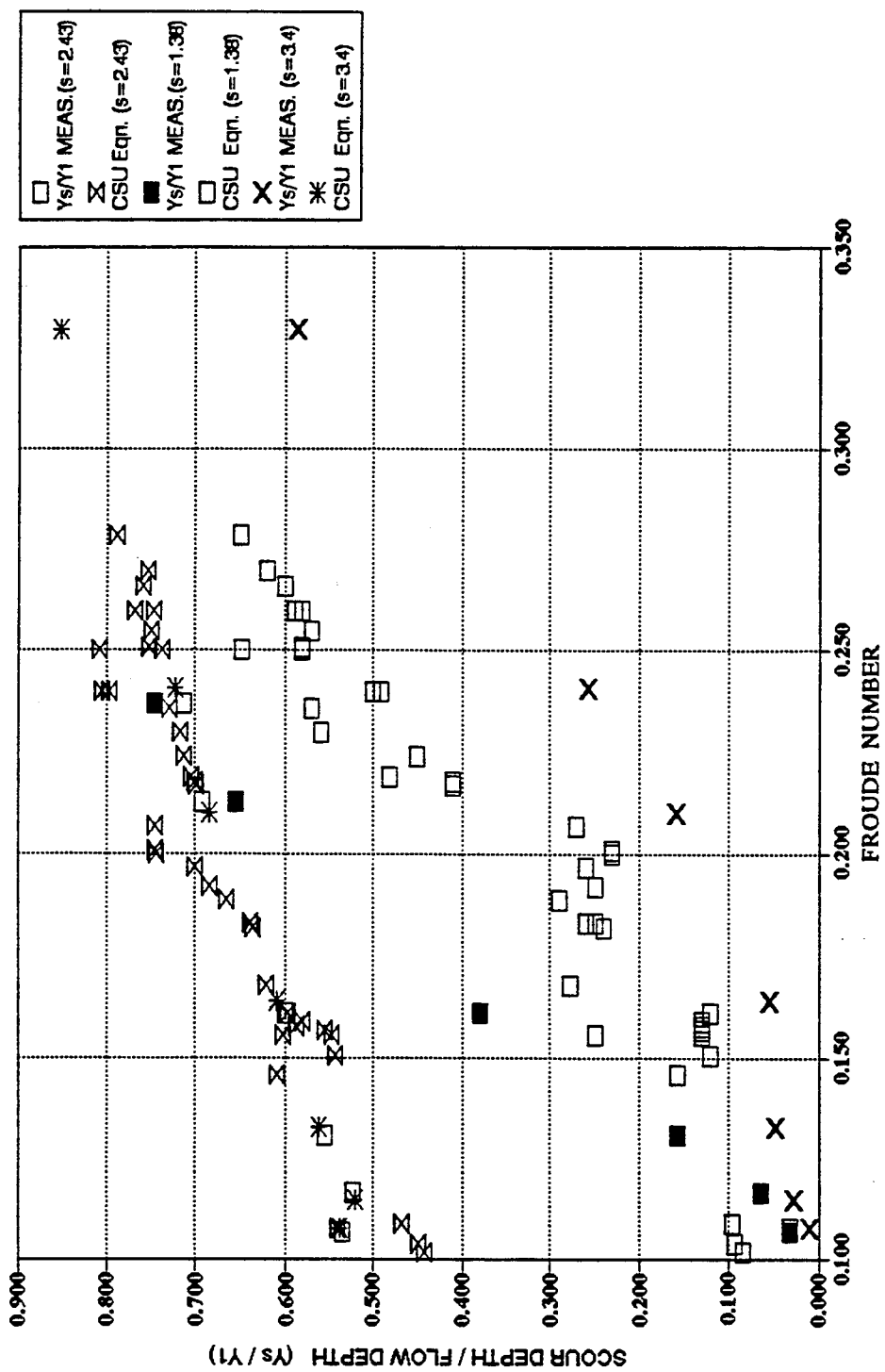


Figure 4.40 Comparison between Measured Data and CSU Equation

- $= b \cos \alpha + L \sin \alpha$
 α = the angle of attack
 L = pier length
 b = pier width
 Y_1 = flow depth
 F_r = Froude number = $V_1 / (g Y_1)^{0.5}$
 d_{50} = mean diameter for bed material
 b'/b = 1.0 for pier aligned with the flow direction.

Therefore Equation 4.3 takes the form:

$$\frac{Y_s}{Y_1} = 0.32 \left(\frac{b}{Y_1} \right)^{0.54} (F_r)^{0.20} \left(\frac{b}{d_{50}} \right)^{0.08} + 1.0 \quad (4.4)$$

The comparison in Figure 4.41 shows that Froehlich's equation over-predicts clear water scour depths for all σ_g values of 1.38, 2.43 or 3.4 and also for any value of Froude number that was tested. This refers to the fact that it is conservative for design purposes because of the addition of the 1.0 to the right hand side of the equation. For example if the measured scour depth ratio is 0.2 or 0.5, the calculated scour depth ratio by the Froehlich equation will be 1.2 or 1.5, thus it is very conservative.

4.8.5 Comparison with New Zealand Equations

A comparison between the measured data of this study and predicted local scour depths from the New Zealand equations, Ettema (1980), Davoren (1985) and Melville and Sutherland (1988) was done. The equations used for these comparisons were as

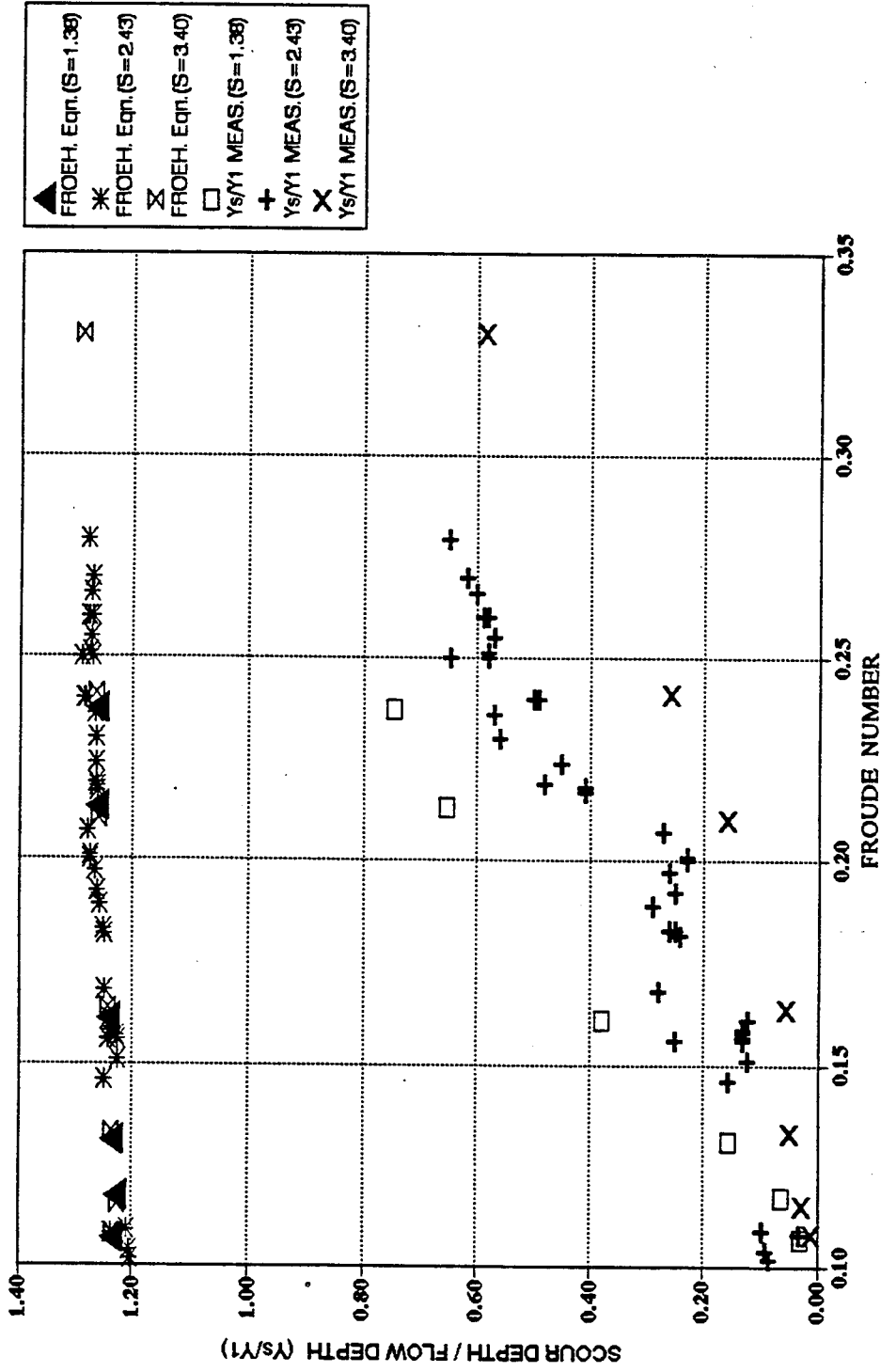


Figure 4.41 Comparison between Measured Data and Froehlich Equation

follow:

Ettema equation (1980)

Maximum equilibrium local clear-water scour depth in uniform material is:

$$\left(\frac{Y_s}{b}\right)_{\max} = 2.3 \quad (4.5)$$

or

$$\left(\frac{Y_s}{Y_1}\right) = \left(\frac{2.3 b}{Y_1}\right) \quad (4.6)$$

Equation 4.6 was used in comparison with measured data corresponding to $\sigma_g = 1.38$.

For non-uniform materials:

$$\left(\frac{Y_s}{b}\right)_{\sigma_g} = K_\sigma \left(\frac{Y_s}{b}\right)_{\max} \quad (4.7)$$

where K_σ is a coefficient equal to or less than 1.0 and can be found using Figure 4.42.

For $\sigma_g = 2.43$, $K_\sigma = 0.40$

For $\sigma_g = 3.40$, $K_\sigma = 0.22$

Then, the Ettema equation takes the following forms:

For $\sigma_g = 2.43$:

$$\frac{Y_s}{Y_1} = \frac{0.920 b}{Y_1} \quad (4.8)$$

For $\sigma_g = 3.40$:

$$\frac{Y_s}{Y_1} = \frac{0.506 b}{Y_1} \quad (4.9)$$

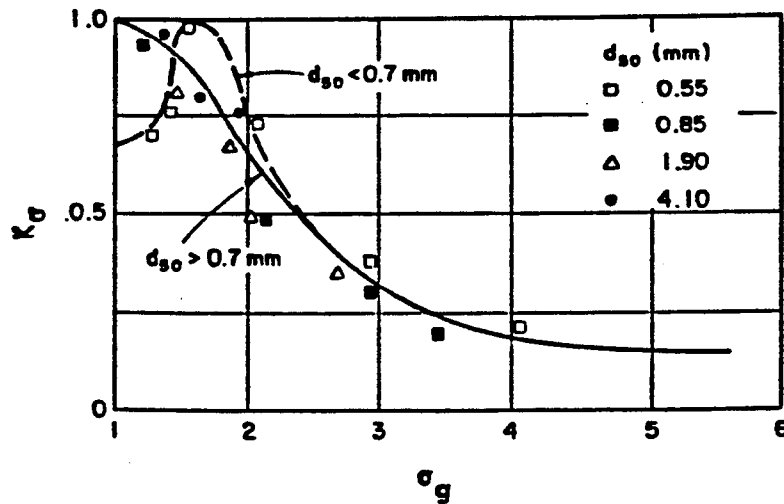


Figure 4.42 Function of K_{σ} versus σ_g by Ettema (1976)

Davoren Equation (1985)

The Davoren equation used in this comparison has the form:

$$Y_s = 0.395 Y_1 \quad (4.10)$$

where:

Y_s = scour depth from mean bed elevation (m)

Y_1 = approach flow depth (m)

or, in the dimensionless form, Equation 4.10 becomes:

$$\frac{Y_s}{Y_1} = 0.395 \quad (4.11)$$

Melville and Sutherland Equation (1988)

Melville and Sutherland (1988) developed the Equation 4.12, for calculating the scour depth based on some multiplication factors to account for flow intensity, flow depth, sediment size, sediment gradation, pier shape and pier alignment. or

$$\frac{Y_s}{b} = K_I K_y K_d K_\sigma K_s K_\alpha \quad (4.12)$$

$$\frac{Y_s}{Y_1} = K_I K_y K_d K_\sigma K_s K_\alpha \frac{b}{Y_1} \quad (4.13)$$

where:

- Y_s = scour depth;
- Y_1 = flow depth;
- b = pier diameter normal to the flow;
- K_I = flow intensity factor;
- K_y = flow depth factor;
- K_d = sediment size factor;
- K_σ = sediment gradation factor;
- K_s = pier shape factor;
- K_α = pier alignment factor;

The K values can be found using the graphs proposed by the authors (1988). For the present study $K_s=1.0$, $K_\alpha=1.0$ (circular piers), $K_d=1.0$ (for $b/d_{50}=237$), $K_y=0.92$ (for

$Y/b=2.0$), and $K_\sigma=1.0$, therefore, Equation 4.13 becomes:

$$\frac{Y_s}{Y_1} = 0.92 K_T \left(\frac{b}{Y_1} \right) \quad (4.14)$$

The comparison is shown in Figures 4.43, 4.44 and 4.45, from which it can be said that Ettema's equation is over predicting clear-water scour depths for the σ_g values of 1.38, 2.43, or 3.4 which were tested in this study. This indicates that calculated scour depths by Ettema's equation are always larger than the measured values in this study. This difference can be referred to as the fact that Ettema's equation gives the largest possible scour depth that can occur at a cylindrical pier, which is $2.3 b$.

Since the flow depth was almost constant (1.0 to 1.10 ft), for lower F_r values tested during the experimental work the scour depths calculated by the Davoren equation gives higher scour depths values than the measured ones for all σ_g values. This equation gives lower scour depth values for values of F_r of 0.20 to 0.25. This is because Davoran equation predicts the maximum value of scour depths for live-bed conditions and not the equilibrium or final scour depths.

In comparison with the Melville and Sutherland equation, it was found that their equation also over predicts measured clear-water scour depths despite the fact that this equation contains multiplying factors for reducing the scour depths than that calculated by Ettema.

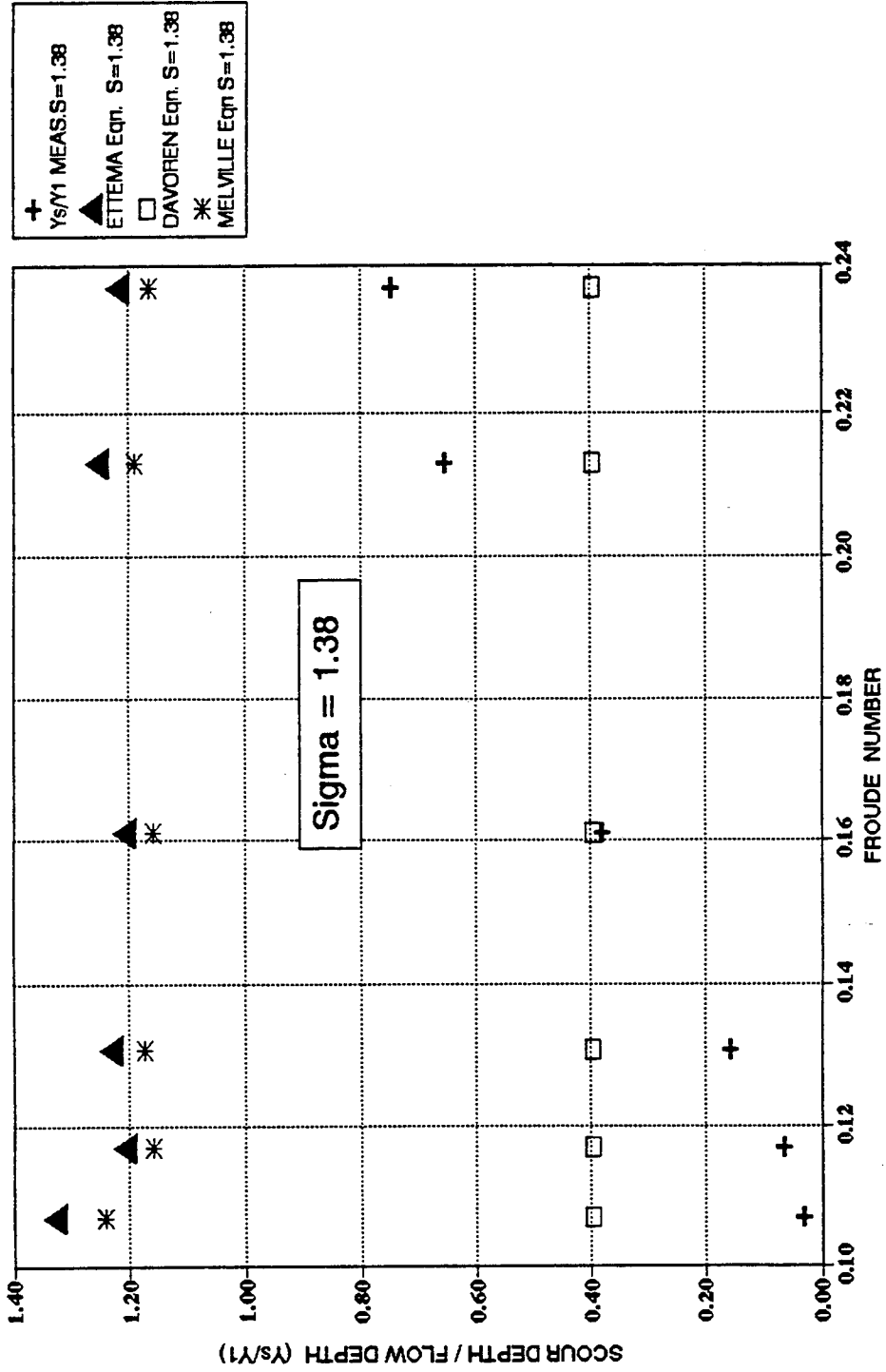


Figure 4.43 Comparison Between Measured Data and New Zealand Equations for $\sigma_g = 1.38$

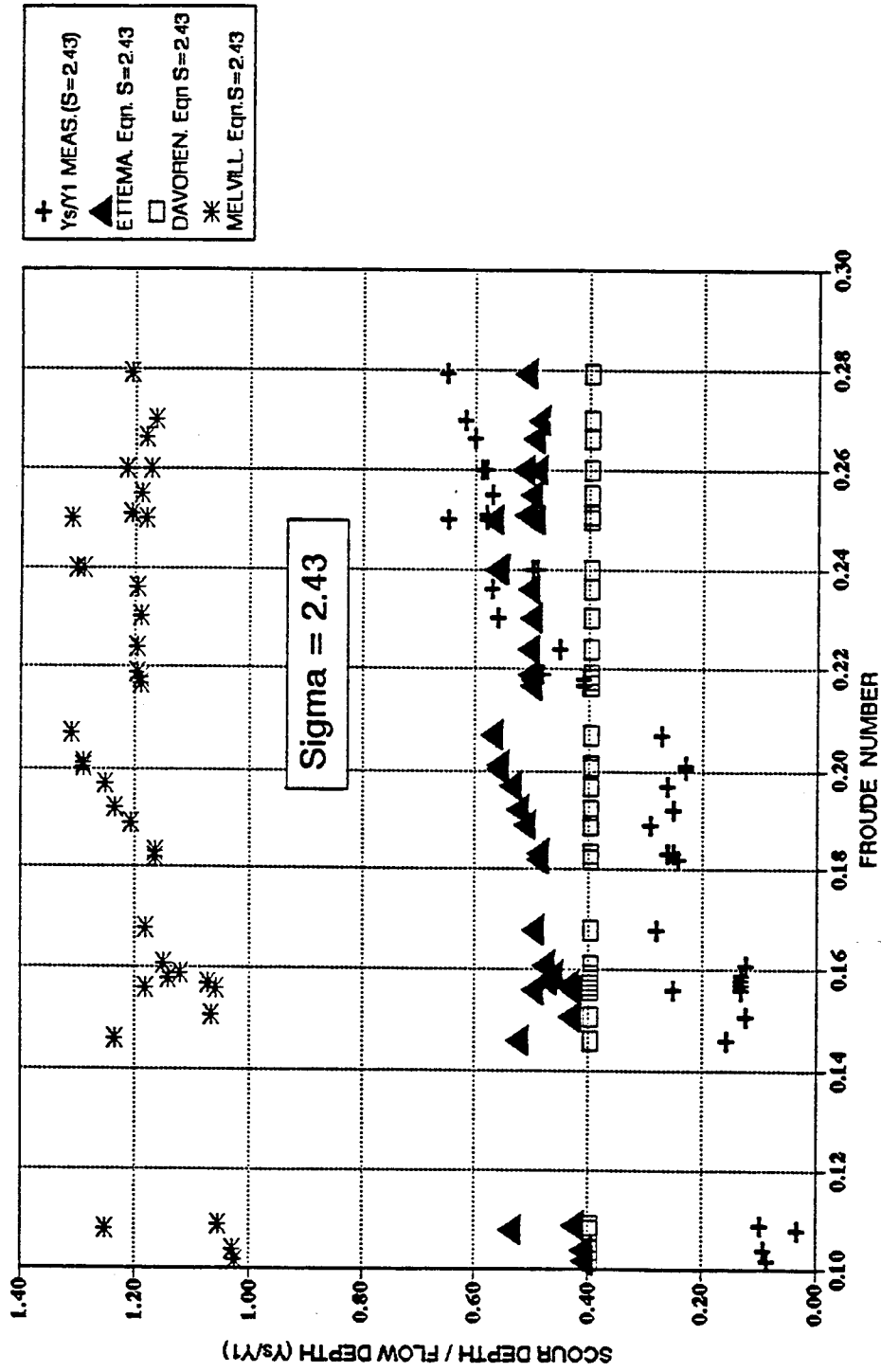


Figure 4.44 Comparison between Measured Data and New Zealand Equations for $\sigma_s = 2.43$

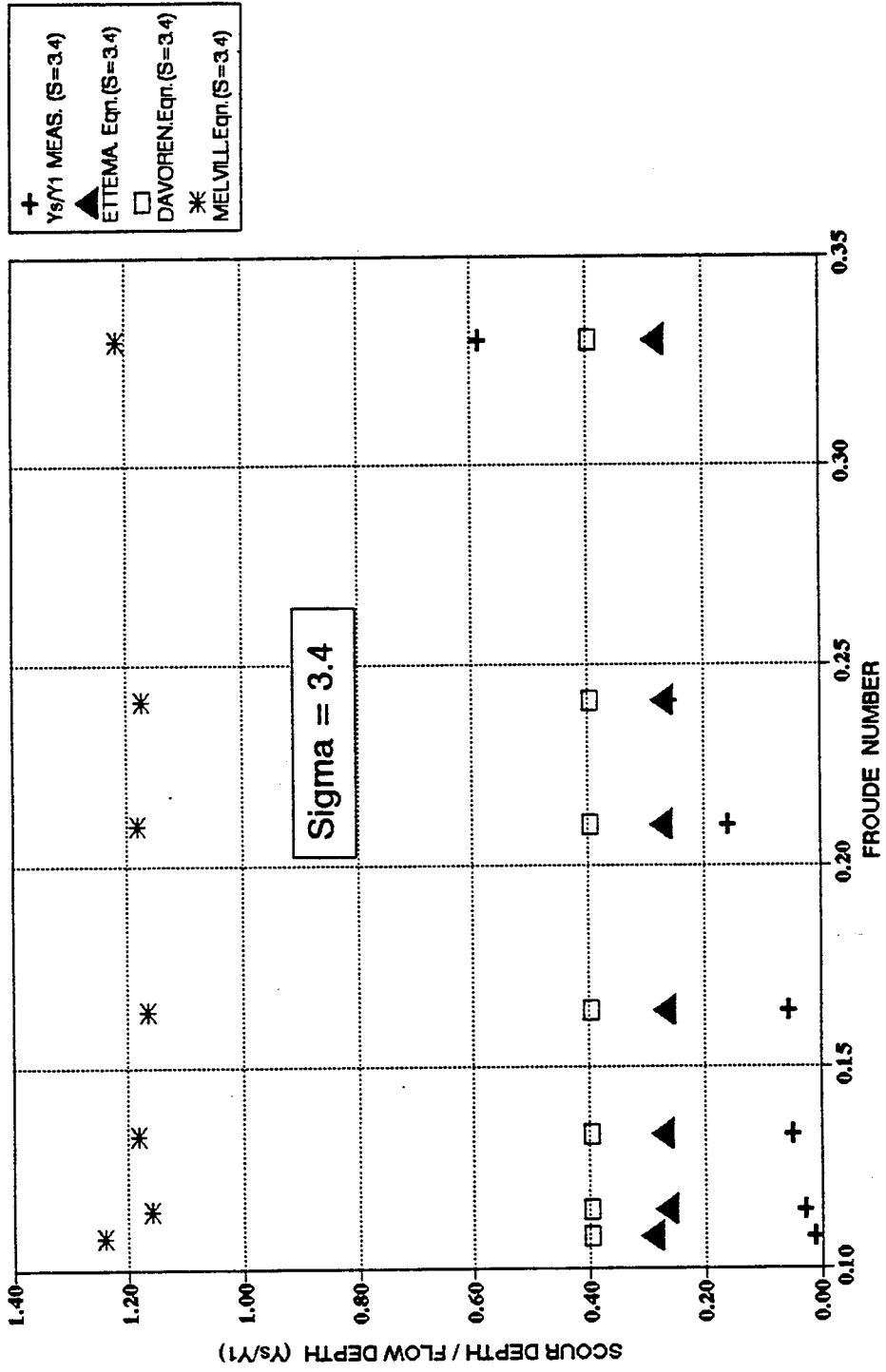


Figure 4.45 Comparison between Measured Data and New Zealand Equations for $\sigma_s = 3.40$

4.9 Regression Analysis

Prediction equations were developed for calculating local scour depth for clear-water scour based on the dimensional analysis performed to determine the parameters affecting scour and the experimental results obtained from this study. The regression analysis was performed for two cases. The first case is to account for the effect of the non-uniformity coefficient of sediment mixtures and the second case accounts for the effect of the parameter d_{90}/d_{50} of the original sediment mixtures to develop a general equation for local scour depth using the whole set of data from present study.

4.9.1 Regression Analysis for Experimental Data

A stepwise regression analysis was used in the MINITAB computer program (which is based on least squares method) to develop equations for local clear-water scour. As presented in detail in appendix A, the following expression was developed from dimensional analysis for parameters affecting the scour process:

$$\frac{Y_s}{Y_1} = K K_1 K_2 \left(\frac{b}{Y_1}\right)^a \left(\frac{d_{50}}{Y_1}\right)^b (\sigma_g)^c \left(\frac{V t}{Y_1}\right)^d (F_r)^e \quad (4.15)$$

Since d_{50} of 0.75 mm and Y , the flow depth was almost constant (about 1.0 ft) were kept constant during the study, the parameter d_{50}/Y was removed from Equation 4.16. For each tested value of σ_g (1.38, 2.43 and 3.4) the dimensionless equation to be used for the regression analysis becomes:

$$\frac{Y_s}{Y_1} = K K_1 K_2 \left(\frac{b}{Y_1}\right)^a \left(\frac{Vt}{Y_1}\right)^b (F_r)^c \quad (4.16)$$

The logarithm of Y_s/Y_1 was regressed against the remaining dimensionless groups using the power equation form (non-linear regression) in the MINITAB computer program. For large experiment durations the value of the term (Vt/Y_1) had a very weak effect on the regression analysis, thus this term was rejected. It was found that the regression which gave the largest coefficient of determination, R^2 was based on the functional relation :

$$\frac{Y_s}{Y_1} = k K_1 K_2 (F_r)^a \quad (4.17)$$

which indicates that the scour depth ratio has a strong dependency on the Froude number of the flow. The above expression was finally used and an equation was obtained for each tested value of σ_g .

For $\sigma_g = 1.38$:

$$\frac{Y_s}{Y_1} = 144.50 (F_r)^{3.47} \quad (4.18)$$

The corresponding statistical analysis for this regression step was as follows:

Power equation :

$$C1 = 2.16 + 3.47 C2 \quad (4.19)$$

	Coefficient	Standard Deviation of coefficient	T-ratio=coeff /SD	P
Constant	2.16	0.5834	3.71	0.021
C2	3.47	0.7091	4.89	0.008
S = 0.1868				
R-square = 91.4%				
R-square = 89.2 % adjusted for D.F.				

Analysis of Variance:

Source	DF	SS	MS=SS/DF	F	P
Regression	1	1.1948	1.1948	23.89	0.008
Residual	4	0.2000	0.0500		
Total	5	1.3948			

Where:

S = an estimate of σ , the estimated standard deviation about the regression line.

DF = degrees of freedom

R² = the coefficient of determination

P = the probability of getting a value as extreme as large in magnitude from a t-distribution.

For $\sigma_g = 2.43$:

$$\frac{Y_s}{Y_1} = 38.00 (F_r)^{3.03} \quad (4.20)$$

The corresponding statistical analysis for this regression step was as follows:

Power equation :

$$C1 = 1.58 + 3.03 C2 \quad (4.21)$$

	Coefficient	Standard Deviation of coefficient	T-ratio = coeff/SD	P
Constant	1.5815	0.1151	13.74	0.000
C2	3.0275	0.1656	18.28	0.000
S = 0.0898				
R-square = 91.30 %				
R-square = 91.0% adjusted for D.F.				

Analysis of Variance:

Source	DF	SS	MS = SS/DF	F	P
Regression	1	2.6939	2.6939	334.04	0.000
Residual	32	0.2581	0.0081		
Total	33	2.9520			

For $\sigma_g = 3.40$:

$$\frac{Y_s}{Y_1} = 23.0 (F_r)^{3.20} \quad (4.22)$$

The corresponding statistical analysis for this regression step was as follows:

Power equation :

$$C1 = 1.36 + 3.20 C2 \quad (4.23)$$

	Coefficient	Standard Deviation of coefficient	T-ratio = coeff/SD	P
Constant	1.3591	0.2876	4.73	0.000
C2	3.2015	0.3681	8.70	0.000
S = 0.1619				
R-square = 93.8 %				
R-square = 92.6% adjusted for D.F.				

Analysis of Variance:

Source	DF	SS	MS=SS/DF	F	P
Regression	1	1.9821	1.9821	75.66	0.000
Residual	5	0.1310	0.0262		
Total	6	2.1131			

Newly developed prediction equations for clear-water scour depths (Equations 4.18, 4.20 and 4.22) from this study show a strong dependence on the Froude number of flow to a power of 3 or more (F^3). These equations take into account the effect of non-uniformity of bed materials.

4.10 Comparison between Predicted Clear-Water Scour Equations from Present Study and other Equations

The prediction equations developed in this study were compared with previous equations developed by other researchers. The measured laboratory data from the present study were applied to some of these equations. The calculated scour depths were compared with the measured data. Figures 4.46 through 4.51 show the comparison with Englis-Poona (1948), Chitale (1960), Breusers (1965), Shen (1966-1969), Neill (1964), Bata (1960), CSU (1975), and Froehlich (1988) equations. These equations and their limitations are given in the literature reviews conducted by other researchers as well as in the publication prepared along with this dissertation under the title "Literature Survey and Compilation of Bridge Pier Scour Data". Figures 4.46 and 4.47 show the comparison for σ_g value of 1.38, and Figures 4.48 and 4.49 show the comparison for σ_g of 2.43. Figures 4.50 and 4.51 present the results for σ_g value of 3.4.

The CSU and Froehlich equations are used to predict live-bed and clear water-scour while the newly developed equations are for clear-water scour only. As shown in the literature, the two modes of transport have different influence on the behavior of

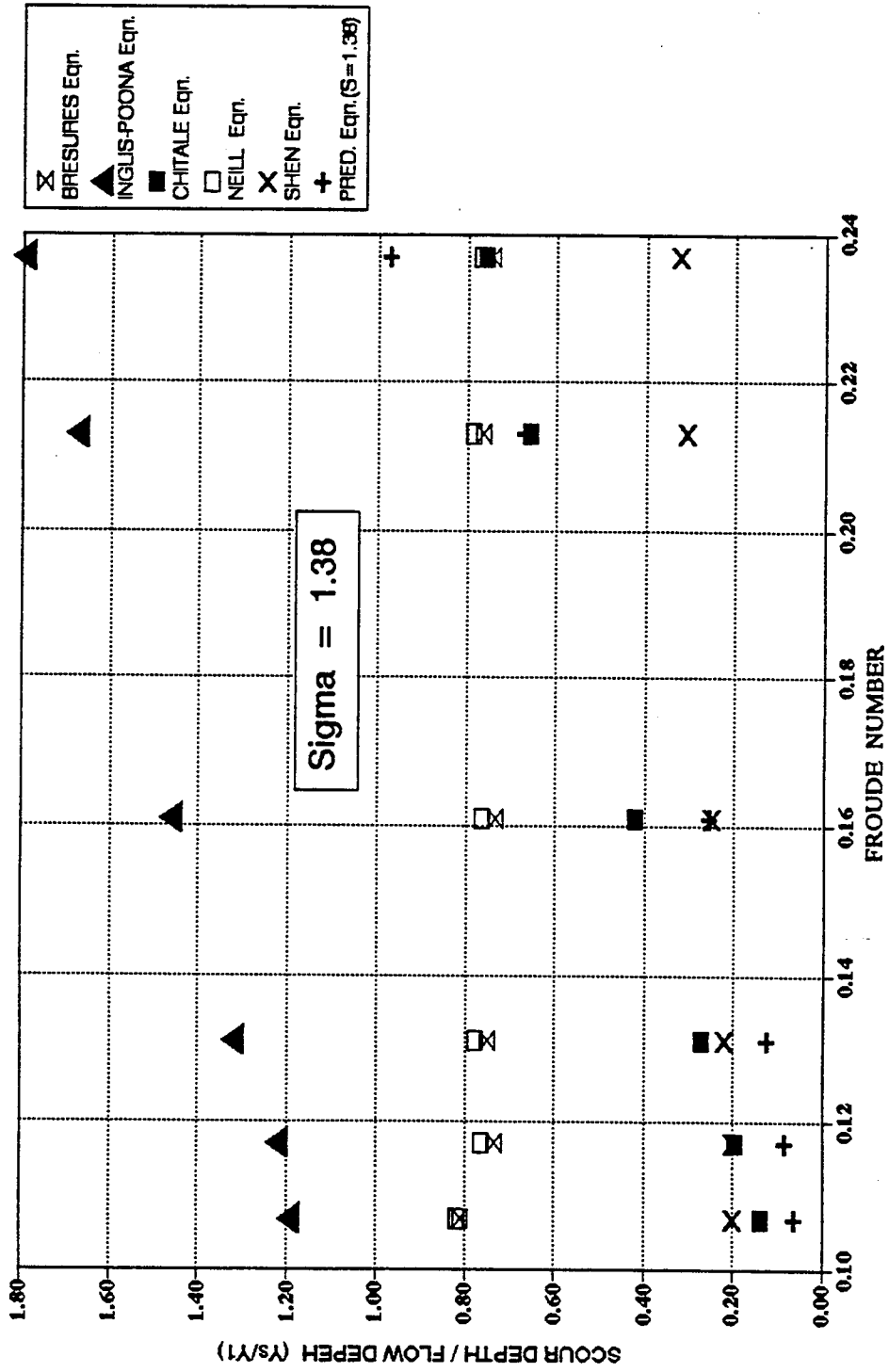


Figure 4.46 Comparison between Newly Developed Prediction Equation and other Equations for $\sigma_s = 1.38$

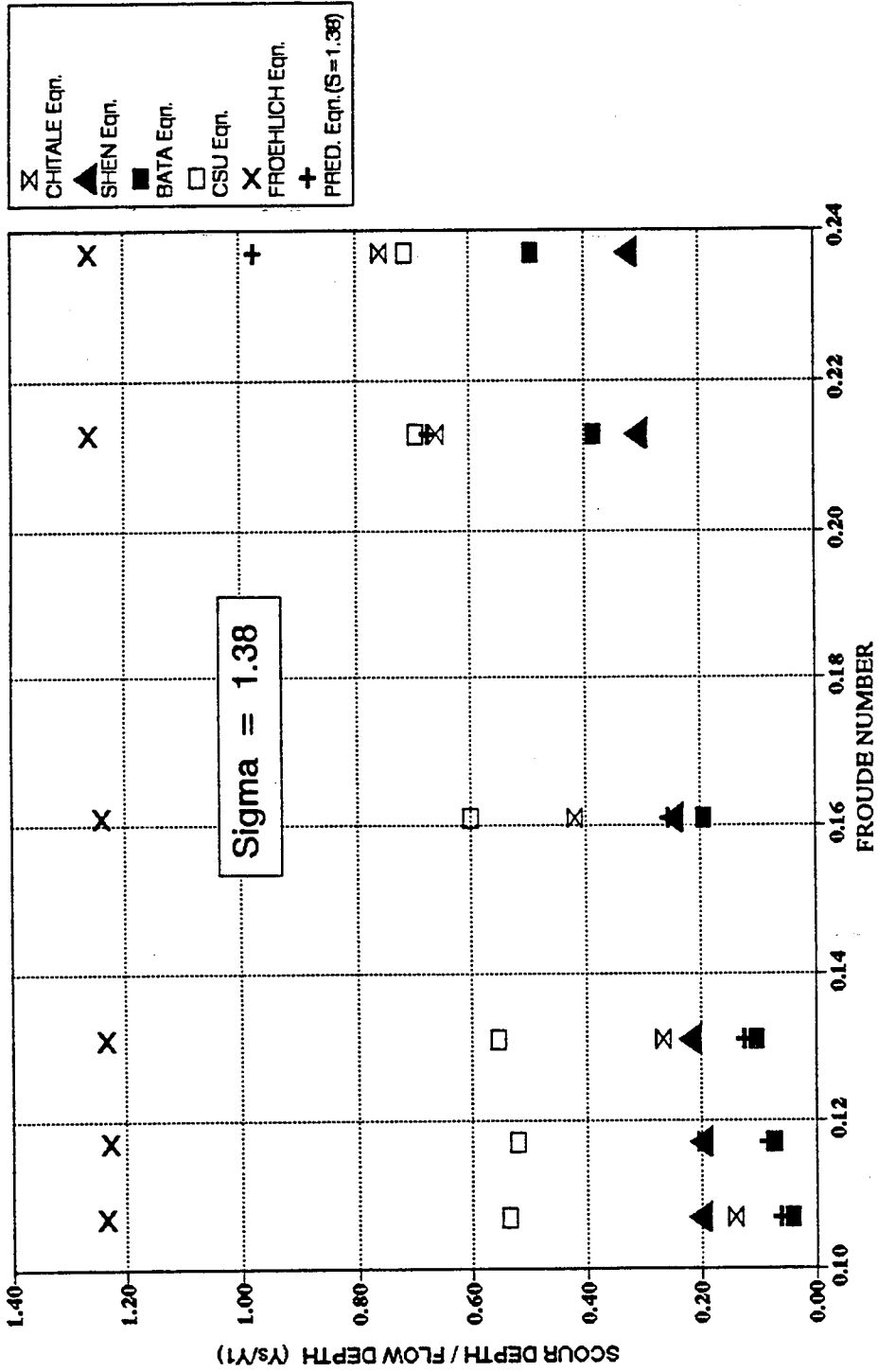


Figure 4.47 Comparison between Newly Developed Prediction Equation and other Equations for $\sigma_s = 1.38$

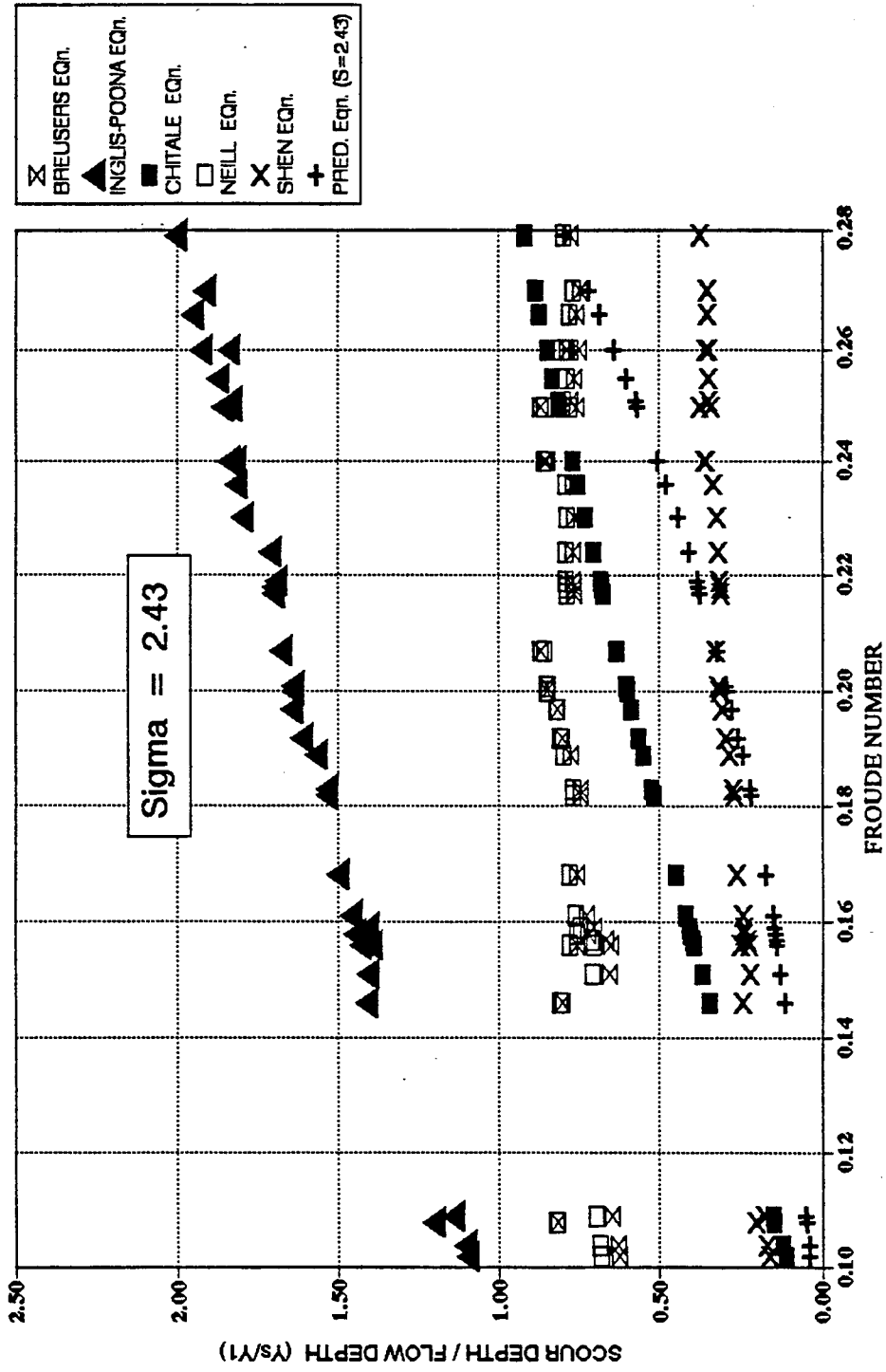


Figure 4.48 Comparison between Newly Developed Prediction Equation and other Equations for $\sigma_s = 2.43$

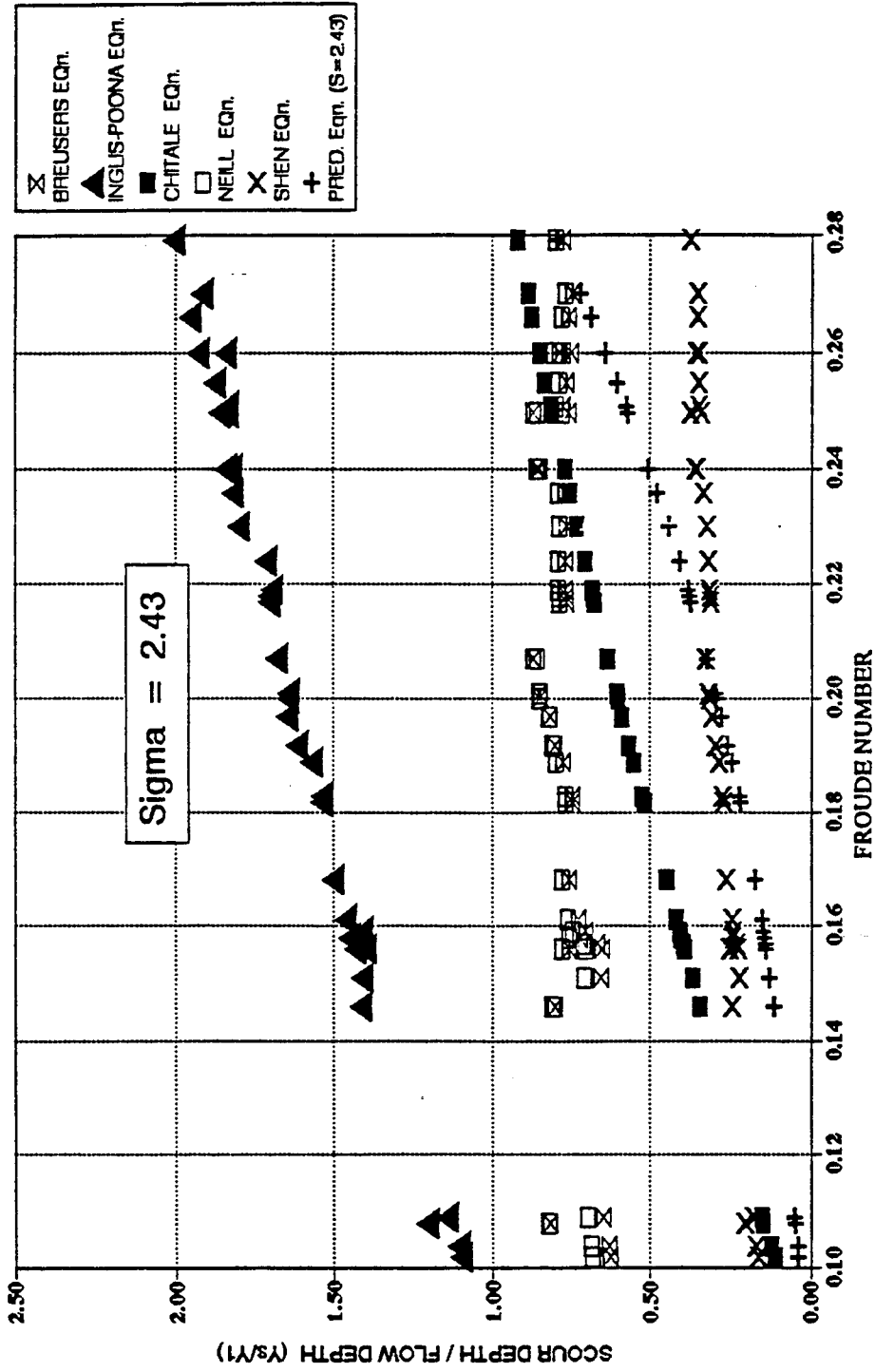


Figure 4.49 Comparison between Newly Developed Prediction Equation and other Equations for $\sigma_s = 2.43$

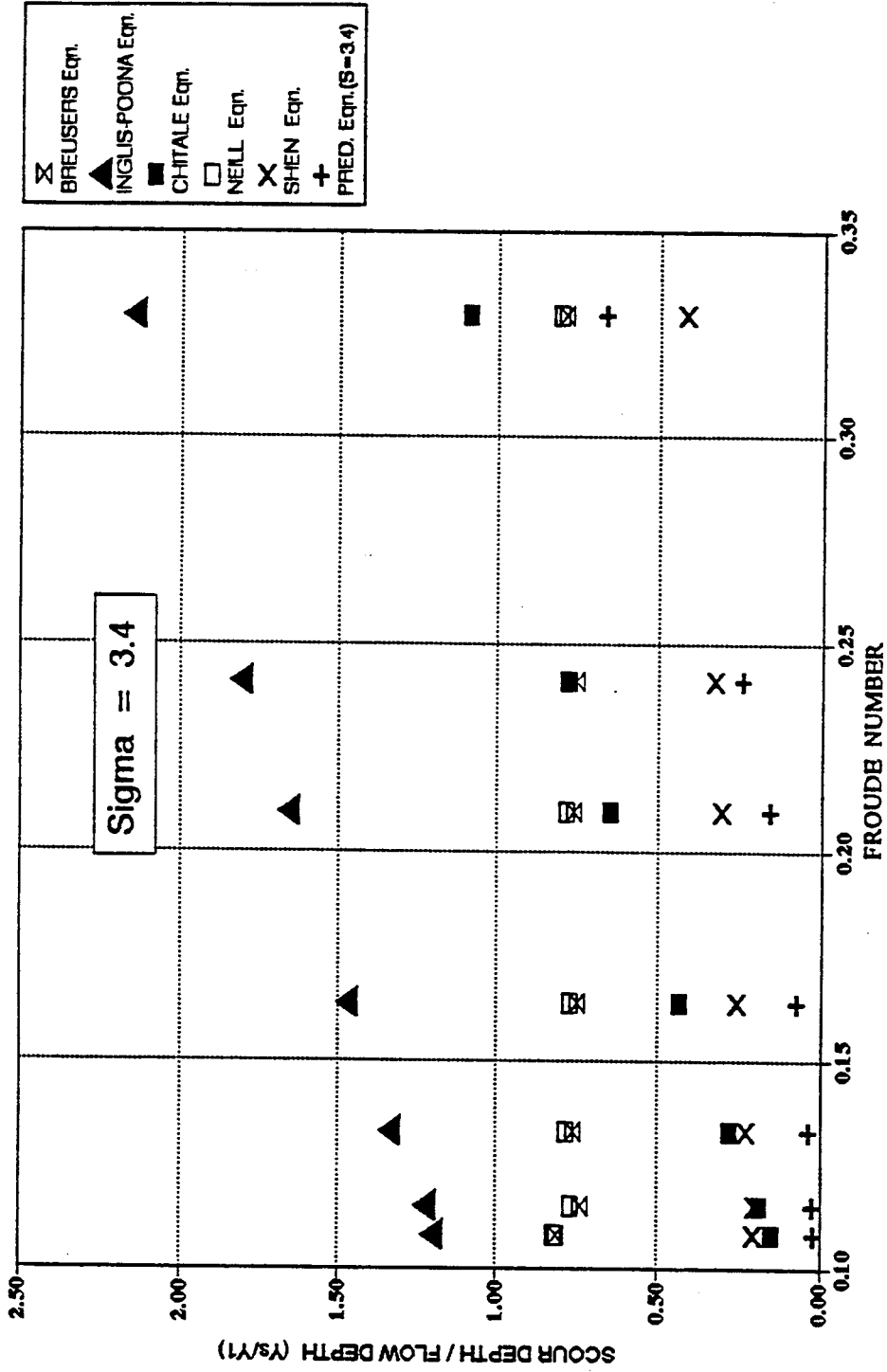


Figure 4.50 Comparison between Newly Developed Prediction Equation and other Equations for $\sigma_g = 3.40$

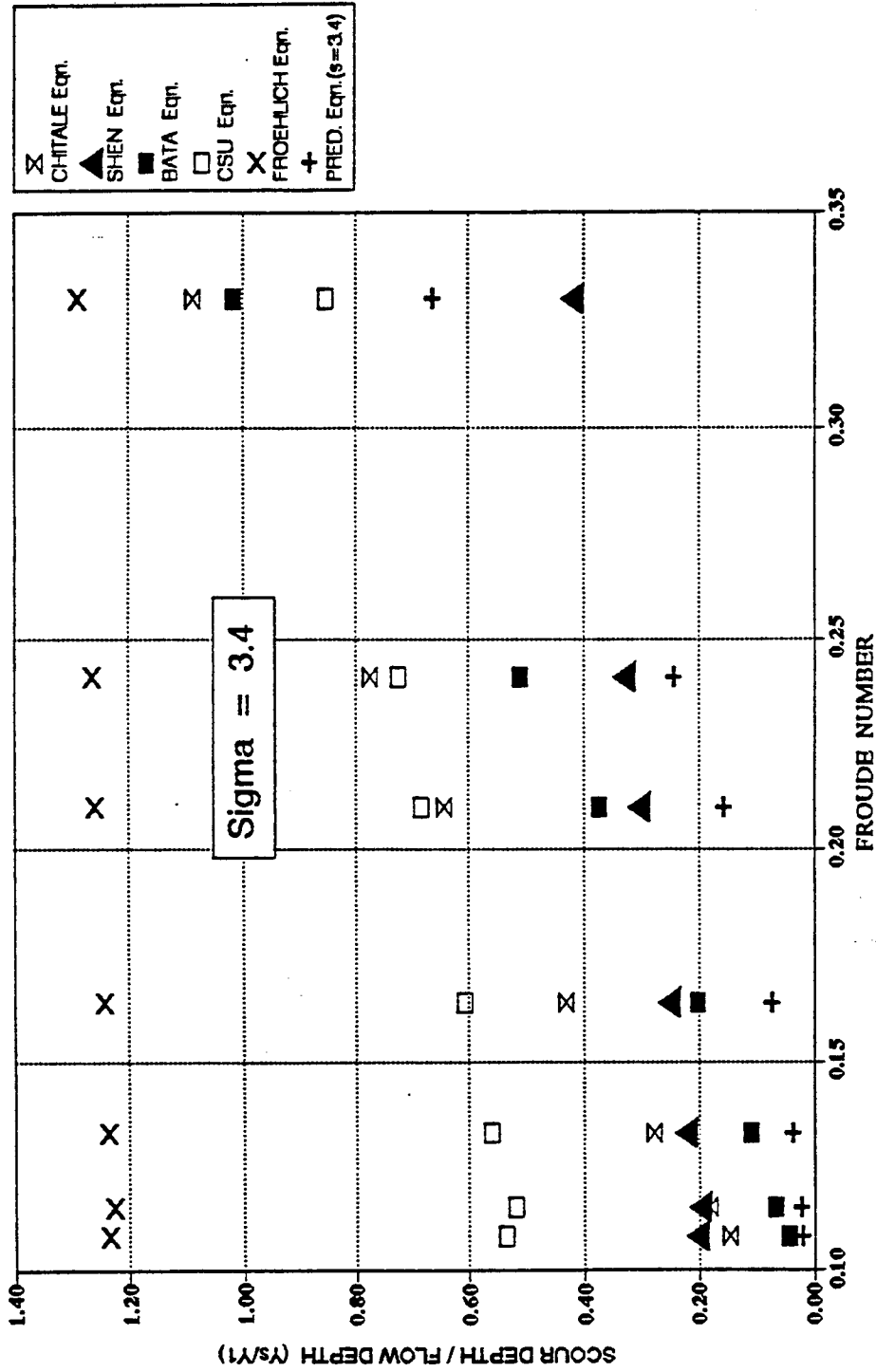


Figure 4.51 Comparison between Newly Developed Prediction Equation and other Equations for $\sigma_g = 3.40$

of scour with time and velocities. CSU equation always predicted larger values of scour depths than the present equations for the range of Froude number and σ_g values tested during the present study. This could be probably due to the factor of safety of 2.0 used in CSU equation or because σ_g in CSU equation had a constant value of 1.0. Thus using the CSU equation for clear-water scour will be conservative because it predicts larger depths of scour.

As a comparison with Froehlich's equation, it can be said that for any value of σ_g that was tested during this study, Froehlich's equation gives almost constant value for the scour depth which at the same time is larger than the values measured or calculated by the new prediction equations. This could be due to the addition of 1.0 to the right hand side of Froehlich equation. This practice is very conservative since a depth of flow is added to the computed scour by the use of a +1.0 at the right hand side of the equation. Therefore comparing Froehlich equation to the new prediction equation for the same experimental data, we can say that Froehlich equation is over-predicting clear water scour depths.

For σ_g values of 3.4, 2.43, and 1.38 Shen's equation which was derived from experiments at CSU Hydraulics laboratory for clear water scour gives comparable values for scour depths with our predicted equations for smaller Froude number values, then it tends to give lower values for higher Froude number values tested during the study. Also, Bata equation for clear water conditions gives almost the same scour depths like the present for small σ_g values of 1.38 and 2.43 but it predicts higher scour depths for higher σ_g value of 3.4 that was tested in the present study. The Chitale equation which

was derived for clear water scour has nearly the same trend for scour depths like the present prediction equation because Chitale equation states that scour depth is a function of Froude number to the second power but it gives higher scour depth values because it was derived for rectangular piers.

Neill and Breusers equations give almost equal values for scour depths which are higher than the values given by our predicted equation. Englis-Poona equation which is believed to be valid for clear water scour, was derived using q , the discharge per unit width in the contraction, which means greater scour could be expected, also this equation was derived for special bridge piers and rivers in India and Pakistan under special conditions. This might explain the big difference between calculated scour depths by Englis-Poona equation which are the highest values in this comparison and our predicted ones. Thus it can be said that this equation is very conservative.

4.11 Comparison between Newly Developed Equations and other Researcher's Measured Data

Now, the opposite operation for what was done in section 4.8 will be done here. Some other measured data will be fitted to the predicted equations developed from present study to see how are the predicted equations in the range of the tested flow conditions compare to other measured data. For three different values of σ_g of 1.3, 2.0 and 2.8 tested by Chiew (1984) in the live bed scour, some measured values of scour depths were picked and plugged the flow conditions under which these scour depths were measured to our predicted equations, the result was that our equations give always

higher values since it predict clear-water scour depths, Figure 4.52 and 4.53.

Also, some of Chee's (1982) data that fits the conditions of this present study were plugged into our equation that predicts scour depths in uniform beds and the results are as shown in Figures 4.54 and 4.55 which indicate that the predicted equation gives higher values for scour depths due to the fact that it predicts clear water scour depths and the measured ones were for live bed scour in uniform beds, thus we are in good shape.

For Baker's (1986) scour depths data that were measured for the live bed scour conditions, Figure 4.56 and 4.57, the comparison with the calculated values by the predicted equations from this study show that our equations always give higher values than measured ones by Baker and this is good since measured ones are in the live bed scour, also the results show the consistency and compatibility between the measured and predicted scour depths for each σ_g value, it is clear that predicted equations for σ_g equals 3.4 and 2.43 give less predicted scour depths than those for σ_g equals 1.38 and this is what it should be.

4.12 General Equation for Local Scour Depth Based on the Present Study

In this section, a generalized equation collecting all experimental data for the three bed material gradations is developed. From the results presented up to this point in this study, the gradation coefficient by itself is not sufficient for describing the armoring phenomena and its behavior in reducing the scour depth effectively. It was observed that the upper portion of the gradation curve above the upper limits of d_{84}

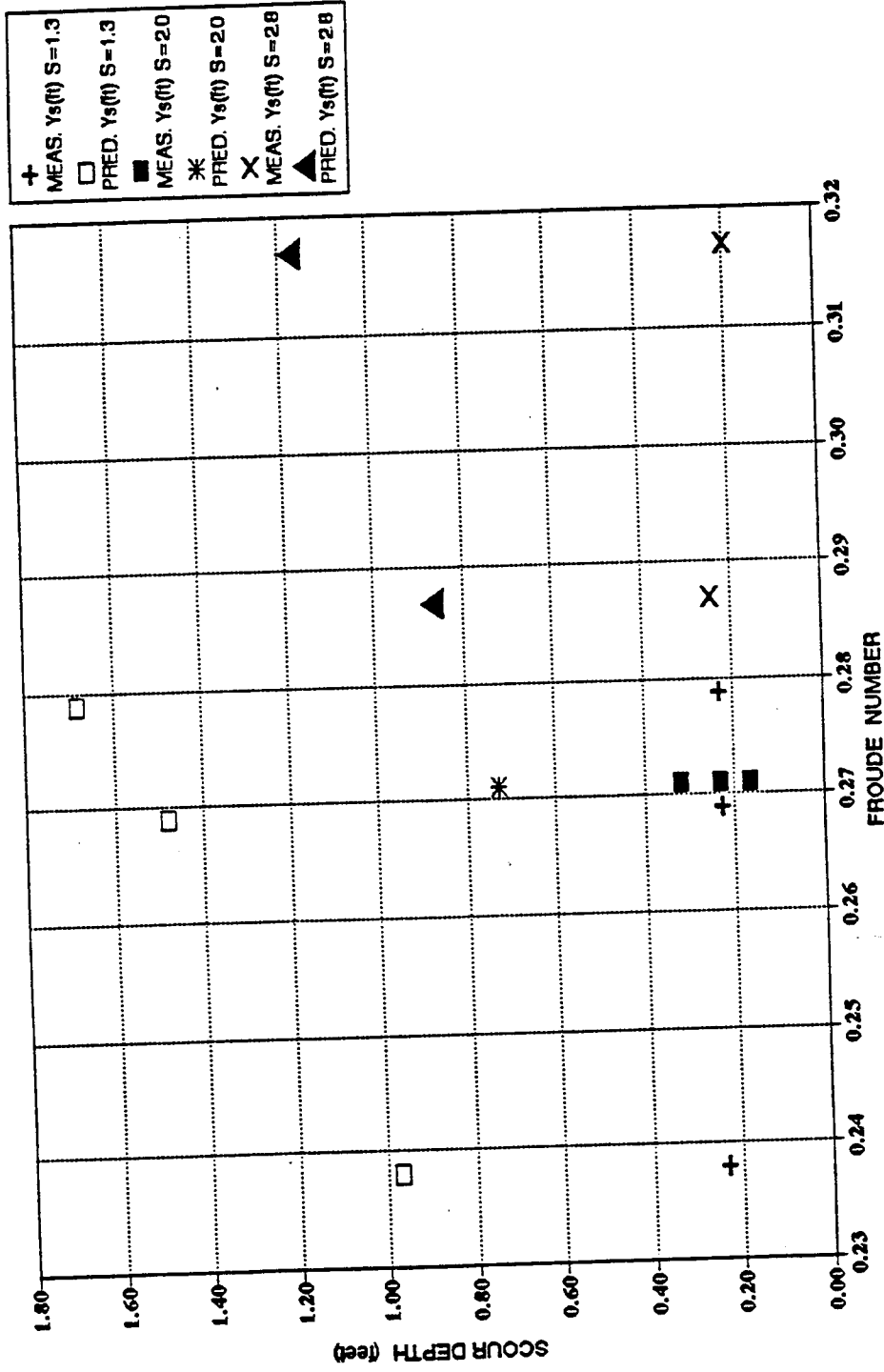


Figure 4.52 Comparison between Newly Developed Prediction Equation and Chiew's Data

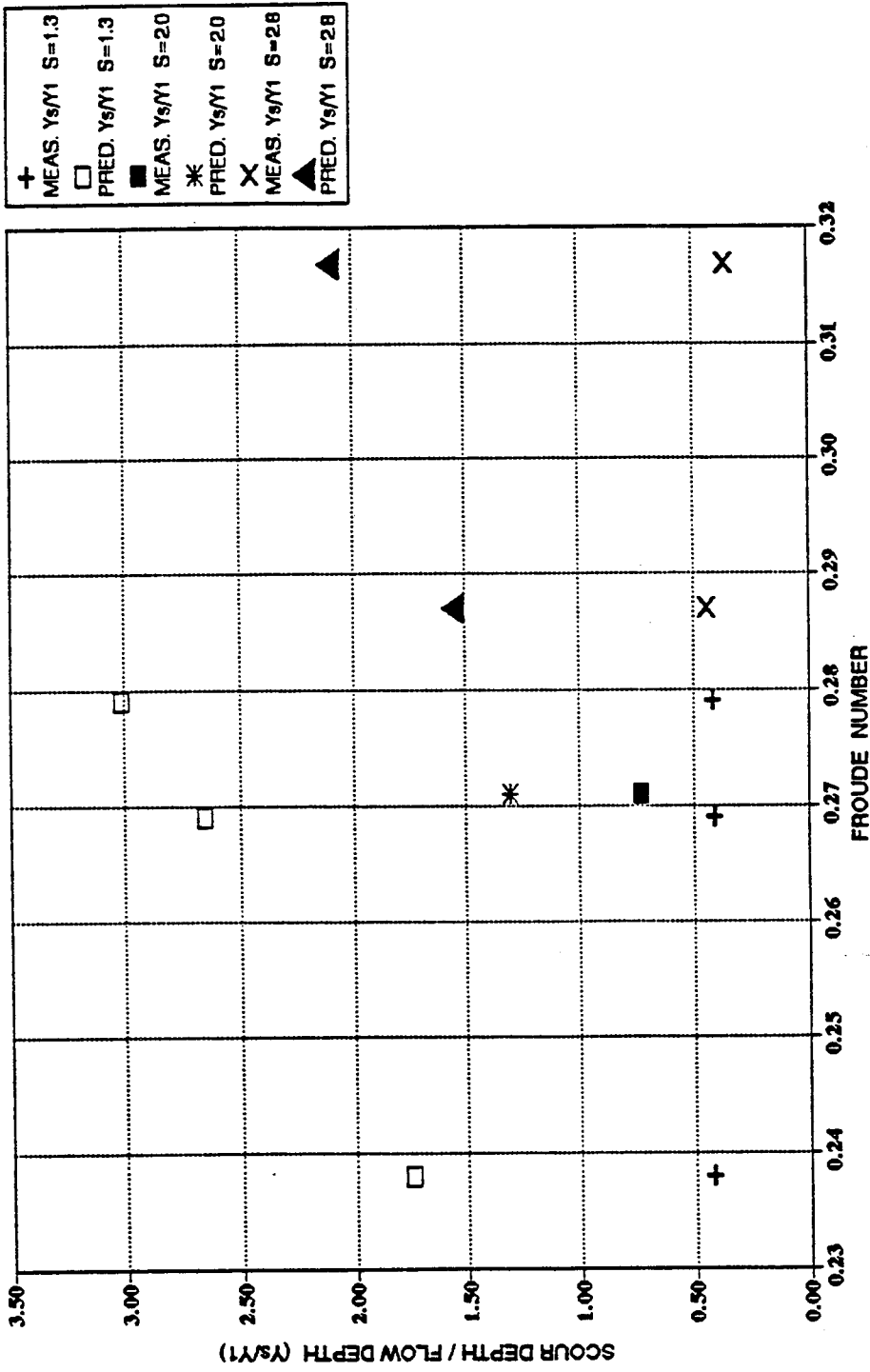


Figure 4.53 Comparison between Newly Developed Prediction Equation and Chiew's Data

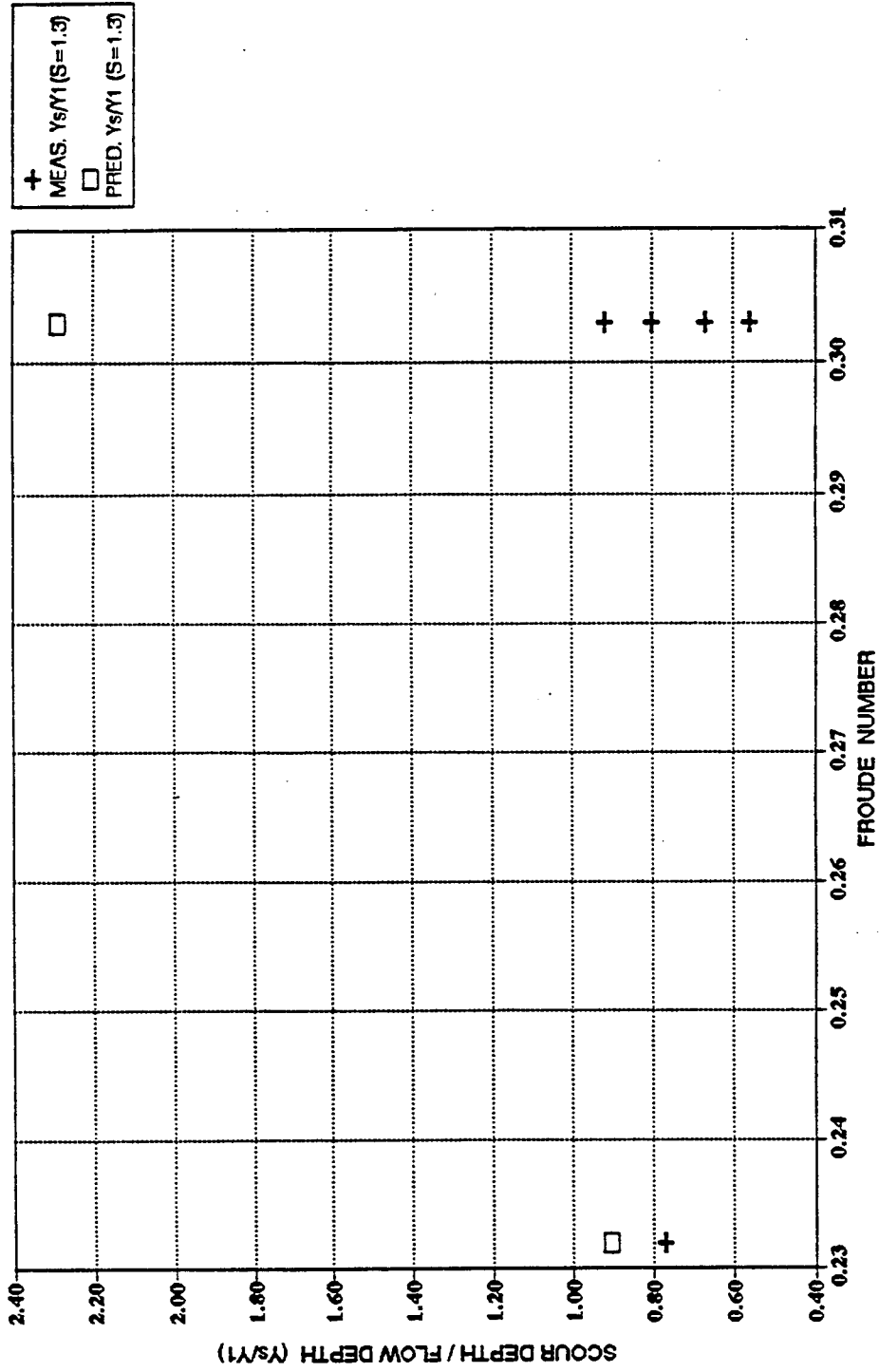


Figure 4.54 Comparison between Newly Developed Prediction Equation and Chee's Data

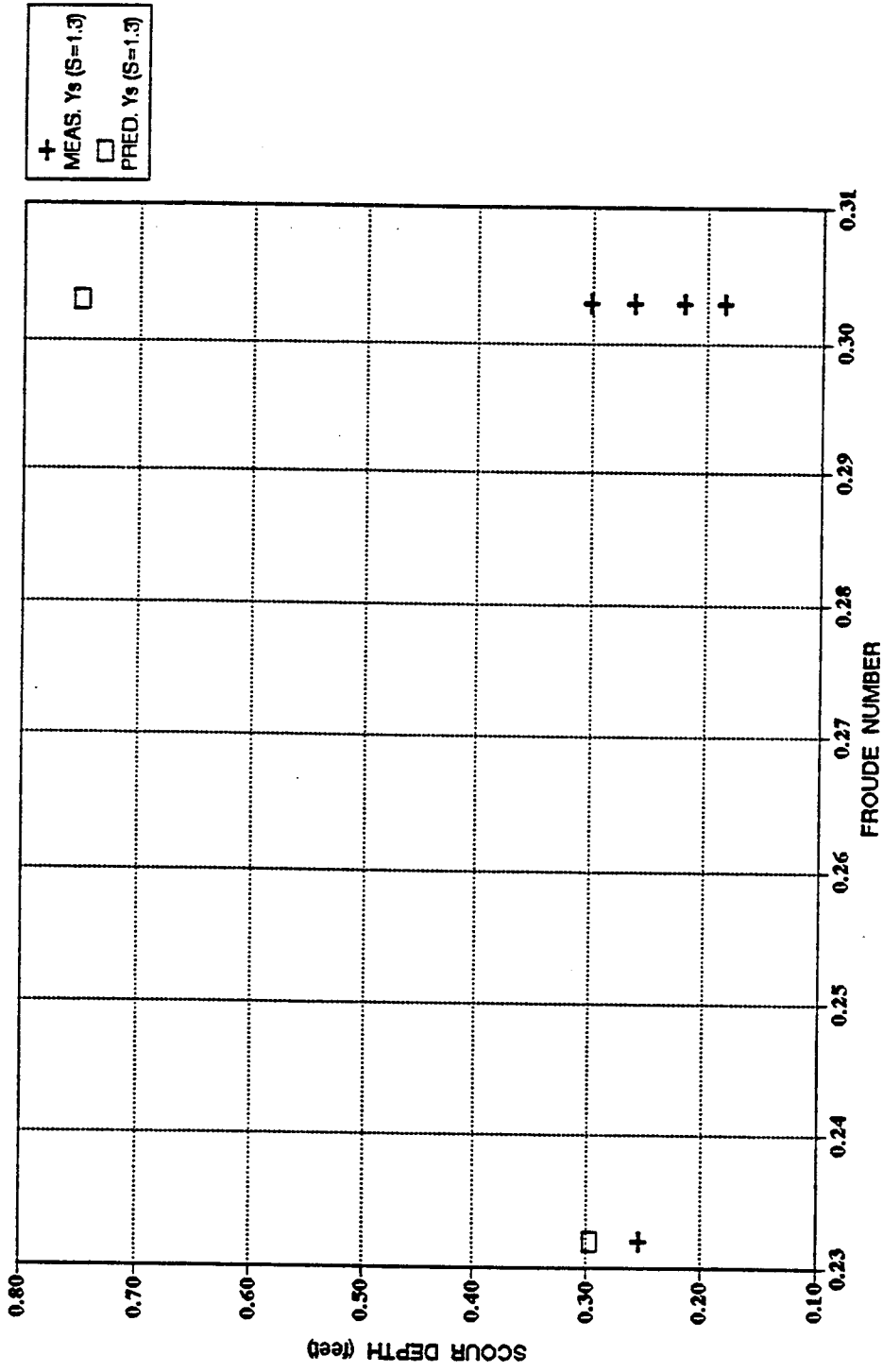


Figure 4.55 Comparison between Newly Developed Prediction Equation and Chee's Data

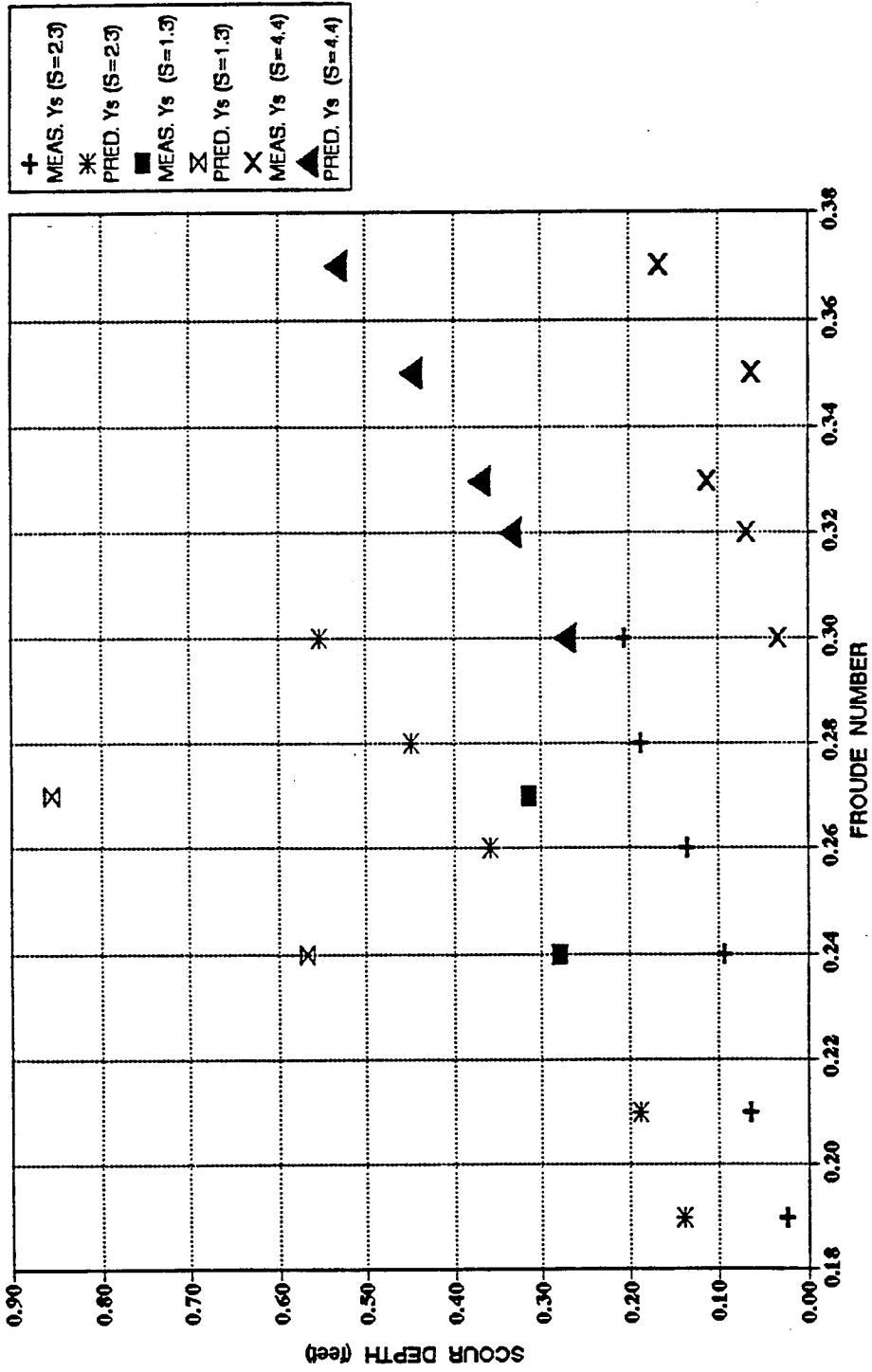


Figure 4.56 Comparison between Newly Developed Prediction Equation and Baker's Data

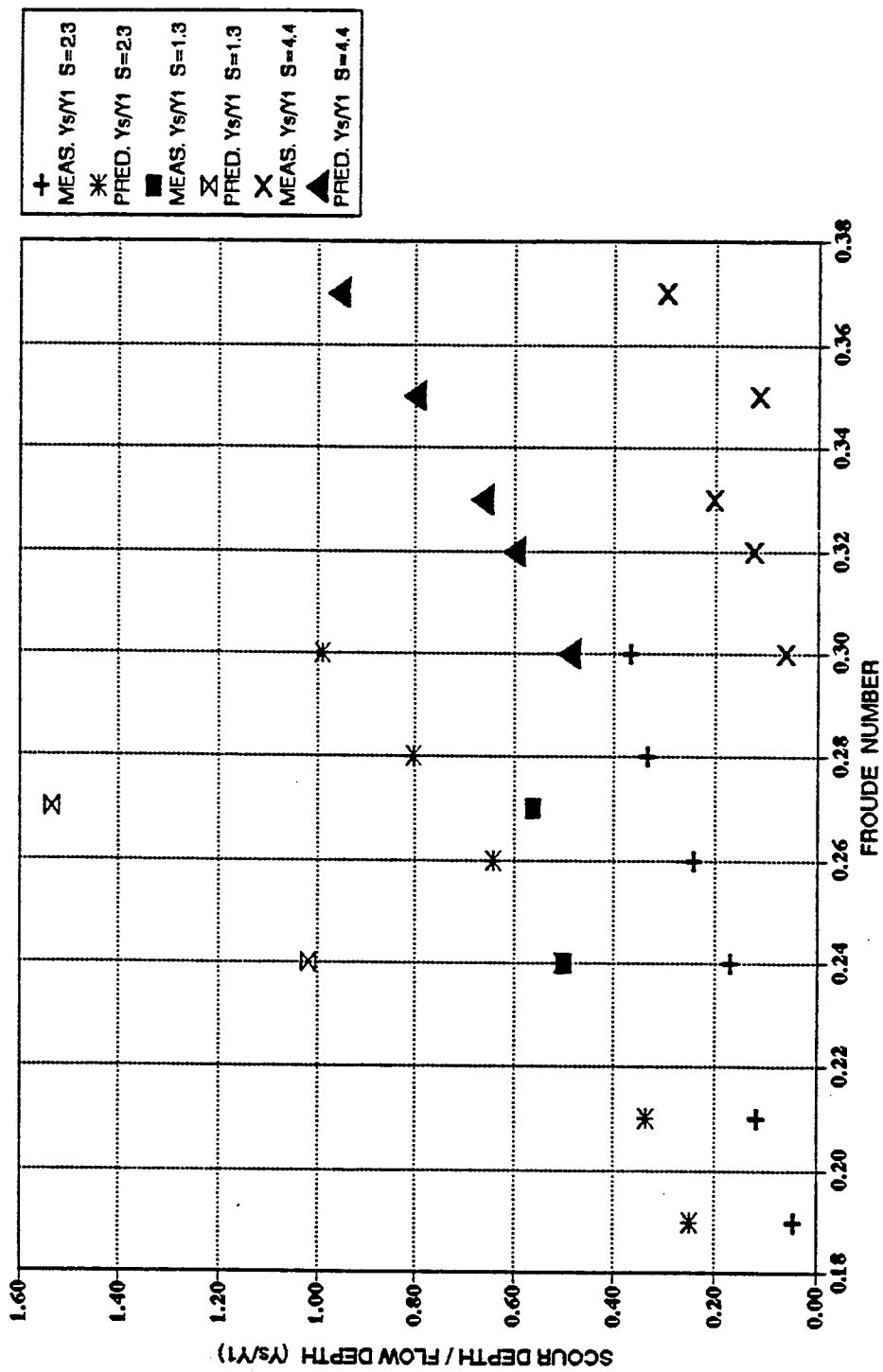


Figure 4.57 Comparison between Newly Developed Prediction Equation and Baker's Data

which define the gradation coefficient play a very important role in reducing the scour depth for graded materials.

It is believed that the coarse fraction above d_{90} is more important than any other portion of the gradation curve in the formation of the armor layers around bridge piers to stop or resist the scouring action of the flowing water. Therefore, the general equation should include a parameter that accounts for the effect of gradation and the ratio d_{90}/d_{50} will be substituted here to replace the effect of σ_g . This is due to the fact that d_{90} was shown to be a more significant parameter than σ_g in the armor layer formation.

A stepwise regression analysis was used by the MINITAB computer program as done earlier to develop a general equation for local clear-water scour. The expression was developed following the dimensional analysis after introducing the parameter d_{90}/d_{50} for each original sediment mixture to account for armoring of bed material instead of σ_g for the parameters affecting scour process:

$$\frac{Y_s}{Y_1} = k K_1 K_2 (F_r)^a \left(\frac{d_{90}}{d_{50}}\right)^b \quad (4.24)$$

where k , K_1 , and K_2 are the proportionality constant, coefficient for pier shape, and coefficient for pier alignment respectively as defined earlier .

The logarithm of Y_s/Y_1 was regressed against the combination of the other two terms F_r and d_{90}/d_{50} , giving the following equation or expression which gave the largest coefficient of determination, R^2 :

$$\frac{Y_s}{Y_1} = 148.0 (F_r)^{2.93} \left(\frac{d_{90}}{d_{50}} \right)^{-1.48} \quad (4.25)$$

The corresponding statistical analysis for this regression step was as follow:

Power equation:

$$C1 = 2.17 + 2.93 C2 - 1.48 C3 \quad (4.26)$$

where C1, C2, and C3 representing log values of Y_s/Y_1 , F_r , and d_{90}/d_{50} .

	Coefficient	Standard Deviation of coefficient	T- ratio=coeff /SD	P
Constant	2.1702	0.1271	17.08	0.000
C2	2.9326	0.1382	21.21	0.000
C3	-1.4847	0.1627	-9.12	0.000
S = 0.1164				
R-square = 91.9 %				
R-square = 91.6% adjusted for D.F.				

Analysis of Variance:

Source	DF	SS	MS=SS/DF	F	P
Regression	2	6.9684	3.4842	256.95	0.000
Residual	45	0.6102	0.0136		
Total	47	7.5785			

CHAPTER 5

SUMMARY, CONCLUSIONS AND RECOMMENDATIONS

5.1 SUMMARY

The main objectives of this study were to investigate the effect of sediment gradation coefficient and increasing the size of coarse material fraction that exists in a sediment mixture on local pier scour, and to develop a prediction equation for clear water scour depth to account for armoring of bed materials. This objective was achieved by conducting a series of physical experiments in a laboratory flume using six different sediment mixtures with a constant mean diameter and known initial gradations.

The mean grain size (d_{50}) was kept constant at 0.75 mm for the six bed materials which were used. One of the three bed materials was considered to be uniform and had a geometric standard deviation (σ_g) of 1.38; the other five had σ_g values of 2.43 and 3.4.

The mixtures were prepared by mixing different kinds of sand and gravel to get a desired mixture with a certain σ_g value and a mean diameter, d_{50} of 0.75 mm. The uniform material was prepared by sieving out the fines and coarse sizes of the sand mixture which had a mean diameter of d_{50} of 0.75 mm and a gradation coefficient σ_g of 2.43 by a group of sieves.

All the three sets of runs were conducted in clear-water scour except the last run at the end of each set of runs was performed when the bed motion had started. This was

to assure that all ranges of flow conditions were covered in clear-water scour regime.

In the first set (runs 1 through 12), the bed material around each of the three piers along the length of the flume had the same d_{50} of 0.75 mm and σ_g of 2.43. The flow conditions were the same at the site of each pier and almost uniform flow conditions over the entire flume test length was maintained. The experiments were continued until the scour depth at each pier was fully developed and the equilibrium was reached for at least 4 hours. Then the discharge was slowly lowered until the flow was stopped completely. The flume was then drained through the aid of an efficient drainage system at the bed of the flume, so that the final bed and scour profiles around each pier could be easily measured. Photographs of the bed were taken, and the armor layers at different areas around each pier were sampled and sieved to determine their sediment size distribution curves.

In the second set (runs 13 through 19), the bed material around Pier No. 1 was kept the same as first set having d_{50} of 0.75 mm and σ_g of 2.43. Around Pier No.2 the size of coarse material fraction above d_{90} was increased but still the bed material had the same d_{50} and σ_g as 0.75 mm and 2.43 respectively. Around Pier No. 3, the size of coarse fraction above d_{95} was increased but d_{50} and σ_g were kept constant at 0.75 mm and 2.43.

In the third set (runs 20 through 27), the bed material around Piers No. 1 and 2 had a geometric standard deviation of 3.4 and a mean diameter of 0.75 mm. The only difference in bed materials around Piers No.1 and 2 was that the size of coarse material fraction above d_{90} was increased around pier No. 1. At Pier No. 3, a uniform

material with σ_g and d_{50} of 1.38 and 0.75 mm, respectively was used.

Prediction equations for the local scour depth in graded and uniform materials were developed using the experimental data from the present study. In addition, an analysis for the effect of increasing coarse material fraction on the resulting scour depth was presented. A comparative analysis between scour depths for bed material having a given value of σ_g with increased d_{90} size and those materials with higher σ_g values are also presented.

A comparison between various prediction equations for local scour depth and the measured data from this study, and a comparison between predicted equations from this study and other data from previous studies were also done.

5.2 CONCLUSIONS

In the experiments conducted for this dissertation scour depth increased with increasing velocities and Froude Numbers. The amount of scour was a function of sediment gradation and d_{90} size. The larger gradation coefficients (and larger d_{90} sizes) resulted in smaller scour depths. Figures 5.1 through 5.3 show the variation of scour depth ratio with approach flow velocity and approach flow Froude number for the different tests conducted during this study. From these figures, it can be seen that up to the critical conditions beyond which live-bed scour is encountered, the amount of scour is a function of both flow velocity and gradation coefficient (or d_{90} size). Beyond

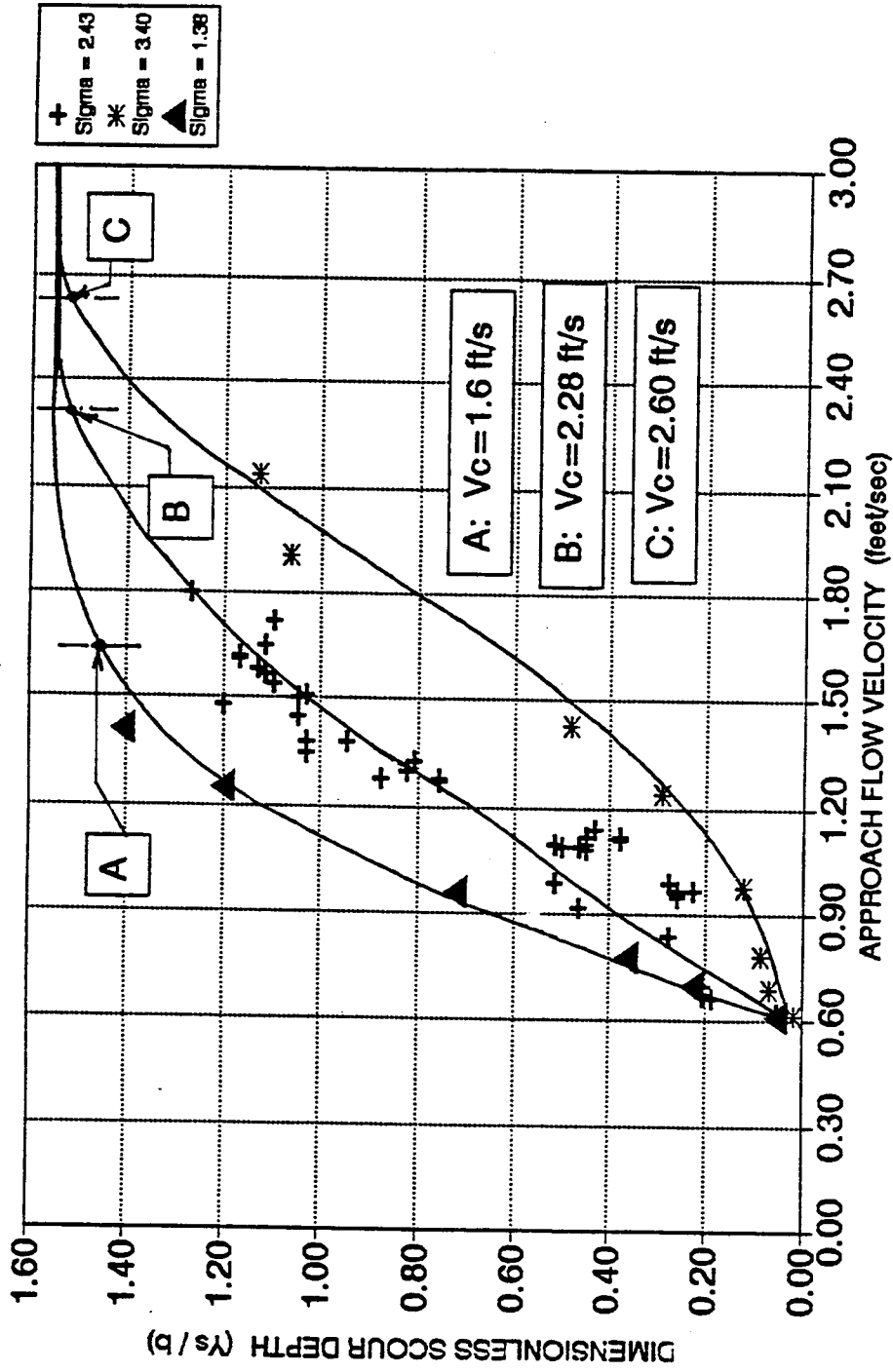


Figure 5.1 Variation of Dimensionless Scour Depth with Approach Velocity for Various Gradation Coefficients Used in Experiments ($D_{50} = 0.75$ mm)

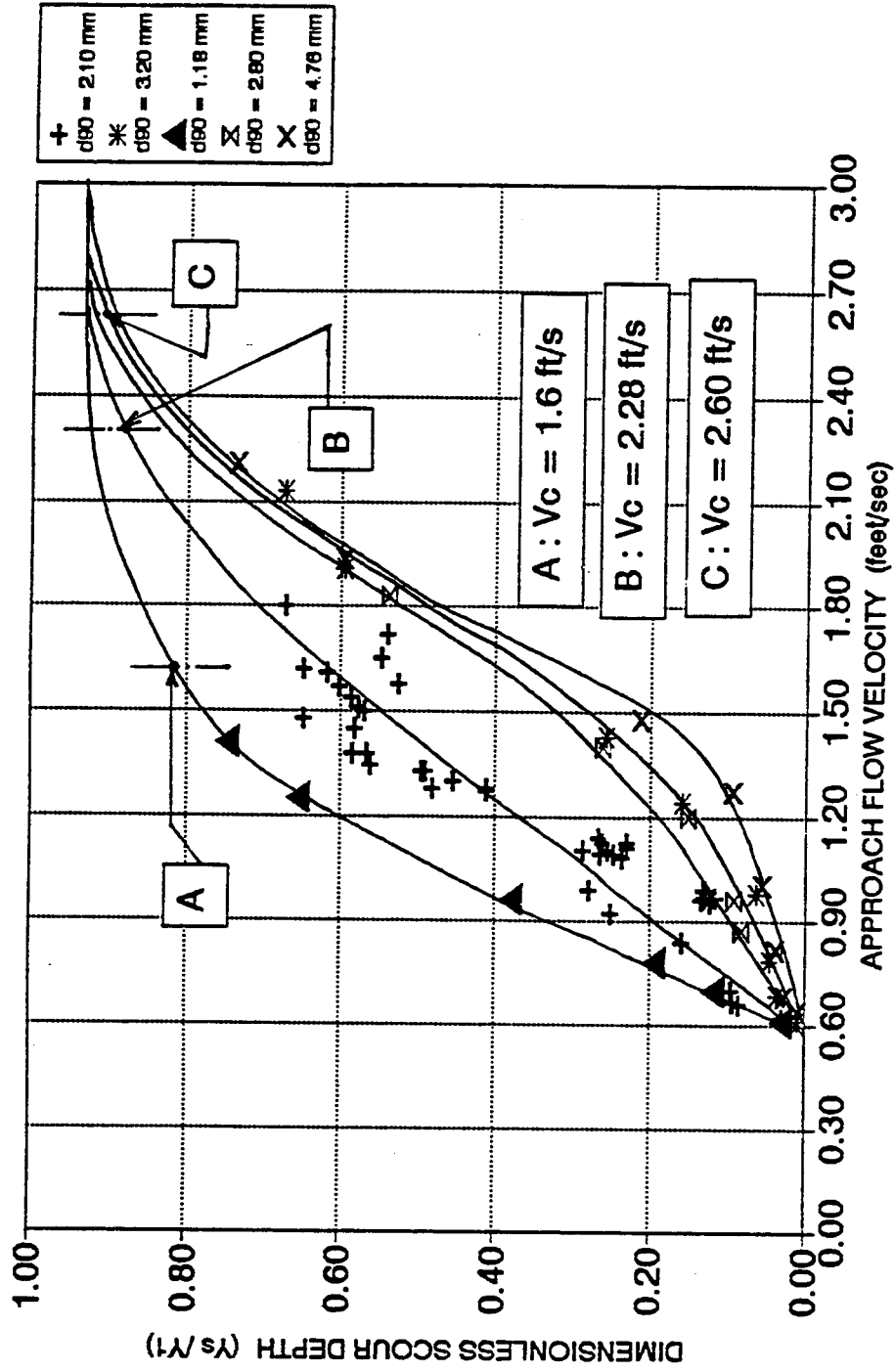


Figure 5.2 Variation of Dimensionless Scour Depth with Approach Velocity for Various D_{50} Sizes Used in Experiments ($D_{90} = 0.75$ mm)

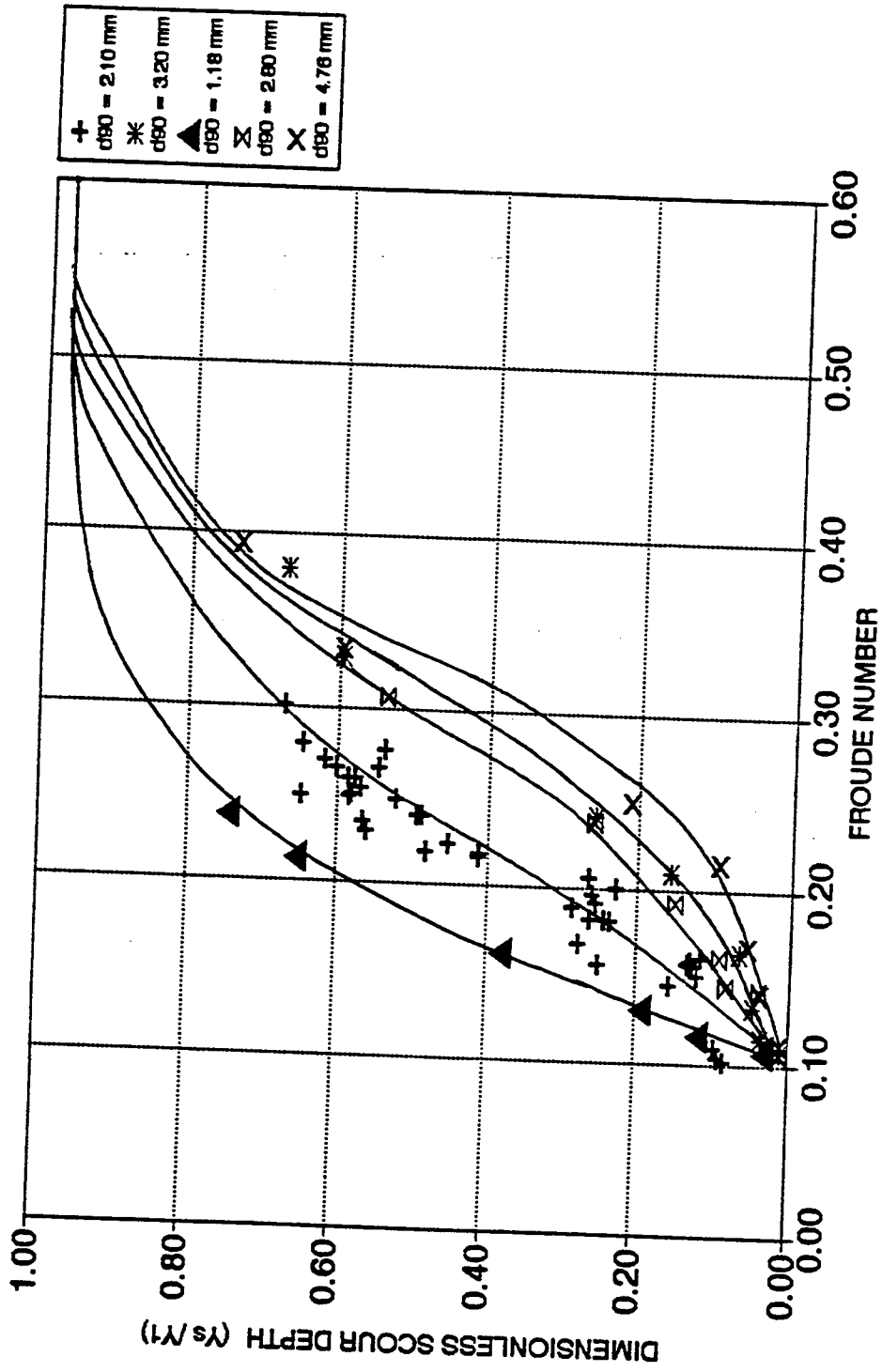


Figure 5.3 Variation of Dimensionless Scour Depth with Approach Flow Froude Number for Various D_{90} Sizes Used in Experiments ($D_{90} = 0.75$ mm)

the limits of clear-water scour conditions, the findings of this study do not apply. For the present experiments the limit of clear-water scour has been successfully estimated by the use of modified Neill equation using d_{90} to represent the sediment mixture size. Future research in establishing this limit condition should be used in conjunction with this study to expand the applicability of the research to wider range of conditions.

The conclusions drawn from this research are as follows:

1. The maximum local scour depth in clear-water scour for uniform materials is much larger than those for graded materials.
2. For flow conditions below critical conditions sediment gradation is important in reducing scour depths because graded materials enhance formation of an armor layer around bridge piers, which in return stops the scour.
3. For a given mean sediment size, the higher the sediment gradation, the less the scour depth will be.
4. Width and depth of scour holes, which take the shape of inverted cones, are a function of flow velocity and sediment gradation when keeping all other parameters that affect scour depth constant.
5. In clear-water scour, no bed formation or contraction scour was observed and only local scour around the piers occurred.
6. The initial rate of scour development decreased with increasing bed material non-uniformity and maximum scour depth was reached in shorter time.
7. Size of bed material fractions above d_{85} play an important role in reducing scour depth as does increasing the gradation coefficient σ_g .

8. Increasing the size of coarse material fraction above d_{90} reduces the scour depth by a greater percentage than does increasing the size of the part above d_{95} . This means that the higher the percentage of coarse material fraction, the higher the reduction in scour depth will be. Increasing σ_g by decreasing the size of finer size fractions does not have the same effect as increasing coarser fraction sizes.
9. For clear-water scour, increasing the size of coarse material fraction in the original sediment mixture dramatically reduces the scour depths at bridge piers due to the formation of coarser armor layers.
10. Bed materials with a gradation coefficient of 2.43 and with increased d_{90} sizes can sustain the same or lesser scour depths than that occurring in bed materials with a higher σ_g value of 3.4. This indicates the importance of size of coarse fractions compared to σ_g .
11. The function of coarse material fraction is to reduce the depth and width of scour holes and to cause the equilibrium scour depth to be attained in a shorter time.
12. The newly developed prediction equations for clear-water scour depths (Equations 4.18, 4.20, and 4.22) from this study show a strong dependence on the Froude number of flow (to a power of 3 or more). These equations take into account the effect of non-uniformity of bed materials.
13. The ratio d_{90}/d_{50} proved to have a significant effect on reducing the scour depth and controlling the armoring process. Therefore scour equations using σ_g should be modified to reflect the size of coarse fractions between σ and 2σ to express the behavior of non-uniform materials in armoring process.

14. For graded materials, 90% to 99% of the maximum scour depth is attained within the first 6.0 hours of the experiments. Experiment run times could be reduced and extrapolations for larger time values could be done without significantly affecting the results.

15. For the clear-water scour range, scour protection or reduction around bridge piers can be achieved by increasing the size of coarse material fraction that exists in the sediment mixture. This technique can provide protection of the bed and the pier foundations as an alternative to the use of riprap.

5.3 RECOMMENDATIONS FOR FUTURE RESEARCH

On the basis of the results of this investigation, the following future research is recommended:

1. Laboratory work results related to effects of gradation should be checked against closely monitored field work.
2. The applicability of increasing the size of coarse fractions to reduce scour depth should be checked by field implementations.
3. For both clear water and live-bed scour conditions, experimental data are required for very shallow flows ($Y/b < 0.2$) and for deep flows ($Y/b > 10.0$ to 20.0) to check the effect of increasing the size of coarse material fraction under these conditions.
4. Experimental data are required for large sediments ($b/d_{50} < 25$) for clear-water scour conditions.

5. Experimental data are required for the influence of increasing the size of coarse material fraction using nearly uniform materials.
6. The highest value of Froude number that was tested in this study for clear-water scour was 0.39 since at higher Froude numbers bed movement occurred. Experimental data are required for Froude numbers beyond the range that was tested during this study.
7. Analytical and numerical turbulence model solutions to the problem of local scour should be explored more rigorously in coordination with experimental work. This integrated approach would provide numerical modelers the experimental coefficients needed in their analytical formulations.

REFERENCES

- Ahmed, M.E. (1989). "Rearrangement of Coarse Grains And Patterns in Armor Coats," Ph.D. Dissertation, Civil Engineering Department, Colorado State University, Fort Collins, Colorado.
- Baker, R. E. (1986). "Local Scour at Bridge Piers in Non-Uniform Sediment," School of Engineering Report No. 402, University of Auckland, New Zealand.
- Bata, C. (1960). "Erezija Eke Novesadskeg Mastorskog Stube (Scour Around Bridge Piers)," Inst. Za Vodoprivedu, Jaroslav. Cerni Beograd, Yugoslavia.
- Blench, T. (1952). "Normal Size Distribution Found in Samples of River Bed Sands," Civil Engineering, Vol. 22.49, Feb.
- Breusers, N. N. C. (1965). "Scour Around Drilling Platforms," Bulletin, Hydraulic Research 1964 and 1965, I.A.H.R., Vol.19, p.276.
- Chabert, J. and Engeldinger, P. (1956). "Etude des Affouillements Autor des Piles des Ponts," Laboratoire National d'Hydraulique, Chatou, France.
- Chee, R. K. W. (1982). "Live Bed Scour at Bridge Sites," School of Engineering Report No. 216, University of Auckland, New Zealand.
- Chiew, Y. M. (1984). "Local Scour at Bridge Piers," School of Engineering Report No. 290, University of Auckland, New Zealand.
- Chitale, S. V. (1960). Discussion of "Scour at Bridge Crossings," by E. M. Laursen. Transactions. ASCE, Vol. 127, pp. 191-196.

- Davies, B. E. (1971). "The Armoring of Alluvial Channel Beds," Unpublished. M. Sc. Thesis, University of Canterbury, Christchurch.
- Davoren, A. (1985). "Local Scour Around a Cylindrical Bridge Pier," Publication No. 3, Hydrology Center, Christchurch, Ministry of Works and Development.
- Day, T. J. (1976). "Preliminary Results of Flume Studies into The Armoring of a Coarse Sediment Mixture," Report of Activities, Part C, Geological Survey, Canada, Paper 76-1C. pp 277-287.
- Ettema, R. (1976). "Influence of Bed Gradation on Local Scour," School of Engineering Report No. 124, University of Auckland, New Zealand.
- Ettema, R. (1980). "Scour at Bridge Piers," School of Engineering Report No. 216, University of Auckland, New Zealand.
- Fleming, G. and Poodle, T. (1970). "Particle Size of River Sediments," Journal of Hydraulic Division, Proc. ASCE, Vol. 96, No. HY2, February, pp. 431-439.
- Franzetti, S., Larcan, E. and Mignosa, P. (1982). "Influence Of Tests Duration On The Evaluation Of Ultimate Scour Around Circular Piers," Hydraulic Modelling Of Civil Engineering Structures, Report No. 304, Milano, Italy.
- Froehlich, D. C. (1988). "Analysis of On-Site Measurements of Scour at Piers," 2 Proc. ASCE, National Hydr. Eng. Conf., Colorado Springs, CO.
- Gessler, J. (1967). "The Beginning of Bed Load Movement of Mixtures Investigated as Natural Armoring in Channels," Translated by E. a. Prych, Translation T-5, W. M. Keck Laboratory of Hydraulics and Water Researches, California Institute of Technology, Pasadena, California, 1967.

- Gessler, J. (1971). "Critical Shear Stress of Sediment Mixtures," Proc. 14th Congress of the IAHR, Paris, France, Vol. 3, No. C1.
- Hancu, S. (1971). "Sur le Calcul des Affouillements Locaux dans la Zone des Piles de Ponts," Proceedings of the 14th I.A.H.R. Congress, Paris, Vol. 3, pp. 299-313.
- Inglis, C. C. (1949). "The Behavior And Control Of Rivers And Canals," Chapter 8, C.W.I. & N., Research Station Poona, Res. Publ. 13.
- Johnson, P.A. (1992). "Reliability-Based Pier Scour Engineering," ASCE Journal Of Hydraulic Engineering Division, Vol. 118 No. 10, pp. 1344-1358.
- Laursen, E. M. and Toch, A. (1956). "Scour Around Bridge Piers and Abutments," Bulletin No. 4, Iowa Road Research Board, Ames, Iowa.
- Little, W. C. and Mayer, P. G. (1972). "The Role Of Sediment Gradation On Channel Armoring," Georgia Inst. Of Technology, Envir. Research Center, Report ERC-0672.
- Melville, B. W. (1975). "Local Scour at Bridge Sites," Ph.D. Thesis, School of Engineering Report No. 117, University of Auckland, New Zealand.
- Melville, B.W., and Sutherland, A.J. (1988). "Design Method For Local Scour At Bridge Piers," Journal Of Hydraulic Engineering, Vol. 114, No. 10 ASCE 1210-1226.
- Neill, C.R. (1964). "River-Bed Scour," A Review for Engineers, Canadian Good Roads Assn. Techn. Publ. No. 23.
- Neill, C. R. (1973). "Guide to Bridge Hydraulics," Edited by C. R. Neill, Published for Roads and Transportation Assn. of Canada by University of Toronto Press,

Toronto.

- Nicollet, G. and M. Ramette (1971). "Affouillements Au Voisinage De Piles De Pont
Cylindriques Circulaires; Proc. 14th I.A.H.R Congress, Paris, 3, pp. 315-322.
- Nicollet, G. (1971). "Deformation Des Lits Alluvionnaires, Affouillelements Autour
Des Piles Des Ponts Cylindriques," E.D.F., Dep. Lab. Nat. d' Hyd. Chatou,
HC 043/689.
- Proffitt, G. T. (1980). "Selective Transport and Armoring of Non-Uniform Alluvial
Sediments," Ph. D. Dissertation, Civil Engineering Dept., University of
Canterbury, Christchurch, New Zealand, October, 1980.
- Raudkivi, A. J. and Ettema, R. (1977a). "Effect of Sediment Gradation on Clear
Water Scour and Measurement of Scour Depth," Proceedings 17th Congress
IAHR, Vol. 4, pp. 521-527, Baden-Baden.
- Raudkivi, A. J. and Ettema, R. (1977b). "Effect of Sediment Gradation on Clear
Water Scour," ASCE Journal of Hydraulics Division, Vol. 103, No. HY10.
- Raudkivi, A. J. and Sutherland, A. J. (1981). "Scour at Bridge Crossings," Road
Research Unit Bulletin 54, National Road Board, New Zealand.
- Richardson, E. V., Simons, D. B. and Julien, P. Y. (1975). "Highways in River
Environment," U.S. Dept. of Transportation, FHWA 1st ed. (2nd ed. 1987),
Fort Collins, CO.
- Shen, H. W., Schneider, V. R., Karaki, S. S. (1966a). "Mechanics Of Local Scour,"
Colorado State University, CER 66 HWS-VRS-SK22.
- Shen, H. W., Schneider, V. R., Karaki, S. S. (1966b). "Mechanics of Local Scour,"

U.S. Department of Commerce, National Bureau of Standards, Institute for Applied Technology.

Shen, H. W., Schneider, V. R., Karaki, S. S. (1969). "Local Scour Around Bridge Piers," JHD, Proc. ASCE, Vol. 95, HY6, pp. 1919-1940.

Shields, A. (1936). "Application of Similarity Principles and Turbulence Research to Bed-Load Movement," translated version.

Vanoni, V. A., and Brooks, N. H. and Kennedy, J.F. (1961). "Lecture Notes on Sediment Transportation and Channel Stability," California Institute Of Tech. Pasadena, California, Report No. KH-R1, January.

APPENDIX A
DIMENSIONAL ANALYSIS FOR THE INFLUENCING PARAMETERS
ON THE SCOUR DEPTH

A.1 Scouring Parameters

The parameters which influence scour around bridge piers can be arranged into four groups:

A.1.1. Fluid variables:

- density of water ρ
- kinematic viscosity of water ν
- acceleration due to gravity g

A.1.2. Flow variables:

- depth of approach flow y
- mean velocity of approach flow V
- angle between flow direction and pier axis α
(angle of attack)

A.1.3 Bed materials variables:

- grain diameter and form d_{50}
- grain size distribution σ_g
- density of sediment ρ_s
- cohesive properties

A.1.4 Bridge pier variables:

- pier dimensions b
- pier shape ϕ
- surface roughness
- number of spacing of the piers

- orientation of piers to approach flow α

A.1.5 Time

The relationship between the scour depth and the parameters which influence it can be summarized as follows:

$$\text{scourdepth} = f [(\text{fluid}), (\text{flow}), (\text{sediment}), (\text{pier}), (\text{time})] \quad (\text{A.1})$$

Because of the complexities and costs of measurement, analysis, and evaluation of all of the above mentioned variables, many investigators assume some restrictive conditions:

- the difference between the laboratory and field values for density, viscosity and acceleration due to gravity can be neglected;
- channels can be considered sufficiently wide so that the bridge pier does not cause a significant contraction;
- the bed material is alluvial (non-cohesive and often uniform particle-sized);
- the piers are perfectly smooth without scour protection systems, such as riprap.

These assumptions and restrictions reduce the list of variables to the following:

1. density ρ and kinematic viscosity ν of water;
2. mean sediment diameter d_{50} and sediment density ρ_s ;
3. approach flow depth y_1 and mean velocity of the approach flow V_1 ;
4. pier width b , pier shape ϕ , and orientation of the pier (angle α).

A.2 Dimensional Analysis

Dimensional analysis is only a technique for grouping the variables, and yields information on the form of the functional relationships. It has been used extensively by many researchers in different forms for grouping or forming the variables used in estimating the depth of local scour.

As stated before, the depth of scour is a function of a number of different parameters. In general, the local scour depth as a function of these affecting parameters can be expressed in the form:

$$d_s = f (y, b, V, d_{50}, \sigma_g, \phi, \alpha, \gamma_s, t, g, \rho, \nu) \quad (\text{A.2})$$

where:

y = approach flow depth;

b = pier width;

V = mean approach velocity;

d_{50} = mean sediment size;

σ_g = sediment gradation;

ϕ = shape factor;

α = angle of attack;

γ_s = specific weight of sediment;

t = time;

g = gravity acceleration;

ρ = water density;

ν = kinematic viscosity.

Using Π -Theorem in performing the dimensional analysis and taking y , V , ρ as the three repeated variables that has the 3 principal lengths M , L , T of mass, length, and time :

Taking $\pi_1 = y^{a_1} V^{b_1} \rho^{c_1} d_s$

therefore $M^0 L^0 T^0 = (L)^{a_1} (LT^{-1})^{b_1} (ML^{-3})^{c_1} (L)$

equating the exponents in both sides of the equation to be in equilibrium, then,

for M : $0 = C_1$, therefore $C_1 = 0$

for T : $0 = -b_1$, therefore $b_1 = 0$

for L : $0 = a_1 + b_1 - 3C_1 + 1$, therefore $a_1 = -1$

therefore: $\pi_1 = d_s y^{-1}$

or $\pi_1 = d_s/y$

Similarly: $\pi_2 = y^{a_2} V^{b_2} \rho^{c_2} b$

therefore: $\pi_2 = b/y$

Taking: $\pi_3 = y^{a_3} V^{b_3} \rho^{c_3} d_{50}$

therefore: $\pi_3 = d_{50}/y$

Taking: $\pi_4 = y^{a_4} V^{b_4} \rho^{c_4} \sigma_g$

therefore: $\pi_4 = \sigma_g$

Similarly: $\pi_5 = \phi$

therefore: $\pi_6 = \alpha$

taking: $\pi_7 = y^{a_7} V^{b_7} \rho^{c_7} \gamma_s$

$$M^0 L^0 T^0 = (L)^{a_7} (LT^{-1})^{b_7} (ML^{-3})^{c_7} (ML^{-2}T^{-2})$$

for M: $0 = C_7 + 1$ therefore $C_7 = -1$

for L: $0 = a_7 + b_7 - 3C_7 - 2$, therefore $b_7 = -2$

for T: $0 = -b_7 - 2$, therefore $a_7 = 1$

Taking: $\pi_7 = y V^{-2} \rho^{-1} \gamma_s$

therefore: $\pi_7 = \gamma_s y / \rho V^2$

Taking: $\pi_8 = y^{a_8} V^{b_8} \rho^{c_8} t$

$$M^0 L^0 T^0 = (L)^{a_8} (LT^{-1})^{b_8} (ML^{-3})^{c_8} (T)$$

for M: $C_8 = 0$

for L: $a_8 + b_8 = 0$

for T: $0 = -b_8 + 1$, therefore $b_8 = 1$

$$a_8 = -1$$

from which: $\pi_8 = y^{-1} V t$

therefore: $\pi_8 = Vt/y$

Taking: $\pi_9 = y^{a_9} V^{b_9} \rho^{c_9} g$

$$M^0 L^0 T^0 = (L)^{a_9} (LT^{-1})^{b_9} (ML^{-3})^{c_9} (LT^{-2})$$

for M: $0 = C_9$

for L: $0 = a_9 + b_9 - 3C_9 + 1$, therefore $a_9 + b_9 = -1$

for T: $0 = -b_9 - 2$, therefore $b_9 = -2$,

$$a_9 = 1$$

Taking: $\pi_9 = y V^{-2} g$

therefore: $\pi_9 = gy/V^2$

Therefore:

$$\frac{d_s}{y} = f\left(\frac{b}{y}, \frac{d_{50}}{y}, \sigma_g, \phi, \alpha, \frac{\gamma_s y}{\rho V^2}, \frac{V_t}{y}, \frac{gy}{V^2}\right) \quad (\text{A.3})$$

Since:

$$\frac{\gamma_s y}{\rho V^2} = \frac{\rho_s g}{\rho} \frac{y}{V^2} = \frac{\rho_s g}{\rho} \frac{1}{g} = \frac{\gamma_s}{\gamma} \quad (\text{A.4})$$

and γ_s, γ being the specific weights of sediment and water respectively and they are constants during the study, also $y/V^2 = 1/g$, therefore:

$$\frac{d_s}{y} = f\left(\frac{b}{y}, \frac{d_{50}}{y}, \sigma_g, \phi, \alpha, \frac{V_t}{y}, \frac{gy}{V^2}\right) \quad (\text{A.5})$$

$$\frac{d_s}{y} = f\left(\frac{b}{y}, \frac{d_{50}}{y}, \sigma_g, \phi, \alpha, \frac{V_t}{y}, \frac{gy}{V^2}\right) \quad (\text{A.6})$$

Since, gy/V^2 is the reciprocal of the square of Froude number, therefore:

$$\frac{d_s}{y} = f \left(\frac{b}{y}, \frac{d_{50}}{y}, \sigma_g, \phi, \alpha, \frac{V_t}{y}, F_r \right) \quad (\text{A.7})$$

or:

$$\frac{d_s}{y} = K \cdot K_1 \cdot K_2 \left(\frac{b}{y} \right)^a \left(\frac{d_{50}}{y} \right)^b (\sigma_g)^c \left(\frac{V_t}{y} \right)^d (F_r)^e \quad (\text{A.8})$$

where K = proportionality constant;

K_1 = shape factor;

K_2 = alignment factor;

a, b, c, d, e = exponents.

